

Evolution of porosity, diffusivity and mineralogy of different cement-clay interfaces

*Inauguraldissertation
der Philosophisch-naturwissenschaftlichen Fakultät
der Universität Bern*

vorgelegt von
Pietro Luraschi
von Bellinzona TI

Leiter der Arbeit:
PD Dr. Thomas Gimmi
Institut für Geologie, Universität Bern und Paul Scherrer Institut

Co-Leiter der Arbeit:
Prof. Dr. Sergey V. Churakov, Universität Bern und Paul Scherrer Institut
Dr. Luc R. Van Loon, Paul Scherrer Institut

Evolution of porosity, diffusivity and mineralogy of different cement-clay interfaces

*Inauguraldissertation
der Philosophisch-naturwissenschaftlichen Fakultät
der Universität Bern*

*vorgelegt von
Pietro Luraschi
von Bellinzona TI*

*Leiter der Arbeit:
PD Dr. Thomas Gimmi
Institut für Geologie, Universität Bern und Paul Scherrer Institut*

*Co-Leiter der Arbeit:
Prof. Dr. Sergey V. Churakov, Universität Bern und Paul Scherrer Institut
Dr. Luc R. Van Loon, Paul Scherrer Institut*

Von der Philosophischen-naturwissenschaftlichen Fakultät angenommen

Bern, den 24. Juni 2024

Der Dekan

Prof. Dr. Marco Herwegh



This work is licensed under a Creative Commons Attribution 4.0 International License. <https://creativecommons.org/licenses/by/4.0> except Chapter 3: © 2020
Published by Elsevier Ltd.

*Quelques fois les hommes trébuchent sur la vérité,
la plupart se relèvent, comme si de rien n'était.*

Modified after W.C.

Abstract

Several countries are planning to store their radioactive waste in deep geological formations. In Switzerland, the repository will be made of tunnels and caverns and will be located several hundred meters underground within the Opalinus Clay (OPA). Concrete and cementitious materials will be used in large amounts inside the repository and will come in contact with OPA and bentonite. There will therefore be several regions where clays (OPA and bentonite) and cementitious materials will form a reactive interface. In fact, when cement and clay come in contact, the strong chemical differences between these two materials lead to mass fluxes and dissolution-precipitation reactions. The result is the formation of thin regions (mm to cm) with altered porosity, mineralogy and transport properties. The understanding of the behavior of such altered regions is relevant for the safety assessment of the nuclear waste repository. In this thesis, different cement paste-clay samples were produced and experimentally investigated in a laboratory by means of different analytical techniques: neutron imaging, X-ray tomography, SEM/EDX, TGA, XRD and through-diffusion experiments. The results are presented and discussed in four main chapters.

The first two chapters focused on high porosity Ordinary Portland Cement paste (OPC) in contact with Na-montmorillonite. The results evidenced a strong decrease of the sample's diffusivity for both tritiated water (HTO) and chloride tracers already within the first 12 months of interaction. The chloride diffusivity was strongly reduced, suggesting that the newly formed phase precipitated in the free porosity (Chapter 3).

Mineralogical and porosity investigations on the same samples allowed detecting a low-porosity region on the montmorillonite side. This was mainly related to the precipitation of C-S-H phases within the first mm from the contact with the cement paste (Chapter 4). The cementitious side showed local porosity variation and various mineralogical alterations in the interface proximity (e.g., portlandite dissolution, Friedel's salt precipitation).

Subsequently, interface samples composed of more realistic materials were produced and investigated by means of different analytical techniques during two years interaction at room temperature and in an oxygen-free atmosphere (Chapter 5). The cement side of the interfacing materials was composed of an OPC or low-pH ESDERD mortar, whereas bentonite or OPA composed the clay side. The experiments allowed to quantify the decrease of the diffusive properties of the different samples and to characterize the mineralogical alteration occurring at the interface. The mineralogical alteration was dependent on the interfacing materials.

In the last part (Chapter 6), new interface samples composed of OPC paste in contact with different clays (montmorillonite, bentonite, OPA) were produced and let react at 70°C for eight months, while the porewater chemistry and the pH were monitored. The experiments allowed gaining information about the chemical evolution of the different systems, and on the effect of the increased temperature on the interface evolution. It was demonstrated that high temperature experiments accelerate the samples reactivity, which is nevertheless comparable to the reactivity at room temperature in terms of mineralogical evolution.

The results of the different performed experiments significantly improved the knowledge regarding the modification occurring when cement and clay are put in contact. The gained information can be implemented in models and further experiments, and they also help understanding relevant processes occurring in a real repository.

Riassunto

Molte delle nazioni che producono rifiuti nucleari hanno scelto come soluzione per lo smaltimento, di stoccare i rifiuti in formazione geologiche profonde. A dipendenza della nazione e delle litologie presenti, differenti tipologie di rocce e formazioni geologiche sono prese in considerazione per ospitare il futuro deposito di scorie radioattive. In Svizzera dopo decenni di ricerche è stata selezionata l'argilla Opalina come sito di stoccaggio. Si tratta una formazione argillosa presente in diverse zone (e diverse profondità) nell'altopiano Svizzero. Il deposito sarà composto da una serie di gallerie e caverne sotterrane situate a circa 800-900 m di profondità. Il sito scelto (che potrebbe ancora essere cambiato in futuro) si trova nelle vicinanze di Stadel, circa 20 km a Nord della città di Zurigo. In una parte del deposito saranno stoccati rifiuti altamente radioattivi provenienti principalmente dalle centrali nucleari. Attorno ad essi è previsto un riempimento composto da bentonite (un granulato argilloso). Le caverne e gallerie del deposito andranno stabilizzate mediante l'uso di calcestruzzo e materiali cementizi. Si creeranno perciò dei contatti (delle interfacce) fra l'argilla Opalina (o la bentonite) e il calcestruzzo. L'argilla e il cemento sono chimicamente molto differenti e formano delle interfacce molto reattive una volta in contatto. Il risultato è la formazione di zone che hanno delle proprietà (mineralogia, porosità) diverse rispetto ai materiali iniziali. Il trasporto di gas e soluti (ad esempio isotopi radioattivi) attraverso queste interfacce sono anch'essi modificati. Per garantire a lungo termine la sicurezza del deposito è dunque necessario conoscere come evolvono le proprietà delle regioni di contatto fra pasta di cemento e argilla.

Nell'ambito di questa tesi, sono stati prodotti diversi campioni di pasta di cemento e argilla, che sono in seguito stato studiati in laboratorio mediante diverse tecniche analitiche: radiografie neutroniche, tomografie a raggi X, SEM/EDX, TGA, XRD ed esperimenti di diffusione tramite acqua superpesante e chloro-36. I risultati sono suddivisi in quattro capitoli principali.

I primi due capitoli si concentrano sull'interazione fra una pasta di -Ordinary Portland Cement (OPC)- ad alta porosità a contatto con montmorillonite sodica. I risultati hanno evidenziato una forte diminuzione della diffusività dei campioni sia per l'acqua superpesante (HTO) sia per il cloro già nei primi 12 mesi di interazione (Capitolo 3). Il coefficiente di diffusione del cloro è risultato essere fortemente ridotto. Questa osservazione suggerisce che la nuova fase formatasi, e responsabile per la diminuzione della diffusività, si è formata nella cosiddetta porosità libera (porosità non affetta da cariche) all'interno della montmorillonite. Il trasporto HTO e quello del cloro sono dunque affetti diversamente dal cambiamento mineralogico che avviene all'interfaccia.

Le indagini mineralogiche e l'investigazione della porosità sugli stessi campioni hanno permesso di individuare una regione a bassa porosità sul lato della montmorillonite. Il calo della porosità è risultato essere principalmente legato alla precipitazione di fasi C-S-H (fasi generalmente osservate nel cemento idratato) entro il primo millimetro dal contatto con la pasta di cemento (Capitolo 4). Nel lato cementizio dei campioni è stata individuata una variazione locale della porosità e diversi cambiamenti mineralogici in prossimità dell'interfaccia (ad esempio, dissoluzione di portlandite e precipitazione di sali di Friedel).

Successivamente, sono stati prodotti campioni più vicini alla composizione reale che vi sarà nel deposito sotterraneo delle scorie. Anche in questo caso i campioni sono stati prodotti in laboratorio e studiati con diverse tecniche durante due anni di interazione (Capitolo 5). Il lato cementizio era composto da OPC e una malta a basso pH (ESDRED), mentre bentonite e OPA costituivano il lato argilloso. Gli esperimenti hanno

permesso di quantificare la diminuzione delle proprietà diffusive dei diversi campioni e di caratterizzare l'alterazione mineralogica che si verifica all'interfaccia. La tipologia di alterazione è fortemente dipendente dai materiali in contatto. Diversi cementi in contatto con la stessa argilla portano a una differente tipologia di alterazione.

Nell'ultima parte della tesi (Capitolo 6), sono stati prodotti nuovi campioni (composti da OPC in contatto con diverse argille) e lasciati reagire a 70°C per otto mesi, durante i quali è stata monitorata l'evoluzione chimica del sistema e il pH. Gli esperimenti hanno permesso evidenziare le differenze e le similitudini fra i diversi sistemi e comprendere l'effetto dell'aumento delle temperature sull'evoluzione dell'interfaccia. È stato dimostrato che l'aumento della temperatura aumenta la reattività dei campioni. Ciò nonostante l'alterazione è paragonabile in termini mineralogici a quella osservata a temperatura ambiente.

I risultati dei diversi esperimenti effettuati hanno migliorato significativamente la conoscenza delle modificazioni che si verificano quando cemento e argilla vengono messi in contatto. Le informazioni acquisite possono essere implementate in modelli o in ulteriori esperimenti e aiutano inoltre a migliorare la comprensione dei processi che avranno luogo nel futuro deposito svizzero di scorie radioattive.

Zusammenfassung

Mehrere Länder planen, ihre radioaktiven Abfälle in tiefen geologischen Formationen zu lagern. In der Schweiz wird das Tiefenlager aus Tunneln und Kavernen bestehen und mehrere hundert Meter unter der Erdoberfläche im Opalinuston (OPA) liegen. Im Endlager werden grosse Mengen an Beton und zementhaltigen Materialien verwendet, die mit OPA und Bentonit in Kontakt kommen werden. Es wird daher mehrere Bereiche geben, in denen Tone (OPA und Bentonit) und zementartige Materialien eine reaktive Grenzfläche bilden werden. Wenn Zement und Ton in Kontakt kommen, führen die starken chemischen Unterschiede zwischen diesen beiden Materialien zu Massenflüssen und Auflösungs-/Ausfällungsreaktionen. Das Ergebnis ist die Bildung von dünnen Bereichen (mm bis cm) mit veränderter Porosität, Mineralogie und Transporteigenschaften. Das Verständnis des Verhaltens solcher Regionen mit modifizierten Eigenschaften ist für die Sicherheitsbewertung des Endlagers von erheblicher Bedeutung, insbesondere im Hinblick auf den Transport von Gasen und Radionukliden.

In dieser Arbeit wurden verschiedene Zement-Ton Proben hergestellt und im Labor mit verschiedenen Methoden experimentell untersucht: Neutronen-Radiographie, Röntgentomographie, SEM/EDX, TGA, XRD und Durchdiffusion Experimente. Die Ergebnisse werden in vier Hauptkapiteln präsentiert.

Die ersten beiden Kapitel befassen sich mit hochporösem Portlandzement (OPC) in Kontakt mit Na-Montmorillonit. Die Ergebnisse zeigten eine starke Abnahme der Diffusivität der Proben sowohl für tritiiertes Wasser (HTO) als auch für Chlorid-Tracer bereits innerhalb der ersten 12 Monate nach dem Kontakt (Kapitel 3). Der Chlorid-Diffusionskoeffizient war stark reduziert, was darauf hindeutet, dass die neu gebildeten Phasen in der freien Porosität entstanden sind. Mineralogische und Porositätsuntersuchungen an denselben Proben ermöglichten die Feststellung einer Region mit geringer Porosität auf der Montmorillonit-Seite. Dies hängt hauptsächlich mit der Ausfällung von C-S-H Phasen innerhalb der ersten Millimeter nach dem Kontakt mit dem Zement zusammen (Kapitel 4). Die Zement-Seite zeigte lokale Porositätsvariationen und verschiedene mineralogische Veränderungen in der Nähe der Grenzfläche (z. B., Portlandit-Auflösung, Ausfällung von Friedelschm Salz).

Anschliessend wurden realitätsnähere Proben hergestellt und mittels verschiedener Techniken während einer zweijährigen Interaktion untersucht (Kapitel 5). Die Zement-Seite bestand aus OPC oder Mörtel mit niedrigem pH-Wert (ESDRED), während Bentonit oder OPA die Ton-Seite bildeten. Die Experimente ermöglichten, die Abnahme der Diffusivität der verschiedenen Proben zu quantifizieren und die an der Grenzfläche auftretenden mineralogischen Veränderungen zu charakterisieren.

Im letzten Teil (Kapitel 6) wurden neue Proben (bestehend aus OPC in Kontakt mit verschiedenen Tönen) hergestellt und acht Monate lang bei 70°C reagieren gelassen. Während des Experiments wurden die Porenwasserchemie und der pH-Wert ständig überwacht. Die beobachteten Modifikationen lieferten Informationen über die chemische Entwicklung der verschiedenen Systeme und über die Auswirkungen der erhöhten Temperaturen auf die Entwicklung der Grenzflächen. Es wurde gezeigt, dass hohe Temperaturen die Reaktivität der Proben beschleunigen. Die Ergebnisse sind jedoch mit denen vergleichbar, die bei Raumtemperatur erzielt wurden. Eine Erhöhung der Temperatur ist daher sinnvoll, um die Mindestdauer der Versuche zu verkürzen.

Die Ergebnisse der verschiedenen durchgeführten Experimente haben das Wissen über die Veränderungen, die beim Kontakt von Zement und Ton auftreten, erhöht. Die gewonnenen Informationen können in Modelle und weitere Experimente einfließen und helfen, relevante Prozesse im zukünftigen Endlager zu verstehen.

Résumé

Plusieurs pays envisagent de stocker leurs déchets radioactifs dans des formations géologiques profondes. En Suisse, le dépôt sera constitué de tunnels et de cavernes et se situera à plusieurs centaines de mètres sous terre dans l'argile à Opalinus (OPA). Le béton et les matériaux cimentaires seront utilisés en grande quantité à l'intérieur du dépôt et entreront en contact avec l'OPA et la bentonite (un autre type d'argile qui sera présent dans le dépôt). Il y aura donc plusieurs régions où les argiles et les matériaux cimentaires formeront une interface réactive. Le contact entre le ciment et l'argile se traduit en effet par des flux de masse et des réactions de dissolution-précipitation en raison des fortes différences chimiques entre ces deux matériaux. Il en résulte la formation de fines régions (mm à cm) dont la porosité, la minéralogie et les propriétés de transport sont modifiées. La compréhension du comportement de ces régions altérées est importante pour l'évaluation de la sécurité du dépôt de déchets radioactifs.

Dans cette thèse, différents échantillons de pâte de ciment et d'argile ont été produits et étudiés expérimentalement en laboratoire au moyen de plusieurs techniques analytiques : imagerie neutronique, tomographie à rayons X, SEM/EDX, TGA, XRD et expériences de diffusion. Les résultats sont présentés en quatre chapitres principaux.

Les deux premiers chapitres se concentrent sur une pâte de ciment (OPC, Ordinary Portland Cement) à haute porosité en contact avec une montmorillonite sodique. Les résultats ont mis en évidence une forte diminution de la diffusivité des échantillons pour les traceurs eau tritiée (HTO) et chlorure-36 dès les 12 premiers mois d'interaction (Chapitre 3). La diffusivité du chlorure a été fortement réduite, ce qui suggère que la nouvelle phase formée a précipité dans la porosité libre.

Des études minéralogiques et de porosité sur les mêmes échantillons ont permis de détecter une région à faible porosité du côté de la montmorillonite. Ceci est principalement lié à la précipitation de phases C-S-H dans les premiers mm à partir du contact avec la pâte de ciment (Chapitre 4). Le côté cimentaire a montré une variation locale de la porosité et divers aspects minéralogiques à proximité de l'interface (par exemple, dissolution de la portlandite, précipitation de sels de Friedel). Par la suite, des échantillons d'interface plus réalistes ont été produits et étudiés au moyen de différentes techniques pendant deux années d'interaction (Chapitre 5). La face cimentaire des matériaux d'interface était composée d'un OPC ou d'un mortier ESDERD à faible pH, tandis que la bentonite ou l'OPA constituaient la face argileuse. Les expériences ont permis de quantifier la diminution des propriétés diffusives des différents échantillons et de caractériser l'altération minéralogique se produisant à l'interface. L'altération minéralogique dépendait des matériaux d'interface. Dans la dernière partie (Chapitre 6), de nouveaux échantillons d'interface (composés d'OPC en contact avec différentes argiles) ont été produits et laissés réagir à 70°C pendant huit mois, tandis que la chimie de l'eau dans le réservoir et le pH étaient surveillés. Les expériences ont permis d'obtenir des informations relatives à l'évolution chimique des différents systèmes ainsi que sur l'effet des températures élevées sur l'évolution de l'interface. Il a été démontré que les expériences à haute température accélèrent la réactivité des échantillons, qui est néanmoins comparable à la réactivité à température ambiante.

Les résultats des différentes expériences réalisées ont permis d'améliorer de manière significative les connaissances sur les modifications qui se produisent lorsque le ciment et l'argile entrent en contact. Les informations obtenues peuvent être mises en œuvre dans des modèles, des expériences complémentaires et également aider à comprendre les processus pertinents qui se produisent au sein du dépôt réel.

Acknowledgments

First of all I would like to deeply thank my supervisor PD Dr. Thomas Gimmi for all the support, the discussions and the meetings during these years. I am really thankful Thomas to have had the chance to work with you, and to learn from you. You were always a guide and an example for me.

I also would like to acknowledge Prof. Dr. Sergey Churakov for co-supervising the thesis, for the discussions and for the precious advices he was always ready to give me. My thanks also goes to Dr. Luc Van Loon, who supported me during the lab work and guided through the complex but fascinating world of diffusion experiments.

I acknowledge Dr. Martin Glaus who patiently helped me with mathematical issues and was always ready for an inspiring comment. Thank you to Dr. Jan Tits and Dr. Erich Wieland for answering all the cement related questions. Many thanks to Dr. Georg Kosakowski and Dr. Wilfried Winkler for the help with geochemical issues and questions. I am very grateful to Dr. Michele Griffa who gave me a precious help and advices during the measurements and interpretation of the X-ray tomography data and the review of the articles. Many thanks also to Dr. Frank Winnefeld for the discussions regarding XRD analysis.

I also would like thank the technicians for the support in the lab. Here of course a special thanks to my friend Petar "Sero-Buno" Bunic. You were always ready to help me with experimental and technical issues, and also there for a lunch at "Maestro's".

My thanks surely go to the PhD students who accompanied me during these years, especially Andrea, Latina, Philipp and Leonardo-Gurì. At this point, I also would like to thank all my friends, which were there with and for me during these years: Oschi, Cico, Proni, Fezz, Pif, Gio, Pampa and all those I may have forgotten. Thanks to my friend Masa, for keeping the "Stimmung" always high.

Thanks to "mon capitaine" Elodie, for your infinite kindness, patience, love and for being the quite place which balances my life.

Infinite thanks to my family, for everything, and for making me remember my home, everywhere I go.

Come sempre il mio ultimo pensiero va al mio vecchio amico Pol. Scrivo queste parole guardando un pallido tramonto di fine inverno, e ancora una volta mi ricordi quanto sono fortunato. Ho letto questa poesia qualche tempo fa, penso ti sarebbe piaciuta. O forse no, chi lo sa..

And in to the forest I go

To loose my mind

And find my soul

Table of Contents

Abstract	i
Acknowledgments.....	vi
1. General introduction	1
1.1 The Swiss deep geological repository.....	2
1.1.1 Waste types.....	4
1.2 Evolution of the repository near field.....	5
1.2.1 Evolution of the L/ILW repository conditions.....	5
1.2.2 Evolution of the HLW/SF repository conditions.....	6
1.3 The Opalinus Clay (OPA) as a host rock.....	8
1.4 Current challenges for a repository in Opalinus Clay.....	10
References.....	13
2. Cement-clay interfaces.....	15
2.1 Composition and structure of cementitious materials	16
2.2 Composition and structure of clay minerals	18
2.3 Relevance for a nuclear waste repository	20
2.4 State of knowledge regarding the interface reactivity.....	22
2.4.1 The pH plume.....	22
2.4.2 Dissolution reactions	22
2.4.3 Mineral precipitation.....	23
2.4.4 Porosity alteration	24
2.4.5 Decrease of the diffusivity	25
2.4.6 Modification of the absorbed cation population	25
2.5 Investigation of the interface reactivity	36
2.5.1 Natural and industrial analogues.....	26
2.5.2 Experiments.....	26
2.5.2.1 Laboratory	26
2.5.2.1 In-situ.....	28
2.5.3 Models.....	29
2.6 Uncertainties and open questions regarding the cement-clay system.....	31
2.7 Goal and structure of the thesis	32
References	36
3. Evolution of HTO and ³⁶Cl⁻ diffusion through a reacting cement-clay interface (OPC paste-Na montmorillonite) over a time of six years	40
4. Evolution of mineralogy and porosity at OPC paste Na-montmorillonite interfaces during 6 years of interaction	54

5. Evolution of diffusive and mineralogical properties of cement-clay interfaces: effects of cement and clay type	95
6. OPC paste-clay interaction at 70°C: Eight months monitoring of properties at materials interfaces	125
7. Discussion and conclusions.....	155
7.1 The evolution of the different types of cement-clay interfaces.....	155
7.1.1 Cement-Na montmorillonite and cement-bentonite interactions	155
7.1.2 Cement-OPA interaction.....	157
7.2 Cement-clay interfaces: relevance of the observed results for a repository	158
7.2.1 Porosity decrease at the interface and bentonite re-saturation.....	158
7.2.2 Radionuclide migration	160
7.2.3 Cement-clay interfaces and their role in gas transport processes.....	160
7.2.4 Liner composition: OPC vs ESDRED	161
References	162
8. Outlook	163
Annex.....	I
Annex A: A brief history of nuclear sciences and nuclear energy use.....	I
Annex B: FT-IR ATR	IX
Annex C: pH and porewater compositions.....	XI
Annex D: Cell composition	XIV

Chapter 1

General introduction

1. General introduction

Nuclear disposal of radioactive waste is since decades a topic of interest for most of the countries operating nuclear power plants. Currently, the most accepted solution among the different countries is to store the radioactive waste in deep geological formations, allowing isolating the waste from the biosphere for a long period of time.

In Switzerland the site-selection process took several decades. After years of investigations, where different lithologies were studied, the cooperative responsible for the storage of the radioactive Waste (Nagra), proposed to store the radioactive waste within a sedimentary formation present in North Switzerland: the Opalinus Clay (OPA). A review about the history of nuclear sciences and of radioactive waste disposal, with a special focus on the Swiss situation, is given in Annex A.

The Swiss repository will be located several hundreds of meters below the surface. The tunnels and caverns excavated within OPA will have to be stabilized with large amounts of concrete and cementitious materials. Cement will therefore come in contact with the OPA, leading to the formation of reactive cement-clay interfaces. Bentonite, another clay rich rock, will also be present inside the repository and interact with cementitious materials. Once put in contact cement and clay will be subjected to a series of complex modifications, which are relevant for the safety assessment of the repository.

Cement-clay interfaces and the chemical, mineralogical and physical alterations following the contact of these two materials are the topic of this thesis.

The following chapters serve as introduction to understand the concept of the Swiss repository for radioactive waste (Chapter 1) and the very complex nature of cement and clay, and especially the interaction between these two materials (Chapter 2).

1.1 The Swiss deep geological repository

In September 2022, Nagra announced the intent to submit the general license application for a combined repository of Low- and Intermediate-Level Waste (L/ILW) and High-Level Waste (HLW) in Opalinus Clay. The strong differences between the two waste types lead to very different repository designs and barrier concepts. A schematic representation of a possible repository is given in Fig. 1.

For the HLW/SF, a series of parallel galleries are planned to be excavated, where the canisters containing the spent fuel and the HLW will be accommodated. A certain distance will be present between the tunnels and the canisters, to limit maximum temperatures. The Waste will in fact produce a remarkable temperature plume for the first decades, related to the residual radioactive decay.

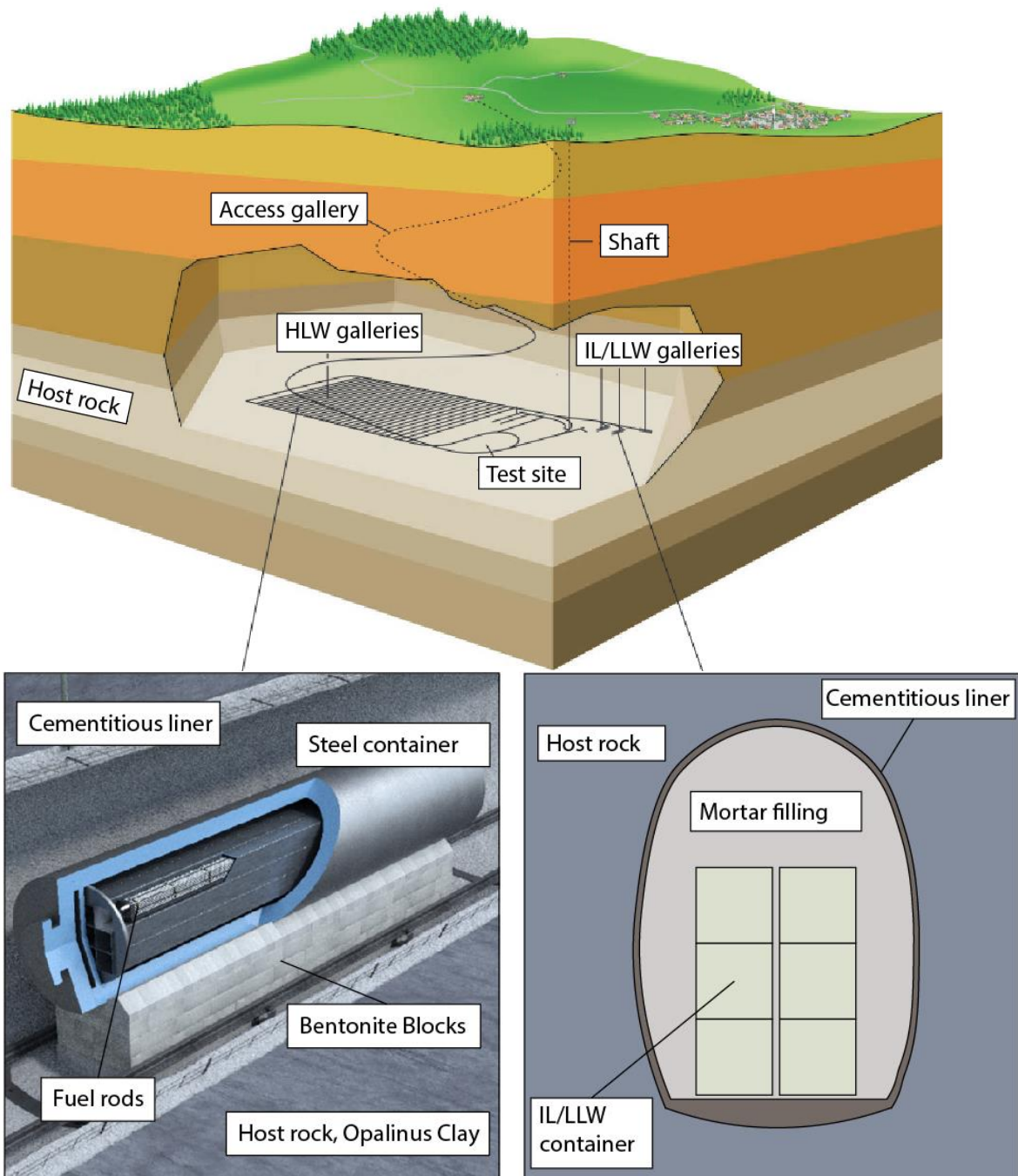


Figure 1 Schematic view of the deep geological repository for SF and L/ILW. Modified after Nagra (2008) and Nagra official website.

Since the HLW and SF will need to be isolated for long periods, an engineered barrier system (EBS) composed of different layers was developed (Fig. 1). The first barrier of the EBS is represented by a ~15 cm thick steel container surrounding the waste (Nagra, 2003). The canister will be put on top of highly compacted bentonite blocks. The tunnel will then be filled with bentonite granulate or blocks (not shown in Fig. 1), which, once saturated, will represent the second barrier. The bentonite will have a double function: i) counterbalance the lithostatic pressure of the host rock, allowing a homogeneous stress distribution, ii) retention of the released radionuclides after canister failure. The third barrier is the surrounding host rock, i.e. the Opalinus Clay in Switzerland.

The L/ILW will be embedded in a cementitious matrix and then put into steel drums. The drums will be placed in concrete containers (Fig. 2) and then stacked into caverns, later filled with mortar/concrete. The technical details about the storage, the different fillings and safety barriers present in the L/ILW repository are extensively discussed in Nagra technical reports (e.g., Nagra, 2016, NTB 14-14).

From 2019 till 2022, Nagra was exploring the underground in three potential siting regions in Northern Switzerland with a series of deep boreholes. These boreholes served to further investigate and confirm the properties of the Opalinus Clay and the surrounding rock formations and to conclude on the most suited siting region. In September 2022, Nagra announced that they will propose the “Nördlich Lägern” region (canton of Zurich) as best suited for the location of an underground repository. The OPA formation in this region has a thickness of more than 100 m; the top of OPA is located between ca. 800 m and 900 m below the (current) surface (Nagra, 2023).

1.1.1 Waste types

Most often, the radioactive wastes are subdivided into Low- and Intermediate-Level radioactive waste (L/ILW) and High-Level radioactive Waste/Spent Fuel (HLW/SF). The first type mostly represents operational waste (e.g., contaminated equipment, cleaning materials, tools..) and waste from decommissioning. A minor part is produced by medicine and industry. Due to their relatively low activity, the L/ILW will reach a natural radiation level in ~100'000 years. The latter represents spent fuel (used fuel rods) from the nuclear reactor and reprocessing products (vitrified activation and fission products). They will reach after 1'000'000 years an acceptable radiation level (comparable with natural uranium ore).

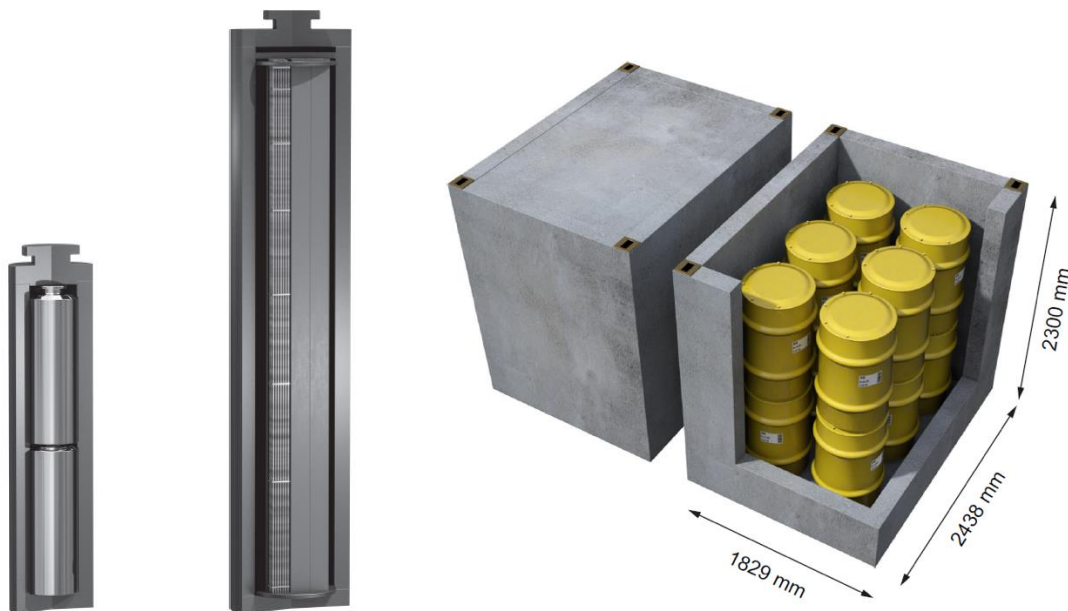


Figure 2 Schematic representation (cross section) of the current design for HLW (left), SF (fuel rods, middle) and low- and intermediate-level waste inserted into metal drums placed into cement containers (right), Nagra (2016, NTB 16-03).

The HLW/SF have a volume of only ~9400 m³ (~10% of the total volume of the waste), but are extremely dangerous. Also, they are characterized by a strong heat production even years after being removed from the reactor (Nagra, official website). Therefore, thermal effects are a major factor when considering the

first period of the underground storage of such HLW/SF waste, even though an intermediate dry storage for several decades is planned. The high temperature gradient around the waste will influence a series of factors that need to be considered for the safety assessment of the repository. For L/ILW, temperature effects are considered as irrelevant since these wastes do not generate significant heat by decay.

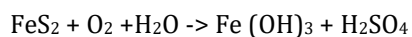
1.2 Evolution of the repository nearfield

The excavation and emplacement of an underground repository is a very complex procedure and there are multitudes of processes that need to be considered (e.g., Fig. 3). Since the major goal of the repository is to obtain the best possible protection of the biosphere from the interaction with radionuclides, the properties of the barrier must be optimal at the time when the remaining radionuclides will be released, i.e., after canister failure. It is therefore crucial to understand the processes occurring in the repository nearfield with respect to any potential changes of properties (geochemical, structural) as a function of time. As the HLW/SF and the L/ILW repositories have different designs, i.e., different storage concepts and a different barrier system, they will experience different geochemical evolutions. Three main phases are generally distinguished for both repository types (e.g., Nagra, 2022):

- i) An operational phase, during which the repository is constructed and operated.
- ii) A transient hydraulic state after the repository closure, during which the partially dried materials (bentonite, Opalinus Clay) will re-saturate.
- iii) A steady hydraulic state after closure, once the clays are fully re-saturated.

1.2.1 Evolution of the L/ILW repository conditions

The repository construction will lead to drying of the OPA (water evaporation) and oxidation processes. For example, the oxidation of pyrite present inside OPA, will lead to an increase in the sulphate concentration inside the porewater, according to



After repository closure, reducing anoxic conditions will be restored. The first (operational) phase is planned to last for 100 years. The transient hydraulic state will instead endure for a very long period. After closure, the re-saturation process will be influenced by the produced gases. According to Nagra (2016, NTB 16-07) the saturation degree of the cavern will not be 100% even after 100'000 years. Heat production in the L/ILW repository will be mainly related to cement hydration (Nagra, 2016, NTB 14-14) and will not have a relevant effect on the repository conditions. Gases will be generated by the anoxic corrosion of metals, from the degradation of organic matter and from radiolysis (Nagra, 2022). The highly porous mortar filling present in the cavern will saturate relatively slowly. Depending on the gas pressure developed in the cavern, the duration of the phase with partial saturation could vary (Nagra, 2022). The gas pressure present in the cavern is dependent on several factors such as the rate of gas generation, the local OPA gas permeability, and the type of the cementitious sealing (e.g., with different transport

properties). The gas permeability of the cement-clay interface present at the contact with OPA will also play a role regarding the gas pressure build-up and ultimately the saturation process.

1.2.2 Evolution of the HLW/SF repository conditions

The three phases of HLW/SF repository evolution described in 1.2 are related each to a major process (Nagra, 2016, NTB 14-13):

- i) heat generation from the canisters
- ii) near-field re-saturation
- iii) hydrogen production

The excavation of an underground tunnel creates an excavation disturbed zone (EDZ) around the galleries, where fracture formation (depending on the local stress field) and drying effects alter the hydro-mechanical and geochemical properties of the host rock. Thanks to the self-sealing properties of OPA, the fractures will very likely close again within some years to decades and the low diffusive properties will be restored (Nagra, 2002b).

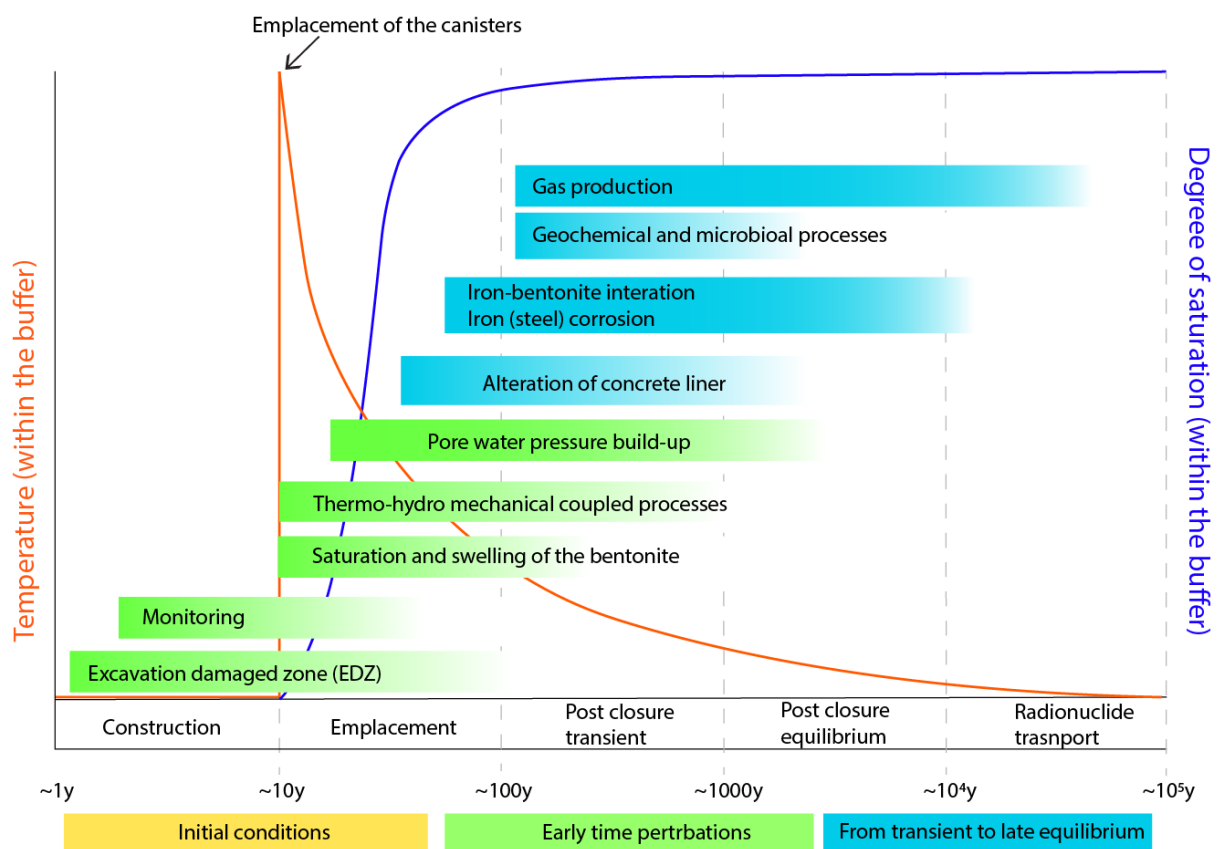


Figure 3 Schematic representation of the evolution of the repository (modified after Bossart et al., 2017). The initial conditions (yellow) represent the conditions before the emplacement of the repository. The early perturbations (green) occur within the first 1000 years. Blue regions represent the period from the transient to late equilibrium (post closure-equilibrium).

The general conditions caused by the tunnel excavation will be the same as those discussed in chapter 1.2.1: desaturation of OPA and oxidation reactions. After repository closure the consumption of the oxygen by different reactions (steel corrosion, buffering capacity of Opalinus Clay) will restore the anoxic conditions.

A concrete liner (shotcrete or pre-fabricated blocks, tubings) will be applied to stabilize the tunnel walls, creating an interface between concrete and Opalinus Clay. Cement and clay will start to interact and the mineralogical and diffusive properties of the interface region between the concrete liner and the Opalinus Clay host rock will probably change.

Once the repository construction will be finalized, the waste containers will be gradually emplaced in the galleries on the bentonite blocks, as showed in Fig. 1. The waste surroundings will be filled with bentonite granulate and the gallery sealed with concrete. Depending on the amount of waste inserted into a canister, the temperature developing at the interface of the canister will vary. For a thermal loading of 1500 W per canister, the temperature at the surface will reach up to $\sim 150-160^{\circ}\text{C}$ (Nagra, 2003), leading to a significant temperature gradient in the bentonite buffer and the Opalinus Clay. This thermal effect will be present at least for the first 100 y after emplacement of the spent fuel. The effective duration and intensity of the thermal output will anyways depend on the (definitive) thermal load pro canister that will be decided to be necessary / optimal. Mazurek et al. (2006) estimated the maximal temperature experienced by Opalinus Clay during burial to be $\sim 80^{\circ}\text{C}$; up to this temperature, the rock will therefore maintain its properties. An excessive thermal output by the waste would lead to mineralogical modifications within the clay and likely alter the mechanical and hydraulic properties. The spatial range of the temperature increase will also depend on the saturation state of the surrounding materials.

The bentonite granulate inserted around the HLW disposal casks will be initially practically dry. The saturation process will occur by Opalinus Clay porewater moving through the concrete liner towards bentonite. Some decades after the emplacement, the temperature will sufficiently decrease to allow the bentonite buffer (at least in the external part) to become close to complete saturation and reaching a porewater pressure around the canisters similar to that in the surrounding saturated Opalinus Clay (Nagra, 2016, NTB 14-13). Also in this case, the definitive thermal load that will be present will affect the re-saturation period, which may even last centuries in case of high initial temperatures of the canisters.

In presence of water, the corrosion of HLW canister will start. During the first decades, the corrosive process will occur in presence of oxygen. Once all the oxygen has been consumed, anoxic corrosion will dominate. The corrosion process has two important consequences. First, the corrosion leads to inevitable failure of the canister. The models predict the steel canister to maintain its integrity for a minimum of 10'000 years after the emplacement and backfilling of the canister in disposal galleries (Nagra, 2003). From then on, the waste matrix will be in direct contact with pore water allowing the leaching and release of the radionuclides. The second important aspect of the anoxic corrosion of steel is the production of hydrogen. Calculations predict that, depending on the corrosion rate, large hydrogen amounts will be produced in the proximity of the disposal casks. It was demonstrated that the dissipation rate by diffusive or advective processes might be not large enough to keep the gas concentration in the liquid phase below the solubility limits. The newly formed gases will then accumulate in partially saturated regions (Nagra, 2016, NTB 16-03). The expected peak pressure depends on the ratio between the gas generation rate and the rate of transport and possible involvement of gas into other chemical reactions. Simulations indicate that the pressure will not reach levels where it could lead to the generation of fractures (Nagra, 2016, NTB 16-03), however this depends on gas generation rate. Gas generation is of course also affecting (delaying) the saturation of the buffer material; this fact also needs to be considered.

The nearfield around HLW/SF, especially the bentonite, will thus be subjected to a very complex superposition of different phenomena (heat, saturation, gas production and transport).

In this context, the behavior of interfaces between cement and clay plays a major role. Transport of gas and of radionuclides, but also the re-saturation of the bentonite buffer will be affected by any changes of porosity and the diffusive properties following mineral reactions at the interface (cf. 2).

1.3 The Opalinus Clay (OPA) as a host rock

Opalinus Clay is a sedimentary rock formed around 174 Ma ago in shallow sea water conditions (Hostettler et al., 2017), where fine-grained particles could settle on the relatively calm seafloor. The name originates from the multitude of fossils of the ammonite “Leioceras Opalinum” observable in this formation. After its deposition, these sediments underwent compaction and diagenesis at the maximum temperature of ~80°C (Mazurek et al., 2006) to become the Opalinus Clay formation as we know it today. In the current region of interest (northern Switzerland) the top of OPA is located between about 800 m and 900 m of depth (Nagra, 2023), and it has a thickness of about 100-110 m. Depending on the site and the position within the formation, the mineralogical composition of the Opalinus Clay can vary (Bossart, 2017). The most interesting facies is the shaly one; composed of clay minerals (illite, kaolinite, chlorite and illite-smectite mixed-layer minerals) and non-clay minerals such as pyrite, quartz and carbonates.

The first investigations on OPA were performed towards the end of the 80s in the canton Jura in the safety gallery of a highway tunnel excavated inside an anticlinal fold of Opalinus Clay (Schaeren and Norbert, 1989; Tripet et al., 1990). This was very convenient since it allowed to easily access a rock that is generally located several hundreds of meters below ground. The first observations which were made allowed to recognize several promising properties of the shaly OPA formation. In 1996, the positive results of the performed experiments led to the opening of the Mont Terri Rock Laboratory. The many experiments performed or still running in this rock laboratory contribute significantly to the understanding of the properties of the Opalinus Clay (Bossart and Thury, 2008; Bossard, 2017).

Thanks to the high amount of clay minerals present, Opalinus Clay has a series of properties which make it a very promising formation to host a repository for radioactive waste, as outlined in the following.

Low permeability and diffusivity

As a result of the very small pore sizes of OPA, the dominant transport regime is diffusion (Bourg and Tournassat, 2015). For the transport mechanism, the porosity, the pore size distribution and the pore connectivity are important. In fact, two rocks with the same porosity can have different diffusivities, depending on the pores sizes shapes and distribution. Since OPA is mainly composed by clay minerals, which generally have a platelet shape, the sedimentation of the rock lead to a preferred orientation of the minerals, which tend to be oriented parallel to the bedding. The diffusivity through OPA perpendicular to the bedding is therefore four to five times lower than parallel to the bedding (Bossart, 2017).

The slow leaching of the waste matrix after canister failure will lead to radionuclide release into the porewater. Part of the radionuclides (mainly cationic species) will sorb on clay and will diffuse slowly

through OPA, while non-sorbing radionuclides (mainly neutral and anionic species) will diffuse faster because of no retardation.

Self-sealing properties

Opalinus Clay contains illite and illite-smectite mixed layer minerals; that latter when in contact with water have the tendency to swell (Mitchell and Soga, 2005). Water molecules are taken up into the interlayer leading to an increase of the interlayer distance, i.e., to expansion (depending on the confining pressure). Montmorillonite represents the smectite with the strongest swelling capacity; the volume increase can reach up to 60% the initial value (Carlson, 2004) under free swelling conditions. Depending on the water activity, distinct hydration forms of montmorillonite corresponding to 1 to 3 water layers are stable.

Thanks to the swelling properties of smectites in presence of water, fractures which may open in Opalinus Clay will tend to close again due to the increase of the volume of the hydrated clay minerals surrounding the fracture. This property is of extreme relevance with regard to a repository, since it allows sealing fractures that may form upon excavation or due to natural reasons (Nagra, 2002b). An example is represented by the Excavation Disturbed Zone (EDZ); which will re-seal within a relatively short time (compared to the repository lifetime) guaranteeing optimal isolating properties (Bossart and Thury, 2008). Clays can have different ionic forms, depending on the cations present in the surroundings (e.g., Ca or Na). Whether predominantly of Ca- or a Na-clay is present can have strong effect on the swelling pressure and on solute diffusion. Variation of the swelling pressure related to the exchange of cations is of great relevance when clay and cement interact (Segad et al., 2010). This topic is extensively discussed in chapter 3 and 4.

High Cation Exchange Capacity (CEC)

CEC is the ability of minerals (or materials) to reversibly bind cations on their negatively charged surfaces. Negative surface charges of clays are the result of isomorphic substitution of cations within the clay structure. The surface charges lead to a strong potential to bind positively charged ions. Depending on the clay, different types and degrees of substitution inside the structure lead to a permanent structural charge of clay particles, which controls the cation exchange. Besides the negatively charged surface, clays are also characterized by a very high specific surface area. The high CEC is extremely interesting in the field of radioactive waste disposal since many radionuclides present in the waste are positively charged (Nagra, 2017) and can adsorb on the surface. Transport of these radionuclides is therefore retarded, providing more time for the radionuclide to decay and thus for lowering the dose that may reach the biosphere.

Porosity

The rock porosity is defined as volume of pores per total volume of sample; it can be derived for instance from densities according to

$$\varepsilon = 1 - \frac{\rho_b}{\rho_g}$$

where ρ_b represents the bulk dry density and ρ_g the grain density. Clay rocks do not have a particularly low porosity, but are characterized by a small pore size. This leads to very low permeability and diffusivity as discussed before.

The negative charge present on the surface of clay minerals affects also the porewater near surfaces. Accordingly, different porosity domains can be distinguished conceptually: i) free porosity, defined as that fraction of porosity unaffected by the charged surfaces and where the pore solution is neutral (accessible to all ions). ii) Interlayer porosity, defined as the narrow region between the negatively charged smectite layers; it contains (almost) exclusively cations in compacted clay rocks. iii) The diffuse layer (DL) porosity, defined as the nearfield of the clays external surface; it contains an excess of cations (and is depleted in anions compared to the free water porewater). Depending on the density and the clay structure, the different porosity domains represent a different amount of the total porosity. This fact is relevant especially regarding diffusive processes of charged species. Water can diffuse through the entire porosity domain; its diffusivity is therefore directly dependent on the available (connected) porosity. If a negatively charged species diffuses through a clay, depending on the compaction a different fraction of the porosity will be accessible. The compaction in fact reduces first the free porosity; with increasing compaction, to a certain degree also the interlayer distance can be reduced (Van Loon et al., 2007). Diffusion coefficients for differently charged species therefore vary for different clays, and they are for instance influenced by the degree of compaction.

Generally, the different porosity types in clays play a distinct role in the mechanism of cement-clay interaction. Their distribution may be decisive for the understanding of clogging phenomena occurring at the interface.

1.4 Current challenges for a repository in Opalinus Clay

Three decades of experiments and modeling demonstrated that Opalinus Clay has the required properties, among which the potential to successfully retard radionuclide transport for the necessary time.

To safely store radioactive waste over periods of hundreds of thousands of years there are many factors that need to be considered, and a multitude of inter-playing processes that need to be understood. The behavior of cement-clay interfaces, which is the topic of this thesis, is in this sense just a minor component of the whole system. In the following, some other still challenging problems are listed (personal choice of the author). The goal is to give an idea about the complexity and the variety of challenges that need to be considered for the storage of radioactive waste.

- *Repository construction and waste emplacement*

The transport and the emplacement of the waste is surely one of the major challenges: the high activity of the SF and HLW will not allow human beings to be in proximity of the containers, therefore all the processes will have to be automatized and conducted with robotics. In the Full Emplacement experiment (FE) at the Mont Terri Rock Laboratory the evolution of the HLW nearfield represented by three full-size cylindrical heaters is investigated. The heaters are placed onto a basement made of highly compacted bentonite blocks; subsequently, using a specially

developed machine, the bentonite granulate was inserted around the heater. The machine to transport the SF/HLW canisters and the method to correctly transport, fill and close the repository still need to be developed.

- *Gas transport*

High amounts of gases will be produced inside the repository, especially in the case of SF/HLW. Gas will be generated by different processes such as metal corrosion, radiolysis of water and microbiological activity. However, the anoxic corrosion of steel and other metal alloys is by far the most relevant gas source. The production, consumption and transport of gases inside the repository is a very complex topic, as extensively described in Nagra (2016, NTB 16-03).

Hydrogen produced by corrosion of steel and alloys will be the dominant gas in the repository for SF/HLW. The gas will have to migrate through the host rock without compromising the rocks integrity, to avoid later enhanced solute transport. Although the amount and types of gases that will be produced are known, there is still uncertainty regarding the gas transport, especially its transport through cement-clay interfaces. Concerning this topic, especially the understanding of the reactivity and long-term evolution of such interfaces is of main interest.

- *The behavior of the bentonite buffer*

Still not completely constrained are the re-saturation times of the bentonite, which will be located around the SF/HLW. This will play an important role primarily for heat dissipation in the beginning of the storage, and for radionuclide and gas transport in a later phase. Also, in this case there is a complex interplay of different factors and the prediction of the re-saturation process is not straightforward. As explained in the chapter 1.2.2, the porewater necessary to saturate the bentonite originates from the OPA host rock. Due to the barrier design, there will be in, the case of SF/HLW, a system composed of OPA-concrete-bentonite. On the other side there will be a hot canister which slows down the saturation as well as contributes to chemical (Fe release) and thermal alteration of bentonite (at least in the canister proximity). The hydraulic properties at the interface between cement and bentonite and the chemical composition of the porewater originating from the interface will play a key role regarding the bentonite re-saturation process.

- *Partial saturation and diffusive processes within bentonite*

During the phase of construction and emplacement some parts of the repository will be (partially) desaturated. The clay and concrete material will be in contact with air and will therefore desaturate. After the repository closure, water will migrate towards the desaturated part of the repository and resaturation will slowly restart. Depending on the repository typology mainly two processes will compete with the resaturation:

- i) Gas production from anoxic steel corrosion, radiolysis and microbial activity
- ii) Heat release leading to temperature increase (relevant only for the SF/HLW repository)

For both clay and cement, the macropores will lose their water first. The smaller the pores, the more strongly the water is kept by capillary and surface forces. The water present in the interlayer is too tightly bound and will not be affected by drying processes related to humidity variations within the tunnels. The rate of the drying process will depend on the relative humidity. Below a certain level of relative humidity the water phase will be less connected, leading to a decrease of solute diffusivity. The interlayers will always allow a certain diffusive flux to be present. This fact affects transport in different ways. Cations can diffuse through the interlayer; whereas anions, due to their negative charge, cannot. This means that a low saturation states the diffusive transport of negatively charged species will be more strongly hindered. To be noted that recent studies of Savoye et al. (2017) show that diffusion of positively charged species (sodium and cesium) is also reduced at lower saturation.

- *Glacial erosion*

It is known that not more than 24'000 years ago the entire Alpine region, and among it Switzerland, was covered with more than one km of ice, depending on the locations (Palacios et al., 2021). Most of the current Swiss lakes are the result of glacial phenomena. How deep the future glaciers will erode the surface is a question which is currently not completely answered (Nagra, 2021). Generally, the glacier incisions found in Northern Switzerland are about 200 m deep. Not clear is the development of very narrow and deeper incisions that can form due to highly pressurized subglacial meltwater (Nagra, 2010). Another relevant factor discussed in Nagra (2010) is the formation of subglacial permafrost, which may affect the underground properties.

- *Information transfer to future generation*

After repository closure the repository nearfield and host rocks will have to remain undisturbed not only by natural processes such as glaciers and tectonics but also by human activity. It is therefore crucial that future generations will be informed about the repository location. Although this may at first sight seem an irrelevant problem, the information flux needs to be guaranteed for a time period of 100'000-1'000'000 of years.

References

- Bourg, I.C., Tournassat, C., 2015. Self-diffusion of water and ions in clay barriers. *Develop. in Clay Sci.* 6, 189–226.
- Bossart, P., Thury, M. 2008. Mont Terri Rock Laboratory. Project, Programme 1996–2007 and results. Reports of the Swiss Geological Survey, No. 3, p. 445. Federal Office of Topography (swisstopo), Wabern, Switzerland.
- Bossart, P., 2017. Twenty years of research at the Mont Terri rock laboratory: what we have learnt. *Swiss J. Geosci.* 110, 405–411.
- Carlson, L., 2004. Bentonite mineralogy. Posiva working report, 2004–02, Posiva OY, Olkiluoto, Finland.
- Hostettler, B., Reisdorf, A.G., Jaeggi, D., Deplazes, G., Blaes, H.R., Morard, A., Menkveld-Gfeller, U., 2017. Litho- and biostratigraphy of the Opalinus Clay and bounding formations in the Mont Terri rock laboratory. *Swiss J. Geosci.* 110, 23–37.
- Mazurek, M., Hurford, A. J., Leu, W., 2006. Unravelling the multi-stage burial history of the Swiss Molasse Basin: Integration of apatite fission track, vitrinite reflectance and biomarker isomerisation analysis. *Basin Res.* 18, 27–50.
- Mitchell, J.K., Soga, K., 2005. *Fundamentals of Soil Behavior*. 3rd Edition, John Wiley & Sons, Hoboken.
- Nagra, 2002b. Projekt Opalinuston – Synthese der geowissenschaftlichen Untersuchungsergebnisse. Entsorgungsnachweis für abgebrannte Brennelemente, verglaste hochaktive sowie langlebige mittelaktive Abfälle. Nagra Tech. Rep. NTB 02–03.
- Nagra, 2003. Canister Options for the Disposal of Spent Fuel. Nagra Tech. Rep. NTB 02-11.
- Nagra, 2010. Glaciological conditions in northern Switzerland during recent Ice Ages. Nagra Arbeitsber. NAB 10-18.
- Nagra, 2014b. SGT Etappe 2: Vorschlag weiter zu untersuchender geologischer Standortgebiete mit zugehörigen Standortarealen für die Oberflächenanlage. Geologische Grundlagen. Nagra Tech. Rep. NTB 14-02.
- Nagra, 2016. High-level waste repository-induced effects. Nagra Tech. Rep. NTB 14-13.
- Nagra, 2016. Low- and intermediate-level waste repository-induced effects. Nagra Tech. Rep. NTB 14-14.
- Nagra, 2016. Production, consumption and transport of gases in deep geological repository according to the swiss disposal concept. Nagra Tech. Rep. NTB 16–03.
- Nagra, 2016. Sensitivity analyses of gas release from a L/ILW repository in the Opalinus Clay including the microbial consumption of hydrogen. Nagra Arbeitsber. NAB 16–07.
- Nagra, 2017. Chemistry of selected dose-relevant radionuclides. Nagra Tech. Rep. NTB 17–05.
- Nagra, 2021. The Nagra Research, Development and Demonstration (R&D) Plan for the Disposal of Radioactive Waste in Switzerland. Nagra Tech. Rep. NTB 21–02.
- Nagra, 2022. Cement - Clay. Synthesis of transport across the Cement-Clay interface. Nagra Arbeitsber. NAB 22–34.
- Nagra, 2023. Reference porewaters for SGT Stage 3 of the Opalinus Clay for the siting regions Jura Ost (JO), Nördlich Lägern (NL) and Zürich Nordost (ZNO). Nagra Arbeitsber. NAB 22–47.

- Palacios, D., Hughes, P. D., García-Ruiz, J.M., de Andrés, N., 2021. European Glacial Landscapes. Maximum Extent of Glaciations. 1st Edition, Elsevier.
- Savoie, S., Lefevre, S., Fayette, A., Robinet, J-C., 2017. Effect of water saturation on the diffusion/adsorption of ²²Na and cesium onto the Callovo-Oxfordian Claystones. Geof. 1683979.
- Schaeren, G., Norbert, J. 1989. Tunnels du Mont Terri et du Mont Russelin — La traversée des “roches à risques”: Marnes et marnes à anhydrite. Juradurchquerungen aktuelle Tunnelprojekte im Jura Mitteilungen der Schweizerischen Gesellschaft für Boden- und Felsmechanik 119, 19–24.
- Segad, M., Jönsson, B., Akesson, T., Cabane, B., 2010. Ca/Na Montmorillonite: Structure, Forces and Swelling Properties. Langmuir 26, 5782–5790.
- Tripet, J. P., Brechbühler, Y. A., Haarpaintner, R. T., Schindler, B., 1990. Hydrogéologie des milieux à faible perméabilité: Étude des Marnes aaléniennes dans la galerie de reconnaissance du Mont Terri (Canton du Jura). Bulletin de la Société Neuchâteloise des Sciences Naturelles 113, 179–189.
- Van Loon, L.R., Glaus, M.A., Müller, W., 2007. Anion exclusion effects in compacted bentonites: towards a better understanding of anion diffusion. Appl. Geochem. 22, 2536–2552.

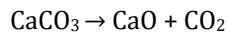
Chapter 2

Cement-clay interfaces

2. Cement-clay interfaces

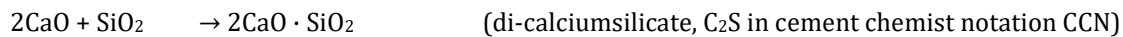
2.1 Composition and structure of cementitious materials

Cement is a binder widely used in the construction industry, mostly mixed with aggregates of different nature and water to form concrete. Cement is generally produced by burning limestone and marls at high temperatures (>1400°C). The removal of CO₂ from the calcareous rocks leads to the formation of the so-called lime (CaO), according to reaction:



This reaction is known as calcination reaction.

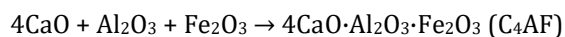
The lime further reacts with silicate forming di- and tri-calcium silicate (belite and alite), according to the reactions:



Some of the lime can also react with alumina (aluminum oxide), leading to the formation of calcium aluminate:



When lime reacts together with alumina and iron oxide, ferrite is formed:



Those four mineral phases (called 'clinkers') are the main components of unhydrated cement and are in disequilibrium with the surrounding environment.

When the clinkers are brought in contact with water the various components start to react (cement hydration). The main products are represented by C-S-H phases (Calcium-Silicate-Hydrate), portlandite, Alumina-Ferric-trisulphate (AFt), Alumina-Ferric-monosulphate (AFm) and carbonates. Depending on a series of parameters (e.g., cement composition, reaction time or environmental conditions) different hydration products (solids) form which are in equilibrium with the surrounding solution (liquid). The composition of the solid and the liquid changes during hydration in a meta-stable system, which reaches a (quite) stable equilibrium after 28 days; this represents the end of the main hydration phase.

The most common cement type is Portland cement (PC), often mixed with small amounts of gypsum, (CaSO₄ · H₂O, added to retard the hardening process), and called Ordinary Portland Cement (OPC).

Modifying the Portland cement by adding different materials gives rise to a multitude of different cement formulations and a wide spectrum of different properties (hydraulic, mechanical, chemical) which can be tailored depending on specific needs.

The PC recipe is often modified with materials of analogous chemistry, such as i) slag rests of steel production (blast furnace slag), ii) remainings of the burning of coal in powerplants (fly ashes), or iii) silica-rich spherical particles obtained as by product of steel alloy production (silica fume).

There are five main types of cements designed to meet different needs of the industries:

CEM I, Ordinary Portland Cement (OPC)

CEM II, mixture of OPC with a maximum of 35% of additives (e.g., fly ashes, blast furnace slag)

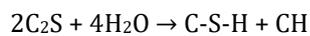
CEM III, OPC mixed with blast furnace slag (between 35% and 95%)

CEM IV, produced by mixing Portland cement clinkers with gypsum and pozzolan, a volcanic ash of silicious amorphous composition, which reacts in the presence of calcium hydroxide (the so-called “pozzolanic reaction”)

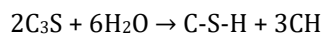
CEM V, sulfate resistant cement, characterized by low amount of C3A. In the presence of sulphate, C3A reacts forming certain minerals (e.g., ettringite) and leading to volume increase and subsequent lowering of the mechanical properties. The main cement phases are:

Calcium silicate hydrate [C-S-H]

C-S-H represent the main phase in most hydrated cement paste and are responsible for the strength of the binder. C-S-H phases form upon hydration of belite



and alite



where CH represents portlandite, $Ca(OH)_2$.

C-S-H are composed of ring silicates, i.e. of SiO_4^- tetrahedra linked at the edges in a circular sheet-like structure, and by CaO sheets. Two silicate sheets and a calcium oxide sheet form a layer. An interlayer space is present between the layers, generally occupied by calcium cations. In presence of other cations (e.g., aluminum or sodium) a partial substitution can occur leading to modified structures (e.g., C-A-S-H). At room temperature C-S-H do not crystallize well and are therefore generally amorphous. Depending on the surrounding condition, the Ca/Si ratio inside the structure can vary, affecting the mechanical properties.

C-S-H phases start to destabilize at pH below 10-10.5, or if the calcium concentration in the surrounding porewater is decreasing.

Portlandite [Ca(OH)₂]

Portlandite is formed from alite and from belite hydration. Similar as C-S-H, portlandite represent one of the major hydration products of Portland cement. It has a layered structure composed of calcium octahedra stacked on each other. If the formation conditions are ideal portlandite forms hexagonal crystals. Although the high amount of portlandite present in Portland cement, it is not particularly relevant for the mechanical properties of the hydrated cement. The presence of portlandite is more important regarding the alkalinity of the porewater, which protects the steel bars of reinforced concrete from corrosion. Portlandite is particularly sensitive to pH conditions and quickly dissolves at pH lower than 12.5.

Af_t, Alumina Ferric trisulfate [3CaO · (Al,Fe)O₃ · [CaSO₄]_{1,3} · nH₂O]

The most common Af_t phase is ettringite, which represents a main phase of cement hydration. Ettringite rapidly forms upon clinker hydrations and plays therefore an important role in the control of the hydration reaction. The crystal structure is composed of columns oriented parallel to the c-axis and that host water and sulphate ions. Ettringite formation is typically observed during “sulphate-attack” of concrete: when

sulphate diffuses into the concrete, secondary ettringite can precipitate leading to expansion and deterioration of the mechanical properties. Sulphate concentration, pH and temperature can quickly affect ettringite stability.

AFm, Alumina-ferric-monosulphate $[Ca_2(Al,Fe)(OH)_6] \cdot X \cdot yH_2O$

AFm phases are a family of hydrated calcium aluminate with a chemical composition similar to hydrocalumite. In cementitious systems, AFm mostly forms when C₃A reacts with dissolved calcium sulfate. According to Taylor (1997) the general structure is composed of $[Ca_2(Al,Fe)(OH)_6]$ octahedrally coordinated and positively charged main layers with a negatively charged interlayer containing anions (X) and water molecules. In the cement system the anion X is generally CO₃²⁻, OH⁻ or SO₄²⁻. In the presence of salt (NaCl) also Cl⁻ can be found in the structure.

Other Hydrated phases

Brucite Mg(OH)₂ has the same structure as portlandite [Ca(OH)₂]. It generally forms in concrete under the presence of magnesium (e.g., magnesium sulfate attack). In concrete rich in dolomite CaMg(CO₃)₂ aggregates, the formation of brucite may lead to internal pressure and shortening of the service life (e.g., Lee et al., 2002).

Hydrogarnet represents a minor hydration phase in cement. It has a cubic structure and the composition can be very variable depending on the surrounding conditions. The structure is similar to that of brucite, where Al³⁺ or Fe³⁺ replaces some of the Mg²⁺ inside the structure. The negative charge formed is then compensated by cations located in the interlayer (together with water).

Carbonates

The most common carbonate mineral present in concrete is calcite. It mostly forms during the carbonation process by the interaction of dissolved CO₂ and calcium present in the pore solutions. Depending on the chemical composition of the cementitious porewater and on the environmental conditions other carbonate phases can be found (Gaucher and Blanc., 2006; Dung et al., 2019).

2.2 Composition and structure of clay minerals

Clay minerals represent an abundant and very wide group of hydrous aluminum phyllosilicates. They naturally occur mainly as weathering product of other rocks (but also during hydrothermal alteration), and are therefore one of the principal constituents of sedimentary rocks. Thanks to their properties, they find use in a wide variety of fields: industry, agriculture, technology, and environment. There is a multitude of possible chemical compositions, and the classification of clays itself is not straightforward. There are several minerals in fact with clay-like structure, or that are classified as clay although the structure does not match completely to the clay (classical) structure.

The clay structure is based on silica tetrahedra (T) organized into sheets connected with alumina octahedra (O), Fig. 4. Depending on the clay type, the basic structure can be composed of layers formed by one tetrahedral and one octahedral sheet, the so called 1:1 (TO) structure. In the other case, one octahedral

sheet is sandwiched between two tetrahedral sheets, leading to the formation of a layer of 2:1 clays (TOT). The Si^{4+} present inside the tetrahedra can be partially substituted by Al^{3+} giving the clays their negative surface charge. Such isomorphic substitution can also occur in the octahedra (e.g., when Al^{3+} is exchanged by Mg^{2+} or Fe^{2+}).

The clay layers are organized into stacks, divided by the so-called interlayer space. This space is occupied by cations, which counterbalance the clay negative charge, and possibly by water. For some clays, variable amounts of water can enter the interlayer space, resulting in clay swelling (increase of the layer distance of the sheets). Different clays have different swelling properties.

Depending on the occupancy of the octahedrally coordinated sites, clays are defined as i) dioctahedral, if 2 out of 3 sites are occupied by trivalent cations (e.g., Fe^{3+} or Al^{3+}), ii) trioctahedral, if all 3 sites are occupied by divalent cations such as Fe^{2+} or Mg^{2+} . Due to the very wide variety of chemical compositions possible there is a large variety of clay minerals, often present in nature as interstratification of different clays. The most common clays are subdivided into groups and are discussed in the following paragraphs. As mentioned previously, due to the variable structure some minerals are sometimes classified as clay, although they can also be considered as belonging to other categories (e.g., chlorite).

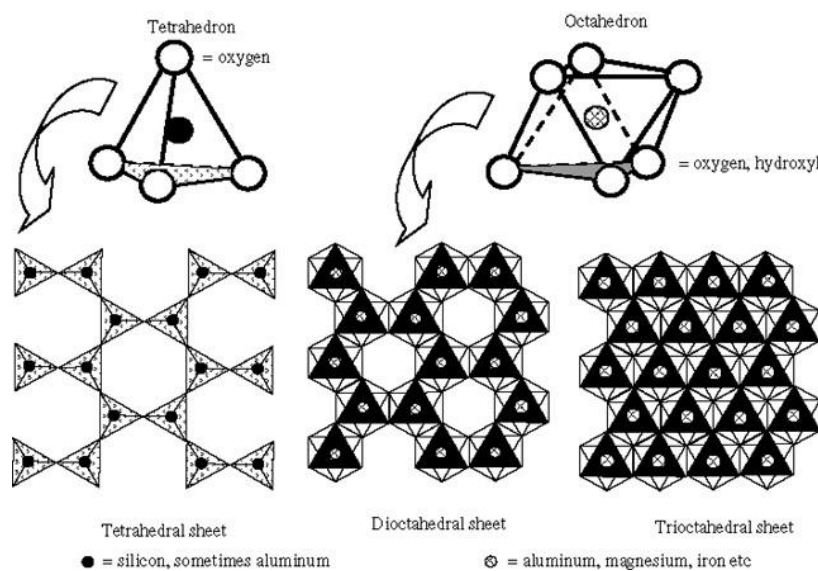


Figure 4 Illustration of the clay basic structure (Hillier, 1978).

The kaolin group show a 1:1 structure (Fig. 5) and has the following general formula: $\text{Al}_2\text{Si}_2\text{O}_5(\text{OH})_4$. The main members of this group are i) kaolinite, which has a triclinic crystal structure and is characterized by relatively low substitution in its structure, and has therefore no (or only weak) permanent charge, ii) hallosite (monoclinic) with the same formula but, when hydrated, can host water molecules (and cations) between the TO layers. When weathering leads to the removal of the silica group, kaolin group members become Gibbsite [$\text{Al}(\text{OH})_3$].

The smectite group comprises 2:1 minerals (Fig. 5), with a wide range of compositions. The most common minerals are montmorillonite, nontronite and beidellite. These three minerals have a similar TOT structure but differ with respect to the occupation of the tetrahedral and octahedral sites. Smectites are furthermore characterized by high swelling properties in presence of water. Inside the interlayer, different cations (e.g.,

Na⁺, Ca²⁺, Mg²⁺, ...) can be present depending on the pore water chemistry in the rocks. Montmorillonite is characterized by isomorphous substitution of Mg for Al in the octahedral sheet, whereas inside beidellite, Al substitutes Si in the tetrahedral sheet. Nontronite represents an iron rich smectite, where Al substitutes for the silica in the tetrahedral positions. Most of the layer charge is therefore located on the tetrahedral side; this charge is then counterbalanced by alkali and earth alkali ions.

Illite is a group of 2:1 clays with variable formulas and characterized by the presence of potassium between the TOT layers. As K dehydrates easily and fits nicely into the hexagonal cavities, this mineral group does not swell in presence of water (Fig. 5). Illite is often formed from diagenetic modification of smectites; typical are interstratifications of illite and smectite. In the field of waste disposal, illitization is a topic of interest since it can affect the swelling properties of the barriers around the waste.

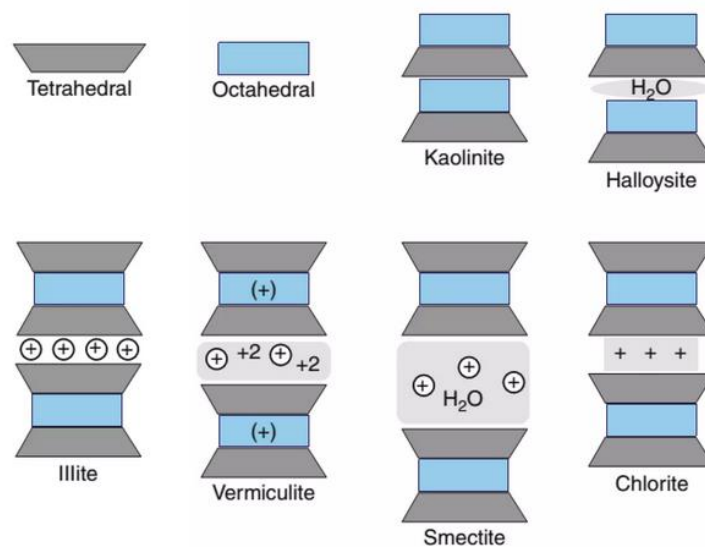


Figure 5 Illustration of different clays and layer types (Négronk-Mendoza, 2015)

Chlorite represents a special category since it is not always considered as a clay mineral due to its special structure. It is a group of 2:1 minerals rich in magnesium and iron. Minerals belonging to this group are characterized by not having single cations in the interlayer but a unit of $(Mg^{2+}, Fe^{2+}, Fe^{3+})OH_6$, a brucite-like layer. Chlorite is commonly found in low-grade metamorphic rocks (green schist facies) and as a product of hydrothermal alteration. It is also typically found in small amounts in sedimentary rocks.

2.3 Relevance for a nuclear waste repository

Cement and clay represent two systems that are well known and studied separately from each other since many decades. Nevertheless, due to their very complex and variable structure there are still several aspects which are not yet completely understood (chemical, micro-structural and mechanical). Combining cement and clay to create an interface multiplies these complications and unknown properties and makes the prediction of the long-term behavior of such a system very challenging. Inside an underground radioactive waste repository there are several regions where a cement and clay will be in direct contact. The two most

important interfaces between cement and clay in the Swiss repository design and their relevance are discussed in the following.

i) Opalinus Clay – cement (tunnel/cavern liner)

To ensure mechanical stability of the tunnel and the cavern walls, shotcrete or prefabricated concrete blocks (tubbings) will be applied to the walls. These two different methods significantly influence the interaction type, since for shotcrete the hydration (the most reactive phase) occurs when the concrete is applied to the wall. An example of the complexity of the reaction is described in Jenni et al. (2014). During an experiment, they observed different stages of hydration of the cement paste, when applied to Opalinus Clay rock (slightly dried, due to exposition to air). Cement porewater will be taken up by the partly dried Opalinus Clay. This phenomenon partially stops the cement hydration, which then restarts in a second wave when the OPA porewater diffuses back to the cement. There are therefore different stages of hydration leading to a complex zonation within the concrete.

The application of hardened blocks instead of shotcrete reduces the initial reactivity (compared to fresh cement), but decreases the quality of the contact with the walls. In both cases, anyway, a cement-clay interface is created. At present, the Swiss concept foresees the application of a low-pH cement liner to the tunnel walls. The cement choice influences the reactions occurring at the interfaces, as extensively discussed in the following chapters. The Opalinus Clay-cement interface will occur in both the L/ILW and the HLW repository.

ii) Opalinus Clay – cement – bentonite

This interface type will occur only around the HLW repository, according to Fig. 1. In this case, a liner of ~15 cm will be applied to the Opalinus Clay walls to stabilize them (Nagra, 2016, NTB 14-13). A bentonite granulate filling comes in a later phase, after the waste installation. The HLW design is more complex than that described before and has three components: Opalinus Clay-concrete-bentonite. Bentonite will naturally saturate with the surrounding porewater, at least in the external part, within the first decades to centuries (Nagra, 2016, NTB 14-13). The water will partially come from the cement and partially from the surrounding clay. This of course introduces further unknowns in the cement-clay system. There will be an OPA-cement and a cement-bentonite interface within a relative short distance (<20 cm). The cement degradation will therefore occur faster, and the prediction of the evolution of the reactivity is quite complex (and also difficult to reproduce experimentally).

HLW/SF are the most hazardous wastes present in the repository and therefore it is crucial to know as accurately as possible how the conditions in the repository nearfield will evolve. In this case, besides the diffusion of radionuclides and the migration of gases, also a question regarding the saturation state of bentonite arises. It is important that bentonite is completely saturated when the canister fails, to allow the barrier to stabilize and seal the galleries. At the same time, diffusion of solutes is slower in partly saturated bentonite compared to full water saturation, which can be regarded as beneficial. Another topic of interest, related to the bentonite saturation, is the dissipation of the heat produced by the radioactive waste: depending on the saturation state of bentonite the dissipation capacity and therefore the temperature reached by the bentonite will vary.

Cement and clay will therefore represent a very dynamic system which is strongly dependent not only on the initial chemical composition of the components, but also on a multitude of other interconnected factor and processes (e.g., condition of emplacement, degree of saturation or temperature conditions).

2.4 State of knowledge regarding the interface reactivity

The strong reactivity of cement-clay interfaces is related to the differences in their chemical composition and finally to the differences in their porewater composition. Cement porewater is strongly alkaline, having generally high amounts of sodium and potassium in solution and a high pH (~13 for standard type II cements). Calcium is also present in relevant concentrations. Sulphate, magnesium and aluminum are also present but in lower concentrations. The clay porewater generally has an almost neutral pH (~7); the concentration of the other elements is strongly dependent on the composition. Potassium is generally significantly lower than in cement or concrete, creating a strong gradient towards the clay. The interface reactivity depends on several factors as the material composition, the temperature and the interaction time. In spite of the great variability, there are several common features that can be generally observed when cement and clay come in contact.

2.4.1 The pH plume

The disequilibrium present at the interface will drive solute transport when cement and clay are put in contact. Regarding the pH, hydroxyl anions will diffuse towards the clay and quickly change the pH regime. The geochemical differences will also lead to the diffusion of cations present in solution towards the clay and ultimately to destabilization of cement phases (e.g., portlandite, C-S-H) and a further release of OH⁻. The pH changes can be indirectly determined thanks to the observed mineral transformations or by means of laboratory techniques. The rate of progress of the pH plume on the clay side depends on molecular diffusion as well as on buffering reactions related to sorption on clay edge sites (Nagra, 2018) and dissolution precipitation reactions (Gaucher and Blanc, 2006).

2.4.2 Dissolution reactions

Dissolution of clay minerals

Clay minerals are not stable under alkaline conditions and start dissolving when in contact with high pH solutions as demonstrated in different experiments (Bauer and Berger, 1998; Cama et al., 2000). This is a key process when considering the cement-clay system since i) the dissolution of the clays results in ions release in solution that are then reused in other reactions which may alter the interface properties. ii) The dissolution of clays buffers the pH plume originating from the cement compartment. Dissolution of clays is a kinetically controlled process, meaning that the thermodynamic equilibrium is not necessarily reached and that there a series of parameters which influence the dissolutive process (e.g., activation energy, reactive surface area and temperature, Cama and Ganor, 2015). Even if clays are not stable under alkaline condition, they do not quickly dissolve since the activation energy necessary for a dissolution is very high. Kinetic constants for the dissolution of clay minerals are poorly constrained and therefore the stability of clays under alkaline conditions is still not well characterized.

Dissolution of accessory minerals

Not only clays dissolve under alkaline conditions, but also accessory minerals such as quartz, or feldspars dissolve (although at different rate). Similarly to clay minerals, their dissolution contributes to buffering the pH, limiting the penetration of the pH plume within the barrier, and liberates ions in solutions available for other reactions.

Dissolution of cementitious phases

The main cementitious phases start to destabilize when the pH drops below a certain value. Therefore, when a cement-clay interface is formed, some cement phases start to dissolve due to the pH decrease in the interface proximity (Gaucher and Blanc, 2006). The two most relevant phases in this case are portlandite and C-S-H. For Portland cement, portlandite is the first mineral that reacts; when the pH decreases below ~ 12.5 , Ca(OH)_2 starts dissolving, liberating Ca^{2+} and OH^- into solution and generating a calcium (Ca^{2+}) and pH (OH^-) plume towards the clay. This reaction is fast, i.e., reaches quickly local equilibrium (Berner, 1992). Once portlandite is consumed and a pH of $\sim 10-10.5$ is reached, C-S-H starts to dissolve. The incongruent C-S-H dissolution is more complex and slower than portlandite dissolution (Baston et al., 2012). During the dissolution, the Ca/Si ratio of the C-S-H will decrease. C-S-H are the strength-giving minerals, holding together the cement matrix; once they dissolve, the mechanical properties of the concrete strongly decrease and silicates and carbonates represent the main solid phases remaining (Ochs et al., 2016).

Although they are present in more limited amounts compared to portlandite or C-S-H, AFm and AFt are also sensitive to pH conditions and dissolve when the pH decreases. Especially ettringite dissolution and re-precipitation phenomena are known to occur in cement-clay systems (Mäder et al., 2017).

2.4.3 Mineral precipitation

The strong initial disequilibrium leads to mass fluxes and mineral dissolution and precipitation on both sides of the interface. The mineralogical alteration strongly varies depending on the interface type and on the surrounding conditions. In the following paragraph, some of the most common newly formed phases are described.

Calcite

Regarding the clay side, most types of material interfaces refer to

- i) the host rocks; sedimentary formations with high clay content, such as the Opalinus Clay (Switzerland), the Boom Clay (Belgium) or the Callovo-Oxfordian (COx) argillite (France);
- ii) bentonite, considered in different countries as a valid filling material;
- iii) montmorillonite or illite, used to experimentally (or in models) simulate a simplified system.

Clay formations, depending on the facies, can be rich in carbonates and fossils (Kneucker and Furche, 2021) and have therefore a relatively high $p\text{CO}_2$. The high CO_2 concentration is related to the diagenetic filling of the fossil's shale; the porewater equilibrates with the CaCO_3 present and has therefore high values of dissolved CO_2 and calcium. For this reason, precipitation of calcite or more generally of carbonates is often observed at cement-clay interfaces (even in absence of atmospheric CO_2 , e.g., experiments in nitrogen-filled

glove boxes). In the case of compacted montmorillonite or bentonite the amount of calcite present is much lower and therefore the resulting $p\text{CO}_2$ is very low. Whether inside the rock formation (or the samples) a high CO_2 partial pressure is present or not makes a relevant difference, since calcite can quickly precipitate (within weeks) and affect the porosity and therefore the interface reactivity.

C-S-H Phases

Formation of these phases at cement-clay interfaces was observed in several experiments (Fernández et al., 2016; Lalan et al., 2019) and also predicted by models (Marty et al., 2009; Kosakowski and Berner, 2013). The formation is triggered by the contemporary presence of silica (originating from the dissolution of clays and possibly other silicates) and calcium (mostly provided by dissolution of cementitious phases). C-S-H phases are generally amorphous and very fine grained. They can accommodate different cations in their structure and also be present in other forms, e.g., including aluminum (C-A-S-H). C-S-H phases have interlayers. Their precipitation in large amounts would remarkably decrease the porosity, but it is unlikely that this could completely clog the porosity. The anion transport through a C-S-H enriched region would instead be strongly affected.

AFm, AFt Phases

The most common AFt phase is ettringite. Precipitation of ettringite is a typical phenomenon during sulfate attack. Ettringite precipitation is observed when clay rocks with porewater rich in sulfate are put in contact with concrete. An example is given by Dauzères et al. (2014), who reported ettringite precipitation within the low-pH cement in contact with CO_x . Chloride AFm can form in the case of contact with high saline porewater (Taylor, 1997).

Magnesium bearing phases

The formation of magnesium phases is also a topic to which much attention was dedicated in the last years. Precipitation of magnesium phases was observed in the CI experiment at Mont Terri (Mäder et al., 2017; Bernard et al., 2020) inside OPA in contact with OPC. Yokoyama et al. (2021) observed instead Mg-phases inside bentonite (MX-80) in contact with low-alkali cement. Jenni et al. (2017) observed Mg-enrichment (brucite, hydrotalcite) when modeling OPA-OPC interfaces.

Other phases described in samples with cement-clay interfaces

Depending on the type of interface and on the experimental or modeling studies, other phases have been described. Zeolites (e.g., phillipsite and analcime) were observed in natural analogues (Savage, 2011) and are often included and observed in models (Marty et al., 2014). Zeolites are mostly observed in experiments at high temperature (e.g., Bouchet et al., 2004; Nakayama et al., 2004; Lalan et al., 2016), but in some cases also at room temperature (Cuevas et al., 2006). Formation of smectites, as beidellite (Bouchet et al., 2004), and illite (illitisation) was reported by Adler et al. (1999) and Mosser-Ruck and Cathelineau (2004).

2.4.4 Porosity alteration

Porosity changes at cement-clay interfaces are a key factor controlling the system evolution, since the pore space governs diffusive processes for exchange of solutes and gases. It has been observed that the overall porosity near interfaces decreases with time (Savage, 2011). Depending on the interface components, the

mineral responsible for the porosity reduction, the location of the low-porosity region and the magnitude of the decrease will vary. Experimentally the determination of the porosity of the interface is quite challenging and there are only few articles addressing this topic in detail. Furthermore, it must also be noted that there are different methods to determine the porosity.

Gaboreau et al. (2011) used autoradiography to investigate the porosity alteration in 15 years old Tournemire mudrock/cement samples. The results indicate an increase of the porosity within cement and a decrease in the clay. The same method was also described in Mäder et al. (2017), where OPA-cement interfaces were investigated after 5 years interaction. Dauzères et al. (2014) reported porosity measurements by means of microtomography on OPC and Low-pH cement paste reacted with synthetic CO_x pore solution. The authors observed a “coarser” porosity in the leached cement region. Porosity decrease (measured with autoradiography) on both sides of the interface was also described by Lalan et al. (2019). Shafizadeh (2019) and Shafizadeh et al. (2020) used neutron imaging to derive water content in saturated OPC Na-montmorillonite samples. A porosity increase in the cement was observed as well as a clear porosity reduction within the first 1-2 mm of the montmorillonite.

2.4.5 Decrease of the diffusivity

The dissolution-precipitation reactions occurring at cement-clay interfaces lead to an alteration of the porosity near the interface. The location and the magnitude of the porosity alteration is dependent on the interface type, but it generally leads to a decrease of the interface diffusivity. This is related to the higher molar volume of the newly forming mineral phases that therefore reduce the available pore space for the diffusive process. As described in chapter 1.3, the clay pore space is composed of the free porosity (anion accessible), the interlayer porosity and the diffusive-layer porosity. The precipitation of solid phases within pores affects therefore the diffusion of anions or cations in different ways. A complete clogging of the pore space would essentially block all mass transport. On the other hand, a local precipitation inside specific domains may strongly affect anions, but to a smaller degree cations (Appelo, 2013). For this reason, investigating and understanding in which pore environment precipitations occur, is a key factor. In this regard, it is also important to determine which mineral is precipitating at the interface. For example, newly precipitated calcite which does not possess an interlayer would completely block the mass transfer. Instead the newly precipitated C-S-H phases, which possess an interlayer space, would not completely block the mass transfer. Identification of the mineral precipitating at the interface is therefore relevant for a correct assessment of the diffusivity evolution. Similarly, the prediction of the diffusive properties of cement-clay interfaces is an important factor. This topic is extensively discussed in chapters 3, 5 and 6.

2.4.6 Modification of the adsorbed cation population

On the clay-side the initial composition of the clay minerals tends to be sodic. In bentonite (e.g., MX-80) the main component is Na-montmorillonite (Carlson, 2004), whereas in Opalinus Clay various cations are present, but sodium is mostly dominating in solution and on the exchange sites. The alkaline plume entering clays is enriched in potassium (originally in the cement porewater) and Ca (mainly from dissolution of portlandite and C-S-H). Since Ca²⁺ and K⁺ have a higher affinity for the interlayer space compared to Na⁺,

they tend to exchange such that sodium is liberated into solution. Within Opalinus Clay, magnesium can similarly be exchanged by the cementitious cations leading to increased Mg concentrations in solution.

2.5 Investigation of the interface reactivity

2.5.1 Natural and industrial analogues

Natural and industrial analogues allow studying systems that are similar to cement-clay interfaces and that already reacted over long periods. These data serve as comparison and indication to set model parameters and then test laboratory experiments. A well-known example is the Maquarin site (Northern Jordan) where the dissolution of natural portlandite gave rise to an alkaline-cement-like porewater (high Ca, high pH), which circulated within fractures of a clay-rich formation for over 100'000 years (Smellie et al., 1998). The natural interaction appeared to pass several episodes of opening and closing of the fractures related to different generations of (complex) mineral reactions. Dissolution of the minerals composing the clay formations was observed together with precipitation of several phases characteristic for a cement-clay system (C-S-H, ettringite, zeolites, carbonates). The alkaline alteration extends up to 40 mm from the fractures, with a 1-4 mm region strongly altered (Smellie et al., 1998; Milodowski et al., 2001; Cassagnabère et al., 2001).

Another interesting example of an analogue (industrial, in this case), is the Tournemire argillite (France). A railway tunnel was excavated in this formation and the argillaceous rock was in contact with cementitious material (used to reinforce the tunnel walls) for approximately 125 years (Savage, 2011). Tinseau et al. (2006) give a detailed overview over the observed interface alterations. The system was for the entire interaction period in contact with air. This fact favored the oxidation of pyrite and the precipitation of carbonates at the interface. Dissolution of quartz and kaolinite was observed in the zone close to the contact with the cement. Tinseau et al. (2006) also describes variations of the illite/smectite presence up to 17 cm from the interface. Furthermore, precipitation of zeolites and calcium sulfates was also observed. Devol-Brown et al. (2006) performed batch experiments using the same mineralogical composition and hyperalkaline fluid and found comparable results.

Mortar from Hadrian's wall mortar (1700a old) was studied by Hodgkinson and Hughes (1999). The initial composition was an amorphous C-A-S-H binder. The mortar was strongly affected by carbonation. When in contact with the present Si-rich sedimentary rock, dissolution precipitation phenomena were observed; the pores were filled and the porosity decreased. The extension of the altered zone is relatively small (<2.5 mm, for non-carbonated regions) and therefore slow reaction kinetics were assumed (at low temperatures).

2.5.2 Experiments

2.5.2.1 Laboratory

From the 90s a multitude of laboratory experiments were performed to study the evolution of cement-clay interfaces. Gaucher and Blanc (2006) and Wilson et al. (2021) offer extensive and detailed reviews on this topic. In the following some of these experiments will be discussed.

Three different experimental setups are common: batch experiments, column or flow-through experiments, and diffusion experiments:

i) Batch experiments represent relatively simple closed systems which allow studying different processes (e.g., dissolution, mineral transformation). This kind of experiments can be easily performed at different temperatures and pressures. The great advantage of this type of (reactor) experiments is that the initial composition and settings (T and P) can be easily chosen, modified and reproduced. However, the simple experimental setup implies some limitations: the transport factor (e.g., diffusion or advection) is not considered and no spatial information can be gained (e.g., precipitation fronts).

Bauer and Berger (1998) used batch experiments to study kaolinite and smectite dissolution rates in alkaline solutions. Ramírez et al. (2005) investigated the mineralogy and the CEC modifications of the Callovo-Oxfordian clay. More recently, Dauzères et al. (2014) studied the interaction of different cement pastes with CO_x pore fluids. There are a multitude of batch experiments which were conducted with focus on the cement-clay system, mostly in the 90s. The experiments were performed with a variety of starting mineralogy, temperature and pressures and are extensively discussed in Gaucher and Blanc (2006).

ii) Column or flow-through experiments are more complex and require more instruments (pumps, reservoirs). In these experiments, a solution flows through a column filled with a given material (e.g., clay or cement paste). These experiments allow monitoring the modifications of some parameters such as porosity/permeability, or the changes in the outflowing solution composition as a function of time. Post mortem it is also possible to investigate the mineralogical alterations in the samples. Bateman (2001a) and Small et al. (2016) report the results of column experiments performed using simulated cement porewater and different host rocks and minerals. Taubald et al. (2000) used column experiments to investigate the effect of OPC leachate on smectites and OPA. They observed after 1.5 years interaction a 2 cm alteration zone within OPA with precipitation of C-A-S-H, carbonate, portlandite and brucite.

iii) Diffusion experiments basically represent a variation of column experiments. The transport regime is in this case diffusive. Therefore, the sample dimension is generally smaller compared to column experiments. The great advantage of diffusion experiments is that the imposed transport regime is close to repository conditions.

Also, there are different possibilities and setups to perform diffusion experiments. The most simple way is to sandwich a sample between two solution reservoirs allowing a diffusive exchange of solutes between the sample and the solutions. Adler et al. (1999) contacted OPA with high pH solutions for up to 18 months and reported a complex mineralogical alteration such as the formation of C-A-S-H, and in later stages zeolite and calcite. A more realistic, but also more complex type of experiments was performed by Dauzères et al. (2010), who performed several diffusion experiments through cement paste/CO_x interfaces. Dauzères et al. (2010) reported ettringite and calcite precipitation, as well as dissolution of portlandite on the cement side of the interface. The use of a real interface add several experimental challenges that need to be solved (extensively discussed in the chapters 3-6).

OPC-argillite (Upper Toarcien from Tournemire) interaction at 70°C was investigated by Lalan et al. (2019). They observed calcite and C-(A)-S-H precipitation and decalcification reactions. Dauzères et al. (2014)

report laboratory experiments based on the interaction of low-alkali cement (LAC) with synthetic clay pore water. LAC is of interest because of the lower pH of the leachate, which may result in a less reactive interaction with the clay host rock. Dauzères et al. (2014) observed portlandite dissolution, C-S-H decalcification and ettringite precipitation for an interaction time of 5 months. Shafizadeh (2019) studied OPC-Na montmorillonite interfaces samples by means of through-diffusion experiments and neutron imaging to investigate porosity changes at the interface. The work presented in chapters 3-6 represent the continuation of the research started by Shafizadeh (2019).

2.5.2.2 In-situ

In-situ experiments have been conducted or are still ongoing in several underground rock laboratories around the world. Some of the most relevant experiments for this thesis will be described in the following. Read et al. (2001) investigated the reactivity of an interface between Portland cement and Boom Clay. The experiments were performed at 25°C and 85°C. The authors reported portlandite dissolution in cement and, in the case of the experiment at high temperature, the formation of a narrow zone with Mg-enrichment within the clay.

The CI-interaction experiment (Mont Terri Underground Rock Laboratory, Switzerland) is focusing on the interaction between cement and clay. The setup is based on two boreholes in OPA filled with three different concretes (two low-alkali cements, one OPC) and one type of bentonite (MX-80). Over the years several sampling campaigns have been performed to investigate the mineralogical changes taking place at the interfaces, and the new boreholes were again filled with various cements or concretes. The large amount of information is presented in Jenni et al. (2014) and Mäder et al. (2017). The most important results can be summarized as follows:

- For both OPC and ESDRED (low-alkali concrete), the extension of the alteration zone inside the claystone is very small.
- The reaction region within the cement matrix is more extended for ESDRED than for OPC. Mäder et al. (2017) explained a higher reactivity of this cement by its chemical composition (silica fume, nanosilica, set accelerators).
- The reaction fronts show similar extensions for the first two sampling campaigns (after 2.2 and 4.9 years of interaction), indicating a reduction of the reaction rates.
- The authors concluded that the use of low-alkali cements instead of OPC is not particularly advantageous, and may even introduce more uncertainties in the system evolution.
- A Mg-enrichment was observed within OPA, approximately 4-6 mm from the interface when clay was contacting OPC. The Mg-enrichment in clay is instead located directly at the interface when OPA is interfacing ESDRED. In this case, the Mg-enrichment is additionally observed within the ESDRED matrix as well.
- At the interface, calcite precipitation was observed within OPC and ESDRED, together with a porosity reduction in the case of OPC.

Gaboreau et al. (2012) studied the interaction of COx claystone (France) and different cements. The investigated interface samples were made from shotcrete applied to tunnel walls or concrete injected into

boreholes. Also in this case, the perturbations observed were very limited (<1 cm) after five years interaction. On the cement side porosity variations, dissolution of portlandite, and carbonate and C-S-H precipitation were reported. In the clay compartment, they observed mainly sulfate precipitation and a change of the adsorbed cation population.

The interaction of cement with the Tournemire Argillite was investigated in the CEMTEX in-situ experiment described in Lalan et al. (2016). The experiments were performed at 70°C. Portlandite dissolution and C-S-H decalcification, together with calcite precipitation were reported up to 0.8 mm within the cement. At the interface, C-S-H, C-(A)-S-H, and zeolites were observed. Another work performed on the Tournemire argillite is described by Gaboreau et al. (2011) who performed measurements on 15a old samples, observing clogging of the macroporosity in clay and increased porosity in the cement compartment. Bartier et al. (2013) investigated 18a old samples of Tournemire Argillite/cement interfaces and described both C-A-S-H and carbonate precipitation inside the claystone.

In the FEBEX experiment (Grimsel Underground Rock Laboratory, Switzerland), a heater surrounded by bentonite was placed in granite for approximately 18 years. The experiment enabled to study a multitude of processes, and cement-clay interactions only represents a small part (Nagra, 2016 NTB 15-04). Kaufhold et al. (2018) reported results of the investigation of bentonite and concrete after 18a interaction. Calcite and sulphate precipitation at the interface up to 1mm from the interface were reported. The heater temperature was maintained constant at 100°C; most of the reactions were observed at the bentonite-heater interface. In parallel to the main experiment several small-scale laboratory experiments were performed.

2.5.3 Models

Natural analogues and experiments are powerful tools allowing understanding the reactivity and the reactions occurring at the interface. One of the major limitations of experimental studies is the relatively short time scale they would typically cover (mostly years to decades). Natural analogues, as discussed, can instead give insights on very long reaction times, although only a limited number of these systems exist; and they generally represent complex interactions or conditions not exactly comparable with the repository scenario (e.g., rock and porewater composition, type of alteration, time).

Modeling therefore is an essential tool, which helps to describe the behavior of cement-clay interfaces over repository time scales. Numerous models were tested to simulate the reactions at cement-clay interfaces. Nagra (2018) give an extensive review of publications starting from the year 2000. There are several possibilities for simulating and acquiring information regarding the concrete-clay system. A model by definition represents a simplification of the reality, and therefore certain parameters or “complexities” are approximated or estimated. Depending on the type of model, and the questions to be answered, they focus on different processes. There are several factors, that are decisive and influence the results. They include: the initial chemistry and mineralogy, the type of transport and the type porosity which are considered, the surface area, the kinetic parameters. There are therefore relevant differences among models. Despite this fact, some similarities are present regarding the thickness of alteration zones, the porosity evolution and the mineralogical alteration (Nagra, 2018):

- The altered region is, according to most models, limited to some centimeters after 10^5 years interaction.
- Cement phases such as portlandite and C-S-H are leached. Ca^{2+} and OH^- diffuse towards the clay. The diffusion of OH^- from the cement compartment into the clay leads to partial dissolution of clays and accessory minerals.
- On the clay side, the clays and the accessory minerals are (partially) replaced by C-(A)-S-H and other minerals (clay interlayering, silicates). The new minerals, due to their higher molar volume, lead to local decrease of the total porosity and therefore also to a decrease in diffusivity. In many models, full clogging of the porosity is observed.
- Clay edge sites will be de-protonated retarding the diffusion of OH^- anions (fast, reversible reaction).
- For interface samples composed of natural clay formations, the high pCO_2 will lead to precipitation of carbonates, which rapidly affect the porosity at the interface.
- Diffusion of Ca^{2+} and K^+ cations from the cementitious porewater enhance their exchange with other cations on the exchanger sites of montmorillonite (fast reversible reaction).

To investigate the uncertainties inherent in any modelling, a typical approach is to produce several possible scenarios considering different values for a certain parameter. Marty et al. (2009) modeled for example interfaces between CO_x and cement and produced several scenarios with kinetic parameters. Berner et al. (2013) used model to simulate bentonite-concrete-OPA interfaces, reporting interesting results for a complex interface model. Jenni et al. (2017) and Jenni and Mäder (2021) presented some of the rare modeling approaches considering the presence of a dual porosity (i.e., free porosity and diffusive-layer porosity). Models offer great possibilities but have also some limitations, as reported in the next section.

Limitations and uncertainties of the modeling approach

Wilson et al. (2021) resumes the most relevant problems modelers are confronted with:

- *Rates of mineral growth*
Especially for complex minerals, these rates are poorly known and are therefore estimated.
- *Dissolution rates of clay minerals*
Currently, there still are relevant differences between in-situ and in laboratory experiments determined dissolution rates of clay minerals. These rates are critical, since clay dissolution releases ions in solution and buffers the high pH of cementitious porewater.
- *Cation exchange and surface complexation*
These two processes are not always considered in models, but play an important role in the interface reactivity.
- *Composition of the precipitated secondary minerals*
Several models have an oversimplified composition of the precipitated secondary minerals (e.g., no inclusions of zeolites). However, zeolite minerals are observed in experiments and in natural analogues and should be taken into account in the future
- *Size of the reactive surface area*

The reactive surface area is often considered as constant and a certain value is therefore fixed. But this parameter is generally not well constrained.

– *Porosity*

Most of the models do not take into account the different porosity domains present in the clay and assumes the entire porosity domain as available for transport and reactions (e.g., mineral precipitation).

2.6 Uncertainties and open questions regarding the cement-clay system

There are several properties of cement-clay interfaces which are relatively well understood, and on which the models, the experiments and the analogues agrees, such as: the general mineralogical evolution, the maximal extension of the interface and the main processes occurring. However, there are also items regarding the cement-clay interaction, which are not fully understood. In the following paragraphs some of the open questions are recapped.

- Evolution of the porosity alteration at the interface

Most of the experiments provide only rough estimations of the porosity alterations occurring at the interface, with a very limited resolution with regard to absolute changes in porosity and zonations within the clay or the cement. Furthermore, very little is known about the 4D evolution of the porosity is given, that is, about the spatial evolution with time (see 2.4.4). A promising study in this regard is the one performed by Shafizadeh (2019), although it only investigated a limited number of simplified systems.

Whether the porosity will completely clogg or which kind of porosity is involved in the precipitation phenomena (e.g., free vs interlayer porosity, see chapter 1.4) remain open questions.

- Evolution of the interface diffusive properties

Only few studies investigated the diffusive properties of cement-clay interfaces. The diffusivity alteration for specific interfaces (e.g., OPA-OPC) is largely unknown, and practically no information exists regarding the diffusive properties of the skins with altered mineralogy forming near the interface. Similarly, the diffusive behaviour of negatively charged species through samples with cement-clay interfaces has been rarely studied.

- Nature of the Mg enrichment

Depending on the interface components, a magnesium enrichment is sometimes described in the literature when cement and clays come in contact. Currently it is still not completely clear which mineral is precipitating and how important the role of such phases in the cement-clay system is, especially with respect to the porosity alterations and the diffusive behaviour.

- Gas transport across the interface

Although gas migration is of great concern in safety assessment of a nuclear waste repositories, there is little knowledge about gas transport through samples with cement-clay interfaces. The lack of knowledge

is mostly related to the practical difficulty of performing such experiments. The study of the porosity evolution as well as diffusive experiments using comparably large solutes or negatively charged species (which are both expected to move mainly through the largest pores, similarly as gas molecules in partly desaturated materials) may shed some light on this topic.

- Effect of the increased temperature on the interface evolution

Several batch experiments were performed at increased temperature to increase the system reactivity. Few experiments investigated the diffusive properties of samples with cement-clay interfaces and no literature is known to the author regarding complete diffusive experiments on samples reacted at high temperature with complex interface systems. Thus, the effect of increased temperature on the evolution of porosity and diffusive properties near cement-clay interfaces is still largely unknown.

- The dissolution of clay minerals

According to thermodynamics, clay minerals are in principle unstable under alkaline conditions; this is known and accepted within the literature. The rate of dissolution instead still remains an open question, which needs to be better investigated to correctly understand the system evolution.

- The evolution of complex and more realistic systems with cement-clay interfaces

There are few experiments performed on geochemically complex systems as for example those foreseen in the Swiss repository design (e.g., low pH cement-OPA). Most experimental investigations focus on simplified systems. For complex, more realistic systems there is very little information regarding the evolution of the porosity and the diffusive properties.

2.7 Goals and structure of the thesis

The present thesis project represents a continuation and extension of an earlier project on cement-clay interfaces (Shafizadeh, 2019), which investigated the porosity and diffusivity evolution at OPC paste-Na montmorillonite interfaces. Shafizadeh (2019) developed a cell allowing performing through-diffusion experiments and porosity investigations using neutrons and collected valuable information regarding this system. Only limited information could, however, be obtained in the frame of that thesis regarding the chemistry and mineralogy of the alterations.

The first aim of the present thesis was to gain further and complementary information regarding the OPC-Na montmorillonite system investigated by Shafizadeh (2019). The investigation of the same interface samples after longer interaction time allows acquiring further knowledge regarding the interface evolution over time, especially with respect to porosity and diffusive properties. In parallel, new OPC-Na montmorillonite samples will be produced and, together with the older ones, they will be investigated with a series of analytical techniques to shed light on the chemical and mineralogical alterations near the interface.

The second goal was to create and study interface samples composed of several different, geochemically more complex and more realistic materials such as OPA, bentonite and various cements. The increased geochemical complexity of such interface samples is expected to lead to a multitude of reactions. The analysis and comparison of the resulting alterations in different sample types will allow to shed some light on processes which so far are not completely understood. These include the understanding of the timing and type of mineralogical alterations depending on the used cement and clay, the relevance of specific dissolution/precipitation reactions in specific sample types, and the coupling between evolution of porosity and diffusivity for these materials.

The results of the thesis are presented in four self-contained parts (Chapters 3-6) in the form of scientific articles.

Chapter 3 (1° Article, published in 2020)

- **Evolution of HTO and $^{36}\text{Cl}^-$ diffusion through a reacting cement-clay interface (OPC paste-Na montmorillonite) over a time of six years**

The first article focuses on the evolution of the diffusive properties of OPC paste-Na montmorillonite interfaces. Several samples produced during the dissertation of Shafizadeh (2019) were investigated regarding their diffusive properties after up to 6 years interaction. The combination of tritiated water (HTO) and chloride-36 ($^{36}\text{Cl}^-$) as tracers allowed to study both, the effect on the total and on the anion accessible porosity. The repeated diffusive experiments performed on differently aged samples, together with information regarding the porosity evolution, allowed gaining new information about diffusive transport through cement-clay interface samples, including the estimation of local diffusion coefficients for the zones of reduced porosity following mineral precipitation.

Key topics

porosity, HTO/ $^{36}\text{Cl}^-$, diffusion

Key questions

- How does the diffusivity of OPC-montmorillonite samples evolve over time?
- What happens to the transport of anions?
- How do the diffusion properties change in zones of reduced porosity?
- In which porosity domain(s) does the precipitation of new minerals happen?

Chapter 4 (2° Article, to be submitted)

- **Evolution of mineralogy and porosity at OPC paste Na-montmorillonite interfaces during 6 years of interaction**

The second article completes the information gained in the first one with chemical and mineralogical investigations. The same samples used for through-diffusion experiments were

investigated by means of several techniques to characterize the mineralogical alteration responsible for the porosity modification, and ultimately for the decrease of the derived diffusion coefficient. The techniques included neutron imaging, scanning electron microscopy (SEM/EDX), X-ray diffraction (XRD), thermogravimetry (TGA-IR), and X-ray tomography. The obtained results allowed gaining relevant mineralogical information that, together with the diffusive data from the first article, elucidate many aspects of the complex and interconnected reactions occurring in an OPC paste-Na montmorillonite system.

Key topics

C-S-H, porosity, AFm, altered skins

Key questions

- What is the thickness of the alteration fronts?
- Which kind of minerals precipitate, which dissolve?
- What is the timing of precipitation and of the porosity alteration?

Chapter 5 (3° Article, to be submitted)

▪ **Evolution of diffusive and mineralogical properties of cement-clay interfaces: effects of cement and clay type**

The goal of this study was to create different types of interfaces closer to those expected in real conditions (more complex mineralogy than those described in the two previous chapters), and to investigate them with different methods to characterize the mineralogical and diffusive behaviour during two years interaction. Bentonite and OPA were the clay materials used, whereas high-porosity Ordinary Portland Cement paste (OPC) and a low pH mortar (ESDRED) were selected as representatives for the cementitious compartment.

Already after 2 years interaction relevant differences could be observed, which allowed characterizing the differences among the systems.

Key topics

OPA, bentonite, OPC paste, ESDRED mortar, diffusivity, dissolution, precipitation

Key questions

- What are the differences between the diffusive properties of the different interface types?
- What are the initial mineralogical differences between the different types of interfaces?
- How do the mineralogy and diffusive properties change over time?

▪ **OPC paste-clay interaction at 70°C: eighth months monitoring of properties at materials interfaces**

The first three parts were focused on alterations at room temperature. In this article, the knowledge acquired during the precedent studies was applied to study the cement-clay systems at higher temperature. Elevated temperatures are likely relevant for a real repository, for instance because of heat release by spent fuel, and also because of higher in-situ temperatures in the underground. Furthermore, the samples were studied in a more complete way, considering additional properties. Different interface types were created and let react at 70°C for several months. During this period, the pH and the porewater evolution were steadily monitored to better characterize the short-term reactions occurring within the system. The increased temperature accelerates the diffusive process and the reactivity of the interface. Furthermore, the higher temperature may lead to the formation of different minerals compared to those observed at room temperature.

Key topics

OPA, bentonite, diffusivity, porewater composition, pH

Key questions

- What is the effect of temperature on the reactivity of the interface cement-clay samples?
- What is the effect of temperature on the mineralogical alterations?
- How do the pH and the porewater chemistry evolve?

References

- Adler, M., Mäder, U.K., Waber, H.N., 1999. High-pH alteration of argillaceous rocks: an experimental study. *Schw. Min. und Petr. Mitt.* 79, 445–454.
- Appelo, C.A.J., 2013. A Review of Porosity and Diffusion in Bentonite. Working Report, Posiva Oy.
- Bartier, D., Techer, I., Dauzères, A., Boulvais, P., Blanc-Valleron, M.-M., Cabrera, J., 2013. In situ investigations and reactive transport modelling of cement paste/argillite interactions in a saturated context and outside an excavated disturbed zone. *Appl. Geochem.* 31, 94–108.
- Baston, G.M.N., Clacher, A.P., Heath, T.G., Hunter, F.M.I., Smith, V., Swanton, S.W., 2012. Calcium silicate hydrate (C-S-H) gel dissolution and pH buffering in a cementitious near field. *Mineral. Mag.* 76, 3045–3053.
- Bateman, K., Coombs, P., Pearce, J.M., Wetton, P.D., 2001a. Nagra/Nirex/SKB Column Experiments; Fluid Chemical and Mineralogical Studies. British Geological Survey Report WE/95/26.
- Bauer, A., Berger, G., 1998. Kaolinite and smectite dissolution rate in high molar KOH solutions at 35°C and 80°C. *Appl. Geochem.* 13, 905–916.
- Bernard, E., Jenni, A., Fisch, M., Grolimund, D., Mäder, U., 2020. Micro-X-ray diffraction and chemical mapping of aged interfaces between cement pastes and Opalinus Clay. *Appl. Geochem.* 115, 104538.
- Berner, U., 1992. Evolution of pore water chemistry during degradation of cement in a radioactive waste repository environment. *Waste Manag.* 12, 201–219.
- Berner, U., Kulik, D.A., Kosakowski, G., 2013. Geochemical impact of a low-pH cement liner on the near field of a repository for spent fuel and high-level radioactive waste. *Phys. Chem. Earth* 64, 46–56.
- Bouchet, A., Cassagnabère, A., Parneix, J.C., 2004. Batch experiments: results on MX80. In: Michau, N. (Ed.), *Ecoclay II: Effect of Cement on Clay Barrier Performance Phase II*. Final report. (ANDRA) European contract FIKW-CT-2000-0028.
- Cama, J., Ganor, J., Ayora, C., Lasaga, C.A., 2000. Smectite dissolution kinetics at 80°C and pH 8.8. *Geochim. et Cosmochim. Acta* 64, 2701–2712.
- Cama, J., Ganor, J., 2015. Dissolution kinetics of clay minerals. *Develop. Clay Sci.* 6, 101–153.
- Carlson, L., 2004. Bentonite mineralogy. Posiva working report, 2004-02, Posiva OY, Olkiluoto, Finland.
- Cassagnabère, A., Parneix, J.C., Sammartino, S., Griffault, L., Maeder, U., Milodowski, A.E., 2001. Mineralogical evolution of bituminous marl adjacent to an alkaline water conducting feature at the maqarin analogue site. *Proceeding of the Tenth International Symposium on Water-Rock Interaction*. Balkema, 367–370.
- Cuevas, J., Vigil de la Villa, R., Ramírez, S., Sánchez, L., Fernández, R., and Leguey, S., 2006. The alkaline reaction of FEBEX bentonite: a contribution to the study of the performance of bentonite/concrete engineered barrier systems. *J. of Ib. Geol.* 32, 151–174.
- Dauzères, A., Le Bescop, P., Sardini, P., Cau Dit Coumes, C., 2010. Physico-chemical investigation of clayey/cement-based materials interaction in the context of geological waste disposal: experimental approach and results. *Cem. Concr. Res.* 40, 1327–1340.
- Dauzères, A., Le Bescop, P., Cau Dit Coumes, C., Brunet, F., Bourbon, X., Timonen, J., Voutilainen, M., Chomat, L., Sardini, P., 2014. On the physico-chemical evolution of low-pH and CEM I cement pastes interacting with Callovo-Oxfordian pore water under its in-situ CO₂ partial pressure. *Cem. Concr. Res.* 58, 76–88.

- Devol-Brown, I., Tinseau, E., Bartier, D., Mifsud, A., Stammose, D., 2006. Interaction of Tournemire argillite (Aveyron, France) with hyperalkaline fluids: batch experiments performed with powdered and/or compacted materials. *Phys. Chem. Earth* 32, 320–333.
- Dung, N.T., Lesimple, A., Hay, R., Celik, K., Unluer, C., 2019. Formation of carbonate phases and their effect on the performance of reactive MgO cement formulations. *Cem. Concr. Res.* 125, 105894.
- Fernández, R., Ruiz, A.I., Cuevas, J., 2016. Formation of C-A-S-H phases from the interaction between concrete or cement and bentonite. *Clay min.* 51, 223–235.
- Hillier, S., 1978. Clay mineralogy. 223-228. In: *Sedimentology. Encyclopedia of Earth Science*. Springer, Berlin, Heidelberg.
- Hodgkinson, E.S., Hughes, C.R., 1999. The mineralogy and geochemistry of cement/rock reactions: high-resolution studies of experimental and analogue materials. *Chem. Cont. Waste Geosph.* 157, 195–211.
- Gaucher, E.C., Philippe Blanc, P., 2006. Cement/clay interactions - A review: Experiments, natural analogues, and modeling. *Waste Manag.* 26, 776–788.
- Gaboreau, S., Prêt, D., Tinseau, E., Claret, F., Pellegrine, D., Stammose, D., 2011. 15 Years of in situ cement–argillite interaction from Tournemire URL characterisation of the multi-scale spatial heterogeneities of pore space evolution. *Appl. Geochem.* 26, 2159–2171.
- Gaboreau, S., Lerouge, C., Dewonck, S., Linard, Y., Bourbon, X., Fialips, C.I., Mazurier, A., Pret, D., Bosrchenck, D., Montouillout, V., Gaucher, E.C., Claret, F., 2012. In-situ interaction of cement paste and shotcrete with claystones in a deep disposal context. *Am. J. Sci.* 312, 314–256.
- Jenni, A., Mader, U., Lerouge, C., Gaboreau, S., Schwyn, B., 2014. In situ interaction between different concretes and Opalinus Clay. *Phys. Chem. Earth, Parts A/B/C*, 70–71. 71–83.
- Jenni, A., Gimmi, T., Alt-Epping, P., Mader, U., Cloet, V., 2017. Interaction of ordinary Portland cement and Opalinus clay: dual porosity modelling compared to experimental data. *Phys. Chem. Earth, Parts A/B/C*, 99, 22–37.
- Jenni, A., Mäder, U., 2021. Reactive Transport Simulation of Low-pH Cement Interacting with Opalinus Clay Using a Dual Porosity Electrostatic Model. *Minerals*, 11.
- Kaufhold, S., Dohrmann, R., Ufer, K., Kober, F., 2018. Interactions of bentonite with metal and concrete from the FEBEX experiment: mineralogical and geochemical investigations of selected sampling sites. *Clay Min.* 53, 745-763.
- Kneuker, T., Furche, M., 2021. Capturing the structural and compositional variability of Opalinus Clay: constraints from multidisciplinary investigations of Mont Terri drill cores (Switzerland). *Environm. Earth Sci.* 80, 107017.
- Kosakowski, G., Berner, U. 2013. The evolution of clay rock/cement interfaces in a cementitious repository for low- and intermediate-level radioactive waste. *Phys. Chem. Earth* 64, 65–86.
- Lee, H., Cody, R.D., Cody, A.M., Spry, P.G., 2002. Observations on brucite formation and the role of brucite in Iowa highway concrete deterioration. *Environm. Eng. Geosci.* 8, 137–145.
- Lalan, P., Dauzères, A., De Windt, L., Bartier, D., Sammaljärvi, J., 2016. Impact of a 70°C temperature on an ordinary Portland cement paste/claystone interface: an in situ experiment. *Cem. Concr. Res.* 83, 164–178.
- Lalan, P., Dauzères, A., De Windt, L., Sammaljärvi, J., Bartier, D., Techer, I., Dettleux, V., Siitari-Kauppi, M., 2019. Mineralogical and microstructural evolution of Portland cement paste/argillite

- interfaces at 70°C – considerations for diffusion and porosity properties. *Cem. Concr. Res.* 115, 414–425.
- Mäder, U., Jenni, A., Lerouge, C., haboreau, S., Miyoshi, S., Kimura, Y., Cloet, V., Fukaya, M., Claret, F., Otake, T., Shibata, M., Lotenbach, B., 2017. 5-year chemico-physical evolution of concrete–claystone interfaces, Mont Terri Rock Laboratory (Switzerland). *Swiss J. Geosci.* 110, 307–327.
- Marty, N.C.M., Tournassat, C., Burnol, A., Giffaut, A.E., Gaucher, E.C., 2009. Influence of reaction kinetics and mesh refinement on the numerical modelling of concrete/clay interactions. *J. Hydrol.* 364, 58–72.
- Marty, N., Munier, I., Gaucher, E.C., Tournassat, C., Gaboreau, S., Vong, C.Q., Giffaut, E., Cochapin, B., and Claret, F., 2014. Simulation of Cement/Clay Interactions: Feedback on the Increasing Complexity of Modelling Strategies. *Transp. in Por. Media* 104, 385–405.
- Milodowski, A.E., Hyslop, E.K., Khoury, H., Hughes, C., Mäder, U.K., Griffault, L., Trotignon, L., 2001. Mineralogical alteration by hyperalkaline groundwater in northern Jordan. In: *Proceedings of the Tenth International Symposium on Water–Rock Interaction*. Balkema, 1347–1350.
- Mosser-Ruck, R., Cathelineau, M., 2004. Experimental transformation of Na, Ca-smectite under basic conditions at 150°C. *Appl. Clay Sci.* 26, 259–273.
- Nagra, 2008. Vorschlag geologischer Standortgebiete für das SMA- und das HAA Lager. Darlegung der Anforderungen, des Vorgehens und der Ereignisse. Nagra Tech. Rep. NTB 08-03.
- Nagra, 2016. High-level waste repository-induced effects. Nagra Tech. Rep. NTB 14-13.
- Nagra, 2016. Main outcomes and review of the FEBEX In Situ Test (GTS) and Mock-up after 15 years of operation. Nagra Tech. Rep. NTB 15-04.
- Nagra, 2018. A review of cement-clay modelling. Nagra Arbeitsber. NAB 18-24.
- Nakayama, S., Sakamoto, Y., Yamaguchi, T., Akai, M., Tanaka, T., Sato, T., Iida, Y., 2004. Dissolution of montmorillonite in compacted bentonite by highly alkaline aqueous solutions and diffusivity of hydroxide ions. *App. Clay Sci.* 27, 53–65.
- Negrónk-Mendoza, A. 2015. Clay. In: Gargaud, M., et al. *Encyclopedia of Astrobiology*. Springer, Berlin, Heidelberg.
- Ochs, M., Mallants, D., Wang, L., 2016. Radionuclide and metal sorption on cement and concrete 2, 5–17. Berlin/Heidelberg, Germany. Springer.
- Ramírez, S., Vieillard, P., Bouchet, A., Cassagnabère, A., Meunier, A., Jacquot, E., 2005. Alteration of the Callovo-Oxfordian clay from Meuse-Haute Marne underground laboratory (France) by alkaline solution. I. A XRD and CEC study. *Appl. Geochem.* 20, 89–99.
- Read, D., Glasser, F. P., Ayora, C., Guardiola, M. T., Sneyers, A., 2001. Mineralgical and microstructural changes accompanying the interaction of Boom Clay with ordinary Portland cement. *Adv. Cem. Res.* 13, 175–183.
- Savage, D., 2011. A review of analogues of alkaline alteration with regard to long-term barrier performance. *Min. Mag.* 75, 2401–2418.
- Shafizadeh, A., 2019. Neutron Imaging Study of Evolution of Structural and Transport Properties of Cement-Clay Interfaces. PhD Thesis. University of Bern, Bern, Switzerland.
- Shafizadeh, A., Gimmi, T., Van Loon, L.R., Kaestner, A.P., Mader, U.K., Churakov, S.V., 2020. Time-resolved porosity changes at cement-clay interfaces derived from neutron imaging. *Cem. Concr. Res.* 127, 105924.

- Small, J.S., Byran, N., Lloyd, J.R., Milodowski, A.E., Shaw, S., Morris, K., 2016. Summary of the BIGRAD Project and its Implications for a Geological Disposal Facility. Report NNL (16) 13817 for RWM, Harwell, UK.
- Smellie, J.A.T., Karlsson, F., Alexander, W.R., 1997. Natural analogue studies: present status and performance assesement implications. *J. contam. hydr.* 26, 3–17.
- Taylor, H.F.W., 1997. *Cement Chemistry*, 2nd Edition. Thomas Telford, London.
- Taubald, H., Bauer, A., Schafer, T., Geckeis, H., Satir, M., Kim, J.I., 2000. Experimental investigation of the effect of high-pH solutions on the Opalinus Shale and the Hammerschmiede smectite. *Clay Min.* 35, 515–524.
- Tinseau, E., Bartier, D., Hassouta, L., Devol-Brown, I., Stammose, D., 2006. Mineralogical characterization of the Tournemire argillite after in situ interaction with concrete. *Waste Manag.* 26, 789–800.
- Wilson, J., Bateman, K., Tachi, Y., 2021. The impact of cement on argillaceous rocks in radioactive waste disposal systems: A review focusing on key processes and remaining issues. *Appl. Geochem.* 130, 104979.
- Yokoyama, S., Shimbashi, M., Minato, D., Watanabe, Y., Jenni, A., Mäder, U., 2021. Alteration of bentonite reacted with cementitious materials for 5 and 10 years in the Mont Terri rock laboratory (CI Experiment). *Min.* 11.

Chapter 3

Evolution of HTO and $^{36}\text{Cl}^-$ diffusion through a reacting cement-clay interface (OPC paste-Na montmorillonite) over a time of six years

-- Manuscript published--

Applied Geochemistry 119 (2020)

<https://doi.org/10.1016/j.apgeochem.2020.104581>



Evolution of HTO and $^{36}\text{Cl}^-$ diffusion through a reacting cement-clay interface (OPC paste-Na montmorillonite) over a time of six years

Pietro Luraschi^{a,b,*}, Thomas Gimmi^{a,b}, Luc R. Van Loon^a, Amir Shafizadeh^{a,b}, Sergey V. Churakov^{a,b}

^a Laboratory for Waste Management, Nuclear Energy and Safety, Paul Scherrer Institute, 5232, Villigen, Switzerland

^b Institute of Geological Sciences, University of Bern, 3012, Bern, Switzerland

ARTICLE INFO

Editorial handling: Michael Kersten

Keywords:

Cement clay diffusion porosity precipitation

ABSTRACT

Cement and clays are proposed as sealing materials in underground repositories for radioactive waste. When cement and clay come into contact, chemical gradients between their very different porewater compositions lead to diffusive exchange of solutes, which can result in mineral transformations and alterations of transport properties at the materials interface. Small samples of cement-clay interfaces were prepared and let react over a period of six years. During this time, the changes in transport properties of the samples were periodically monitored by means of through-diffusion experiments. This technique allows studying the evolution of the diffusive flux across the reacting interface and characterizing the variation of the corresponding effective diffusion coefficient (D_e) over time. All experiments were performed on samples consisting of a hardened high porosity OPC paste and Na-montmorillonite. These model materials were chosen in order to simplify the mineralogy of the system. The experiments allowed obtaining relevant information regarding the development of the diffusive properties and the reactivity of such a cement-clay interface system. HTO and $^{36}\text{Cl}^-$ were used as tracers to study the evolution of both the total and the anion accessible porosity. After six years of reaction a considerable reduction of the flux for both HTO and $^{36}\text{Cl}^-$ was observed. The flux of HTO did, however, not approach zero, which means that connected porosity for diffusive transport of water is still available. The periodic monitoring of the sample evolution showed a strong reduction of the effective diffusion coefficient D_e of the samples within the first 1.5 years of the experiment and a less prominent decrease in the period between 1.5 and 6 years. The D_e of $^{36}\text{Cl}^-$ showed a stronger reduction compared to that of HTO; for some cells no chloride flux at all could be measured anymore at $t > \sim 4$ a. Using additional information on the extension of porosity changes from a neutron imaging study performed in parallel on the same samples, the diffusive properties of each component of the interface, or of a clay zone with reduced porosity could be estimated. For HTO the relation between the evolution of D_e and of the porosity in the clay part can be well described with Archie's empirical law. For chloride large uncertainties regarding the accessible porosity do not allow a precise correlation. Whether a complete porosity clogging will take place or some fraction of connected pore space will persist in the sample over reaction times \gg than 6 years remains an open question.

1. Introduction

Several countries are planning to dispose radioactive wastes in an underground geological repository in clay-rich rock formations. Most concepts of Engineered Barrier Systems (EBS) in the geological repository foresee a wide use of cementitious materials as tunnel backfill or shotcrete liner (e.g., Nagra, 2002; IAEA, 2009; Nagra, 2014). Accordingly, cement and clays will come into contact. Strong chemical

disequilibrium between their pore waters will drive mass fluxes that can lead to dissolution and/or precipitation reactions and the formation of so called "skins": regions close to the interface with clearly altered physicochemical properties (Read et al., 2001; Cuevas et al., 2006; Dauzeres et al., 2010; Kosakowski and Berner, 2013). These newly formed skins may have a strong impact on safety relevant properties of the repository, such as solute and gas transport or re-saturation.

The extension and the type of alteration of these skins vary

* Corresponding author. Laboratory for Waste Management, Nuclear Energy and Safety, Paul Scherrer Institute, 5232, Villigen, Switzerland.

E-mail address: pietro.luraschi@psi.ch (P. Luraschi).

<https://doi.org/10.1016/j.apgeochem.2020.104581>

Received 21 October 2019; Received in revised form 22 February 2020; Accepted 25 March 2020

Available online 26 May 2020

0883-2927/© 2020 Published by Elsevier Ltd.

depending on the interfacing materials. Field experiments and natural analogues indicate that after years to decades of interaction the altered region extends over mm to cm scale (Tinseau et al., 2006; Fernández et al., 2017; Mäder et al., 2017). Experimental investigations of such interfaces beyond decades are not available and their evolution on the repository timescale still remains uncertain. The quantitative understanding of reactive transport phenomena at these interfaces, that is, of the formation, extent and properties of the skins is therefore important for long-term model-based assessment of the repository under in situ conditions. To better understand the reactions taking place at such mineral interfaces, the study of natural analogues (Hodgkinson and Hughes, 1999; Martin et al., 2016; Tineasu et al., 2006; Smellie et al., 1998), laboratory experiments (Ramírez et al., 2002; Claret et al., 2002; Melkior et al., 2004; Karnland, 2004; Fernández et al., 2010) and a multitude of modelling approaches (Steeffel and Lichtner, 1998; De Windt et al., 2004; Watson et al., 2009; Berner et al., 2013; Vieliard et al., 2014; Jenni et al., 2017) have been applied. Valuable reviews on the state of knowledge and future challenges regarding cement-clay interaction are provided by Gaucher and Blanc (2006), Savage (2011) and Savage and Cloet (2018). The review by Marty et al. (2014) demonstrates that the variability of modelling predictions for cement-clay interfaces in terms of porosity, mineralogical variation and position of the altered region is strongly dependent on the initial mineralogy/chemistry of the system as well as on several badly constrained model parameters. It is therefore clear that despite of the great body of research data available in this field considerable uncertainties still remain.

One of the still missing information are the properties of the skins forming at the interface when cement and clay come in contact. Especially the evolution of the diffusivity through such interfaces remains a nearly uninvestigated field where data are limited. Albinsson et al. (1996) performed diffusion experiments with different ions across clay-concrete interfaces and could estimate some diffusion coefficients. Melkior et al. (2004) studied the evolution of the HTO and chloride diffusion coefficient of bentonite after contact with alkaline porewater; and observed a decrease of the diffusivity with increasing interaction time. Yamaguchi et al. (2016) reported also a decrease of HTO diffusion coefficients to 70% of the initial value after 600 d in samples prepared from hardened cement paste and bentonite.

The present study embarks on a non-destructive methodology for studying the temporal evolution of the diffusive properties through a reacting interface composed of cement and clay material. A special cell was designed and filled with hardened high porosity cement paste and compacted Na-montmorillonite (Shafizadeh et al., 2019). These materials were chosen to build a fast reacting and relatively simple cement-clay model system. The idea was to be able to monitor the progress of the reactions within a reasonable time frame and to have a comparably simple initial chemical composition, which should facilitate the quantitative interpretation of the chemical and transport processes occurring at the interface. During six years the transport properties of the reacting samples were repeatedly investigated by measuring the steady state diffusive flux across the samples using HTO and $^{36}\text{Cl}^-$ radioactive tracers. The combined use of HTO and $^{36}\text{Cl}^-$ tracers allows quantification of diffusive transport of a neutral and a negatively charged species simultaneously. As anions are expected to be partly excluded from regions near the negatively charged clay surfaces, such data provide insight regarding the evolution of the total and the anion accessible pore space. Recently, the same samples were investigated by means of neutron imaging (Shafizadeh et al., 2015, 2020). There, the time evolution of water content across the interface was derived, which is a proxy for the porosity in the sample at saturated conditions. The observed data suggested that interactions between Na-montmorillonite and OPC result in i) a slightly increased porosity in the cement compartment close to the interface, likely related to dissolution of portlandite, and ii) a low porosity region formed within the first mm of the clay, likely related to precipitation of new mineral phases. The

investigation of the same samples by means of through-diffusion experiments in the present study makes it possible to correlate the changes in the transport properties with the reported porosity evolution. Accordingly, the evolution of the diffusivity can be interpreted taking into account the variation of the porosity across the interface.

Although this system represents a simplification, it is expected to behave similarly as an interface between OPC and bentonite (mainly composed of Na-montmorillonite, Carlson, 2004), which potentially represents an interface that will be present in a deep geological repository for radioactive waste (e.g., Nagra, 2014). The data gained for the Na-montmorillonite-OPC paste system are therefore important; at the same time, they build a good basis to investigate more complex systems.

2. Material and methods

2.1. The experimental cell

The cell was developed at the Paul Scherrer Institut (Shafizadeh et al., 2015, 2020) to allow simultaneous through-diffusion and neutron imaging investigations of cement-clay interfaces. A schematic view of the layout is shown in Fig. 1. The cement (1) and the clay (2) plugs (5 mm diameter, about 5 mm length, cf. Table 1) were emplaced in a polytetrafluoroethylene (PTFE) cylindrical holder (3). This material is relatively flexible, resistant to the highly alkaline cement porewater, and transparent for neutrons. Mechanical stability and sample confinement are reinforced by the aluminum ring (4) around the PTFE cylinder. Polyether ether ketone (PEEK) screw caps on each side of the cells allow keeping the cell tight and the interface in contact (5). In- and outlet channels in the cap allow porewater circulation inside the cell (6). A small reservoir of $\sim 30 \text{ mm}^3$ (7) is separated from the sample by a PEEK filter (8). The tightness of the cells is maintained by fluoroelastomer (FKM) O-rings (9). Possible leaking of solutes around the cell is considered as irrelevant because of the tight fit of the swelling Na-montmorillonite and the high porosity of the cement.

2.2. Composition and preparation of samples

Na-montmorillonite and cement paste samples were prepared and saturated separately with their corresponding pore waters (Table 2) and then introduced into the cell to start the interaction. Samples were kept for most of the time in a glove box under nitrogen atmosphere ($24 \text{ }^\circ\text{C} \pm 2$) to avoid potential carbonation. The cells had to be removed out of the glove box occasionally for short periods for complementary measurements. The characteristics of the interface samples are listed in Table 1.

2.2.1. Na-montmorillonite

Na-montmorillonite from Milos (Greece) was converted into a homoionic form by cation exchange with a NaCl solution according to Glaus et al. (2010). The montmorillonite composition determined by XRF is listed in Shafizadeh et al. (2015). The samples were compacted to a bulk-dry density between 1310 and 1670 kg m^{-3} and then inserted into the cell. The compaction was performed using a dedicated press

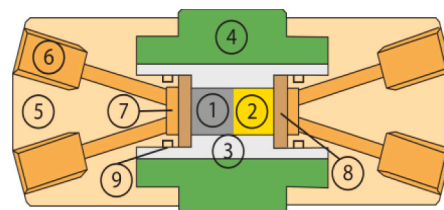


Fig. 1. Schematic view of the experimental cell used to perform through-diffusion experiments (modified after Shafizadeh et al., 2015). See text for explanation of labels.

Table 1
Characteristics of the cement paste and the Na-montmorillonite in the different samples.

Sample	Interface contact	Clay		Cement			
		Length (mm)	Dry density (kg m ⁻³)	Porosity ^a (-)	Length (mm)	Dry density (kg m ⁻³)	Porosity ^b (-)
C1	March 14, 2013	5.5	1670	0.40	4.5	700	0.63
C3	September 25, 2013	5.0	1500	0.46	5.0	700	0.63
C4	June 25, 2013	5.5	1310	0.53	4.5	700	0.63
C5	September 25, 2013	5.1	1440	0.49	4.9	700	0.63
C8	June 02, 2014	4.7	1540	0.45	5.3	700	0.63
C11	June 13, 2014	5.0	1490	0.47	5.0	700	0.63
C15	June 13, 2014	5.0	1450	0.48	5.0	700	0.63
C20	July 18, 2014	4.9	1520	0.46	5.1	700	0.63
D6	September 25, 2017	5.0	1560	0.44	5.0	700	0.63
D11	October 06, 2017	5.0	1530	0.45	5.0	700	0.63

^a Calculated from the dry density using a grain density of 2800 kg m⁻³

^b Determined by MIP (Sarott et al., 1992).

Table 2
Composition of the used synthetic porewater (total concentrations) for OPC (Wieland et al., 1998) and for Na-montmorillonite (Shafizadeh et al., 2019).

	OPC [M]	Na-montmorillonite [M]
Na	0.114	0.3
K	0.18	-
Ca	1.6 × 10 ⁻³	-
Cl	-	0.3
S ^{VI}	3 × 10 ⁻³	-
Al	5 × 10 ⁻⁵	-
pH	13.3	8.7

designed for this type of cell. The finally obtained bulk dry densities in the sample led to a porosity range of 0.40–0.53 (Table 1), with the porosity values calculated according to

$$\varepsilon = 1 - \frac{\rho_b}{\rho_s} \quad (1)$$

where ε is the porosity (-), ρ_b the bulk dry density (kg m⁻³) and ρ_s the grain density (kg m⁻³). For the grain density a value of 2800 kg m⁻³ was used; similar values were considered by Muurinen (1994), Bourg et al. (2006) and Van Loon et al. (2007). Subsequently, the Na-montmorillonite plugs were saturated for 2 weeks with the corresponding porewater solution (Table 2) calculated with GEMS (Kulik, 2013) according to Shafizadeh et al. (2019), with a cylindrical metallic dummy occupying the space in the Teflon holder foreseen for the hardened cement paste.

The interaction of the highly alkaline cement porewater with Na-montmorillonite is likely to modify the interlayer cation inside the montmorillonite. Therefore additional samples of homoionic Ca- and K-montmorillonite were prepared to measure reference diffusive properties of these forms. Ca- and K-montmorillonite were produced by contacting the Na-montmorillonite with CaCl₂ and KCl solutions, respectively.

2.2.2. OPC cement paste

Hardened Portland cement paste (Type CEM I 52.5 N HTS, Lafarge, France) was cast in 2003 (Tits et al., 2003). The cement paste was produced using a special procedure (Döhning et al., 1994) and a high water cement ratio of 1.3 leading to a porosity of 63% ± 5% determined by MIP (Sarott et al., 1992). The high porosity of the cement was selected to increase the diffusivity and thus to accelerate the reactions at the interface. The cement was produced using plexiglas moulds and let hydrate at air conditions for 6 months. After that, the samples were introduced in a solution (Table 2) in equilibrium with the cement (Tits et al., 2003). The samples were kept saturated all the time in the corresponding cement solution in a sealed container. A slice of about 1 cm was cut from the samples, then cylindrical samples of 5 mm diameter

were drilled out of the slices. These cylinders were then placed into the cells in close contact to the Na-montmorillonite. Jakob et al. (1999) investigated the evolution of the hydraulic conductivity for the same type of cement and observed that after 3 months the hydraulic conductivity of this cement reached a constant value. Measurements performed months to years after the production indicated the same value. We assume therefore that the cement properties were not significantly changing in the following years.

The cement porewater composition, which was used in the reservoirs attached to the sample, is listed in Table 2. The chemical composition of the cement, determined by XRF, is listed in Shafizadeh et al. (2015).

2.3. Through-diffusion experiments

After emplacement in the cell, the cement-clay samples were saturated for two weeks by connecting each part of the cell with a reservoir containing the corresponding porewater solution (Table 2). To start the diffusion experiment the tracer had to be added to one of the reservoirs ('high concentration side'). The tracer was inserted on the cement side in a 50 mL reservoir. For the different experiments the used activity concentration varied between 500 and 2000 Bq mL⁻¹ for HTO (GE Healthcare, UK) and 500–40000 Bq mL⁻¹ for ³⁶Cl⁻ (Eckert and Ziegler, D). The reservoir connected to the clay ('low concentration side') had a volume of 20 mL and was frequently replaced to keep its concentration near zero.

The accumulated HTO and ³⁶Cl⁻ activity was subsequently measured by liquid scintillation counting (Tri-carb 2250 CA, Canberra-Packard) using Ultima Gold XR (Canberra-Packard) as scintillation cocktail, with a ratio of 5 mL of sample to 15 mL of cocktail. The radioisotopes were obtained from Isotope Products Europe (Blaseg, Germany). For solution preparation the reagents used were provided by Fluka (Buchs, Switzerland) or Merck (Dietikon, Switzerland), and the de-ionized ultrapure water was Milli-Q® (Merck, Switzerland).

Tritiated water is an uncharged species and should be able, in principle, to diffuse through the entire porosity domain. HTO is in general considered as a non-sorbing tracer, although Tits et al. (2003) reported some sorption on the same cement used in this experiment. A slight retardation in some cases was observed as well in the experiments discussed in this article.

Chloride-36 is negatively charged. Some aspects need to be considered while performing diffusion experiments on cement-clay interfaces with this tracer: (i) due to the negative charge of the clay surfaces, ³⁶Cl⁻ diffusivity through clay samples is known to be lower than that of HTO; this feature is related to the relatively small portion of total porosity accessible for anions in montmorillonite (Pusch, 2001; Van Loon et al., 2007). (ii) Glaus et al. (2010) showed how the diffusivity of ³⁶Cl⁻ in clay depends on the chloride content in the electrolyte solution. (iii) On the cement side, the OPC paste contains AFm and C-S-H phases (both represent hydration products of Portland cement), on which chloride

can be sorbed. Afm are a family of hydrated Ca–Al phases, which possess positively charged surfaces (Taylor, 1997). C–S–H are the main hydration product of OPC and are mainly responsible for the cement strength; they can also take up anions (Beaudoin et al., 1990; Plusquellec and Nonat, 2016). Accordingly, chloride interacts with cement when diffusing through it; such sorption phenomena have been extensively investigated in the literature (Page et al., 1981; Jensen et al., 1999; Hirao et al., 2004). During our experiments chloride sorption was observed as retardation during the transient phase; for the calculation of D_e , however, only the steady state diffusion was considered (see chapt. 2.4), which is independent of sorption.

2.4. Through-diffusion experiments: data analysis

Given the experimental set-up, diffusion can be considered as a one-dimensional process, where the tracer diffuses through a 1D domain with a length L , with a flux J . For a steady-state condition, Fick's first law can be applied:

$$J = -D_e \frac{\partial C}{\partial x} \quad (2)$$

J is the flux [Bq m⁻² s⁻¹ or mol m⁻² s⁻¹], D_e is the effective diffusion coefficient of the sample [m² s⁻¹], C is the tracer concentration [Bq m⁻³] or [mol m³] and x is the length [m].

In a non-steady-state system Fick's second law applies:

$$\frac{\partial C}{\partial t} = \frac{D_e}{\alpha} \frac{\partial^2 C}{\partial x^2} \quad (3)$$

where t is time, α is the rock capacity, defined as:

$$\alpha = \varepsilon + \rho_b K_d \quad (5)$$

K_d is the equilibrium distribution coefficient [m³ kg⁻¹], ε the (accessible) porosity and ρ_b the bulk dry density [kg m⁻³]. For a non-sorbing tracer K_d is zero and therefore the rock capacity is equal to the (accessible) porosity.

Eq. (3) only applies for spatially constant parameters. More generally for our cement-clay system where D_e is varying along the sample, eq. (3) has to be rewritten as

$$\alpha(x) \frac{\partial C}{\partial t} = \frac{\partial}{\partial x} D_e(x) \frac{\partial C}{\partial x}, \quad (6)$$

Because D_e is calculated in our experiments from the steady state, $\frac{\partial C}{\partial t} = 0$ and eq. (2) can be used for the determination of the domain averaged D_e of the sample.

The effective diffusion coefficient D_e gives an indication of the diffusive properties of the sample, and can be expressed as

$$D_e = \varepsilon \frac{D_w}{G} \quad (7)$$

D_w [m² s⁻¹] is the diffusion coefficient of the species in pure water, and G [-] is a term accounting for geometrical factors (González Sánchez et al., 2008) including the tortuosity and the constrictivity of the porous network. These two parameters are difficult to be measured separately and therefore lumped into G .

The initial and the boundary conditions are:

$$\begin{aligned} c(x, t) &= 0 & x > 0 & t = 0 \\ c(0, t) &= C_0 = \text{constant} & x = 0 & t > 0 \\ c(L, t) &= 0 & x = L & t > 0 \end{aligned} \quad (8)$$

The concentration C_0 [mol m⁻³] of the tracer on the cement side (high concentration side) is assumed to be constant, whereas $c(L, t)$ [mol m⁻³], the concentration on the clay side (low concentration side), is assumed to be zero (Van Loon and Soler, 2003).

The flux at the low concentration side is therefore given by:

$$J(L, t) = D_e \left. \frac{\partial c}{\partial x} \right|_{x=L} \quad (9)$$

Solving eq. (3) for the given initial and boundary conditions results in an analytical expression for the cumulated diffused activity A_{dif}^t [Bq] or [mol] of a tracer in the low concentration reservoir as a function of time (Crank, 1979):

$$A_{dif}^t = S \cdot L \cdot C_0 \cdot \left(\frac{D_e \cdot t}{L^2} - \frac{\alpha}{6} - \frac{2 \cdot \alpha}{\pi^2} \sum_{n=1}^{\infty} \frac{(-1)^n}{n^2} \cdot \exp\left(-\frac{D_e \cdot n^2 \cdot \pi^2 \cdot t}{L^2 \cdot \alpha}\right) \right) \quad (10)$$

where S is the cross-sectional area [m²] and t is the time [s]. At steady state conditions ($t \rightarrow \infty$) the solution reduces to:

$$A_{dif}^t = S \cdot L \cdot C_0 \cdot \left(\frac{D_e \cdot t}{L^2} - \frac{\alpha}{6} \right) \quad (11)$$

and the accumulated activity becomes a linear function of time

$$A_{dif}^t = a \cdot t + b \quad (12)$$

where $a = \frac{S \cdot C_0 \cdot D_e}{L}$ and $b = -\frac{S \cdot L \cdot C_0 \cdot \alpha}{6}$.

Thus, an average sample D_e can be derived from the slope of the accumulated activity in the linear regime (Van Loon and Soler, 2003). In such a simplified description, the resulting rock capacity α represents a combined contribution of the two components (cement and clay). The resulting value of α is therefore difficult to interpret.

2.5. Determination of the effective diffusion coefficient for the clay ($D_{e,clay}$) and for the clay skin ($D_{e,skin}$)

The measured effective diffusion coefficient represents the diffusive flux through the entire cell domain which consists of filters, clay and cement (Fig. 2). The filters need therefore to be considered in the calculation to obtain only the diffusive properties of the cement and of the clay. The filters are taken into account by considering the system as a series of resistances (Glaus et al., 2015):

$$\frac{1}{R_{tot}} = \frac{1}{R_{clay}} + \frac{1}{R_{cem}} + \frac{2}{R_{filters}} \quad (13)$$

where R is

$$R = \frac{\Delta x}{D_e} \quad (14)$$

and Δx is the dimension of each component of the domain. Using eq. (13) the properties of the clay domain and subsequently of the clay skin can be estimated assuming known properties of all other components. We

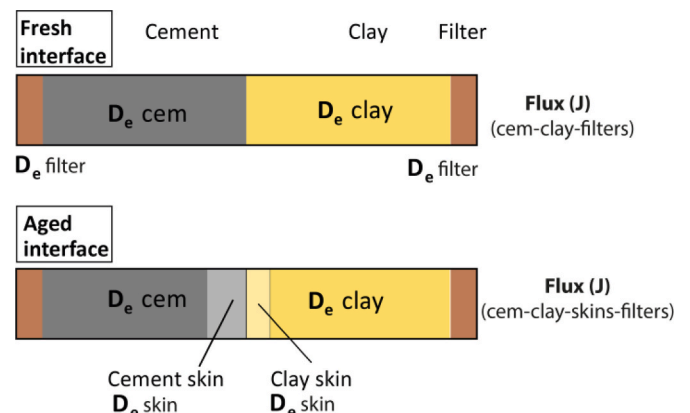


Fig. 2. Schematic view of a fresh and an aged cement-clay interface sample.

generally assumed in our analysis a constant D_e of the cement, but considered the effect of a potential alteration in the error estimation in the following section. The filter properties and the cement and clay diffusion coefficients used for this derivation are listed in Table 3. Fig. 3 illustrates how the diffusion coefficients of different components were determined.

2.6. Error estimation on the derived diffusion coefficients

The estimation of the error on the total diffusion coefficient (raw D_e) was performed according to Van Loon and Soler (2003). In general, the derived diffusion coefficients have a relatively small error ($\sim\pm 6\%$). The errors of D_e for the other models were calculated following first order error propagation. Some additional errors may arise from (unknown) changes in filter and cement properties, or from the choice of the steady state interval from which D_e was calculated. Glaus et al. (2008) performed diffusion experiments on similar filters as those used for the present study, and reported for filters previously used with Na-montmorillonite a decrease of up to 45% of the derived filter D_e (reaching a value of $1.1 \times 10^{-10} \text{ m}^2 \text{ s}^{-1}$). In this study for some samples the filters were exchanged during the diffusion experiments (once steady state conditions were reached since several days) to study the variation of the total diffusive properties. For the tested samples only slight variations of the flux were observed confirming the low impact of the filters on the derived sample D_e . For the $D_{e,\text{sample}}$ derivation we considered for both filters the value of a used filter ($1.1 \times 10^{-10} \text{ m}^2 \text{ s}^{-1}$). Cement may affect less strongly the filter properties than clay, but a slight decrease of the diffusive properties is also likely to take place. Therefore, we considered the same value also for the filter on the cement side, leading to a maximum value for the derived sample diffusion coefficient ($D_{e,\text{sample}}$).

According to eqs. (13) and (14), to derive the $D_{e,\text{clay}}$, the cement diffusion coefficient must be known. For our calculation $D_{e,\text{cem}}$ was set to that measured by Tits et al. (2003), which is $2.8 \times 10^{-10} \text{ m}^2 \text{ s}^{-1}$ (cement porosity: 0.63). This assumption is based on observations made by Sarott et al. (1992) on cement samples produced in the same way, where hydraulic conductivity was measured over longer period, concluding that the hydration was largely completed after 3 months and that the hydraulic conductivity remains constant after that time. Moreover the samples were stored under nitrogen atmosphere, strongly reducing the carbonation chances, which may influence the cement diffusive properties. Although the cement properties are not expected to be significantly altered, we estimated the effect of a modified cement diffusion coefficient ($D_{e,\text{cem}}$) on the derived $D_{e,\text{clay}}$ (Fig. 4a). We furthermore estimated the error arising from neglecting the alteration of the diffusion properties of the cement skin. Shafizadeh et al., 2020 observed on the cement side porosity variations with a local maximum of +10% porosity. The impact of this cement skin (with different spatial extension) is shown in Fig. 4b.

The high porosity of the used cement paste results in a high $D_{e,\text{cem}}$. Therefore, according to eq. (13), a variation of the cement diffusion coefficient would only slightly affect the derived $D_{e,\text{clay}}$. Furthermore, with increasing interaction time the formation of the low porosity region inside the clay further reduces the overall diffusivity of the system, making the variation of the cement properties progressively less influent. Thus, a modification of the cement diffusion coefficient, or the

formation of a cement skin with slightly altered porosity will have little impact on the derived clay diffusion coefficient as clearly visible in Fig. 4a and b.

For the error estimation we considered a variation of the filters and of the cement properties by 10% (on the initial value). This led to a general error of $\sim \pm 20\%$ for the entire clay domain (model 2). For the skin region (model 3), additional uncertainties (e.g., skin extension, unaltered clay D_e) increased the propagated error up to $\pm 45\%$.

3. Results

3.1. HTO through-diffusion experiments

The data shown in Fig. 5a, representing the derived raw D_e (filters, cement and clay), can be divided into two subgroups. For the first subgroup (red symbols in Fig. 5a), a remarkable reduction of the determined D_e during the first 12–17 months is observed, followed by a subsequent moderate reduction until 73 months. There is a certain scatter between the data obtained on different cement-clay samples for this subgroup. This fact is certainly related to i) slight variations in the density of the clays and ii) slight variations in the length of the cement and clay parts of the samples (see Table 1), possibly also to iii) partial clogging of filter pores, leading to a decrease of the diffusive properties of the entire system, or also iv) small fractures or heterogeneities which may occur during the insertion or during the reaction of the cement with the clay, resulting in diffusivity change. The second subgroup showed a clearly different overall trend: the D_e of these samples does not significantly vary over time (blue squares, Fig. 5a), it decreases only slightly with respect to the initially measured values. Shafizadeh et al. (2019) using neutron imaging did not detect any significant porosity variation for such samples; the reason why the low porosity region did not form in these samples is unclear and under investigation. Table 3 resumes the derived effective diffusion coefficients for all the interface samples that were measured.

From the raw D_e values (Fig. 5a), first the D_e values of the entire samples ($D_{e,\text{sample}}$) consisting of cement and clay were calculated according to Eq. (13) and Table 1. In order to reduce the variability in the derived diffusion data caused by the slight variation of the clay and cement domain sizes, effective diffusion coefficients for the clay part ($D_{e,\text{clay}}$) were then calculated from the overall sample diffusion coefficients ($D_{e,\text{sample}}$), assuming that the main changes affecting diffusion occurred in the clay. This assumption is based on the results of Shafizadeh et al. (2020), who reported a region with only slightly higher porosity developing on the cement side of the interface, but a low porosity region of about 1 mm developing on the clay side close to the interface. The derived average D_e of the ~ 5 mm clay plug represents the properties of the region with unvaried porosity (unaltered clay), and the properties of the skin (Fig. 3). Assuming a constant effective diffusion coefficient in the cement plug equal to the one reported by Tits et al. (2003), D_e values for the clay part were obtained using eq. (13) (Fig. 5b). The general trend is similar to the one observed for the derived $D_{e,\text{raw}}$ (Fig. 5a): a strong decrease of diffusivity during the first 12–17 months and a subsequent slower D_e decrease after 17 months. The scatter between the data points became visibly smaller compared to that of the raw D_e shown in Fig. 5a, confirming that an important variability of the sample D_e is related to the variability of the lengths of the cement and

Table 3
Effective diffusion coefficients (D_e , in $\text{m}^2 \text{ s}^{-1}$) used for calculation of the interface properties.

	D_e HTO	D_e $^{36}\text{Cl}^-$	Comment
Hardened OPC paste	2.8×10^{-10}	1.6×10^{-10}	Tits et al. (2003) and Sarott et al. (1992)
Filter (Peek)	1.1×10^{-10}	1.1×10^{-10}	Glaus et al. (2008)
Na-mont. 1500 kg m^{-3}	6.1×10^{-11}	5.2×10^{-12}	Present study, average value (Table 5)
K or Ca-mont. 1500 kg m^{-3}	1.0×10^{-10}	1.5×10^{-11}	Present study, average value (Table 5)

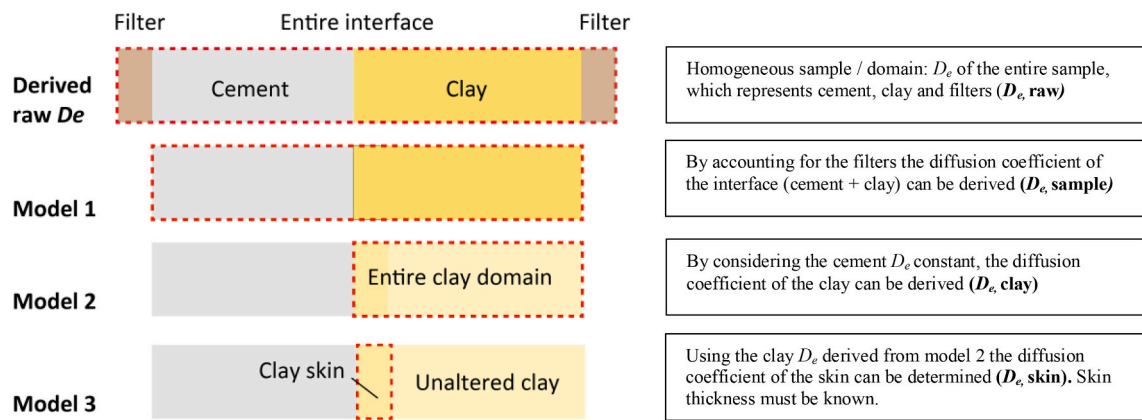


Fig. 3. Schematic representation of the region or component for which D_e was obtained. The red dashed line represents the region taken into consideration for D_e derivation in each model.

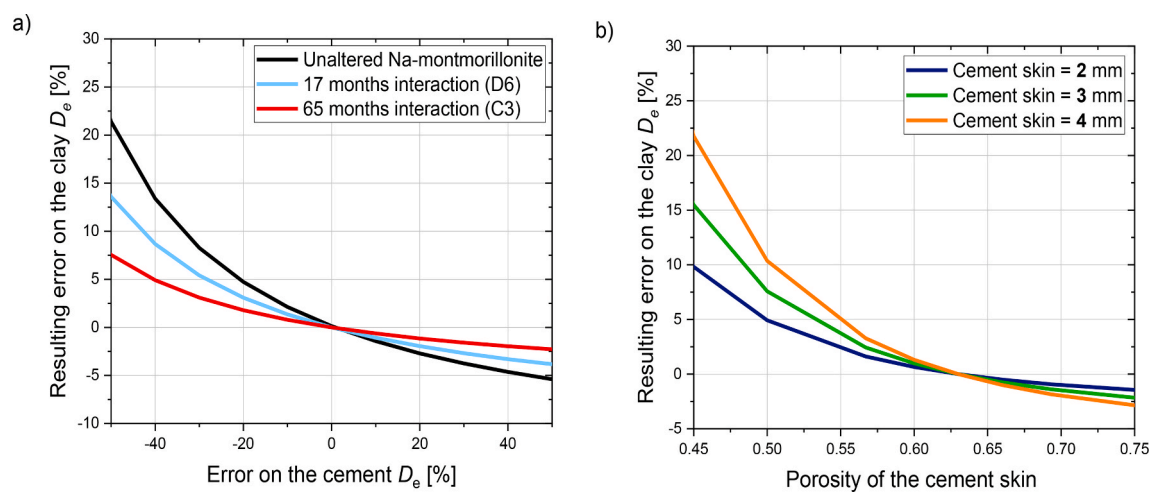


Fig. 4. Variation of the derived diffusion coefficient D_e of the clay part (in %) upon a variation of the diffusion properties of the cement part. (a) Variation of D_e clay depending on the hypothetical error of the used D_e of the cement part. The three lines represent different interaction times of the cement-clay interface. (b) Variation of D_e clay depending on assumed porosity and extent of cement skin, at an interaction time of 65 months. The longer the interaction time, the smaller is the influence of the cement skin properties on D_e of the clay part.

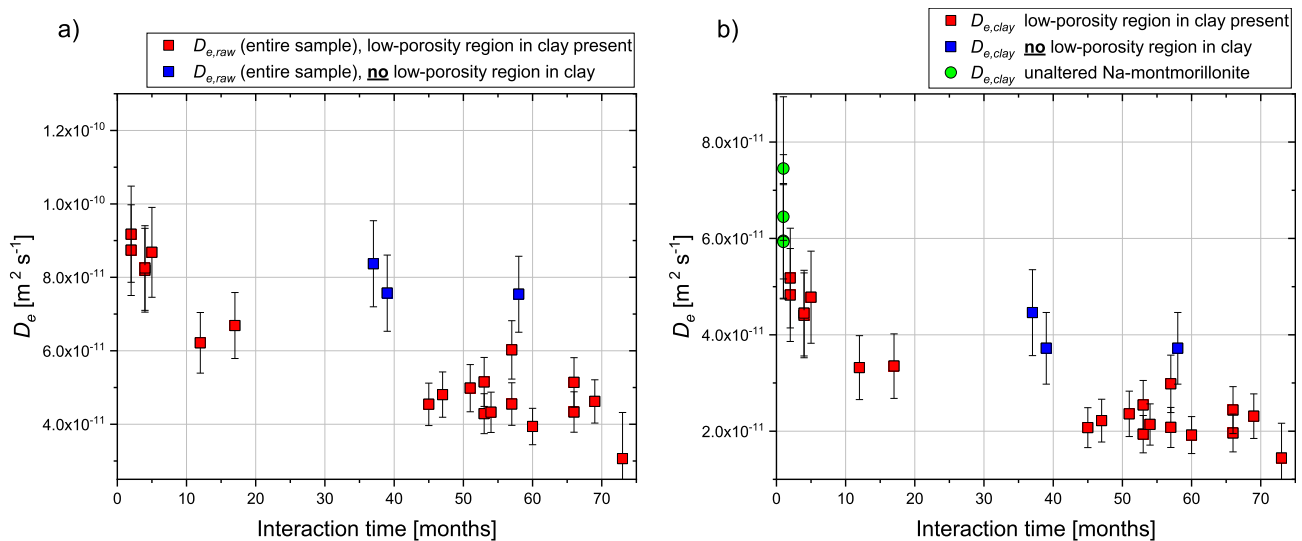


Fig. 5. Evolution of the average diffusion coefficient (D_e) of HTO for (a) the entire system ($D_{e, \text{raw}}$) composed of filters, cement and clay); and (b) for the clay part only ($D_{e, \text{clay}}$).

Table 4

Effective diffusion coefficients of HTO ($\text{m}^2 \text{s}^{-1}$) for the various regions of the clay domain (subdivided in 4 parts, see Fig. 4). Raw D_e : obtained D_e for sample and filters. Model 1: the interface sample (cement, clay). Model 2: the entire clay region. Model 3: skin region evaluated assuming either a diffusion coefficient of Na-montmorillonite (model 3a) or of K, Ca-montmorillonite (model 3b) for the unaltered clay part (Table 3). For the $D_{e,skin}$ calculation, a skin thickness of 1 mm was used (2 mm for C1) according to Shafizadeh et al. (2019, 2020).

Sample	Interaction time (months)	D_e of the entire sample ($D_{e,raw}$)	D_e interface without filters (Model 1)	D_e of the entire clay domain, (Model 2)	D_e of the skin region. Unaltered clay = Na-mont. (Model 3a)	D_e of the skin region. Unaltered clay = Ca, K-mont. (Model 3b)
C1	12	6.2×10^{-11}	5.5×10^{-11}	3.3×10^{-11}	2.1×10^{-11}	1.5×10^{-11}
	54	4.3×10^{-11}	3.7×10^{-11}	2.1×10^{-11}	1.1×10^{-11}	9.0×10^{-12}
	60	3.9×10^{-11}	3.3×10^{-11}	1.9×10^{-11}	9.2×10^{-12}	7.9×10^{-12}
	73	3.1×10^{-11}	2.5×10^{-11}	1.4×10^{-11}	6.4×10^{-12}	5.8×10^{-12}
C3	5	8.7×10^{-11}	8.2×10^{-11}	4.8×10^{-11}	2.6×10^{-11}	1.5×10^{-11}
	47	4.8×10^{-11}	4.1×10^{-11}	2.2×10^{-11}	6.3×10^{-12}	5.4×10^{-12}
	53	4.3×10^{-11}	3.6×10^{-11}	1.9×10^{-11}	5.2×10^{-12}	4.6×10^{-12}
	66	4.3×10^{-11}	3.7×10^{-11}	2.0×10^{-11}	5.3×10^{-12}	4.6×10^{-12}
D6	2	8.7×10^{-11}	8.2×10^{-11}	4.8×10^{-11}	2.6×10^{-11}	1.6×10^{-11}
	4	8.2×10^{-11}	7.6×10^{-11}	4.4×10^{-11}	2.1×10^{-11}	1.3×10^{-11}
	17	6.7×10^{-11}	6.0×10^{-11}	3.3×10^{-11}	1.2×10^{-11}	9.1×10^{-12}
D11	2	9.2×10^{-11}	8.7×10^{-11}	5.2×10^{-11}	3.2×10^{-11}	1.7×10^{-11}
	4	8.3×10^{-11}	7.7×10^{-11}	4.4×10^{-11}	2.1×10^{-11}	1.4×10^{-11}
C5	51	5.0×10^{-11}	4.3×10^{-11}	2.4×10^{-11}	6.7×10^{-12}	5.7×10^{-12}
	53	5.2×10^{-11}	4.4×10^{-11}	2.5×10^{-11}	7.3×10^{-12}	6.0×10^{-12}
	66	5.1×10^{-11}	4.5×10^{-11}	2.4×10^{-11}	7.2×10^{-12}	6.0×10^{-12}
C15	45	4.5×10^{-11}	3.9×10^{-11}	2.1×10^{-11}	5.7×10^{-12}	5.0×10^{-12}
	57	6.0×10^{-11}	5.3×10^{-11}	3.0×10^{-11}	9.6×10^{-12}	7.6×10^{-12}
C8	39	7.6×10^{-11}	6.9×10^{-11}	3.7×10^{-11}	–	–
	58	7.5×10^{-11}	6.9×10^{-11}	3.7×10^{-11}	–	–
C20	37	8.4×10^{-11}	7.8×10^{-11}	4.5×10^{-11}	–	–
C11	57	4.5×10^{-11}	3.9×10^{-11}	2.1×10^{-11}	5.7×10^{-12}	5.0×10^{-12}
C4	69	4.6×10^{-11}	3.9×10^{-11}	2.3×10^{-11}	6.1×10^{-12}	5.2×10^{-12}

clay part. The remaining variabilities are probably related to minor variations of the material density (and composition) and the contamination of the filters.

The earliest measured D_e value for the clay region, defined as the average value after 2–4 months, is $4.7 \times 10^{-11} \text{ m}^2 \text{ s}^{-1}$, which is lower than values measured for unaltered Na-montmorillonite samples at a similar density (green circles Fig. 5b; Table 5). One has to keep in mind that any variation of the cement or of the filters diffusion coefficient directly affects the derived D_e value of the clay. But more importantly, this ‘initial’ D_e of the clay region represents a value after 2–4 months of interaction, due to the time needed to perform the through-diffusion experiments. The difference between this ‘initial’ value and that of unaltered Na-montmorillonite means that reactions at the interface already occurred and possibly a skin already started forming, leading to a decrease of the D_e . After 12–17 months the $D_{e,HTO}$ rapidly decreased to $3.3 \times 10^{-11} \text{ m}^2 \text{ s}^{-1}$. Between 17 and 73 months the $D_{e,HTO}$ decreased further to an average value of $2.2 \times 10^{-11} \text{ m}^2 \text{ s}^{-1}$. Interestingly from 45 to 73 months the $D_{e,HTO}$ remained quite stable. This fact suggests that from 45 months on the interface reactivity is clearly reduced. Since no data were obtained between 17 and 45 months of interaction it is possible that the reactivity of the interface was reduced already earlier.

Table 5

Effective diffusion coefficients for $^{36}\text{Cl}^-$ ($\text{m}^2 \text{ s}^{-1}$) for the various regions of the clay domain (subdivided in 4 parts, see Fig. 4). Raw D_e : obtained D_e for sample and filters. Model 1: the interface sample (cement, clay). Model 2: the entire clay region. Model 3: skin region evaluated assuming an average diffusion coefficient of Na-montmorillonite for the unaltered clay part (Table 3). For the $D_{e,skin}$ calculation, a skin thickness of 1 mm was used according to Shafizadeh et al. (2020).

Sample	Interaction time (months)	D_e of the entire sample ($D_{e,raw}$)	D_e interface without filters (Model 1)	D_e of the entire clay domain (Model 2)	D_e of the skin region. Unaltered clay = Na-mont (Model 3)
D11	2	2.0×10^{-11}	1.6×10^{-11}	8.4×10^{-12}	–
	4	1.5×10^{-11}	1.2×10^{-11}	6.4×10^{-12}	–
D6	17	5.7×10^{-13}	4.4×10^{-13}	2.2×10^{-13}	4.6×10^{-14}
C4	69	3.1×10^{-13}	2.4×10^{-13}	1.3×10^{-13}	2.5×10^{-14}
C11	57	3.8×10^{-14}	2.9×10^{-14}	1.5×10^{-14}	3.0×10^{-15}
C15	57	6.4×10^{-13}	4.9×10^{-13}	2.5×10^{-13}	5.1×10^{-14}
C8	58	1.4×10^{-11}	1.1×10^{-11}	5.5×10^{-12}	–

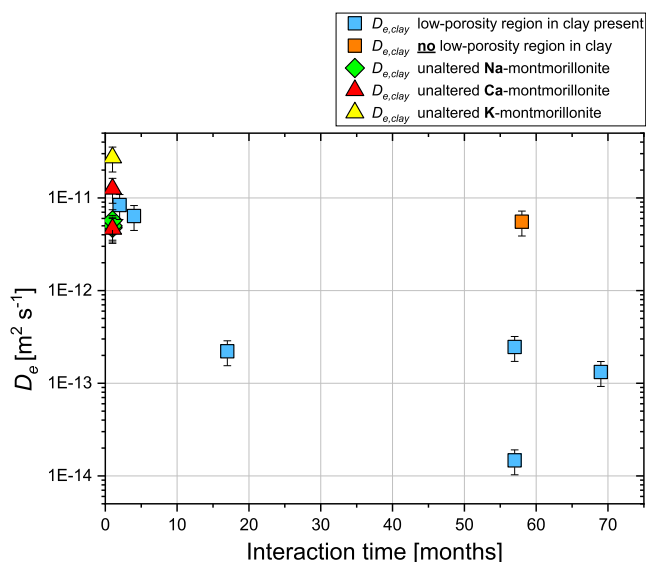


Fig. 6. Evolution of the diffusion coefficient (D_e) of $^{36}\text{Cl}^-$ for the clay part only; for all measured interface samples and for various unaltered montmorillonite samples.

flux even when using the highest initial activity (40 kBq mL^{-1}). Furthermore, as mentioned in the previous section, not all the samples reacted similarly: some of them show a very small reduction of the diffusive flux over time. In one of these samples (where porosity hardly evolved, as observed by Shafizadeh et al., 2019) the D_e of $^{36}\text{Cl}^-$ changed similarly as that of HTO. In fact, the $D_{e,\text{Cl}}$ was only slightly lower than the initial value in this sample (orange symbol, Fig. 6).

4. Discussion

4.1. Interface reactivity: evolution of diffusivity and porosity

The observed changes of the diffusive fluxes for HTO and chloride indicate a strong reduction of the D_e of the entire sample ($D_{e,\text{sample}}$), or also of the clay part ($D_{e,\text{clay}}$), during the first 12–17 months and a subsequent slower reduction. According to eq. (7) a reduction of the diffusion coefficient is related to a decrease of the (average) porosity ϵ and an increase of the geometrical factor G , which includes the tortuosity. The strong chemical differences between cement and clay porewater trigger mass fluxes at the material interface and lead to quick mixing of the porewater in the interface region. This change in the pore water composition induces dissolution-precipitation reactions and mineralogical changes, which affect both the porosity and the geometry of the pores.

Analysis of the samples conducted by Shafizadeh et al. (2015, 2020) showed a reduction of the porosity inside the first mm of the clay and a slight increase of porosity on the cement side. This porosity evolution certainly affects fluxes measured in our through-diffusion experiments. At the same time, the remaining part of the clay region without clear porosity evolution, which was called “unaltered or unreacted clay part”, may have undergone chemical changes too. Due to the high alkalinity of the cement porewater and the higher cation exchange selectivity of montmorillonite for Ca and K compared to Na, the montmorillonite is expected to transform from the initial Na form into a K and Ca form near the interface. As cation exchange reactions are fast compared to mineral alterations, it is likely that this transformation into a K and Ca form has extended clearly beyond the zone of altered porosity, possibly throughout the whole clay plug. Ca- and K-montmorillonite have different diffusive (González Sánchez et al., 2008) and swelling properties (Karland, 2006) compared to Na-montmorillonite. González

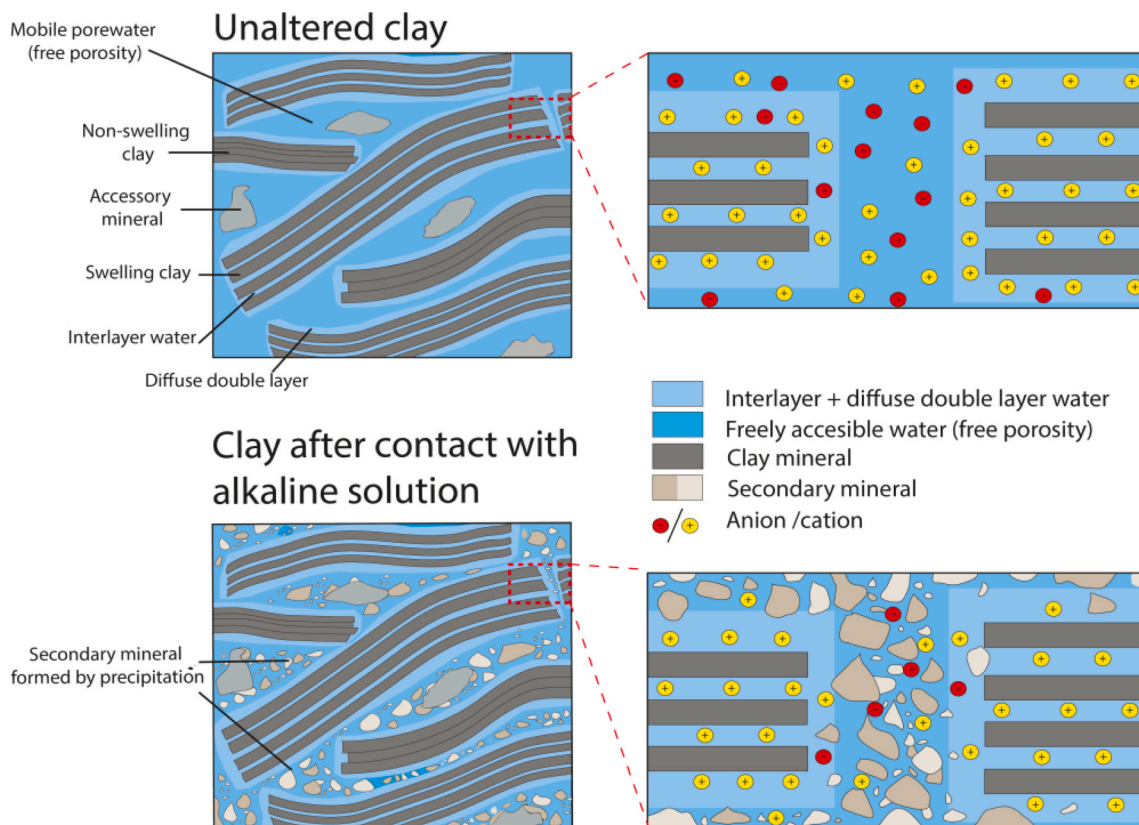


Fig. 7. Schematic illustration of clay minerals and respective pore environments for unaltered clay, and for clay after contact with alkaline solution (e.g. cement porewater). Precipitation location (free porosity only or interlayer/diffuse double layer) and precipitation type (homogeneous vs heterogeneous) are not clear.

Sánchez et al. (2008) investigated diffusion coefficients of Ca and Na-montmorillonites for a bulk dry density of 1900 kg m^{-3} and two different ionic strengths. In these experiments the D_e of HTO in Ca-montmorillonite was found to be about $\sim 60\%$ higher than that in Na-montmorillonite. In the experiments performed during the present study, for a compaction of $1500 \pm 100 \text{ kg m}^{-3}$ the D_e of HTO in Ca- and K-montmorillonite were found to have similar values, and were $\sim 40\%$ higher than the D_e of HTO in Na-montmorillonite. Thus the dependence of the HTO diffusivity on the composition of the montmorillonite needs to be considered while dealing with the evolution of the diffusivity of the clay at the interface. Preliminary (unpublished yet) investigation on the present samples by means of SEM/EDX, indicate a partial transformation of Na-montmorillonite into the Ca and K form, as already described in the literature (Mosser-Ruck and Cathelineau, 2004; Gaucher and Blanc, 2006).

The stronger reduction of the diffusion coefficient of chloride with respect to HTO is related to the montmorillonite structure. The distinction of different pore environments in clays (Fig. 7) and the magnitude of diffusive fluxes or generally of solute transport in these environments remain a matter of debate (Wersin et al., 2004; Appelo, 2013). Often the total porosity in clay rocks is subdivided into (i) free porosity, a domain with a charge balanced electrolyte solution, (ii) interlayer porosity between single TOT layers of swelling clay minerals, containing hydrated cations that compensate the negative structural charge, and (iii) diffuse double layer (DDL) porosity, containing water, charge compensating cations and anions. Interlayer water is generally thought to contain mainly (or even only) cations, whereas the DDL displays an excess of cations and the free porosity is charge neutral (Mitchell and Soga, 1992; Bradbury and Baeyens, 2003; Appelo, 2013). Interlayer and diffuse double layer are partly also considered as a single compartment, which can be described by a Donnan approach (Jenni et al., 2017), where the Donnan pore water contains also an excess of cations. At a bulk dry density of 1500 kg m^{-3} most of the porosity of Na-montmorillonite is interlayer porosity (Pusch, 2001). Precipitation of new mineral phases is thought to occur preferably in the free porosity. Interlayer pores are expected to be less accessible or inaccessible for anions. Therefore precipitation of new minerals taking place in the free porosity is expected to affect the chloride flux more strongly than the HTO flux. This conclusion is supported by the observed evolution of the diffusion coefficients ratio: the initial $D_{e,\text{HTO}}/D_{e,\text{Cl}}$ for unaltered

Na-montmorillonite samples is about 10; after 17 months of reaction this ratio is around 150. At longer interaction times, ratios between 120 and 1400 were obtained. It has to be noted that in several cells no chloride flux at all could be measured after 4 years or more of interaction, even though the initial activity at the inlet was increased in repeated experiments to possibly overcome the detection limit at the low concentration side for very low $^{36}\text{Cl}^-$ fluxes. For the cells where no $^{36}\text{Cl}^-$ flux was detected, it can be stated that the diffusion coefficient of the entire sample had to be lower than $10^{-14} \text{ m}^2 \text{ s}^{-1}$ (no flux observed with a C_0 activity of 40 kBq mL^{-1}), which indicates an almost complete blocking of the anion accessible porosity.

Mineralogical investigation and simulation of bentonite-OPC interaction made by other authors indicate the possible formation of many different mineral phases, depending on the system composition and condition (Cuevas et al., 2006; Savage et al., 2011; Fernández et al., 2017). In our case the nature of the phase/s precipitating is currently under investigation; but the experimental conditions (CO_2 free environment and ambient temperature) suggest that carbonates and/or zeolite are unlikely to be the major phase responsible for the porosity decrease.

4.2. Temporal development of the reactivity at the interface

The D_e evolution of the clay domain (model 2, see Fig. 3) for both HTO and $^{36}\text{Cl}^-$ (Figs. 5 and 6) give an estimate of a characteristic time required for substantial mineral transformations at the interface. Two distinct phases could be identified: a first period (0–17 months) related to a strong decrease of the diffusivity (46% $D_{e,\text{HTO}}$ reduction, and $\sim 96\%$ decrease for $D_{e,\text{Cl}}$) and a second period (17–73 months) with moderate decrease of the D_e . It was further noted that the $D_{e,\text{HTO}}$ remained quite stable during the period between 45 and 73 months. The two periods with different evolution of the diffusive properties are likely related to stages of dissolution-precipitation reactions occurring at the interface. Although only limited data are available at the moment, it can be hypothesized that most of the reactions occurred already during the first 1.5 years. For the same samples, Shafizadeh et al. (2020) observed by means of neutron imaging a strong porosity reduction in the clay within the first 17 months and a less prominent porosity decrease after this period. The porosity reduction following mineral reactions slows down diffusive mass transfer and thus reduces the further reactivity of the

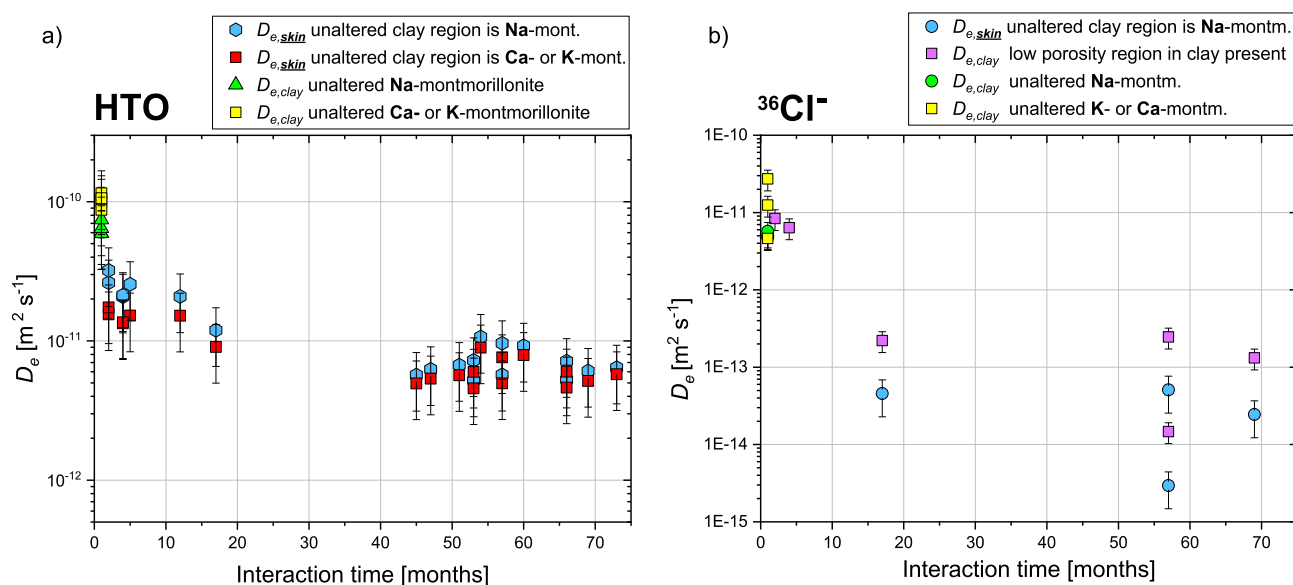


Fig. 8. a) Evolution of the effective HTO diffusion coefficient of the clay skin ($D_{e,\text{skin}}$). The diffusion coefficient is calculated considering the unreacted part of the clay as Na-montmorillonite (blue) or K/Ca-montmorillonite (red). b) Evolution of the effective diffusion coefficient, for $^{36}\text{Cl}^-$, of the entire clay domain (pink) and of the clay-skin (blue). The diffusion coefficient of the skin ($D_{e,\text{skin}}$) is calculated considering the unreacted part of the clay as Na-montmorillonite.

interface. This trend was observed as well in field experiments (Mäder et al., 2017) or in numerical simulations (Kosakowski and Berner, 2013).

4.3. Considerations on the skin properties

Measurements performed by Shafizadeh et al. (2020) provide an estimate of the thickness (~1 mm) of the low porosity alteration zone developing inside the clay. According to eqs. (13) and (14), by making some assumption as previously discussed, it is possible to derive a rough estimation of the diffusive properties of the clay skin. The obtained values are only an approximation because of other unknown factors such as changes in the diffusive properties of filters, and the slight variation of cement porosity (Shafizadeh et al., 2020). Nevertheless, it can be assumed with high confidence that the low porosity region in the clay compartment next to the interface represents the bottleneck domain which limits the overall HTO and ion flux through the interface. In such a system slight changes in the diffusive properties of cement or of the filters should have a minor impact on the overall properties of the sample. The clay domain was split in two regions: an unaltered clay compartment and an altered skin at the interface (Fig. 8a and b). As has been discussed earlier the diffusive properties of the clay with more or less unaltered porosity are not certain. Some chemical reactions (e.g. cation exchange in the interlayer) are very likely to take place on the time scale of the experiments due to the high contents of K^+ and Ca^{2+} of the cement porewater. Therefore the calculated skin parameters are subject to relatively large uncertainties. The diffusion coefficient of montmorillonite can vary remarkably depending on its cationic composition (Table 6). Assuming that all montmorillonite turned into Ca- or K-montmorillonite via cation exchange, the calculated $D_{e,HTO}$ of the skin is lower by about 26% (12 and 17 months interaction) or about 15% (>45 months interaction) compared to assuming the clay remained Na-montmorillonite (Fig. 8a). In the former case, $D_{e,skin}$ for HTO becomes $\sim 1.2 \times 10^{-11}$ after 12–17 months of interaction and reaches an average value of 6×10^{-12} between 45 and 73 months. In the latter case, the clay skin D_e for HTO after 12–17 months becomes $\sim 1.7 \times 10^{-11} \text{ m}^2 \text{ s}^{-1}$ and reaches an average value of 7×10^{-12} between 45 and 73 months.

Regarding chloride (Fig. 8b), the measured diffusivity values are so low and their variability at later times so large that considering the diffusive properties of the unreacted clay part as that of Na-

montmorillonite or of K or Ca-montmorillonite does hardly affect the resulting diffusion coefficients obtained for the skin. After 17 months of interaction the chloride $D_{e,skin}$ is calculated as $4.6 \times 10^{-14} \text{ m}^2 \text{ s}^{-1}$; at more than 57 months the $^{36}\text{Cl}^- D_{e, skin}$ varies between 5.1×10^{-14} and $3.0 \times 10^{-15} \text{ m}^2 \text{ s}^{-1}$.

4.4. Relation to Archie's law

The effective diffusion coefficient and the porosity can often be correlated according to a relationship given by Archie (1942),

$$D_e = D_w \cdot e^m \quad (15)$$

where m is a cementation factor [-], which depends on the connectivity and the geometry of the pores and is rock specific. Several modified versions of this relationship were used to describe different rock properties (Boudreau, 1996; Muurinen, 1994; Rosanne et al., 2003; Van Loon et al., 2015; Tyagi et al., 2013). Fig. 9 displays in a logarithmic plot the conventional Archie's relationship for some literature data and the D_e of HTO for Na-montmorillonite derived in the present study (for estimation of the $D_{e,skin}$ the unaltered clay part was considered to be Na-montmorillonite). For unreacted fresh samples the porosity values were calculated according to eq. (1). For the skin region in the montmorillonite the porosity was estimated based on the measurements performed by Shafizadeh et al. (2020). Porosity values for the skins have a considerable uncertainty, since the estimation of the thickness, of the porosity and the definition of the skin itself is not straightforward. The HTO data, including those of the reacted clay skins, can be approximately described by Archie's relationship using a cementation factor of $m = 4.4$. The other way round, this means also that Archie's relationship may be used in numerical simulations, which aim at modelling Na-montmorillonite contacting cement or alkaline porewater, to estimate the diffusive properties of such newly forming skins based on the evolving porosity.

The analogous plot for the chloride diffusion coefficients is more controversial and more difficult to interpret (Fig. 10). This fact is related to the uncertainty of the estimation of the anion accessible porosity. For unreacted clay samples the anion accessible porosity was estimated based on data in Van Loon et al. (2007). For the skin-regions the average total porosity of ~30% estimated from the data of Shafizadeh et al.

Table 6

Summary of D_e values for HTO and Cl ($\text{m}^2 \text{ s}^{-1}$) in various montmorillonites and bentonites (MX-80) from literature and measured in the present work.

Author	HTO Na-mont.	$^{36}\text{Cl}^-$ Na-mont.	HTO Ca-mont.	$^{36}\text{Cl}^-$ Ca-mont.	HTO K-mont.	$^{36}\text{Cl}^-$ K-mont.	Comment	Bulk dry density kg m^{-3}
Glaus et al. (2010)	1.7×10^{-11}	7.2×10^{-14}					0.1 M NaClO ₄	1900
		2.5×10^{-13}					0.5 M NaClO ₄	1900
	1.9×10^{-11}	4.7×10^{-13}					1.0 M NaClO ₄	1900
González Sánchez et al. (2008)		7.2×10^{-13}					2.0 M NaClO ₄	1900
			3.5×10^{-11}				0.5 M CaCl ₂	1900
			3.7×10^{-11}				0.005 CaCl ₂	1900
Melkior et al. (2004)	1.4×10^{-11}						1.0 M NaCl	1900
	1.5×10^{-11}						0.01 M NaCl	1900
	7.4×10^{-11}	5.5×10^{-12}					^a Bent. sample	1700
Melkior et al. (2009)	7.3×10^{-11}						^a Bent. sample	1700
	4.4×10^{-11}	1.5×10^{-12}					^a Bent. sample	2000
	4.2×10^{-11}						^a Bent. sample	2000
Present Study	5.3×10^{-11}		5.1×10^{-11}				^a Bent. sample	1600
	5.0×10^{-11}		5.1×10^{-11}				^a Bent. sample	1600
P_Na1	6.0×10^{-11}	4.8×10^{-12}					0.3 M NaCl	1450
P_Na2	5.9×10^{-11}	5.0×10^{-12}					0.3 M NaCl	1450
P_Na1B	6.5×10^{-11}						0.3 M NaCl	1550
P_Na2B	^a 7.5×10^{-11}	5.7×10^{-12}					0.3 M NaCl	1520
P_K1					1.1×10^{-10}	2.7×10^{-11}	0.3M KCl	1450
P_K2					8.8×10^{-11}		0.3M KCl	1450
P_Ca1B			1.0×10^{-10}	1.3×10^{-11}			0.1M CaCl ₂	1450
P_Ca2B			1.2×10^{-10}	4.6×10^{-12}			0.1M CaCl ₂	1450

^a Value not considered to obtain average unaltered Na-montmorillonite D_e .

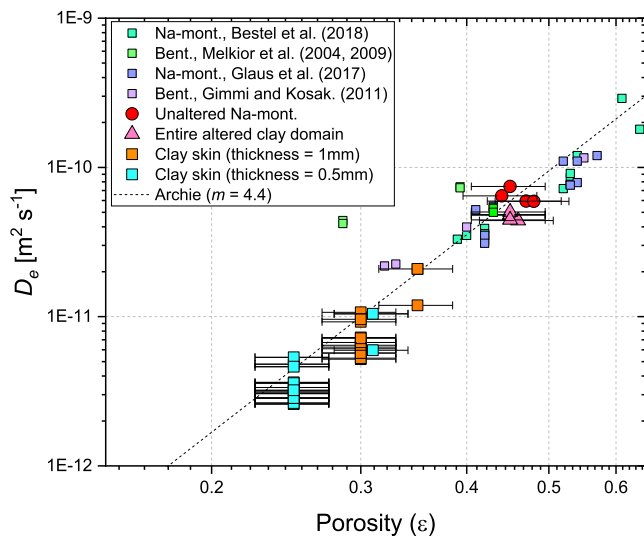


Fig. 9. Relationship between the effective HTO diffusion coefficient and the diffusion accessible porosity for Na-montmorillonite (and bentonite), with data from the literature (Bestel et al., 2018; Gimmi and Kosakowski, 2011; Glaus et al., 2017; Melkior et al., 2004, 2009) and values reported here. The dashed line represents the classical Archie's relation, eq. (15) with $m = 4.4$. Porosities for the skin regions were derived from the data of Shafizadeh et al. (2020); the error on these porosities is estimated to be $\pm 10\%$.

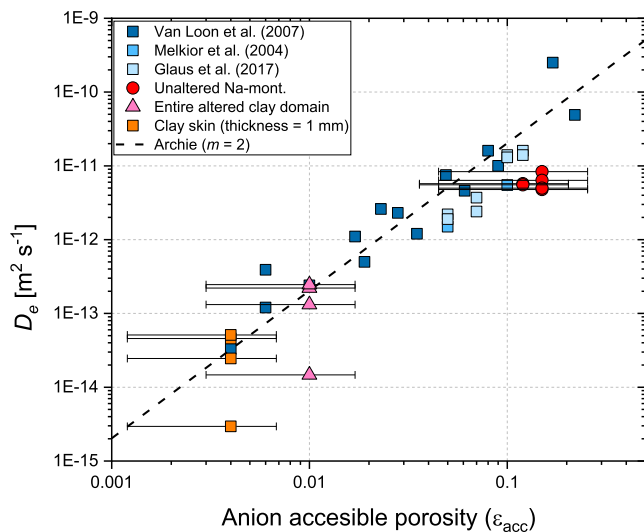


Fig. 10. Relationship between the effective $^{36}\text{Cl}^-$ diffusion coefficient and the diffusion accessible porosity for chloride in Na-montmorillonite (and bentonite), with data from the literature and derived in this study. The dashed line represents the classical Archie's relation, eq. (15) with $m = 2$. Accessible porosities for the entire clay domain (pink) and the clay skin (orange) are only rough estimates with very large uncertainties.

(2020) would relate to an anion accessible porosity of less than 2% according to Van Loon et al. (2007). It has to be mentioned that Van Loon et al. (2007) use porosities for differently compacted samples, whereas in our case porosities were reduced by mineral precipitations. Precipitation is likely to take place in the free porosity, drastically reducing the anion accessible porosity (Fig. 7). Accordingly, the anion accessible porosity estimated for our skins in this way is very uncertain, leading to a large uncertainty when estimating a cementation exponent with Archie's empirical law. In fact, due to the very large uncertainty of the anion accessible porosity of the skins, it cannot be decided whether or not the skin data follow the same trend as the other data. Nevertheless

the very low diffusivity values measured (in some cases no flux was observed) suggest that only a very small portion of the porosity remains available for anions.

4.5. Transferability and implications for other cement-clay systems and other processes

The mineralogy of the interface samples studied in this work was intentionally kept as simple as possible to facilitate the interpretation of the measurements. Using cement-claystone samples or concrete-bentonite samples made of materials as will be used in disposal sites is very complex in terms of handling, sample preparation, characterisation and interpretation of the observations, mainly due to the high heterogeneity of the phases and their chemical variability. The exact parameters of mass transport, interaction kinetics and the consequent mineral reactions modifying the transport properties of interfaces are expected to depend on the specific materials. Despite the simplicity, the samples prepared from Na-montmorillonite and OPC paste studied in this work are a good proxy to a bentonite-OPC interface that is foreseen in a geological repository for radioactive wastes (e.g., Nagra, 2002). Bentonite (MX-80) contains up to 85% of Na-montmorillonite. Other minerals are quartz, feldspars, calcite and accessory minerals in minor amounts (Carlson, 2004). The accessory mineral dissolution in alkaline conditions will for sure play a role (Soler and Mäder, 2010), but due to the high amount of montmorillonite present in the MX-80 bentonite it is likely that at least during the initial period of interaction bentonite-OPC interfaces will behave in a similar way as Na-montmorillonite-OPC interfaces. For other interface types (e.g., Opalinus Clay-OPC or Boom Clay-OPC), a direct inference on the evolving diffusivity or porosity is difficult due to the completely different initial conditions of the interface. Nevertheless, the results of the present study may provide a general indication in terms of expected times of reactions and magnitudes of diffusivity changes.

Besides transport of solutes, as investigated in this study, many other processes are important for the assessment of the safety of a geologic repository for radioactive waste. These processes include the (re-)saturation of clay rocks or clay granulates surrounding the waste canisters, or also transport of gases (dissolved or in the gas phase). The (re-)saturation occurs via advective water transport and diffusive water vapour transport. Clay skins with reduced porosity will certainly also affect these processes, leading to a slower mass transfer in general. The performed experiments indicate an extremely low diffusivity for the anion $^{36}\text{Cl}^-$. This experimental evidence probably has consequences for other species: i) the flux of the anion OH^- through the clay at larger times is likely to be limited as well to a relative small extent; accordingly, the (initially probably fast) propagation of the pH front will later slow down. ii) In a similar way, diffusion of negatively charged radionuclides may be strongly reduced. iii) Diffusion of large dissolved gas molecules (e.g. CH_4 , CO_2) will probably be influenced as well by the reactions at the interfaces, because diffusion of large gas molecules tends to occur through the same porosity as that of anions.

At the same time, a generalisation of the present findings to the much larger space and time scale relevant for a repository would certainly require additional investigations. For instance, questions of the homogeneity or heterogeneity of skins at larger spatial scales should be addressed. Also, the performed experiments on OPC paste Na-montmorillonite interfaces do not allow an extrapolation of the porosity/diffusivity behaviour over very long time scales, even though the previously discussed trends of the evolution of the diffusion coefficient suggest that in short term a total reduction of the porosity will not be reached.

5. Conclusions

Na-montmorillonite/OPC paste interface samples have been reacting under controlled conditions over six years. The evolution of transport

properties across the interface was periodically monitored by through-diffusion experiments. Two distinct phases of the interface reactivity could be identified. The first phase (0–17 months) was characterised by a strong decrease of the diffusion coefficient (46% reduction of D_e for HTO, and ~96% decrease of D_e for $^{36}\text{Cl}^-$). The second phase (17–73 months) was characterised by a slow further decrease of the diffusivity across the interface. Combining the diffusive flux measurements presented here and non-destructive analysis of the sample porosity across the interface presented by Shafizadeh et al. (2020), it was concluded that the changes of transport properties across the sample are dominated by a narrow low porosity/low diffusivity alteration zone in the clay compartment close to the interface. This alteration zone is likely to form as a result of precipitations following mineral transformations. A reduction of diffusive transport with time was observed for both HTO and $^{36}\text{Cl}^-$ tracers. The chloride D_e showed a much stronger reduction compared to HTO. This suggests that precipitation of new phases occurred likely in the porosity that was accessible to anions (free porosity), such that these pathways were partly blocked for $^{36}\text{Cl}^-$. The neutral tracer HTO is less affected by this partial blocking of the free porosity, because it can still diffuse via interlayer or DDL porosity. The $D_{e,\text{Cl}}$ values determined for the entire clay domain are very low ($<2.5 \times 10^{-13} \text{ m}^2 \text{ s}^{-1}$), and in some cases no anion flux at all was observed. A complete clogging, that is, a complete blocking of the pore space for diffusion of HTO, was, however, not observed up to a time of six years. Combining information gained from the precedent neutron investigation measurements (Shafizadeh et al., 2020) with the present data allowed estimating the diffusive properties of the skin region for HTO and chloride. These skin regions in the clay (after at least 45 months interaction) have an estimated average diffusivity of $7.0 \times 10^{-12} \text{ m}^2 \text{ s}^{-1}$ for HTO (considering the unaltered clay part as Na-montmorillonite) and $<5.1 \times 10^{-14} \text{ m}^2 \text{ s}^{-1}$ for chloride. A series of assumptions and simplifications had to be made to derive these numbers, leading to comparably large uncertainties. For HTO the evolution of the effective diffusion coefficient of the entire clay domain ($D_{e,\text{clay}}$) and of the skin ($D_{e,\text{skin}}$) can be well described with Archie's empirical law, whereas for chloride the unknown accessible porosity of the skins does not allow a precise statement.

Declaration of competing interest

The authors declare that they have no known competing financial interests or personal relationships that could have appeared to influence the work reported in this paper.

Acknowledgments

The authors would like to acknowledge Petar Bunic and Sabrina Frick for their highly appreciated support in the laboratory. Additional thanks go to Martin Glaus and Jan Tits for the many helpful discussions. Partial financial support by Nagra, the Swiss Cooperative for the Disposal of Radioactive Waste, is gratefully acknowledged.

References

Albinsson, Y., Andersson, K., Börjesson, S., Allard, B., 1996. Diffusion of radionuclides in concrete and concrete-bentonite systems. *J. Contam. Hydrol.* 21, 189–200.

Appelo, C.A.J., 2013. A Review of Porosity and Diffusion in Bentonite. Posiva Working Report 2013-29. Posiva OY, Olkiluoto, Finland.

Archie, G.E., 1942. The electrical resistivity log as an aid in determining some reservoir characteristics. *Trans. AIME* 146, 54–62.

Beaudin, J.J., Ramachandran, V.S., Feldman, R.F., 1990. Interaction of chloride and C-S-H. *Cement Concr. Res.* 20, 875–883.

Berner, U., Kulik, D., Kosakowski, G., 2013. Geochemical impact of a low-pH cement liner on the near field of a repository for spent fuel and high-level radioactive waste. *Phys. Chem. Earth* 64, 46–56.

Bestel, M., Glaus, M.A., Frick, S., Gimmi, T., Juranyi, F., Van Loon, L.R., Diamond, L.W., 2018. Combined tracer through-diffusion HTO and ^{22}Na through Na-montmorillonite with different bulk dry densities. *Appl. Geochem.* 93, 158–166.

Boudreau, B.P., 1996. The diffusive tortuosity of fine-grained unlithified sediments. *Geochem. Cosmochim. Acta* 60, 3139–3142.

Bourg, I.C., Sposito, G., Bourg, A.C.M., 2006. Tracer diffusion in compacted, water-saturated bentonite. *Clay Clay Miner.* 54, 363–374.

Bradbury, M.H., Baeyens, B., 2003. Porewater chemistry in compacted re-saturated MX-80 bentonite. *J. Contam. Hydrol.* 61, 329–338.

Carlson, L., 2004. Bentonite Mineralogy. Posiva Working Report, 2004-02. Posiva OY, Olkiluoto, Finland.

Claret, F., Bauer, A., Schafer, T., Griffault, L., Lanson, B., 2002. Experimental investigation of the interaction of clays with high-pH solutions: a case study from the Callovo-Oxfordian formation, Meuse- Haute Marne underground laboratory (France). *Clay Clay Miner.* 50, 633–646.

Crank, J., 1979. *The Mathematics of Diffusion*. Oxford University Press.

Cuevas, J., Vigil de la Villa, R., Ramirez, S., Sanchez, L., Fernández, R., Leguey, S., 2006. The alkaline reaction of FEBEX Bentonite: a contribution to the study of the performance of bentonite/concrete engineered barrier systems. *J. Iber. Geol.* 32, 151–174.

Dauzeres, A., Le Bescop, P., Sardini, P., Cau Dit Coumes, C., 2010. Physico-chemical investigation of clayey/cement-based materials interaction in the context of geological waste disposal: experimental approach and results. *Cement Concr. Res.* 40, 1327–1340.

De Windt, L., Pellegrini, D., van der Lee, J., 2004. Coupled modeling of cement/claystone interactions and radionuclide migration. *J. Contam. Hydrol.* 68, 165–182.

Döhning, L., Görlich, S., Rüttener, W., Schwerzmann, R., 1994. Herstellung von homogenen Zementsteinen mit hoher hydraulischer Permeabilität. Nagra, Wettingen, Switzerland. Nagra Internal Report NIB 94-29.

Fernández, R., Rodríguez, M., Vigil de la Villa, R., Cuevas, J., 2010. Geochemical constraints on the stability of zeolites and C-S-H in the high pH reaction of bentonite. *Geochem. Cosmochim. Acta* 74, 890–906.

Fernández, R., Torres, E., Ruiz, A.I., Cuevas, J., Cruz Alonso, M., García Calvo, J.L., Rodríguez, E., Turrero, J.M., 2017. Interaction processes at the concrete-bentonite interface after 13 years of FEBEX-Plug operation. Part II: bentonite contact. *Phys. Chem. Earth* 99, 49–63.

Gaucher, E.C., Philippe Blanc, P., 2006. Cement/clay interactions - a review: experiments, natural analogues, and modeling. *Waste Manag.* 26, 776–788.

Gimmi, T., Kosakowski, G., 2011. How mobile are sorbed cations in clays and clay rocks? *Environ. Sci. Technol.* 45, 1443–1449.

Glaus, M.A., Rossé, R., Van Loon, L.R., Yaroshchuk, A.E., 2008. Tracer diffusion in sintered stainless steel filters: measurement of effective diffusion coefficients and implications for diffusion studies with compacted clays. *Clay Clay Miner.* 56, 677–685.

Glaus, M.A., Frick, S., Rossé, R., Van Loon, L.R., 2010. Comparative study of tracer diffusion of HTO, $^{22}\text{Na}^+$ and $^{36}\text{Cl}^-$ in compacted kaolinite, illite and montmorillonite. *Geochem. Cosmochim. Acta* 74, 1999–2010.

Glaus, M.A., Aertsens, M., Maes, N., Van Laer, L., Van Loon, L.R., 2015. Treatment of boundary condition in through-diffusion: a case study of $^{85}\text{Sr}^{2+}$ diffusion in compacted illite. *J. Contam. Hydrol.* 177–178, 239–248.

Glaus, M.A., Frick, S., Van Loon, L.R., 2017. Diffusion of Selected Cations and Anion in Compacted Montmorillonite and Bentonite. PSI Bericht 17-08. Paul Scherrer Institut, Villigen PSI, Switzerland.

González Sánchez, F., Van Loon, L.R., Gimmi, T., Jakob, A., Glaus, M.A., Diamond, L.W., 2008. Self-diffusion of water and its dependence on temperature and ionic strength in highly compacted montmorillonite, illite and kaolinite. *Appl. Geochem.* 23, 3840–3851.

Hirao, H., Yamada, K., Takahashi, H., Zibara, H., 2004. Chloride binding of cement estimated by binding isotherms of hydrates. *J. Adv. Concr. Technol.* 3, 77–84.

Hodgkinson, E.S., Hughes, C.R., 1999. The mineralogy and geochemistry of cement/rock reactions: high-resolution studies of experimental and analogue materials. *Chem. Contain. Waste Geosphere* 157, 195–211.

IAEA, 2009. Geological Disposal of Radioactive Waste: Technological Implications for Retrievability. NW-T-1.19.

Jakob, A., Sarott, F.A., Spieler, P., 1999. Diffusion and Sorption on Hardened Cement Pastes - Experiments and Modelling Results. Paul Scherrer Institut, Villigen PSI, Switzerland. PSI Report 99-05.

Jenni, A., Gimmi, T., Alt-Epping, P., Mäder, U., Cloet, V., 2017. Interaction of ordinary Portland cement and Opalinus Clay: dual porosity modelling compared to experimental data. *Phys. Chem. Earth* 99, 22–37.

Jensen, O.M., Hansen, P.F., Coats, A.M., Glasser, F.P., 1999. Chloride ingress in cement paste and mortar. *Cement Concr. Res.* 29, 1497–1504.

Karland, O., 2004. Laboratory experiments concerning compacted bentonite contacted to high pH solutions. In: Michau, N. (Ed.), *EcoClay II: Effect of Cement on Clay Barrier Performance Phase II*. Final Report. (ANDRA) European contract FIKW-CT-2000-0028.

Karland, O., Olsson, S., Nilsson, U., 2006. Mineralogy and Sealing Properties of Various Bentonites and Smectite-Rich Clay Materials. Svensk Kärnbränslehantering AB, Stockholm, Sweden. SKB Technical Report TR-06-30.

Kosakowski, G., Berner, U., 2013. The evolution of clay rock/cement interfaces in a cementitious repository for low- and intermediate level radioactive waste. *Phys. Chem. Earth* 64, 65–86.

Kulik, D., Wagner, T., Dmytrieva, S.V., Kosakowski, G., Hingerl, F.F., Konstantin, Chudnenko, K.V., Berner, U.R., 2013. GEM-Selektor geochemical modeling package: revised algorithm and GEMS3K numerical kernel for coupled simulation codes. *Comput. Geosci.* 17, 1–24.

Mäder, U., Jenni, A., Lerouge, C., haboreau, S., Miyoshi, S., Kimura, Y., Cloet, V., Fukaya, M., Claret, F., Otake, T., Shibata, M., Lotenbach, B., 2017. 5-year chemico-

- physical evolution of concrete–claystone interfaces, Mont Terri Rock Laboratory (Switzerland). *Swiss J. Geosci.* 110, 307–327.
- Martin, L.H.J., Leemann, A., Milodowski, A.E., Mäder, U.K., Münch, B., Giroud, N., 2016. A natural cement analogue study to understand the long-term behaviour of cements in nuclear waste repositories: maqarin (Jordan). *Appl. Geochem.* 71, 20–34.
- Marty, N.C.M., Munier, L., Gaucher, E.C., Tournassat, C., Gaboreau, S., Quang Vong, C., Giffaut, E., Cochepin, B., Claret, F., 2014. Simulation of cement/clay interactions: feedback on the increasing complexity of modelling strategies. *Transport Porous Media* 104, 385–405.
- Melkior, T., Mourzagah, D., Yahiaoui, Y., Thoby, D., Alberto, J.C., Brouard, C., Michau, N., 2004. Diffusion of an alkaline fluid through clayey barriers and its effect on the diffusion properties of some chemical species. *Appl. Clay Sci.* 26, 99–107.
- Melkior, T., Gaucher, E.C., Brouard, C., Yahiaoui, S., Thoby, D., Clinard, C., Ferrage, E., Guyonnet, D., Tournassat, C., Coelho, D., 2009. Na⁺ and HTO diffusion in compacted bentonite: effect of surface chemistry and related texture. *J. Hydrol* 370, 9–20.
- Mitchell, J.K., Soga, K., 1992. *Fundamentals of Soil Behaviour*, third ed. John Wiley and Sons, p. 592pp.
- Mosser-Ruck, R., Cathelineau, M., 2004. Experimental transformation of Na,Ca-smectite under basic conditions at 150 °C. *Appl. Clay Sci.* 26, 259–273.
- Muurinen, A., 1994. Diffusion of Anions and Cations in Compacted Sodium Bentonite. VTT Publications 168, Espoo, Finland. Technical Research Centre of Finland.
- Nagra, 2002. Project Opalinus Clay – Safety Report, Demonstration of Disposal Feasibility for Spent Fuel, Vitrified High-Level Waste and Long-Lived Intermediate-Level Waste ("Entsorgungsnachweis"). Nagra, Wettingen, Switzerland. Nagra Technical Report NTB 02–05.
- Nagra, 2014. SGT-Etape-2: Vorschlag weiter zu untersuchender geologischer Standortgebiete mit zugehörigen Standortarealen für die Oberflächenanlage: Charakteristische Dosisintervalle und Unterlagen zur Bewertung der Barrierensysteme. Nagra, Wettingen, Switzerland. Nagra Technical Report NTB 14-03.
- Page, C.-L., Short, N.R., El Tarras, A., 1981. Diffusion of chloride in hardened cement pastes. *Cement Concr. Res.* 11, 395–406.
- Plusquellec, G., Nonat, A., 2016. Interactions between calcium silicate hydrate (C-S-H) and calcium chloride, bromide and nitrate. *Cement Concr. Res.* 90, 89–96.
- Pusch, R., 2001. *The Buffer and Backfill Handbook. Part 2: Materials and Techniques.* SKB, Stockholm, Sweden. SKB Technical Report TR-02–12.
- Ramírez, S., Cuevas, J., Vigil, R., Leguey, S., 2002. Hydrothermal alteration of "La Serrata" bentonite (Almería, Spain) by alkaline solutions. *Appl. Clay Sci.* 21, 257–269.
- Read, D., Glasser, F.P., Ayora, C., Guardiola, M.T., Sneyers, A., 2001. Mineralogical and microstructural changes accompanying the interaction of Boom Clay with ordinary Portland cement. *Adv. Cement Res.* 13, 175–183.
- Rosanne, M., Mammari, N., Koudina, N., Prunet-Foch, B., Thovert, J.-F., Tevissen, E., Adler, P.M., 2003. Transport properties of compact clays. II. Diffusion. *J. Colloid Interface Sci.* 260, 195–203.
- Sarott, F.A., Bradbury, M.H., Pandolfo, P., Spieler, P., 1992. Diffusion and adsorption studies on hardened cement paste and the effect of carbonation on diffusion rates. *Cement Concr. Res.* 22, 439–444.
- Savage, D., 2011. A review of analogues of alkaline alteration with regard to long-term barrier performance. *Min. Mag.* 75, 2401–2418.
- Savage, D., Cloet, V., 2018. A Review of Cement-Clay Modelling. Nagra Arbeitsgemeinschaft NAB 28-24. Nagra, Wettingen, Switzerland.
- Shafizadeh, A., Gimmi, T., Van Loon, L.R., Kaestner, A., Lehmann, E., Mäder, U., Churakov, S.V., 2015. Quantification of water content across a cement-clay interface using high resolution neutron radiography. *Phys. Proc.* 69, 516–523.
- Shafizadeh, A., Gimmi, T., Van Loon, L.R., Mäder, U., Churakov, S.V., 2019. Neutron Imaging Study of Evolution of Structural and Transport Properties of Cement-Clay Interfaces. PhD Thesis. University of Bern, Bern, Switzerland.
- Shafizadeh, A., Gimmi, T., Van Loon, L.R., Kaestner, A.P., Mäder, U.K., Churakov, S.V., 2020. Time-resolved porosity changes at cement-clay interfaces. *Cement Concr. Res.* 127, 105924.
- Smellie, J.A.T., 1998. Executive Summary: Maqarin Natural Analogue Project: Phase III. SKB, Stockholm, Sweden. SKB Technical Report (TR 98-04).
- Soler, M.J., Mäder, U.K., 2010. Cement-rock interaction: infiltration of a high-pH solution into a fractured granite core. *Geol. Acta* 8, 221–233.
- Steeffel, C.I., Lichtner, P.C., 1998. Multicomponent reactive transport in discrete fractures II: infiltration of hyperalkaline groundwater at Maqarin, Jordan, a natural analogue site. *J. Hydrol* 209, 200–224.
- Taylor, H.W.F., 1997. *Cement Chemistry.* Academic press.
- Tinseau, E., Bartier, D., Hassouta, L., Devol-Brown, I., Stammose, D., 2006. Mineralogical characterization of the Tournemire argillite after in situ interaction with concretes. *Waste Manag.* 26, 789–800.
- Tits, J., Jakob, A., Wieland, E., Spieler, P., 2003. Diffusion of tritiated water and ²²Na⁺ through non-degraded hardened cement pastes. *J. Contam. Hydrol.* 61, 45–62.
- Tyagi, M., Gimmi, T., Churakov, S.V., 2013. Multi-scale micro-structure generation strategy for up-scaling transport in clays. *Adv. Water Resour.* 59, 181–195.
- Van Loon, L.R., Soler, J.M., 2003. Diffusion of HTO, ³⁶Cl⁻, ¹²⁵I⁻ and ²²Na⁺ in Opalinus Clay: Effect of Confining Pressure, Sample Orientation, Sample Depth and Temperature. Nagra, Wettingen, Switzerland. Nagra Technical Report NTB 03-07.
- Van Loon, L.R., Glaus, M.A., Müller, W., 2007. Anion exclusion effects in compacted bentonites: towards a better understanding of anion diffusion. *Appl. Geochem.* 22, 2536–2552.
- Van Loon, L.R., Mibus, J., 2015. A modified version of Archie's law to estimate effective diffusion coefficients of radionuclides in argillaceous rocks and its application in safety analysis studies. *Appl. Geochem.* 59, 85–94.
- Vieillard, P., Ramírez, S., Bouchet, A., Cassagnabère, A., Meunier, A., Jacquot, E., 2014. Alteration of the calovo-oxfordian clay from meuse-haute marne underground laboratory (France) by alkaline solution: II. Modelling of mineral reactions. *Appl. Geochem.* 19, 1699–1709.
- Watson, C., Hane, K., Savage, D., Benbow, S., Cuevas, J., Fernández, R., 2009. Reaction and diffusion of cementitious water in bentonite: results of 'blind' modeling. *Appl. Clay Sci.* 45, 54–69.
- Wersin, P., Curti, E., Appelo, C.A.J., 2004. Modelling bentonite–water interactions at high solid/liquid ratios: swelling and diffuse double layer effects. *Appl. Clay Sci.* 26, 249–257.
- Wieland, E., Tits, J., Dobler, J.P., Spieler, P., 1998. Interaction of Eu(III) and Th(IV) with sulphate-resisting Portland cement. *Mater. Res. Soc. Symp. Proc.* 506, 573–578.
- Yamaguchi, T., Sawaguchi, T., Tsukada, M., Hoshino, S., Tanaka, T., 2016. Mineralogical changes and associated decrease in tritiated water diffusivity after alteration of cement–bentonite interfaces. *Clay Miner.* 51, 279–287.

Chapter 4

**Evolution of mineralogy and porosity at OPC paste Na-montmorillonite interfaces
during 6 years of interaction**

-- Manuscript in preparation for publication --

Evolution of mineralogy and porosity at OPC paste-Na montmorillonite interfaces during 6 years of interaction

Pietro Luraschi^{a,b,*}, Thomas Gimmi^{a,b*}, Michele Griffa^c, Frank Winnefeld^c, Anders Kaestner^d, Sergey V. Churakov^{a,b}

^aLaboratory for Waste Management, Nuclear Energy and Safety, Paul Scherrer Institute, 5232 Villigen, Switzerland

^bInstitute of Geological Sciences, University of Bern, 3012 Bern, Switzerland

^cSwiss Federal Laboratories for Materials Science and Technology, Empa, 8600 Dübendorf, Switzerland

^dLaboratory for Neutron Scattering and Imaging, Research with Neutrons and Muons, Paul Scherrer Institute, 5232 Villigen, Switzerland

* Corresponding authors

E-mail addresses: pietro.luraschi@psi.ch (P.Luraschi), thomas.gimmi@psi.ch (T. Gimmi)

Keywords: cement clay porosity mineralogy

Abstract

Cement pastes and concretes are important materials for the construction of underground repositories for radioactive waste in clay-rich sedimentary rocks. In such repositories, cement-based composites and clay will be in contact and will form strongly reacting interfaces. Understanding the alteration of the mineralogical and diffusive properties at such material interfaces is critical for the repository safety assessment. Here, the coupled evolution of mineralogy and porosity at the interface of compacted Na-montmorillonite and an Ordinary Portland Cement (OPC) paste was investigated in the laboratory for a period of six years by means of different analytical methods. On the cement paste side, continuous portlandite dissolution and partial C-S-H destabilisation resulted in an initial porosity increase. Friedel's salt precipitation was observed throughout the cement side of the samples, but increasingly towards the interface. The calcium released by portlandite dissolution and partially by C-S-H decalcification diffused into the clay, leading to the new formation of C-S-H phases and to a region with a remarkable porosity reduction in the clay. This "skin" showed an extension of ~1 mm. The measured porosity in the skin decreased from initial ~0.40-0.45 (depending on the sample) down to ~0.30-0.35 m³ m⁻³. Montmorillonite was partially dissolved by the highly alkaline paste's porewater, releasing silica and aluminium into solution available for further chemical reactions. Beyond the strongly altered region at the interface (extent of ~1 mm), the original mineralogical composition of the clay side was about preserved, but i) sodium was substituted by calcium on the montmorillonite exchanger sites, ii) the pH quickly increased from ~7 to ~12 (when the cells were detached from the porewater reservoirs for longer than 2 weeks). This study provides a comprehensive geochemical dataset for a mechanistic understanding of the long-term cement-based composite-clay interaction and for validation of reactive transport models.

Introduction

Clay-rich formations are considered by several countries as possible host rocks for disposal of radioactive waste. The radiological safety of an underground repository is provided by a system of natural and engineered barriers. In the current Swiss concept of the geological disposal of radioactive waste, cement-based composites and clay will be in contact in several parts of the engineered barrier system (EBS). The strong differences between the porewater chemistry of clay and that of the cementitious material trigger dissolution-precipitation reactions which may alter safety-relevant properties of the natural and engineered barriers (Nagra, 2002, 2014). Short-term mineralogical alterations taking place at these interfaces were extensively studied in laboratory experiments during the last 30 years, while long-term alterations were inferred from natural analogues and models. Gaucher and Blanc (2006), Nagra (2018), and Wilson et al. (2021) offer extensive literature reviews in this area. The question of highest concern is the long-term behaviour of such interfaces. Especially the coupled evolution of the porosity and the diffusivity remains an open question. As various feedbacks exist between the involved physical, chemical and mineralogical processes, the correct interpretation of experimental results, and the correct parameterization of reactive transport models is not at all straightforward.

Depending on the chemical/mineralogical properties of the interfacing materials (e.g., cement-based composite mix design or clay composition), the extent and direction of mineralogical alterations can vary significantly. In general, the interaction of the strongly alkaline cementitious porewater with the more neutral porewater in clay-rich materials leads to partial dissolution of both, clay minerals and cement hydrate phases, precipitation of new phases, e.g. calcium silicate hydrates (C-S-H) or zeolites, and modification of the clays cation exchange composition and capacity (Hodgkinson and Hughes, 1999; Dauzeres et al., 2010; Kosakowski and Berner, 2013; Jenni et al., 2014; Lalan et al., 2019; Wilson et al., 2021). More specifically, when hydrated Ordinary Portland Cement (OPC) comes in contact with clay rocks, portlandite dissolution, C-S-H decalcification and calcite precipitation are typical, observed alterations on the cementitious side, whereas a porosity decrease and various chemical/mineralogical alterations occur on the clay side (Gaucher and Blanc 2006; Bartier et al., 2013; Mäder et al., 2017).

Several experiments were performed to study cementitious materials-clay interactions. Some of them investigated the interaction of clay with alkaline solutions, while other specifically focussed on the interaction of cement paste and clay materials, as for example samples with OPC-montmorillonite (or bentonite) interfaces. Cuevas et al. (2004) studied the interaction of bentonite with NaOH at several temperatures and reported the precipitation of different zeolites and C-S-H. Bouchet et al. (2004), by means of batch experiments, investigated the interaction of montmorillonite with different alkaline solutions and observed, as well, the precipitation of zeolites and C-S-H. They observed furthermore beidellite formation. The experiments were performed at various temperatures (>60°C). More recently, Fernández et al., (2016) studied cementitious materials-bentonite samples and found the precipitation of - among other minerals - calcium aluminate silicate hydrates (C-A-S-H). On the cementitious side, leaching of portlandite and C-S-H was generally observed (Berner, 1992). Depending on the clay or porewater type also other mineral phases can form (e.g., Mg-hydrates, Bernard et al., 2020; Wilson et al., 2021).

The quantification of local porosity variations with respect to time and space is especially challenging, due to the slow reaction kinetics, limited alteration extent, the chemical system's complexity and the fragility of such interfaces. The extent of local porosity change depends on the system composition and the distance to the interface. Most often, an overall local porosity decrease at the interface region was observed in experiments and natural analogues. The formation of an impermeable zone (due to pore space clogging) was reported in some cases, e.g. Gaboreau et al. (2011). Models often indicate a complete pore space occlusion at the interface (Smellie, 1998; Savage et al., 2002; Marty et al., 2009; Kosakowski and Berner 2013). However, their results depend partly on not so well supported assumptions, including those related to the largely unknown feedback between porosity alterations and transport coefficients.

Several destructive and non-destructive methods have been applied to investigate the local porosity change. Post-mortem autoradiography analysis was applied by Gaboreau et al. (2011), Mäder et al. (2017), Lerouge et al. (2017) and Lalan et al. (2019). This method is based on impregnation of a polished section with a resin (e.g., Methylmethacrylate, MMA) containing a short-lived radioactive isotope (e.g., ^{14}C), whose emitted radiation is collected on a detector plane directly in contact with the section. The resulting spatial map of resin concentration therefore allows retrieving a spatial map of local porosity at a specific moment in time. The imaging is conducted in 2D and does not allow to precisely resolve local variations because of limited spatial resolution (very small pore sizes may not be impregnated). In addition, being intrinsically a 2D, projective imaging method, the interfacial surface misalignment and curvature, may introduce artefacts, in the imaging of the local porosity spatial gradients. The interpretation of the data is further complicated by the lack of a reference image of the original state. An alternative to autoradiography of impregnated polished surface is neutron imaging. It is a completely non-destructive technique, which can be repeatedly applied over time on the same exact samples, giving insights into the dynamics of the porosity evolution (2D or 3D, depending on the modality + time imaging). Shafizadeh (2019) used 2D neutron imaging (i.e., neutron radiography) to quantify local porosity changes in OPC paste-Na montmorillonite samples, identical to the interfacial systems analysed in the present study. For small samples prepared from hardened OPC paste and Na-montmorillonite (cylinders of 5 mm length for each material), Shafizadeh (2019) and Shafizadeh et al. (2020) reported a small net increase of porosity in the first 2-3 millimetres within the OPC paste over a time of about two years, and a strong decrease of porosity in the Na-montmorillonite about 1-2 mm away from the interface. Luraschi et al. (2020) investigated, for the exact same samples, the evolution of the diffusivity during six years of interaction. They observed a strong decrease of the effective diffusion coefficient of the entire interface, which mainly took place during the first 12 months of interaction. The combination of results from the diffusion experiments and spatially resolved information from neutron radiography allowed an estimation of the diffusive properties for the low-porosity region close to the interface on the clay side (termed "clay skin"). At that time, no information on chemical and mineralogical alterations at the interface were available for the analysis.

For the type of material interface investigated in this article, C-S-H and possibly C-A-S-H are likely to be observed within the montmorillonite skin. However, it remains unknown whether and where other minerals can precipitate and eventually contribute to the porosity evolution. Furthermore, the clay dissolution extent and the temporal evolution of the skin properties remains poorly constrained.

In this study, information regarding physical, chemical and mineralogical alterations of small laboratory interface samples, composed of hardened, high porosity OPC paste and Na-montmorillonite, were combined. During a period of six years, such samples, mimicking a cement-based material-clay interface, were investigated repeatedly by a series of methods (neutron radiography, X-ray tomography, Scanning Electron Microscopy (SEM), X-ray Diffraction (XRD), Thermogravimetric Analysis (TGA)). In summary, two distinct system evolution patterns were observed at the OPC paste-Na montmorillonite interface. In one set of samples, a localized, partial dissolution of minerals on the cementitious side and consequent formation of a low-porosity region on the clay side were observed. In other samples (defined here as -homogeneously reacted samples-), an extended dissolution on the cementitious side, but no formation of a low-porosity region on the clay side were observed. These two patterns were already described in Luraschi et al. (2020). The current article completes the study of OPC paste-Na montmorillonite interfaces with respect to diffusive properties (Luraschi et al., 2020) by adding detailed chemical, mineralogical and local porosity information. The combination of different analytical and imaging techniques allowed to precisely characterize the typology, the timing and the extension of the alterations which took place on both the cementitious and the clay side, that is, to characterize the alterations in 3D (space + time). Such information is essential for a mechanistic understanding of the interface reactivity and for constraining and benchmarking of reactive transport models.

Materials

Cement, clay and experimental setup

Na-montmorillonite (Milos, Greece) was compacted by cold compression with a custom built press to a dry density of 1310-1670 kg m⁻³ and then inserted into the reaction cell, to be saturated with the corresponding clayey porewater for two weeks (see Luraschi et al., 2020). The cement paste (CEM I 52.5 N HTS) was produced in 2001 (Tits et al., 2003). After casting, the paste was cut into segments and stored under a nitrogen atmosphere in the corresponding porewater solution (Wieland et al., 1998; Luraschi et al., 2020). Plugs of 5 mm diameter were carefully drilled out, cut to 5 mm length, and put in contact with the pre-saturated Na-montmorillonite. The paste and clay were introduced in a polytetrafluoroethylene (PTFE or Teflon™) holder. In the implemented cell, two polyether ether ketone (PEEK) frits are located in the external parts of the holder to stabilize the interface. Mechanical stability was ensured by an aluminum ring surrounding the PTFE and two PEEK screw caps on the ends. In- and outlet channels in these caps allowed solutions to circulate on each side of the cell. A ~30-mm³ reservoir was located in the caps after the frits (Fig. 1).

The details of the cell setup is described in Shafizadeh (2019). The chemical composition of the paste and clay, as well as the chemistry of the porewaters circulated on each side are given in the Supplementary Material (S4). Once the interface samples were prepared, they were let react in a glovebox under a nitrogen atmosphere for up to six years, during which several through-diffusion experiments (Luraschi et al., 2020), non-destructive imaging by neutron radiography and X-ray tomography measurements, and finally different postmortem mineralogical and chemical investigations were performed.

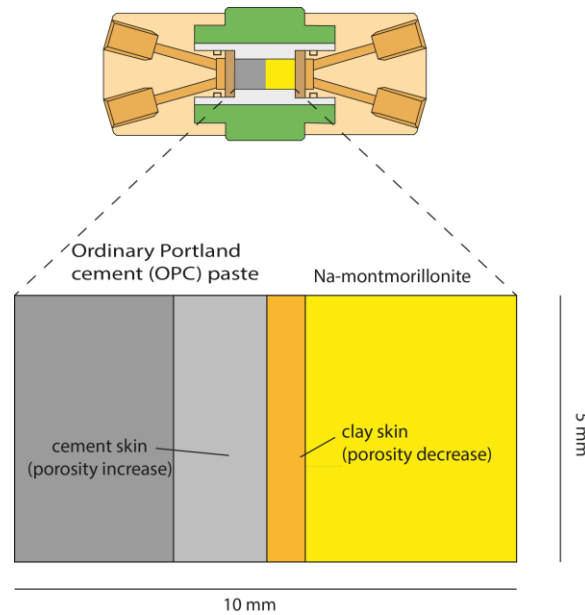


Fig. 1 The experimental cell with a sketch of the interface sample (modified after Luraschi et al., 2020). Top: cell and initial state of sample (yellow: Na-montmorillonite, gray: OPC paste), bottom: schematic state of sample after extended contact time.

In order to perform the non-destructive investigations, the samples (sealed) had to be removed from the glovebox with nitrogen atmosphere and were thus exposed to normal atmospheric conditions. Due to limited laboratory space and equipment, most of the cement paste-clay interface samples had to be disconnected from the corresponding fluid reservoirs for extended periods (up to 2 years). During these periods it was possible or even likely that the porewaters in the two materials, even at the end opposite to the interface contact zone, did not retain their original composition but equilibrated to some degree, affecting also the pH conditions. This fact probably enhanced some reactions, such as portlandite dissolution (pH sensitive) or exchange of the cation occupancy on the clay side.

Tab. 1 List of OPC paste-Na montmorillonite samples and performed investigations

Sample	Performed experiments	Low-porosity region in clay
C1	Diffusion exp. ¹ , neutron radiography	Yes
C2	TGA	No
C3	Diffusion exp. ¹ , neutron radiography, X-ray tomography, XRD, TGA	Yes
C4	Diffusion exp. ¹ , neutron radiography, X-ray tomography	Yes
C5	Diffusion exp. ¹ , neutron radiography	Yes
C8	Diffusion exp. ¹ , neutron radiography	No
C11	Diffusion exp. ¹ , neutron radiography, SEM/EDX	Yes
C12	Neutron radiography, XRD	No
C15	Diffusion exp. ¹ , neutron radiography, X-ray tomography	Yes
C20	Diffusion exp. ¹ , neutron radiography	No
C25	Neutron radiography, SEM/EDX	Yes
C29	Neutron radiography, SEM/EDX	No
D5	SEM/EDX	Yes
D6	Diffusion exp. ¹ , neutron radiography, X-ray tomography	Yes

¹Through-diffusion experiments described in Luraschi et al. (2020).

Methods

Neutron imaging

Neutron imaging relies on the differences in the neutron scattering and absorption (also called capture) probabilities (scattering and absorption cross sections) for the atomic nuclei of distinct elements. In particular, neutrons are strongly attenuated by hydrogen, making neutron imaging to a powerful tool for non-destructive analysis of water distribution in porous media (Kaestner et al., 2016). In a fully saturated sample, the water content can be considered as a proxy for the porosity. Therefore, the porosity evolution can be monitored over time by performing time-lapse imaging over the entire duration of the experiment. In this study, the interface samples were investigated at the cold neutron imaging beamline (ICON, Kaestner et al., 2011) of the Swiss Spallation Neutron Source (Paul Scherrer Institut, Villigen, Switzerland) by performing time-lapse radiography, i.e., 2D projection imaging. When a sample is exposed to a collimated neutron beam, a fraction of the neutrons interacts with the sample's nuclei. Each neutron of such fraction is either (1) scattered off the trajectory it had before interacting with the sample or (2) absorbed. The remaining, transmitted neutrons, along with some of the scattered ones, are collected by a neutron detector. In these experiments, the detector consisted first of a Gadolinium (Gd) scintillator screen (field of view: of 27 x 27 mm²). The Gd atomic nucleus has, among all elements, the highest total interaction cross-section for neutrons, mainly contributed by the absorption component. The scintillator converts the absorbed neutrons into emitted light, which is then directed to a charge-coupled device (CCD) photon detector, producing a 16-bit gray-scale image. In this study, the cells containing the samples were fit into an aluminium support, only weakly interacting with the neutron beam, and then exposed to it for 90 seconds to acquire a single neutron radiograph. A detailed description of the experimental setup and the imaging parameters is given in Shafizadeh et al. (2015; 2020). During the measurements and the subsequent radioactivity decay phase, the (sealed) cells were exposed to ambient conditions under air atmosphere.

Given a radiograph acquired at a time point t , the local water content of the sample portion along the straight path (line or ray), orthogonal to the detector plane and crossing the detector plan at a pixel position, was estimated following a multistep procedure based on the Lambert-Beer law,

$$I_T(t) = I_0(t) \exp(-\sum_i \mu_i d_i) \quad (1)$$

where I_T represents the transmitted beam intensity recorded at that pixel position (radiograph's pixel value), I_0 the incoming beam intensity along the same ray and t the neutron radiograph acquisition time. Eq. (1) is valid for each detector's pixel. The sample's total attenuation coefficient μ_i is a measure for the total neutron beam interaction (scattering or absorption) with a corresponding material i being present along such ray. d_i represents the thickness of each material along the ray. In first approximation and along each ray, the sample can be thought of as a composite made of an equivalent column of water and a series of successive columns of distinct solid phases (the solid skeleton). This simplified description is valid for what concerns the sample's interaction with the neutron beam. Assuming time independent values for the μ_i of the solid materials, $I_T(t)$ can be normalized with the dry sample's intensity $I_{T,dry}$. Then, by knowing

the attenuation coefficient of water, μ_w , and the relative intensity (also called transmission coefficient T) of a dry sample ($T_{dry} = \frac{I_{T,dry}}{I_{0,dry}}$), the thickness d_w of the water column can be determined from the relative beam intensity $T = I_t/I_0$ and the relative intensity of the dry sample $T_{dry} = I_t/I_0$, according to

$$d_w = \frac{1}{\mu_w} \left[\left(\frac{I_T}{I_0} \right) / \left(\frac{I_{T,dry}}{I_{0,dry}} \right) \right] = \frac{1}{\mu_w} [T/T_{dry}] \quad (2)$$

The volumetric water content θ is then given as

$$\theta = \left(\frac{d_w}{d_T} \right) \quad (3)$$

where d_T represents the total thickness of the measured sample (along the specific ray). Here, the cylindrical shape of the sample has to be taken into account, since both the projected variable sample thickness (d_T) and the projected water thickness (d_w) vary with the position along the detector plane. Furthermore, estimations based upon a constant value for μ_w lead to wrong θ estimates, as a consequence of neutron multiple scattering-related artifacts, which is not taken into account in the radiograph formation model of Eq. (2). To compensate for such artifacts, an effective value, $\mu_{w,eff}$, for water's neutron attenuation coefficient, as function of d_w , can be used instead of the constant μ_w in Eq. (2). A calibration procedure, described in the Supplementary Materials S2 (details in Shafizadeh et al., 2020) and used in this work, showed that $\mu_{w,eff}$ could be modelled as a linearly decreasing function of d_w , i.e.,

$$\mu_{w,eff} = \mu_0 + \beta d_w \quad (4)$$

where β is the slope and μ_0 the intercept derived from a linear fit of the attenuation coefficient through unaltered cement paste or clay with known water content according to the procedure described in Shafizadeh et al. (2020). Such a calibration needs to be performed repeatedly (e.g., for each measurement time and each sample), as the incident beam's temporal variations as well those of the neutron multiple scattering by the sample, during the experimental campaign, very likely affect the calibration parameters through multiple scattering effects. The water content can then be estimated according to

$$\theta = \frac{d_w}{d_T} = -\frac{1}{d_T} \left[\left(\frac{\mu_0}{2\beta} \right) + \sqrt{\left(\frac{\mu_0}{2\beta} \right)^2 + \frac{1}{\beta} \ln \left[\frac{T_{dry}}{T} \right]} \right] \quad (5)$$

The details of the radiography data evaluation are extensively discussed in Shafizadeh (2019) and Shafizadeh et al. (2020). A summary is give in the Supplementary Materials (S2).

Preparation of sub-samples

Due to the interface fragility and the small size of the paste-clay samples, a special preparation is required to perform further, post-mortem investigations.

First of all, the samples need to be dried while simultaneously minimizing water movement inside the paste and the clay. To achieve such goal, the interface samples inside the Teflon cylinder were flash-frozen using liquid nitrogen and subsequently freeze-dried ($\sim 2\text{Pa}$, -55°C) for several hours, allowing the frozen water to sublimate.

For Scanning Electron Microscopy (SEM), a flat polished surface is necessary and must be produced by minimizing damage to the sample's microstructure. Therefore, epoxy resin was used as stabilizing agent. A previously degassed epoxy resin was introduced under vacuum into the interface samples. This method allows the resin to enter (shrinkage-related) openings and fractures, giving the sample a very good stability for further processing (sawing and polishing). Once embedded in resin, the samples were cut perpendicular to the material interface and grinded using different non-polar liquids and oil-based suspensions.

For mineral identification (XRD and TGA), the majority of the samples were flash-frozen and subsequently freeze-dried as described previously. This technique allows to avoid water migration upon drying; on the other hand it can be problematic since it may affect the stability of ettringite and AFm phases (Snellings et al., 2018). After drying, the samples were then cut into thin slices (1 to 2 mm) and crushed by hand in an agate mortar to produce a homogeneous powder.

SEM/EDX

The polished samples were investigated using a SEM (Zeiss EVO-50 XVP) in low vacuum mode (18 Pa) with 9 mm working distance, a beam acceleration of 20 kV and a current of 500-1000 pA. To obtain a general overview, the entire prepared interface samples were investigated using Energy Dispersive X-ray spectroscopy (EDX). A series of small EDX maps were produced and then stitched together to create a complete picture of the chemical evolution of the interface samples (e.g., Fig. 4). After acquisition, the EDX measurements were analysed using the EDAX genesis software. The brightness and the contrast were adapted to evidence determinate features.

X-ray diffraction (XRD)

The powder was inserted into glass capillaries with an outer diameter of 0.5 mm and a wall thickness of 0.01 mm. The samples were measured using a PANalytical X'Pert³ powder diffractometer in capillary geometry with a Cu source ($\lambda = 1.5406 \text{ \AA}$ Cu $K\alpha$) and a PIXcel^{3D} detector. On the incident beam side, the following diffractometer components were applied: a $1/2^\circ$ divergence slit, a focusing mirror, a 20 mm mask and a $1/4^\circ$ anti-scatter slit. On the diffracted beam side, a 5.0 mm anti-scatter slit and a 0.04 rad Soller slit were applied. The capillary containing the sample was rotated at 4 rpm. The diffraction patterns were acquired between 5° and 70° degrees 2θ using a continuous scan with a step size of $0.026^\circ 2\theta$. The phase identification was performed using the X'Pert Highscore software V. 4.9.

Thermogravimetric analysis (TGA)-IR

TGA-IR was performed using a Netzsch STA 449 F3 Jupiter TGA coupled with a Bruker Fourier-transform infrared (FT-IR) spectrometer for the analysis of the exhaust gases. The infrared absorption signal was integrated in the wavenumber ranges of $3400\text{-}4000 \text{ cm}^{-1}$ (O-H stretching vibration) and $2200\text{-}2450 \text{ cm}^{-1}$

(C=O stretching vibration) characteristic for H₂O and CO₂, respectively, and used as relative measures for H₂O and CO₂ contents in the gas phase released upon heating.

The samples were prepared as described above, and ~15 mg were inserted into alumina crucibles and heated (20°C/min) up to 1000°C. The measured mass loss is mostly related to H₂O release (and partially to CO₂ release), which occur at characteristic temperatures allowing mineral characterisation. The coupling of TGA with infrared analysis indicates which gas (e.g. CO₂ or H₂O) is released at which temperature, supporting the identification of the minerals present (e.g. carbonates).

X-ray tomography

The cement paste-clay samples were investigated by performing attenuation-contrast X-Ray tomography, allowing to infer information on the interface micro-structure. The voxel value from the acquired tomograms can be considered as a proxy for the X-ray attenuation coefficient μ_{X-ray} [cm⁻¹]. The latter is, at a single photon energy, proportional to the product between the bulk mass density ρ and a nonlinear function of the effective atomic number Z_{eff} , whose value increases with increasing Z_{eff} (Jackson and Hawkes, 1981). Within any single component of an investigated material, a region with smaller average voxel value (which can be seen in a simplified way as pixel intensity) may be more porous than one with larger value. However, the difference in average voxel value between the two components of an interface may stem not only from a different mass density but also from a different chemical composition. Thus, the tomographic voxel value cannot be considered uniquely as a proxy of local porosity. Still, X-ray tomography was used complementarily to neutron radiography to gain information about the interfacial local porosity spatial distribution: while neutron radiography could indicate more uniquely the presence of higher or lower local porosity but only in 2D, the fully 3D information about the μ_{X-ray} spatial distribution on both sides of the information could be interpreted at the light of the neutron radiography results (as well as of the chemical and mineralogical analysis ones), i.e., it was possible to infer whether a lower μ_{X-ray} values region also corresponded to a more porous one. The voxel size of the tomograms was ~6 μ m, resulting in an effective spatial resolution between 12 and 13 μ m. Details of the measurements are given in the supplementary materials (S1). The samples were extracted from the cells (but remained in the Teflon holder), to decrease the size of the tomographed volume, thus increasing the spatial resolution. As such, the samples were exposed to normal air conditions during the measurement (approximately constant temperature of 23°C and relative humidity of 40%). This also removed the confining pressure present on the sample. Since compacted Na-montmorillonite rapidly swells in the absence of confining pressure, and the paste tends to carbonate in the presence of CO₂, the acquisition time was set to approx. 1 hour. This optimized acquisition time allowed to safely investigate the samples but limited the tomographic spatial resolution (because of a lower number of faster acquired radiographs). In total three samples were investigated. They had reacted for 2, 4 and 6 years respectively.

Results

pH conditions and sample storage

Small amount of solutions (<20 μ L) were taken during the intermediate storage of the cells and were used to obtain an indicative value of the pH regime present on the different sides (paste and clay) of the interface. The pH was estimated by means of pH indicator paper. No other methods were possible due to the very limited amount of reservoir porewater present inside the cell reservoir located outside the peek frits (30 mm³), see Fig. 1. The results consistently indicated a pH > 13 for the cementitious side. For the clay side, all the measured values were ~12 for samples which were detached from the large reservoirs (using during saturation or diffusion experiments) for longer than ~2 weeks. As already discussed previously, due to limited laboratory space and equipment the experimental cells containing the interface samples were disconnected from the reservoirs for extended periods (up to 2 years), as already discussed in Luraschi et al. (2020). The pH regime on the montmorillonite side was therefore for long periods >12.

Neutron radiography

The initial porosity of the cement paste side was 0.63 (as determined by mercury intrusion porosimetry, Jakob et al., 1999), whereas on the clay side the initial porosity varied depending on the sample between 0.39 and 0.53. Shafizadeh (2019) indicated for the exact same samples the formation of a local high porosity region on the cementitious side and a local low-porosity on the clay side. Due to mineral dissolution the local porosity on the cement paste side and near the interface increased, depending on the sample, up to ~0.68 (Shafizadeh, 2019). With increasing reaction time, the high porosity region extended further from the interface, suggesting further (net) mineral dissolution (Shafizadeh et al., 2020). A similar local porosity increase close to the interface is shown in Fig. 2b (light blue line). The neutron radiographs performed on the same sample during the present study did not detect the marked high porosity region on the paste side (Fig. 2a, Fig. 2b red line). The porosity derivation procedure required an internal self-calibration using the most external part of the cement as reference porosity (0.63). As a consequence, for samples reacted for long times (more than 2 years), the uncertainty on the derived porosity for the cementitious part increased, since the reference porosity may no longer be exactly 0.63. The 30-40 μ m resolution of the neutron radiography, the partly slightly inclined interface contact and the necessity for independent calibration for clay and paste do not allow to precisely resolve what happens in the first 200 μ m of the cement part (Fig. 2). Still, the different radiographs suggest that a slight porosity decrease is present at the contact with the clay on the cementitious side (see also Supplementary Materials, S3), although the general porosity trend a bit further into the paste indicates a porosity increase. This feature was observed in most of the samples reacted >4 years (Fig. 2a, red line; Supplementary Materials S3).

On the clay side, the initial porosity (and thus the reference porosity on the external side) varied depending on the samples between 0.39-0.53 (Shafizadeh, 2019). In the clay region next to the interface, a clear porosity reduction was observed in several samples (Tab. 1) for interaction times exceeding 2-4 months (e.g., Fig. 2b, Supplementary Materials S3). The total extension of this region ("clay skin") was ~1 mm. Beyond this skin, the porosity showed only slight changes. However, for a single sample, the region with a porosity still slightly below the initial value extended partly up to 1.5-2 mm (Shafizadeh, 2019). Most part

of the local porosity changes (on both sides of the interface) took place during the first 9-12 months (Fig. 2a, b), with only small porosity variations after the initial 12 months period. Not all the samples showed a clear local porosity reduction in the Na-montmorillonite on the proximity of the interface. As already observed by Shafizadeh (2019), some samples did not display a significant porosity alteration. Rather it remained quite stable over the years. It has to be considered that this could in principle be related to the uncertainty introduced by the calibration procedure. However, Luraschi et al., (2020) reported only a small diffusivity decrease after >4 years interaction. The latter results suggested that, for these samples, the porosity was not strongly altered. In this article we refer to such samples as “homogeneously reacted samples”. Besides the general trends described above, in some cases local porosity variations were observed in measurements of the same sample within a short time interval (e.g., weeks, as described in Shafizadeh et al., 2020). These observations may be related to the uncertainty of the calibration procedure, including the effects of unavoidable neutron beam intensity fluctuations. However, they may also stem from true porosity variations near the interface, due to a temporal variation of local chemical conditions during the experiment. Figure 2b displays the evolution of the porosity after 2, 20, 23 and 62 months, with only the last measurement (62 months) having performed in the present study. It can be noted that the minimum porosity on the clay side (0.39), after 62 months (red line), is less high than that observed after 20 and 23 months (0.31 and 0.29 respectively). It is unclear whether such a variation represents a real porosity modification. A re-dissolution of newly formed phases (e.g., during the extended time when the sample was not connected to the respective solution reservoirs) cannot be excluded. But the variation could also be related to problems with the necessary calibration after the long interaction time (because the long time may have invalidated the assumption of a constant porosity at the external part of the clay), or problems with the correction for H in the solid by using the dry original clay (because newly formed phases probably have a different mineralogy).

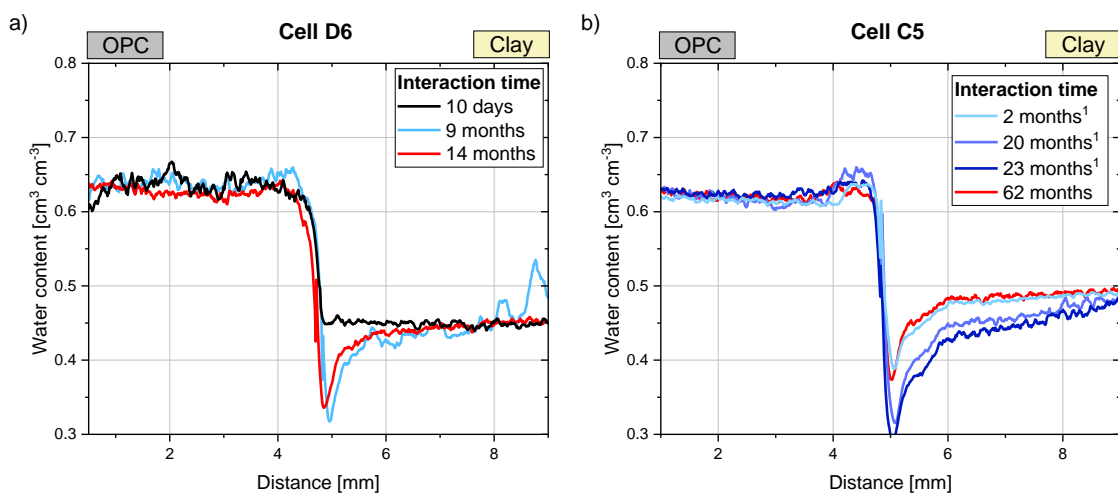


Fig. 2 Evolution of the water content for a) sample D6 during 14 months of interaction. b) Sample C5 during 62 months of interaction. ¹Data from Shafizadeh (2019).

X-ray tomography

The tomogram of sample C3 (Fig. 3), which reacted for six years, gives additional indications on the extension of the clay skin at the contact with the paste. A region with higher voxel value (and thus probably

also with lower porosity) is visible on the clay side (1). Its thickness was $\sim 1\text{mm}$, consistent with the thickness of the lower-porosity region deduced from the neutron radiographs (see Supplementary Materials S3). Such a thickness value was found for all the different samples. Another clay skin region's feature common to all samples and particularly evident from the X-ray tomograms as well as from the neutron radiographs was that it displays a relatively sharp boundary (2). The X-ray tomograms also confirmed another feature already observed by neutron radiography: the remaining clay part (from 1 to 5 mm away from the interface) exhibited a high degree of microstructural homogeneity (3), mirrored by relatively constant voxel values throughout, with exception of bright spots, likely representing heavy accessory minerals (4). The comparison between voxel and pixel value spatial distributions of the X-ray tomograms and 2D spatial maps of local water content, respectively, thus hinted at considering the voxel values also as proxies of local density values, positively correlated with the local porosity ones. In all samples the region with the highest voxel values (i.e., likely lowest porosity) is located in the clay at $\sim 500\ \mu\text{m}$ from the paste contact (5), and is clearly visible in the X-ray tomograms (see, for an example, the bright domain in Fig. 3a or, equivalently, the dark blue one in Fig. 3b, the latter showing the voxels with value above a certain high threshold).

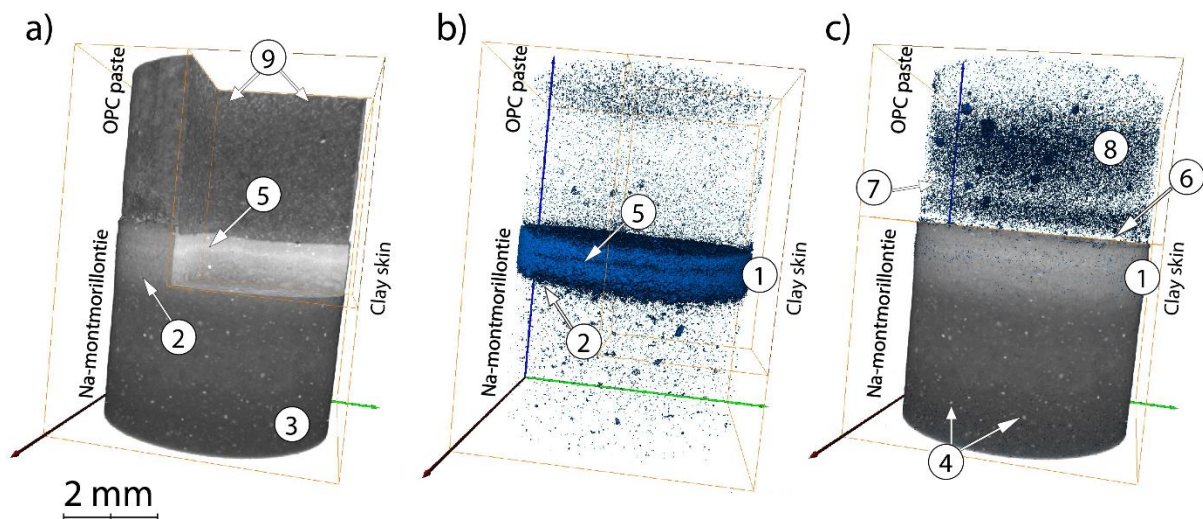


Fig. 3 3D rendering of sample C3's X-ray tomogram, after 6 years of interaction (a). More than one octant of the tomogram's volume was not rendered in order to allow a view inside it. From the tomogram, the low-porosity region on the clay side was segmented and rendered in dark blue (b) whereas, on the cement side, a part of the resolved pore space was segmented by voxel value threshold selection and rendered (c), with dark blue regions showing single pores.

On the cementitious side, binary segmentation by the choice of a low voxel value threshold, allowed mapping out part of the resolved pore space (Fig. 3c). Approximately within the first $200\ \mu\text{m}$ of such side, a higher voxel value region (6) is present (comparably bright in Fig. 3a, fewer segmented pores in 3c). Such thin, less porous layer is likely related to new minerals precipitation (thus, possibly, also to lower porosity). At 1 mm distance from the interface, the resolved pore distribution shown in Fig. 3c shows a thin layer of lower local porosity (7). Still focusing on the segmented pore space shown in Fig. 3c, the mid region of the cementitious side was characterized by a significant increase in local porosity (8), followed, towards the cement paste side's end, by a significant drop. Such final drop region exhibited not only a significant increase in voxel value, partly recognizable in Fig. 3a (9). It also showed a punctuated, random distribution

of high X-ray attenuation spots (see Fig. S1 in the Supplementary Materials). Such spots are significantly less present in the middle region.

SEM/EDX

Several samples that interacted for different time periods were investigated by means of SEM/EDX. To highlight determinate chemical features, only selected channels of the acquired the multispectral EDX images are shown in the following paragraphs (e.g., Fig. 4).

The cement paste side

On the cement paste side, the sample which reacted for a relatively short period (8 months of interaction, Fig. 4a) shows portlandite $[\text{Ca}(\text{OH})_2]$ dissolution for the first 2 mm from the interface (1), whereas the portlandite dissolution front extends further away from the interface (2) in the sample that reacted for longer time (4 years, Fig. 4c). In the other sample that reacted also for 4 years, but where no low-porosity region formed (homogeneously reacted samples) on the clay side (Fig. 4e), portlandite dissolved throughout the entire cement paste side (3). On the cement paste side darker regions are well recognizable at the border and surrounding fractures. These regions are not a result of mineral alteration but are an effect of the high porosity of the cement paste, allowing the resin to penetrate into the sample resulting in a lower intensity (4).

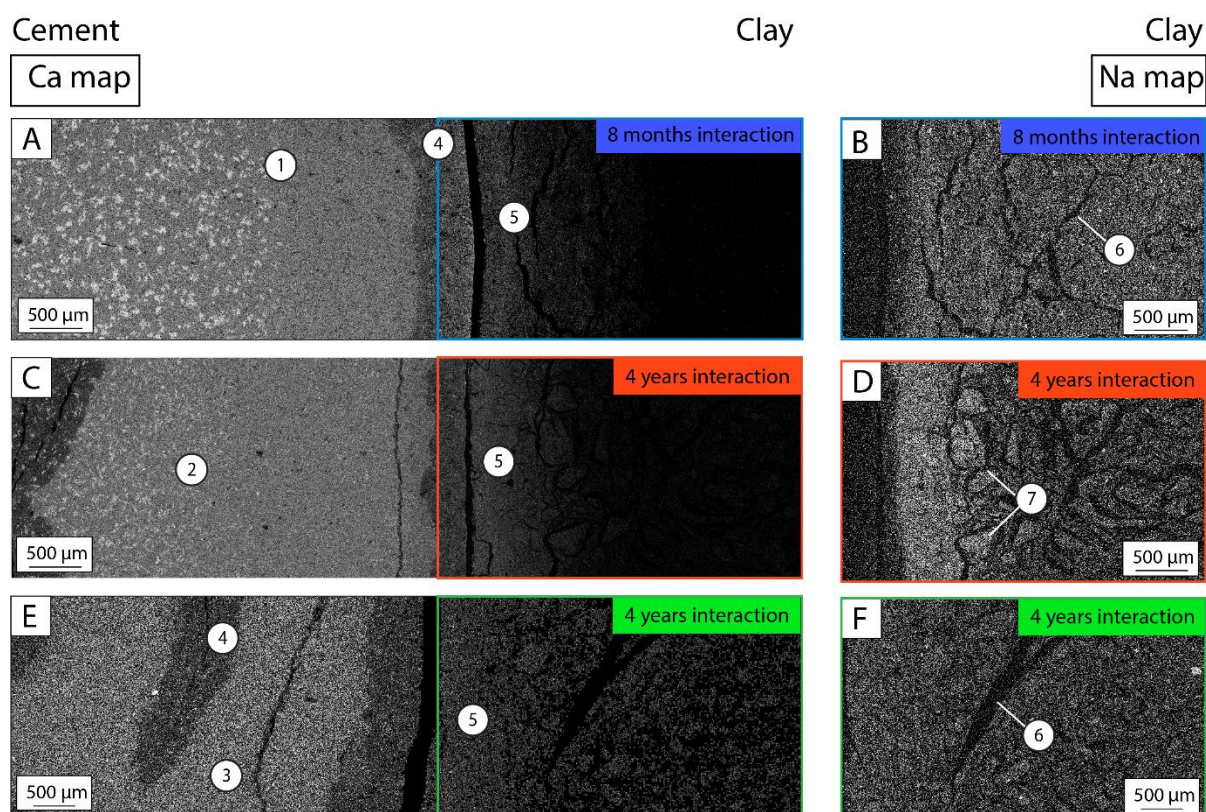


Fig. 4 Calcium and sodium EDX maps of three different Na montmorillonite-OPC paste samples (left column: OPC paste on the left side, Na montmorillonite on the right side; right column: only Na-montmorillonite). A) Ca map for a sample (D5) reacted for 8 months. B) Corresponding Na map of the clay side. C) Ca map for a sample (C25) reacted for 4 years. D) Corresponding Na map of the clay side. E) Ca map for a sample (C29) reacted for 4 years (homogeneously reacted sample). For this sample on the clay side no low-porosity region was detected. F) Corresponding Na map of the clay side. Figure numbering: 1) portlandite stability front, 8 months interaction. 2) Portlandite stability front, 4 years interaction. 3) Absence of portlandite (homogeneously reacted sample). 4) High-density and compacted region on the clay side close to the interface. 5) Drying-related cracks, subsequently filled with epoxy resin. 6) agglomerated-like regions in montmorillonite.

Element ratios 1D profiles along the direction approximately orthogonal to the interface, derived from the EDX data, provide a more quantitative picture. A decrease of the Ca/Si ratio towards the interface (Fig. 5a) is mainly caused by portlandite dissolution. The corresponding 2D portlandite dissolution fronts are also well visible in Figs. 4a, b. The longer the interaction time, the stronger is the portlandite dissolution and the further the front advances away from the interface. In all the samples, the sodium concentration on the cement paste side is slightly increasing towards the interface (Fig. 4b). In the most external part (5 mm from the interface) high Na concentrations are probably partially related to the presence of resin which alters the Na detection. By looking at the Aluminum distribution (Fig. 4c) on the cement side it is possible to observe a progressive increase of the Al content approaching the interface for samples with a low-porosity region on the clay side.

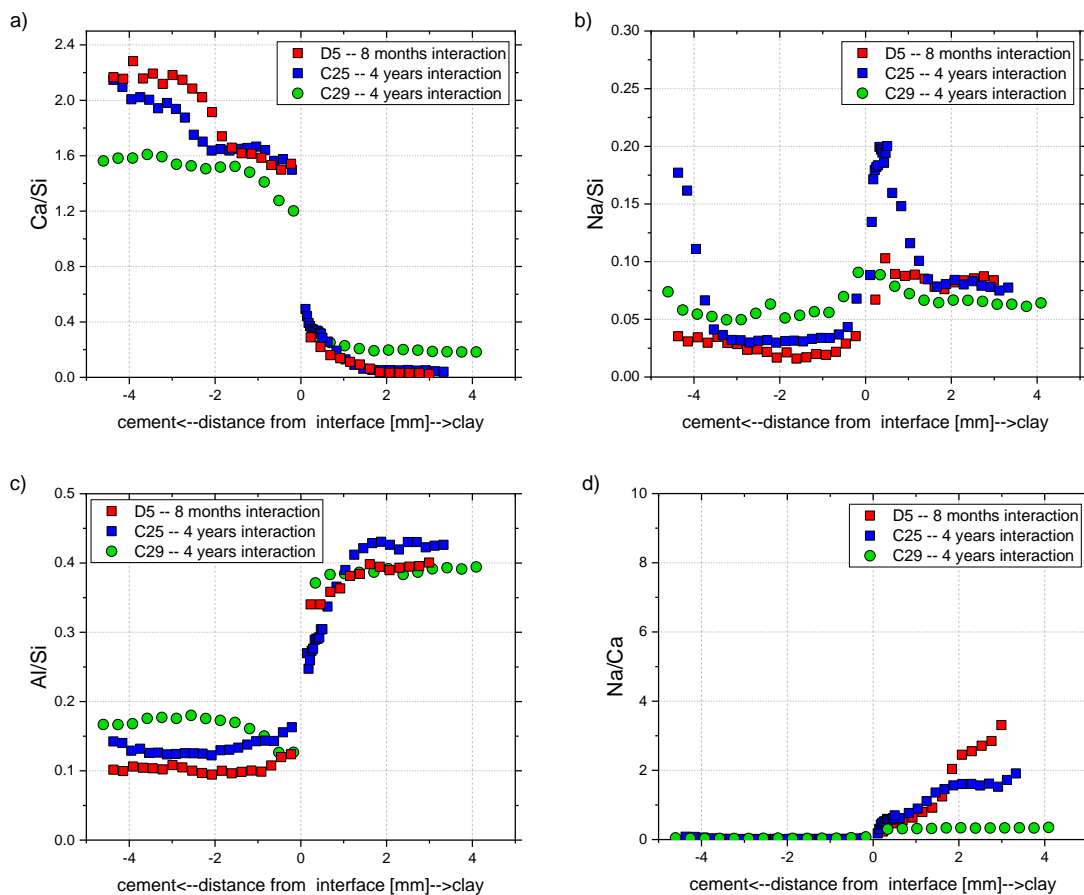


Fig. 5 1D profiles of different element ratios orthogonally to the interface, as derived by EDX mapping, of the three interfaces of Fig. 4. Sample C 29 represents a sample where no low porosity region formed on the clay side.

The clay side

On the clay side, it is possible to observe, close to the interface, a region which appears more compacted, showing less fractures than the unaltered clay part (Fig. 4, first mm of the clay side (5)). The cracks and openings in montmorillonite (6) are related to the sample preparation procedure, as explained in the methods: montmorillonite strongly shrinks upon drying. The montmorillonite does not appear completely homogeneous in samples which were in contact with the alkaline pore solution. Rather, some agglomerated

regions appeared (7). As they were also visible in X-ray tomograms, they appear to be related to structural alterations, and not to drying artefacts.

Figures 4a, c and 5a, clearly show a strong enrichment in Ca within the first mm from the interface. This is a feature typically observed in all the samples exhibiting a low-porosity region in the neutron radiographs (see Tab. 1 for their list). The homogeneously reacted samples also showed an enrichment but not limited to a rim at the interface (Fig. 4e, 5a).

A clear enrichment in sodium concentration was observable on the clay side close to the interface, in all investigated samples. For samples with a low-porosity region, the longer the interaction time, the stronger the enrichment tends to be (Fig. 4b, 4d). In detail, the Na distribution shows a depletion in the first hundreds of μm from the interface and an enrichment at $\sim 500 \mu\text{m}$ away from the interface (Fig. 5b). The Na-rich region was observed also in homogeneously reacted samples, although not so prominent as in the other samples. Also, in this case the partial disconnection of the reservoir for some periods may have slightly influenced the enriched Na rim's position. On the clay side, the Na/Ca ratio was steadily increasing towards the external part of the samples less influenced by the cementitious porewater, and therefore considered as less altered. The Na/K ratio is stable outside the clay skin (see Supplementary Material, S6). These observations suggest (partial) Ca substitution of Na inside the montmorillonite (Fig. 5d). Regarding aluminum, within the low-porosity region, the Al/Si ratio is clearly lower compared to the values in the external less altered clay regions (Fig. 5c). This observation may indicate the precipitation of Si-rich phases (i.e. C-S-H).

Thermogravimetric analysis combined with FTIR (TGA-FTIR)

The cementitious side of a homogeneously reacted sample (C2) was subjected to TGA-FTIR characterization (Tab. 1). Fig. 6a, first of all, clearly shows the absence of the typical portlandite DTG signal peak, at $\sim 470^\circ\text{C}$, in two successive regions of a sample (C2) covering the first 5 mm from the interface, while such peak is clearly evident for an unaltered paste sample. Correspondingly, no IR absorption H_2O peak (Fig. 6c) was observed for the same regions, compared with the unaltered sample, suggesting massive or even complete portlandite dissolution within the first 5 mm from the interface (in homogeneously reacted samples).

From 50°C to 250°C , the regions closer to the interface exhibited a more prominent and wider peak than that of the unaltered sample in the DTG and the H_2O signal. This peak indicates the formation of new minerals with weakly bound water (e.g., AFm, C-S-H or C-A-S-H). Furthermore, between 280°C and 400°C , a considerable amount of mass was lost (4% absolute, Fig. 6b). The FTIR spectrum shows a strong CO_2 release and a small H_2O release related to this mass loss peak. This temperature interval and the respective CO_2 release could suggest the presence of hydrotalcite (Lothenbach et al., 2016). However, the CO_2 peak could also be related to the presence of amorphous (possibly monohydrated) CaCO_3 . The CO_2 release FTIR peak and the corresponding increased mass loss between 600°C and 700°C may point at a slightly higher presence of a carbonate phase in the region at 3-5 mm from the interface. This could be possibly explained by the exposure of the samples to atmospheric conditions during storage, preparation and measurements, with consequent CO_2 mixing in the pore solution. The peak could be related to several phases (e.g., calcite (or polymorphs), carbonate-AFm), but a definitive identification was not possible.

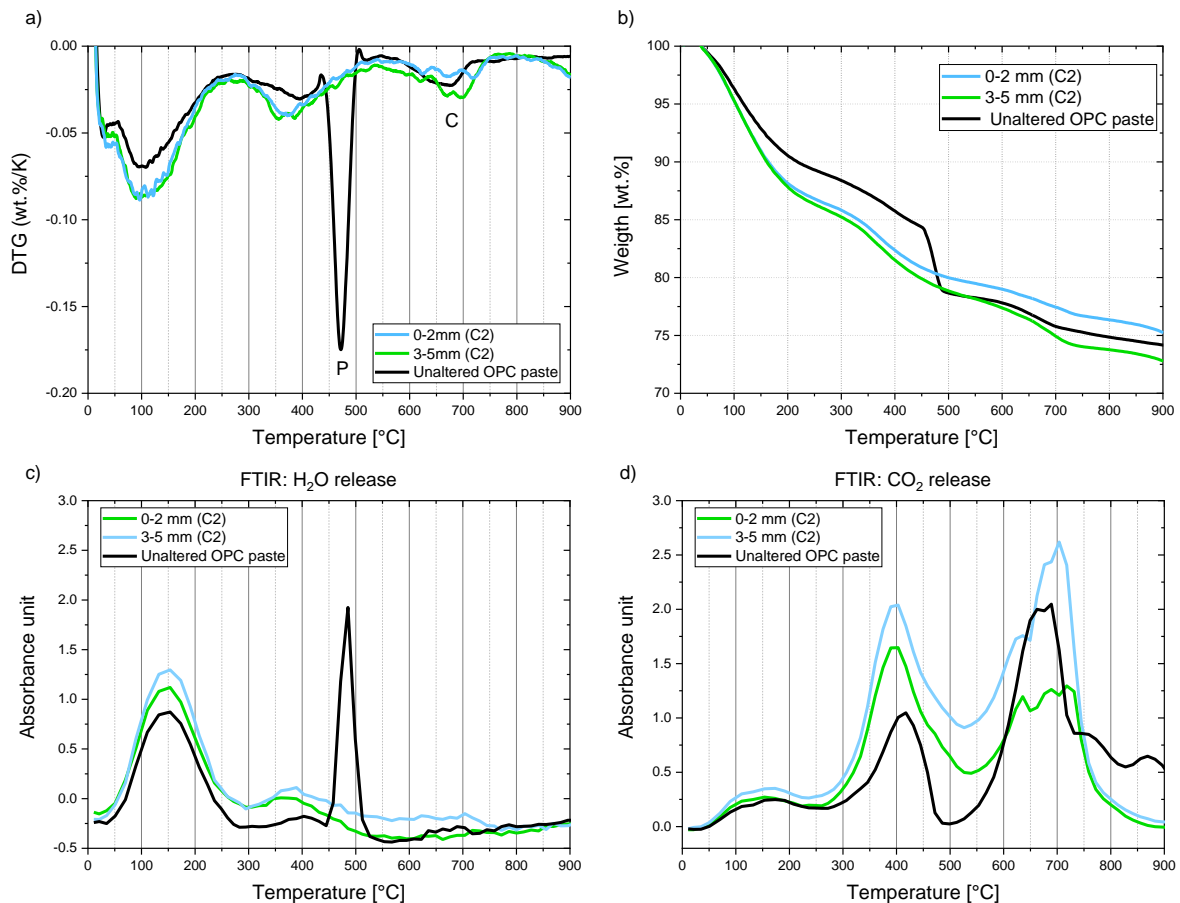


Fig. 6 a) DTG of the cement side of the homogeneously reacted sample C2 (freeze dried) after 70 months of interaction and of an unaltered OPC paste (freeze dried). P: portlandite. C: calcite. b) Corresponding TGA/DTG. c) H₂O exhaust analysis using FT-IR during TGA. d) CO₂ exhaust analysis using FT-IR during TGA.

The unaltered Na-montmorillonite DTG curve is characterized by a sharp negative peak at about 100°C, extending to about 200°C (black line, Fig. 7a), representing the dehydration of the clay interlayers, as also evidenced in Fig. 7c (H₂O loss). Mass loss is also observable at 700°C, related to clay dehydroxylation. The curves for clay parts from sample C3 (with low-porosity region) furthest away from the interface (Fig. 7a, blue lines) show a relatively homogeneous dehydration pattern, quite similar to the one of unaltered Na-montmorillonite. This suggests that the main mineralogy is still dominated by the original Na-montmorillonite layout. However, it has to be remarked that, in the 0-200 °C region, the negative peaks of the furthest away regions are broader than those in the unaltered region, indicating that some (minor) mineralogical changes occurred.

The clay sample from the skin area (0-1 mm), compared to the unaltered Na-montmorillonite sample, shows a weaker water loss up to 100°C, but then a remarkably broader and stronger mass loss (Fig. 7a, b) from 100°C to 300°C. Furthermore, a negative peak at 400-600°C is observable, related to a significant mass loss. A continuous mass loss between 200°C and 700°C has been described for instance for M-S-H phases (Lothenbach et al., 2016; Bernard et al., 2017). However, it is unclear whether Mg has been present in large enough quantity in the samples to form such phases. The continuous dehydration between 100°C and 300°C suggests the presence of C-S-H (Lothenbach et al., 2016; Gruskovnjak et al., 2011). Compared to the external part of the sample (>1 mm), in the skin region a large fraction of the mass is lost within the first

300°C, suggesting that C-S-H minerals dominate the skin composition. The absence of the negative DTG peak at 700 °C, which is characteristic of clay dehydroxylation, suggests that the clay amount inside the skin is reduced with respect to the unaltered sample. The green line in Fig. 7 represent the external clay part (3-5 mm from the interface) of the homogeneously reacted sample C2. The DTG curve show a reduced peak between 100-200°C compared to the unaltered Na-montmorillonite samples and also compared to the external parts of the sample C3 (showing a low-porosity region in clay). Furthermore, between 100-200°C there is a greater mass loss compared to the unaltered sample. These observations suggest that homogeneously reacted samples were altered also in the external regions.

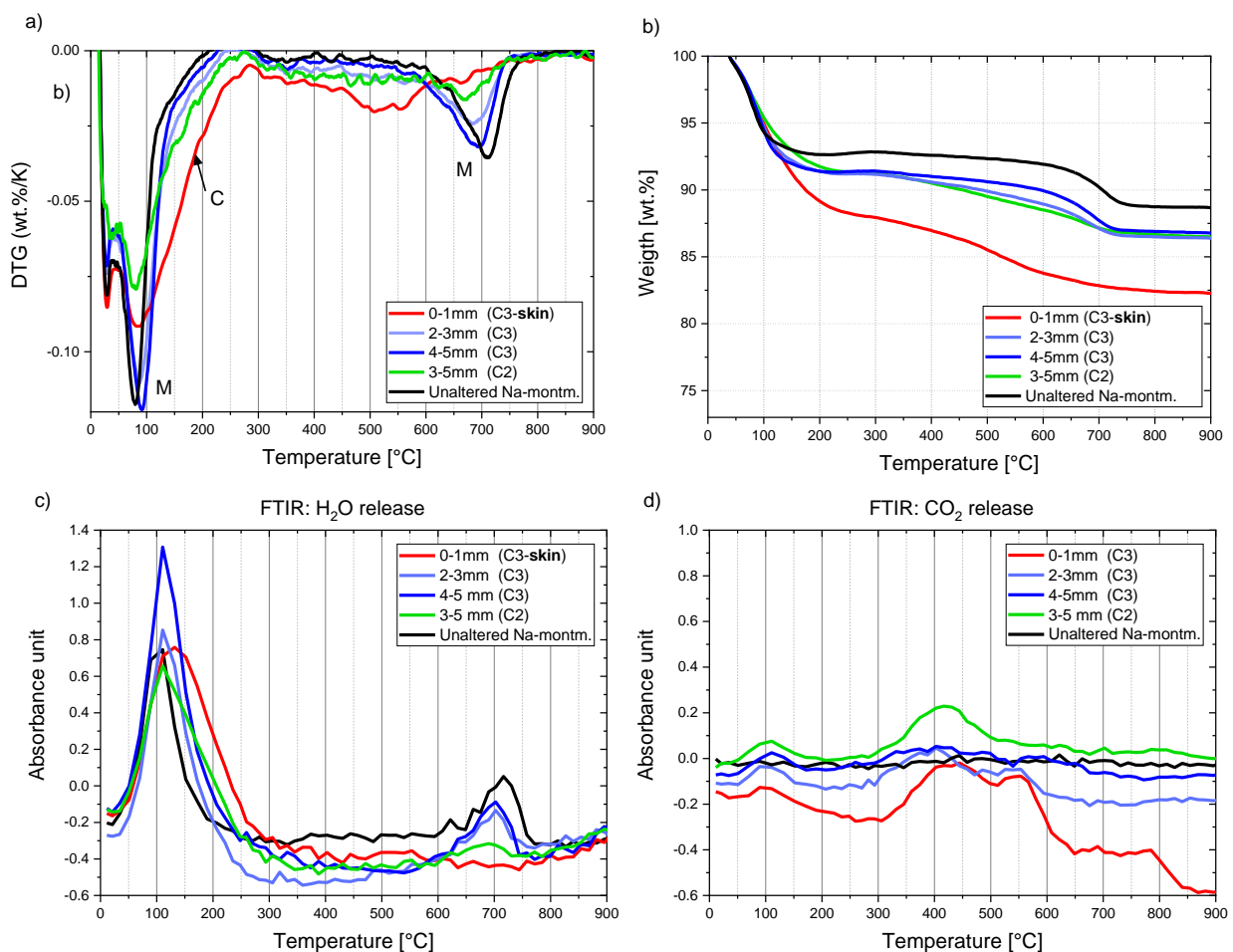


Fig. 7 a) DTG of the C3 sample (clay part only, freeze dried) after 70 months of interaction, of the C2 sample (homogeneously reacted sample, freeze dried) and of unaltered Na-montmorillonite (freeze dried). b) Corresponding TGA/DTG. c) H₂O exhaust analysis using FT-IR during TGA. d) CO₂ exhaust analysis using FT-IR during TGA.

X-ray diffraction

The cement side

The unaltered paste samples are composed of portlandite (main reflections at 18.0° and 34.0° 2θ CuKα), C-S-H (main reflections at 29.1°, 32.5° and 49.6° 2θ CuKα) and ettringite (AFt, main reflections at 9.1°, 15.8° and 23.0° 2θ CuKα). The reflection at ~29.4° 2θ CuKα represents as well the main reflection of calcite, which is also present. For the sample C3 (Fig. 8a), which developed a low-porosity region on the clay side, no

ettringite was observed. In sample C12 ettringite is instead well recognizable (Fig. 8b); the reflection intensity decreases towards the interface.

In the samples with an interaction time >5 years, the XRD portlandite fingerprint was, in general, only weakly observable, a further hint that the mineral was almost completely dissolved throughout the sample. Very weak portlandite peaks were for example detected in the external region (4-5 mm from interface) of sample C3 (blue line in Fig. 8a). Moving from the external region of the cementitious side (less altered) towards the interface (progressively more altered), an increase of the intensity of a reflection that matches with AFm can be observed, with a major reflection at $11.2^\circ 2\theta$ CuK α . In sample C12, (Fig. 8b), which shows a homogenous alteration, portlandite's XRD fingerprints are completely absent, and a very weak AFm reflection is observable at $11.2^\circ 2\theta$ CuK α .

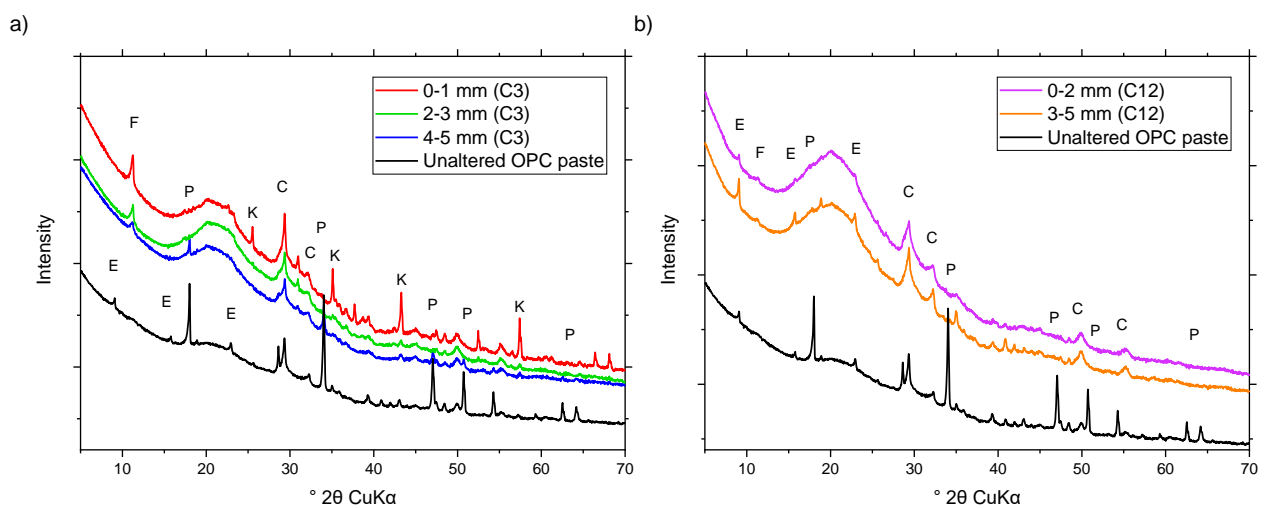


Fig. 8 XRD pattern for cementitious side in C3 (freeze dried) and C12 (freeze dried) samples with and without low porosity zone respectively. The dark line represents unaltered OPC paste (dried in a desiccator). A) Sample C3: low porosity region formed on the clay side leading to different alteration within the sample. B) Sample C12: no low porosity region formed on the clay side; the whole paste sample reacted homogeneously. Peak identification, F for AFm, P for portlandite, C for C-S-H, K for corundum (polishing paper), E for ettringite. The hump visible between $\sim 15^\circ$ and $\sim 25^\circ 2\theta$ CuK α is related to the capillary holder.

The clay side

Unaltered Na-montmorillonite is characterized by a prominent reflection at $\sim 19.6^\circ 2\theta$ CuK α , corresponding to an interlayer distance of 4.5 \AA , followed by a series of minor reflections also related to montmorillonite (Fig. 9). A small reflection at $21.9^\circ 2\theta$ CuK α may possibly indicate the presence of cristobalite ($d = 4.05 \text{ \AA}$), but it could also be possibly related to stacking faults (structural displacement of layered minerals which lead to complex XRD pattern, see Jansen et al., 2024). The reflection at $26.6^\circ 2\theta$ CuK α is related to quartz. For all the Na-montmorillonite samples in contact with the paste, a similar pattern was observed independently from the formation or not of the low-porosity region on the clay side: i) absence of the reflection at $21.9^\circ 2\theta$ CuK α ; ii) reduction of the Na-montmorillonite reflection at $19.6^\circ 2\theta$ CuK α ; iii) a very prominent reflection appears at $7.2^\circ 2\theta$ CuK α ($d = 12.5 \text{ \AA}$). The latter reflection is observed in every measured sample and matches potentially with several minerals: Na-beidellite, zeolites and Ca/Na-montmorillonite. Although the conditions are favorable for zeolite formation, they are generally observed only at higher temperatures (Gaucher and Blanc, 2006), and therefore unlikely to be found in our

samples. The formation of Na-beidellite instead cannot be excluded, as already observed by Karnland et al. (2004) for similar conditions. However, the composition of the sample and the alkaline conditions let the authors consider this reflection as being mainly related to a Ca/Na-montmorillonite. For the sample with a low-porosity region on the clay side (Fig. 9a, 0-1 mm), a new (quite broad) reflection at 29.1° 2θ CuK α ($d=3.07\text{\AA}$) is observed, indicating the possible presence of calcite as well as of formed C-S-H. The significant reflection width also points at the C-S-H formation within such clay side. The reflections at 31.9° and 49.6° 2θ CuK α is also characteristic for C-S-H. The high intensity of the Na-montmorillonite reflection (19.6° 2θ CuK α) observable in the unaltered sample, is remarkably decreased inside the skin region, suggesting partial montmorillonite dissolution. For the samples, where a low-porosity region is present (Fig. 9a), most of the mineralogical alteration seems to have taken place within the first mm from the interface. The remaining regions were characterized by Ca substitution in Na-montmorillonite and possible cristobalite dissolution (although the presence of this mineral was not certain). No C-S-H formation can be inferred beyond the skin. For homogeneously reacted samples, where no low-porosity region formed, the clay mineralogy is nearly identical throughout the clay sample (Fig. 9b) and is about identical to the one inside the skin region (e.g., Fig. 9, C3-skin in inset a) vs 0-2 mm C12 in inset b)).

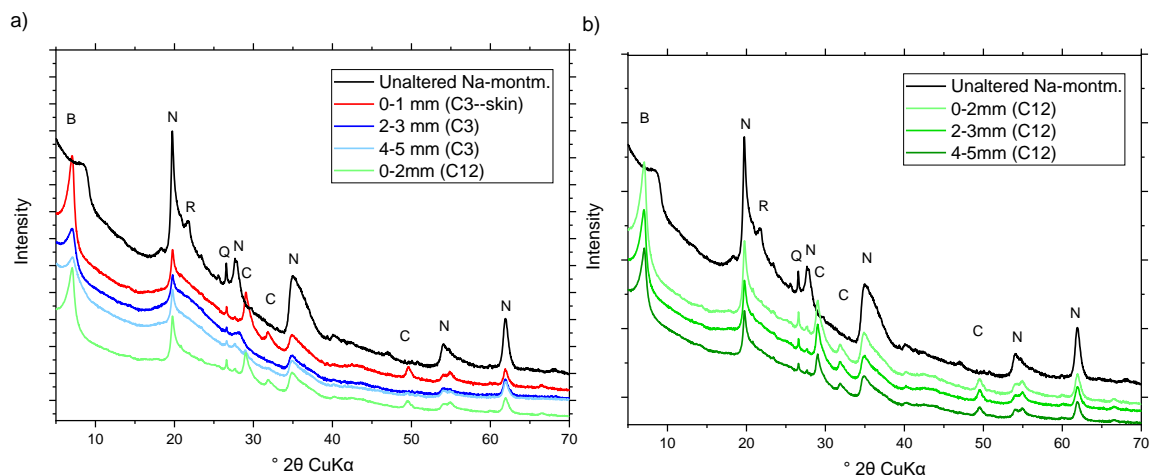


Fig. 9 XRD pattern for different sections of the clay compartment in samples C3 (a, with a low porosity region on the clay side; 6 years interaction time) and C12 (b, homogeneously reacted, without low porosity region on the clay side; 5 years interaction time). Peak identification: B for Ca/Na-montmorillonite; N for Na-montmorillonite; C for C-S-H; Q for quartz; R for cristobalite or clay Staking faults.

Discussion

Mineralogical evolution of the interface

The cementitious side

The experimental observations for the cement side are summarized in Tab. 2 and in Fig. 11. The paste's water content was relatively high (between 60 vol.-% and 65 vol.-%, as estimated by neutron radiography, Fig. 2), pointing at favorable conditions for transport and mixing of its pore solution with the claystone's, with consequent pH decrease. A decrease in pH leads to subsequent dissolution of cement hydrates. One of them, portlandite, is soluble already at a $\text{pH} < 12.5$ and delivers Ca^{2+} and OH^- to the solution. Portlandite dissolution is the most commonly and first observed and observable reaction in OPC-clays systems, given that ettringite gets structurally destabilized at $\text{pH} < 11$ (Jacques et al., 2010) and C-S-H at $\text{pH} < 9.5-10$

(Swanton et al., 2016; Bernard et al., 2017). In addition, portlandite very high crystallinity degree simplifies its identification and the monitoring of its dissolution. The latter starts as soon as the cement paste gets in contact with the clay's porewater.

We would like to underline that the time-resolved locations of the portlandite fronts (depending on the interaction time) could be detected with the different methods in all samples (Fig. 3, 4, 6, 8). Once portlandite was dissolved, as mentioned above, C-S-H were the next cement hydrate prone to dissolution and recrystallization. The C-S-H decalcification process depends on the Ca/Si ratio and on the pH conditions (Mainguy and Coussy, 2000; Gaitero et al., 2008; Butcher et al., 2012). Partial C-S-H decalcification, at least close to the interface (where portlandite was completely dissolved), was therefore likely to have taken place in the investigated interface systems. The XRD measurements indicate an increasing presence of one AFm phase, towards the interface (Fig. 8a, reflection at about $11.2^\circ 2\theta$ CuK α). The high chloride content of the montmorillonite porewater suggest that the AFm is likely to be Friedel's salt [$\text{Ca}_2\text{Al}(\text{OH})_6(\text{Cl}, \text{OH}) \cdot 2 \text{H}_2\text{O}$]. Chloride could have diffused towards the paste, inducing the formation of the Cl-AFm phase. This process is often observed during sea water alteration of concrete (Taylor, 1997; Glasser et al., 2008; Yuan et al., 2009). Part of Friedel's salt is likely to form by exchange of anions in AFm phases (e.g., CO_3^{2-} , SO_4^{2-}) already present in the hydrated cement (e.g., mono-/hemicarbonates, monosulfate and related phases), while it may also precipitate as new phase due to the favorable geochemical conditions. In the latter case, calcium ions would be provided mainly by the portlandite dissolution, whereas aluminum ions would originate from the partial dissolution of the clay under alkaline conditions (Bauer and Berger 1998). The temporal increase in aluminum on the cement paste side, detected by EDX mapping (Fig. 5c), can be explained by the enrichment with Friedel's salt. Another possibility would be the incorporation of aluminum in C-S-H leading to a transformation into a C-A-S-H phase. However, no clear evidence was found supporting this hypothesis. Ettringite was detected in some samples far away from the interface, where pH conditions allow its stabilization (Fig. 8b). In certain samples ettringite was completely dissolved (e.g., Fig. 8a). Ettringite dissolution and re-precipitation was observed by Jenni et al. (2014) and Mäder et al. (2017). In general, the paste and its porewater were, close to the interface, strongly influenced by the clay contact. High contents of Na^+ and Ca^{2+} , the latter released by portlandite and C-S-H dissolution, were observed. The dissolution of clay would also lead to the release of Mg^{2+} into solution, but no evidence of any local Mg enrichment, on the cementitious side, was found, different to what reported for example by Mäder et al. (2017).

Tab. 2 Summary of the applied characterization techniques and the identified material phases and their modifications on the cementitious side.

Technique	Cementitious external part	Cementitious skin at the interface
Neutron radiography	Relatively unaltered local porosity	Small porosity increase (with local variations)
X-ray tomography	Relatively unaltered composition	Dissolution of a high density mineral. Local porosity/density variation between 1-3mm from the interface. High density/low-porosity region at the interface (<200 μm)
EDX	Relatively Homogeneous chemical composition	Ca/Si decrease, Al/Si, Na/Si increase
TGA-IR	Portlandite, C-S-H, calcite	C-S-H
XRD	Portlandite, C-S-H, calcite, Friedel's salt	Friedel's salt, C-S-H

The clay side

All the clay samples, where a low-porosity region (clay skin) was detected with neutron imaging, show a very similar mineralogy (as summarized in Tab. 3 and Fig. 11). At the interface, starting after ~6 months interaction, a zone (called skin) with very high calcium and sodium content was observed, as evinced from the corresponding EDX images (Fig. 4) and their respective 1D profiles (see Fig. 5a and b). The extension of such skin was limited to ~1 mm. The calcium enrichment slightly increased progressively with increasing reaction time. At any time point, a maximum was observed close to the cementitious side (see Figs. 4, 5). In contrast, the highest concentration of sodium was measured at ~500 μm from the interface, and was well recognizable in the EDX images (Fig. 4b, d) as well as in their respective 1D profiles. The lowest local porosity, detected on the clay side by neutron radiography, was approximately located in the same region as this high sodium and calcium region (Fig. 2 and, for a conceptual scheme, 11). Whether first a Na phase precipitates and leads to the porosity decrease, or whether another (e.g., Ca) phase first precipitates and then later Na enriches within this phase, remains an open question. XRD and TGA investigations identified the presence of C-S-H inside such skins (Figs. 9, 10). C-S-H was observed throughout the entire clay side in homogeneously reacted samples. Furthermore, the XRD and TGA patterns of these samples were similar to those of the low-porosity skin region in samples where it formed (Fig. 9). Neutron imaging did reveal a homogenous local porosity spatial distribution for the homogeneously reacted samples. Luraschi et al. (2020) did observe only a weak decrease in diffusivity through such samples, meaning that, very likely, the porosity only slightly decreased. C-S-H formation in the clay side was reported by several authors from both modelling and experimental studies (Hodgkinson and Hughes, 1999; Ramirez et al., 2002; Cuevas 2004; Tinseau et al., 2006; Kosakowski et al., 2009). In some cases, where bentonite and concrete were put in contact, the formation of C-A-S-H was observed (Adler et al., 1998; Claret et al., 2002; Fernández et al., 2016). Our investigation did not clearly evidence the formation of C-A-S-H. Although no specific method to detect C-A-S-H was applied (e.g., Nuclear magnetic resonance spectroscopy, NMR). Nevertheless, the XRD-observed formation of Friedel's salt (Fig. 8b) is compatible with temporally increased aluminum contents in solution, observed via EDX imaging (Fig. 5c). It is therefore possible that in some cases Al substitution in C-S-H took place as well.

XRD (Fig.7) and TGA (Fig. 9, 10) results suggest partial montmorillonite dissolution. It has to be mentioned that, although clays are known to dissolve under alkaline conditions, the kinetics of this process is still under debate (Gaucher and Blanc, 2006). It is thus uncertain how much clay really dissolved in our experiments, and a precise quantification is difficult from our data.

Tab. 3 Overview of the applied characterization techniques and the identified material phases on the clay side

Technique	Clay external part	Clay skin
Neutron radiography	Relatively unaltered local porosity	~0.1 porosity decrease
X-ray tomography	Relatively homogenous properties	High density region, 1 mm extension. Max. at 500 μm
EDX	Na/Ca lower than unaltered Na-montmorillonite	Ca-Na rich region, 1mm extension
TGA-FTIR	montmorillonite	C-S-H. clay dissolution
XRD	Na-montmorillonite, quartz	C-S-H, Ca-Na montmorillonite, cristobalite dissolution (?)

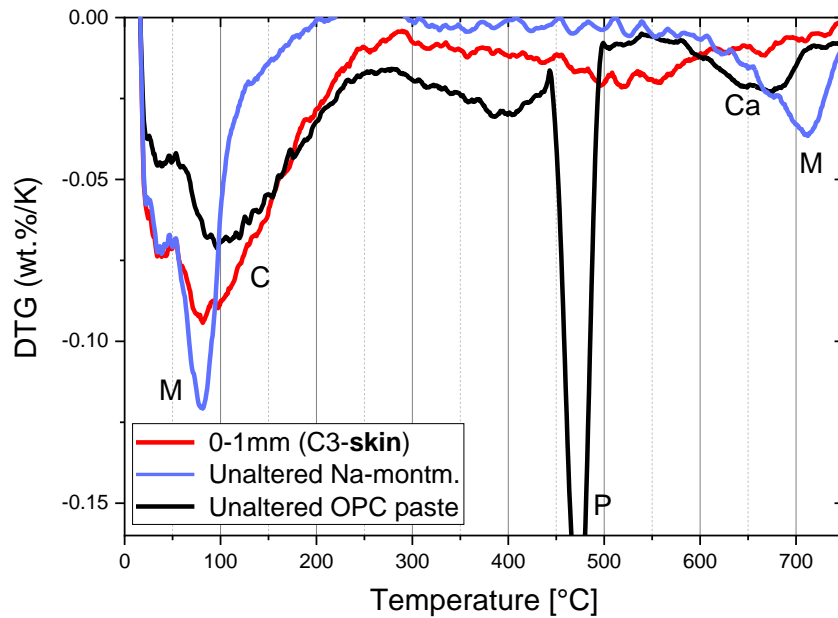


Fig. 10 DTG of a clay skin (freeze dried) compared to an unaltered OPC (dried in dessicator) and Na-montmorillonite (freeze dried). Peak identification: M for montmorillonite, C for C-S-H, P for portlandite, Ca for calcite.

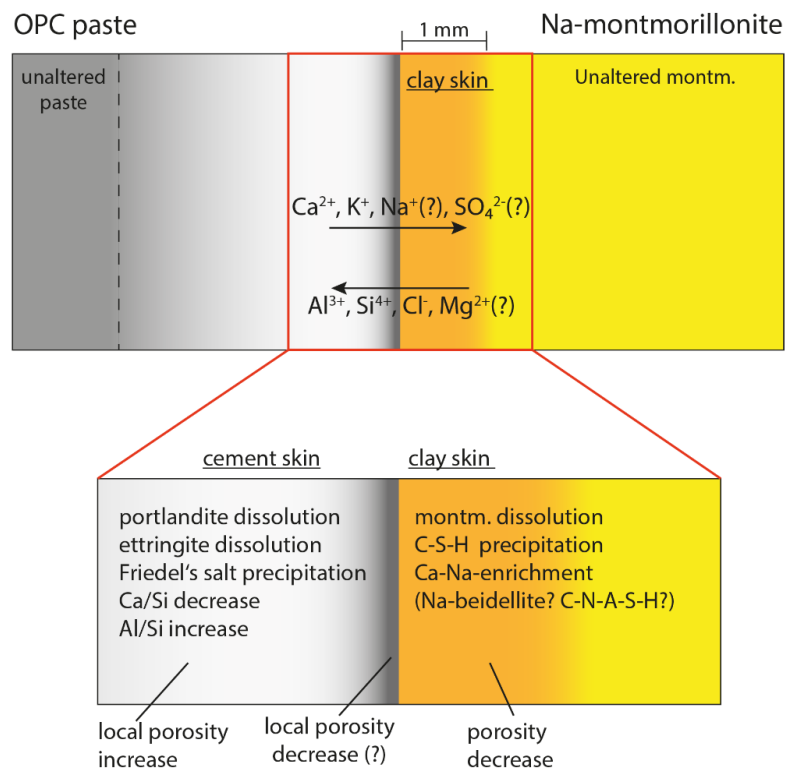


Fig. 11 Schematic view of the reactions observed at OPC paste-Na montmorillonite interfaces

Evolution of the local porosity at the interface

The neutron radiography results point at a rather homogeneous spatial distribution of local porosity throughout the cementitious side, at any time point, except for a local region directly at the interface with a small maximum (Fig. 2b) observed for interaction times <2 years (Shafizadeh et al., 2020). The latter feature was not observed systematically (compare Fig. 2a with b) and was not fully confirmed by the X-ray tomogram of one sample (C3) different from those of Fig. 2. The X-ray tomogram shows a very thin (approximately 200 μm), denser (i.e., likely also less porous) layer directly at the interface, followed by a lower local porosity region. The comparison of such results, obtained from two distinct imaging modalities, highlights what already mentioned before and also by Bernard et al. 2020, i.e., the difficulty in characterizing the spatio-temporal distribution of local porosity. On the one side, neutron radiography and X-ray tomography allow actual, time-lapse monitoring of such distribution. On the other side, they are limited in terms of spatial and quantitative resolutions. SEM/EDX imaging and autoradiography are two imaging techniques, which have been often used for mapping out the local porosity (Prêt et al. 2010; Jenni et al. 2014; Sardini et al. 2015; Mäder et al. 2017; Lerouge et al. 2017). While they allow achieving much higher spatial resolution than what obtainable, for similar sample size, by the two previous imaging modalities, they do not allow actual time-lapse monitoring, due to the respective sample preparations, which are destructive. Although not possible for the same exact sample, the combination of these four imaging modalities, applied to distinct samples, might offer the only possibility to achieve a reliable characterization of the pore space at multiple length scales.

The XRD, TGA-FTIR, EDX and X-ray tomography results presented in this work already showcase the information gain stemming from the combination of distinct characterization techniques. While XRD and TGA-FTIR clearly allowed detecting portlandite dissolution, such bulk information has allowed interpreting and correlating the EDX imaging and X-ray tomography results, with consequent hypothesis of an extension, with time and starting from the interface, of the region where the dissolution takes place. Based upon the data collected in this work, the portlandite dissolution seems to have been associated with a region of decreased local porosity, a feature of the dynamics of such interface systems worth of a dedicated time-lapse experimental campaign. Beside portlandite dissolution, there are other minor mineralogical modifications on the cementitious side which may also slightly have had affected the porosity, as the formation of Friedel's salt in the C3 sample and/or of C-S-H phases). Concerning the specific case of the C3 sample, the higher spatial resolution achieved by X-ray tomography, in comparison with neutron radiography, allowed correlating the higher density region formed in the first 200 μm away from the interface with a correspondingly thin region with slightly lower porosity, also forming at the interface, observed in the respective neutron radiographs (see Supplementary Material, S3). This feature may suggest that some new minerals may precipitate at the interface, leading to a local porosity decrease, while the general trend, on the cementitious side, being more likely an increase in bulk porosity due to hydrates destabilization/dissolution.

The porosity within the clay-skin on the clay side (with 1mm extension) decreased relatively rapidly, thus supposedly causing a strong slowdown of the further reactivity of the interfacial regions. Already after one

year the local porosity reached often a minimum, although porosity variations (increase and decrease) were observed for the same sample during different measurements (Fig. 2b). These variations are most likely related to the measuring conditions and do not represent real modification of the porosity. Depending on the sample, the initial montmorillonite porosity varied between 0.39 and 0.54. Within the limitations regarding the porosity quantification by means of neutron imaging, some indicative porosity trends could be observed: i) the minimal measured porosity in the clay skin region (after >1 year interaction) varied (depending on the initial density) between ~ 0.3 and ~ 0.4 . ii) For most samples where a low-porosity formed, a porosity decrease of ~ 0.1 was determined.

The region inside the skin with the lowest porosity was very thin (<200 μm) and could be well visualized with both neutron radiography and X-ray tomography. In some other samples (homogeneously reacted), no low-porosity region formed, but they showed similar mineralogical modification (e.g., Ca enrichment) after contact with the paste's alkaline pore solution. This observation suggests that small local differences between the samples can influence the porosity development and the reactivity of the interface. Notably, it is possible that a fast decreasing porosity could lead to reduced solute diffusion and could enforce a strong localization of the alterations, while in the absence of a fast porosity reduction the alterations would be more diffuse.

Interpretation of time evolution and extensions of the altered regions

In the cementitious side, the portlandite dissolution appeared to be a fast and pH sensitive process (equilibrium controlled). As soon as the pH drops below 12.5, portlandite is destabilized. Its dissolution front may have started to migrate away from the interface, leaving behind new local pore space. At the same time, in the clay side, C-S-H may have started to form, affecting the pore space, creating a region (clay-skin) with altered physicochemical properties. The first local porosity variations were measured by neutron radiography already after 2-4 months (Shafizadeh, 2019) depending on the sample, with a clear effect for most of the cells after 6 months. The through-diffusion experiments performed on the same samples by Luraschi et al. (2020) indicated a reduction of the effective diffusion coefficient of the clay already after 2 months of interaction. As discussed in Luraschi et al. (2020), the porosity decrease may reduce further the diffusive transport of ions. This process may then slow down the further alkaline attack of the clay and the extension of the ion exchange in the clay side. At the same time, the portlandite dissolution rate in the cement paste side may start to slow down, as less interaction with the clay pore water is taking place. The lower the porosity, the slower and weaker is the diffusive transport, and the more time is needed for any further modifications near the interface, putting up some limitations for experimental investigations of such systems. Although, there is some uncertainty, the derived local porosity profiles could be used as input values for simplified transport modeling. The extension of the low-porosity region is ~ 1 mm, and it seems to remain about stable, at least during the time of the experiments of about 6 years, throughout all the samples. The high porosity region developing on the cement paste side, mainly related to portlandite dissolution, seems to have advanced fast at the beginning and to have slowed subsequently down, still reaching clearly larger extents.

An important remark concerns the boundary conditions of the experiments, which deviate somewhat from those in a repository. Initially, the samples were connected on each side to the larger reservoirs with the

corresponding pore solutions. Thus, these reservoirs defined boundary conditions with constant composition, leading to comparably large gradients of the ion concentrations. However, later the samples had to be detached from the solutions several times for various non-destructive measurements as well as for prolonged intermediate storage. It is likely that during this time, where the samples were not in contact with the buffering solution at both sides, the pH dropped at the external cement boundary, and increased at the external clay boundary, leading to partial equilibration and, for instance, probably increased portlandite dissolution compared to a system evolution under constant pH boundary conditions (even though gradients become smaller). The experimental situation for such samples may in fact be closer to that in a real repository. Preliminary data regarding experiments constantly connected to the reservoirs indicate indeed a lower extension of the region without portlandite compared to those detached from the reservoirs for extended times.

pH conditions: clay and cement paste stability

Clays are known to be unstable under alkaline conditions, but there is still considerable uncertainty regarding their dissolution kinetics (Bauer and Berger, 1998; Hodgkinson and Hughes, 1999; Cama et al., 2000; Huertas et al., 2004; Nakayama et al., 2004). pH measurements in our system conducted by pH paper (due to the small amount of solution available in the cells reservoirs) indicate that, after detachment of the cells from the reservoir, although small diffusive transport is taking place, the pH at the external part of the clay is reaching alkaline regime (pH~12) very fast (~ 2 weeks). Nevertheless, even though the Na-montmorillonite was exposed to high pH for many years (with intermittent phases at normal clay pH during the through-diffusion experiments), it remained the dominant mineral phase outside the skin region as observed by means of TGA (Fig.7) and XRD (Fig. 9).

Inside the cement paste side, close to the interface, an increase of the aluminum content (Fig. 5c) and the Friedel's salt formation (Fig. 8a) were observed. To form this chloride-bearing AFm phase, aluminum needs to be provided. It is likely that it originated from partial clay dissolution. Honty et al. (2010) showed in leaching experiments with clay minerals under alkaline conditions that aluminum was enriched in the solution. It can therefore be concluded that, although a significant part of the clay seems to be preserved, part of it dissolved, providing aluminum for Cl-AFm formation (and potentially C-A-S-H, e.g. Fernández et al., 2016). On the cement paste side, portlandite was homogeneously dissolved within the first 2-3 mm from the interface. On the external part, portlandite was detected in every investigated sample where a low-porosity skin formed on the clay side, although often it was partially dissolved and not well preserved compared to unreacted samples. This observation indicates that the minimal pH reached on the cementitious side was about 12.5, buffered by the presence of portlandite. At the interface, especially when the samples were connected to the corresponding reservoirs, the pH is likely to have dropped to a lower value, destabilizing C-S-H.

Comparison to other systems

The samples prepared from Na-montmorillonite and OPC paste represent a simplified analog of more complex cementitious composites-clay interfaces present in deep geological repositories for radioactive waste. The experimental system was kept as simple as possible with regard to mineralogy, in order to ease

the interpretation and the understanding of the reactions occurring at the interface. Nevertheless, some similarities with other cementitious composite-clay systems, especially concrete-bentonite exist. Bentonite (e.g. MX-80) has a mineralogy mainly composed of Na-montmorillonite (Carlson 2004, Karnland et al., 2006). Therefore bentonite-OPC interfaces are expected to react similarly as the samples investigated here, as already discussed in Luraschi et al. (2020). The interaction of alkaline solutions with bentonite as well as samples with bentonite-OPC interfaces were extensively studied in several experiments (Fernández et al., 2006; 2009 and 2016; González-Santamaría, 2020). The samples characterized in this work and samples with bentonite-OPC interfaces show similarities regarding i) the chloride enrichment on the cementitious side, resulting in Friedel's salt precipitation, ii) portlandite dissolution close to the contact with the clay, and iii) C-S-H precipitation in the clay side. Calcite precipitation, described by several of the mentioned authors, was not observed here since very little CO₂ is expected to be present in our system. We had no or only a very small amount of CO₃²⁻ in the clay porewater (different to typical porewaters of geological formations, Gaucher and Blanc, 2006; Jenni et al., 2014) and also low ingress of external CO₂ due to N₂ atmosphere storing conditions. A preliminary MX-80 bentonite-OPC paste study using the same high porosity OPC paste as here shows similar reactions regarding diffusive properties, calcium enrichment and porosity decrease (magnitude and extension) on the bentonite side. We can therefore consider our Na-montmorillonite OPC samples as a good proxy for bentonite-OPC interactions.

Summary and conclusions

The study of samples with OPC paste-Na montmorillonite interfaces over a period of six years allowed characterizing the type, the spatial extension and the temporal evolution of the mineralogical and local porosity alterations occurring at these interfaces. In the cement paste part, portlandite and ettringite dissolution were observed, as well as Friedel's salt precipitation. The montmorillonite side can be subdivided in a region with strongly altered chemical and transport properties (clay skin; Luraschi et al., 2020), and an external only weakly altered region. The extension of the clay skin was constant for all the samples (~1 mm). Neutron radiography evidenced a remarkable local porosity decrease within such skin (by ~0.1). Ca²⁺ from portlandite dissolution likely diffused towards the clay and precipitated forming C-S-H phases. Part of the calcium substituted sodium in the montmorillonite leading to Ca-Na montmorillonite inside the clay skin. The skin was enriched in sodium (with a maximum at a distance of 500 µm from the interface). The nature of the mineral phase accommodating the sodium is not clear and should be an investigation target for future studies. The remaining weakly altered part of the clay experienced substitution of Ca and possibly K for Na on the cation exchange sites of montmorillonite. The samples (on both sides of the interfaces) showed a very strong reactivity during the first 12 months of contact. This phase was characterized by a strong mineralogical and porosity variation. After this period the decrease of diffusivity slowed down further reactions, leading to more localized effects and slowing down the further development of the alterations.

The experimental study presented here allowed quantifying the evolution (timing, location, extension) of regions with altered porosity forming on both sides of the OPC-Na montmorillonite interface. It is

confirmed that the altered region was restricted to a very narrow area (mm) and that no clogging will occur within the first years when montmorillonite is put in contact with an OPC paste. The porosity evolution furthermore suggests that for the first decades no porosity clogging should occur with such interface samples. It was also confirmed that precipitation of C-S-H phases should represent the main mineralogical alteration occurring on the clay side. The precipitation of a phase possessing interlayer porosity suggest that part of the pore space will always be available for transport processes.

Acknowledgments

The work was partially financed by Nagra, the Swiss Cooperative for the Disposal of Radioactive Waste. Andreas Jenni and Alfons Berger are acknowledged for the support during the SEM investigations. Additional thanks to the entire LES team (Paul Scherrer Institut, Switzerland) for the helpful discussions.

References

- Adler, M., Mäder, U.K., Waber, H.N., 1999. High-pH alteration of argillaceous rocks: an experimental study. *Schweiz. Mineral. Petrogr. Mitt.* 79, 445–454.
- Bauer, A., Berger, G., 1998. Kaolinite and smectite dissolution rate in high molar KOH solutions at 35°C and 80°C. *Appl. Geochem.* 13, 905–916.
- Bartier, D., Techer, I., Dauzères, A., Boulvais, P., Blanc-Valleron, M.-M., Cabrera, J., 2013. In situ investigations and reactive transport modelling of cement paste/ argillite interactions in a saturated context and outside an excavated disturbed zone. *Appl. Geochem.* 31, 94–108.
- Bernard, E., Lothenbach, B., Le Goff, F., Pochard, I., Dauzères, A., 2017. Effect of magnesium on calcium silicate hydrate (C-S-H). *Cem. Concr. Res.* 97, 61–72.
- Bernard, E., Jenni, A., Fisch, M., Grolimund, D., Mäder, U., 2020. Micro-X-ray diffraction and chemical mapping of aged interfaces between cement pastes and Opalinus Clay. *Appl. Geochem.* 115, 104538.
- Berner, 1992. Evolution of pore water chemistry during degradation of cement in a radioactive waste repository environment. *Waste Manag.* 12, 201-219.
- Bouchet, A., Cassagnabère, A., Parneix, J.C., 2004. Batch experiments: results on MX80. In: Michau, N. (Ed.), *Ecoclay II: Effect of Cement on Clay Barrier Performance Phase II*. Final report. (ANDRA) European contract FIKW-CT-2000-0028.
- Butcher, J., Borowick, J., Collierands, N., Williams, J., 2012. Long term leachate evolution during flow-through leaching of a vault backfill (NRVB). *Mineral. Mag.* 76, 3023–3031.
- Cama, J., Ganor, J., Ayora, C., Lasaga, C.A., 2000. Smectite dissolution kinetics at 80°C and pH 8.8. *Geochim. Cosmochim. Acta* 64, 2701–2712.
- Carlson, L., 2004. Bentonite mineralogy. Posiva working report, 2004-02, Posiva OY, Olkiluoto, Finland.
- Claret, F., Bauer, A., Schäfer, T., Griffault, L., Lanson, B., 2002. Experimental investigation of the interaction of clays with high-pH solutions: a case study from the Callovo-Oxfordian formation, Meuse-Haute marne underground laboratory (France). *Clays and Clay Min.* 50, 633–646.

- Cuevas, J., 2004. Geochemical reactions between the FEBEX bentonite and Portland-type cement porewater. In: Michau, N. (Ed.), *Ecoclay II: Effect of Cement on Clay Barrier Performance Phase II*. Final Report. (ANDRA) European contract FIKW-CT-2000-0028.
- Dauzères, A., Le Bescop, P., Sardini, P., Cau Dit Coumes, C., 2010. Physico-chemical investigation of clayey/cement-based materials interaction in the context of geological waste disposal: experimental approach and results. *Cem. Concr. Res.* 40, 1327–1340.
- Fernández, R., Cuevas, J., Sánchez, L., Vigil de la Villa, R., Leguey, S., 2006. Reactivity of the cement-bentonite interface with alkaline solutions using transport cells. *Appl. Geochem.* 21, 977–992.
- Fernández, R., Mäder, U.K., Rodríguez, M., Vigil de la Villa, R., Cuevas, J., 2009. Alteration of compacted bentonite by diffusion of highly alkaline solutions. *Eur. J. Mineral.* 21, 725–735.
- Fernández, R., Ruiz, A.I., Cuevas, J., 2016. Formation of C-A-S-H phases from the interaction between concrete or cement and bentonite. *Clay Min.* 51, 223–235.
- Gaitero, J.J., Campillo, I., Guerrero, A., 2008. Reduction of the calcium leaching rate of cement paste by addition of silica nanoparticles. *Cem. Concr. Res.* 38, 1112–1118.
- Gaboreau, S., Prêt, D., Tinseau, E., Claret, F., Pellegrini, D., Stammose, D., 2011. 15 Years of in situ cement-argillite interaction from Tournemire URL: characterisation of the multi-scale spatial heterogeneities of pore space evolution. *Appl. Geochem.* 26, 2159–2171.
- Gaucher, E.C., Blanc, P., 2006. Cement/clay interactions - A review: Experiments, natural analogues, and modeling. *Waste Manag.* 26, 776–788.
- Glasser, F.P., Marchanda, J., Samson, E., 2008. Durability of concrete - Degradation phenomena involving detrimental chemical reactions. *Cem. Concr. Res.* 38, 226–246
- González-Santamaría, D.E., Fernández, R., Ruiz, A.I., Ortega, A., Cuevas, J., 2020. Bentonite/CEM-II cement mortar interface experiments: A proxy to *in situ* deep geological repository engineered barrier system surface reactivity. *Appl. Geochem.* 117, 104599.
- Gruskovnjak, A., Lotenbach, B., Winnefeld, F., Munch, B., Figi, R., Ko, S., Adler, M., Mäder, U., 2011. Quantification of hydration phases in supersulfated cements: review and new approaches. *Adv. Cem. Res.* 23, 265–275.
- Hodgkinson, E.S., Hughes, C.R., 1999. The mineralogy and geochemistry of cement/rock reactions: high-resolution studies of experimental and analogue materials. *Chem. Contain. Waste Geosph.* 157, 195–211.
- Honty, M., De Craen, M., Wang, L., Madejova, J., Czimerova, A., Pentrak, M., Stricek, I., Van Geet, M., 2010. The effect of high pH alkaline solutions on the mineral stability of the Boom Clay - Batch experiments at 60 °C. *Appl. Geochem.* 25, 825–840.
- Huertas, F.J., Rozalen, M.L., Garcia-Palma, S., Iriarte, I., Linares, J., 2004. Dissolution kinetics of bentonite under alkaline conditions. In: Michau, N. (Ed.), *Ecoclay II: Effect of Cement on Clay Barrier Performance Phase II*. Final Report. (ANDRA) European contract FIKW-CT-2000-0028.
- Lalan, P., Dauzères, A., De Windt, L., Sammaljärvi, J., Bartier, D., Techer, I., Dettleux, V., Siitari-Kauppi, M., 2019. Mineralogical and microstructural evolution of Portland cement paste/argillite interfaces at 70°C - Considerations for diffusion and porosity properties, *Cem. Concr. Res.* 115, 414–425.
- Lerouge, C., Gaboreau, S., Grangeon, S., Claret, F., Warmont, F., Jenni, A., Cloet, V., Mäder, U., 2017. In situ interactions between Opalinus clay and low alkali concrete. *Phys. Chem. Earth Parts A/B/C*, 99, 3–21.

- Lothenbach, B., Durdziński, P. and De Weerd, K., 2016. Thermogravimetric analysis. In: K. L. Scrivener, R. Snellings and B. Lothenbach, Eds. *A Practical Guide to Microstructural Analysis of Cementitious Materials*. Boca Raton, London and New York: CRC Press, 177-211.
- Luraschi, P., Gimmi, T., Van Loon, L.R., Churakov, S.V., Shafizadeh, A., 2020. Evolution of HTO and ^{36}Cl -diffusion through a reacting cement-clay interface (OPC paste-Na montmorillonite) over a time of six years. *Appl. Geochem.* 119, 104581.
- Jackson, D.F., Hawkes, D.J., 1981. X-Ray attenuation coefficients of elements and mixtures. *Phys. Rep.* 70, 169-233.
- Jacques, D., Wang, L., Martens, E., Mallants, D., 2010. Modelling chemical degradation of concrete during leaching with rain and soil water types, *Cem. Concr. Res.* 40, 1306–1313.
- Jakob, A., Sarott, F.A., Spieler, P., 1999. Diffusion and sorption on hardened cement pastes - experiments and modelling results. Paul Scherrer Institut, PSI-Bericht, 99-05.
- Jansen, D., German, A., Ectors, D., Winnefeld, F., 2024. Stacking faults of the hydrous carbonate-containing brucite (HCB) phase in hydrated magnesium carbonate cements. *Cem. Concr. Res.* 175, 107371.
- Jenni, A., Mäder, U., Lerouge, C., Gaboreau, S., Schwyn, B., 2014. In situ interaction between different concretes and Opalinus Clay. *Phys. Chem. Earth, Parts A/B/C* 70, 71–83.
- Karnland, O., 2004. Laboratory experiments concerning compacted bentonite contacted to high pH solutions. In: Michau, N. (Ed.), *Ecoclay II: Effect of Cement on Clay Barrier Performance Phase II*. Final Report. (ANDRA) European contract FIKW-CT-2000-0028.
- Karnland, O., Olsson, S., Nilsson, U., 2006. Mineralogy and sealing properties of various bentonites and smectite-rich clay materials. SKB TR-06-30, Svensk Kärnbränslehantering AB.
- Kaestner, A.P., Hartmann, S., Kuhne, G., Frei, G., Grunzweig, C., Josic, L. Schmid, F., Lehmann, E., 2011. The ICON beamline - a facility for cold neutron imaging at SINQ, *Nucl. Instrum. Methods Phys. Res. Section A* 659, 387–393.
- Kaestner, A.P., Trtik, P., Zarebanadkouki, M., Kazantsev, D., Snehota, M., Dobson, K.J., Lehmann, E.H., 2016. Recent developments in neutron imaging with applications for porous media research, *Solid Earth* 7, 1281–1292.
- Kosakowski, G., Blum, P., Kulik, D., Pflingsten, W., Shao, H., Sing, A., 2009. Evolution of a generic clay/cement interface: First reactive transport calculations utilizing a Gibbs energy minimization based approach for geochemical calculations, *J. of Env. Science for Sust. Soc.* 3, 41–49.
- Kosakowski, G., Berner, U.R., 2013. The evolution of clay rock/cement interfaces in a cementitious repository for low and intermediate level radioactive waste. *Phys. Chem. Earth A/B/C* 64, 65–86.
- Mäder, U., Jenni, A., Lerouge, C., Gaboreau, S., Miyoshi, S., Kimura, Y., Cloet, V., Fukaya, M., Claret, F., Otake, T., Shibata, M., Lotenbach, B., 2017. 5-year chemico-physical evolution of concrete–claystone interfaces, Mont Terri Rock Laboratory (Switzerland). *Swiss J. Geosci.* 110, 307–327.
- Mainguy, M., Coussy, O., 2000. Propagation fronts during calcium leaching and chloride penetration, *J. Eng. Mech.* 126, 250–257.
- Marty, N.C.M., Tournassat, C., Burnol, A., Giffaut, E., Gaucher, E.C., 2009. Influence of reaction kinetics and mesh refinement on the numerical modelling of concrete/clay interactions. *J. of Hydrol.* 364 (1–2), 58–72.

- Nagra, 2002. Project Opalinus Clay – Safety Report, Demonstration of Disposal Feasibility for Spent Fuel, Vitrified High-level Waste and Long-lived Intermediate-level Waste ("Entsorgungsnachweis"). Nagra Tech. Rep. NTB 02–05.
- Nagra, 2014. SGT-Etape-2: Vorschlag weiter zu untersuchender geologischer Standortgebiete mit zugehörigen Standortarealen für die Oberflächenanlage: Charakteristische Dosis Intervalle und Unterlagen zur Bewertung der Barrierensysteme. Nagra Tech. Rep. NTB 14–03.
- Nagra, 2018. A review of cement-clay modelling. Nagra Arbeitsber. NAB 18-24.
- Nakayama, S., Sakamoto, Y., Yamaguchi, T., Akai, M., Tanaka, T., Sato, T., Lida, Y., 2004. Dissolution of montmorillonite in compacted bentonite by highly alkaline aqueous solutions and diffusivity of hydroxide ions. *Appl. Clay Sci.* 27, 53–65.
- Prêt, D., Sammartino, S., Beaufort, D., Fialin, M., Sardini, P., Cosenza, P., Meunier, A., 2010. A new method for quantitative petrography based on image processing of chemical element maps: Part II. Semi-quantitative porosity maps superimposed on mineral maps, *Am. Min.* 95, 1389–1398.
- Ramirez, S., Cuevas, J., Vigil, R., Leguey, S., 2002. Hydrothermal alteration of “La Serrata” bentonite (Almeria, Spain) by alkaline solutions. *Appl. Clay Sci.* 21, 257–269.
- Savage, D., Noy, D., Mihara, M., 2002. Modelling the interaction of bentonite with hyperalkaline fluids. *Appl. Geochem.* 17, 207–223.
- Sardini, P., Caner, L., Mossler, P., Mazurier, A., Hellmuth, K.-H., Graham, R.C., Rossi, A.M., Siitari-Kauppi, M., 2015. Calibration of digital autoradiograph technique for quantifying rock porosity using ¹⁴C-PMMA method, *J. Radioanal. Nucl. Chem.* 303, 11–23.
- Shafizadeh, A., Gimmi, T., Van Loon, L.R., Kaestner, A., Lehmann, E., Mäder, U., Churakov, S.V., 2015. Quantification of water content across a cement-clay interface using high resolution neutron radiography. *Phys. Proc.* 69, 516–523.
- Shafizadeh, A., 2019. Neutron Imaging Study of Evolution of Structural and Transport Properties of Cement-Clay Interfaces. PhD Thesis. University of Bern, Switzerland.
- Shafizadeh, A., Gimmi, T., Van Loon, L.R., Kaestner, A.P., Mäder, U.K., Churakov, S.V., 2020. Time-resolved porosity changes at cement-clay interfaces. *Cem. Concr. Res.* 127, 105924.
- Smellie, J.A.T., 1998. Executive Summary: Maquarin Natural Analogue Project: Phase III. SKB, Stockholm, Sweden. SKB Technical Report (TR 98-04).
- Snellings, R., Chwast, J., Cizer, Ö., De Belie, N., Dhandapani, Y., Durdzinski, P., Elsen, J., Haufe, J., Hooton, D., Patapy, C., Santhanam, M., Scrivener, K., Snoeck, D., Steger, L., Tongbo, S., Vollpracht, A., Winnefeld, F., Lothenbach, B., 2018. Report of TC 238-SCM: hydration stoppage methods for phase assemblage studies of blended cements-results of a round robin test. *Mater. Struct. Constr.* 51.
- Swanton, S.W., Heath, T.G., Clacher, A., 2016. Leaching behaviour of low Ca:Si ratio CaO–SiO₂–H₂O systems, *Cem. Concr. Res.* 88, 82–95.
- Taylor, H.F.W., 1997. *Cement Chemistry*, 2nd Edition. Thomas Telford, London.
- Tinseau, E., Bartier, D., Hassouta, L., Devol-Brown, I., Stammose, D., 2006. Mineralogical characterization of the Tournemire argillite after in situ interaction with concretes. *Waste Manag.* 26, 789–800.
- Tits, J., Jakob, A., Wieland, E., Spieler, P., 2003. Diffusion of tritiated water and ²²Na⁺ through non-degraded hardened cement pastes. *J. Contam. Hydrol.* 61, 45–62.

- Wieland, E., Tits, J., Dobler, J.P., Spieler, P., 1998. Interaction of Eu(III) and Th(IV) with Sulphate-resisting Portland cement. *Mater. Res. Soc. Symp. Proc.* 506, 573–578.
- Wilson, J., Bateman, K., Tachi, Y., 2021. The impact of cement on argillaceous rocks in radioactive waste disposal systems: A review focusing on key processes and remaining issues. *Appl. Geochem.* 130. 104979.
- Yuan, Q., Shi, C., De Schutter, G., Audenaert, K., Dehua Deng, D., 2009. Chloride binding of cement-based materials subjected to external chloride environment – A review. *Constr. Build. Mat.* 23, 1–13.

Supplementary Materials (S1) - X-ray tomography

X-ray tomography was performed on the interface samples with the EasyTom XL tomograph manufactured by RX Solutions (<https://www.rxsolutions.fr/>) and located at Empa's Center for X-ray Analytics (<https://www.empa.ch/web/s499/nano-ct>).

The X-ray source of such tomograph consists of an open X-ray tube, manufactured by Hamamatsu Photonics K.K. (model L10711-23), which was equipped with a Lanthanum hexaboride (LaB₆) filament and a 1 μm -thick tungsten (W) target deposited on a 500 nm-thick diamond substrate. When operated at less than 100 kV of acceleration voltage, such X-ray tube can focus the accelerated electron beam on the W target within a focal spot with size slightly smaller than 1 μm , thus allowing reducing the source-related blur in the X-ray images to the sub- μm scale.

The tomograph is equipped with an X-ray detector being a 2D flat panel of 1920 \times 1536 amorphous-Silicon (a-Si) pixels, each coated with a CsI X-ray scintillator screen. The X-ray photons transmitted through the specimen are converted into visible light photons by the CsI thin film. The latter get converted at each pixel into electrical charge as they interact with a-Si. The physical pixel size of such detector is $p = 127 \mu\text{m}$.

The X-ray source acceleration voltage and current were set to 90 kV and 56 μA , corresponding to a power delivered on the target of about 5 W. 1792 radiographs were acquired for the tomogram. Each radiograph was acquired at a distinct orientation angle, θ , of the specimen around an axis approximately parallel to the vertical direction of the detector's plane and to the sample's symmetry axis. θ spanned the range 0° - 360°, typical for cone beam tomography measurements. Each radiograph consisted of the pixel-wise average of 8 distinct and successive radiographs acquired with θ fixed (frame averaging). The acquisition time *per* frame was 250 ms. In addition to the 1792 radiographs with the sample into the X-ray beam, 128 in the sample absence and 128 with the X-ray source switched off were acquired at the start of the measurement for performing the flat-field and dark current corrections of the sample radiographs, respectively.

The X-ray source-to-detector distance was $d_{s-d} = 257.96 \text{ mm}$ and the source-to-specimen distance was $d_{s-s} = 12.7 \text{ mm}$, leading to a geometrical magnification factor $M = \frac{d_{s-d}}{d_{s-s}} \cong 20.31$ for the sample's projection onto the detector plane, as a consequence of the conical geometry of the X-ray beam. The voxel/pixel size of the tomogram/radiographs was thus $\tilde{p} = \frac{p}{M} \cong 6.25 \mu\text{m}$. We remind the reader that the effective spatial resolution of the tomogram/radiographs is always a multiple of the actual voxel size. A ball-park estimate of the upper bound of the spatial resolution is $2 \times \tilde{p} \cong 12.5 \mu\text{m}$.

Each tomogram was obtained from the respective set of 1792 radiographs by using an implementation of the Feldkamp-David-Kreiss cone beam filtered back-projection tomographic reconstruction algorithm (Feldkamp et al., 1984) into RX Solutions' XAct Ver. 1.0 software, optimized for GPU-processing.

The reconstructed tomograms, with real-valued voxel, were then saved in the format of a stack of 2D 16-bit unsigned integer TIFF images (tomographic slices), spaced along the vertical axis or rotation at a

distance $\tilde{\rho}$. The voxel values in the range 0.45 – 1.75 were mapped from real to integer numbers between 0 and $2^{16}-1$ with a linear transform.

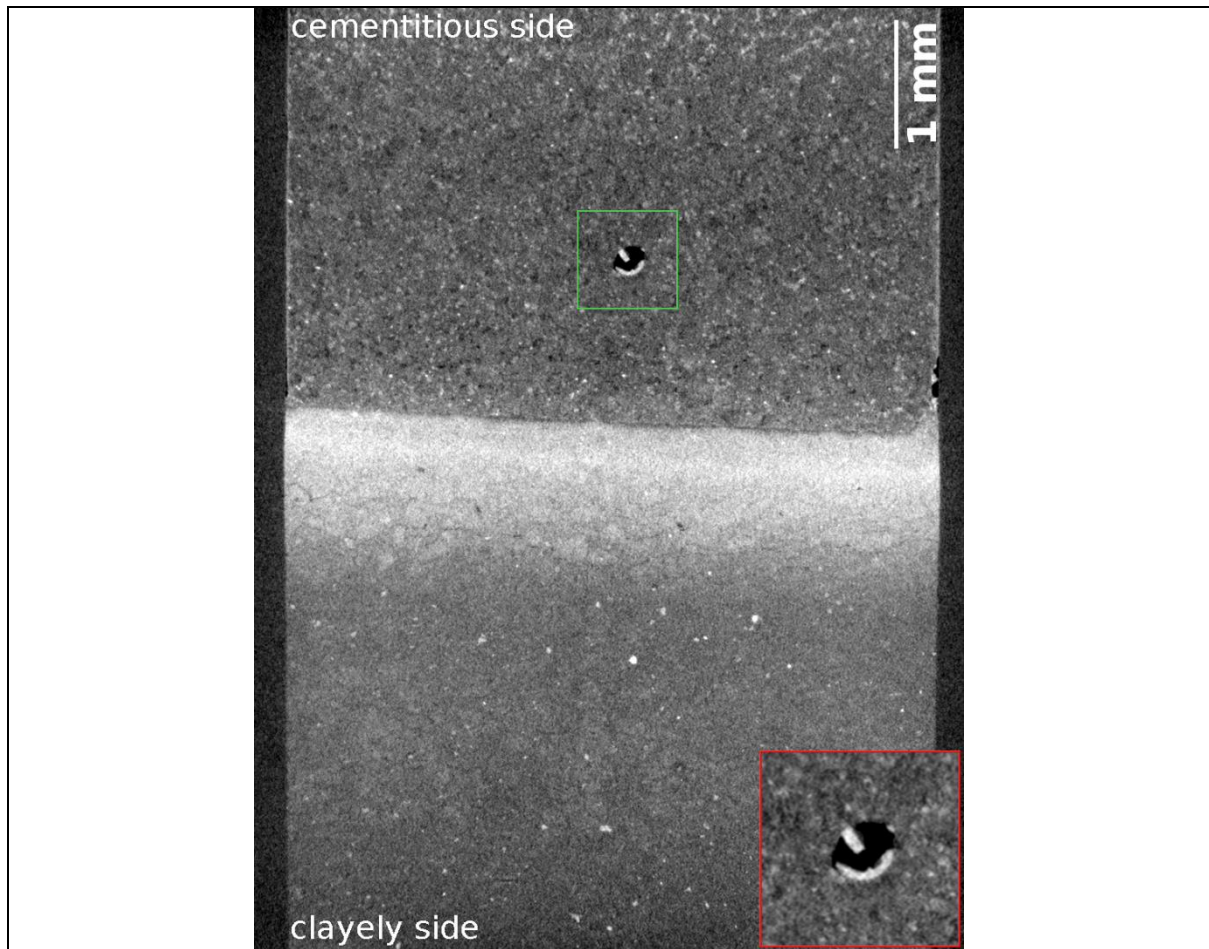


Figure S1: vertical cross-section of the X-ray tomogram of the C3 sample, acquired after a 6-year interaction period. A zoom into the green, rectangular region of interest (ROI) is provide at the bottom-right corner. At that location, the sample had an air void with macroscopic crystallites growing inside it, very likely being of portlandite, given their higher X-ray attenuation compared with on average. At the top of the image, a region, inside the cementitious side of the interface system and characterized by higher average X-ray attenuation coefficient than the rest of such side, is clearly visible.

Feldkamp, L.A., Davis, L.C., Kress, J.W., 1984. Practical cone-beam algorithm, J.Opt. Soc. Amer. A. 1, 612–619.

Since of all OPC hydrates portlandite has the highest $\mu_{X\text{-ray}}$ values, as shown experimentally in Deboodt et al. (2017), such spots could be interpreted as regions of higher Portlandite concentration, under the assumption of very high cement hydration degree. Thus, such region at the end of the cementitious side, could have had a higher content of Portlandite than the middle region.

Supplementary Material (S2) – Neutron radiography

Neutron radiography: calibration procedure

The calibration procedure was developed by Shafizadeh (2019), who offers together with Shafizadeh et al., (2020) a complete and detailed explanation. The following paragraphs resume the calibration procedure used to derive the effective water attenuation coefficient μ_{eff} .

For the derivation of the water content from the radiography, the cylindrical geometry of the sample need to be considered. The total water content (which can be visualized as a water column) variate indeed within the sample, according to:

$$d_t = 2\sqrt{2yr - y^2} \quad \text{eq. (S2.1)}$$

Where d is the water thickness, r is the sample's radius and y is the lateral position within the radiograph. The sample extends from $y = 0$ to $y = 2r$

With increasing water thickness, there is increasing multiple scattering which need to be considered for. Furthermore, the distance between sample and detector also affects multiple scattering. The use of a single water attenuation coefficient μ_w , for the calculation of the water content would lead to over- and underestimation of the -real- water content. The effective water attenuation coefficient μ_{eff} needs therefore to be calculated for the clay and the cement paste separately. This procedure need to be performed for every radiograph.

The external region of the cement and the clay are considered as -unaltered- regions (having the initial known porosity). The water content of these regions is therefore known and can be used to derive the calibration parameters μ_0 and β (eq. (5) in the methods section).

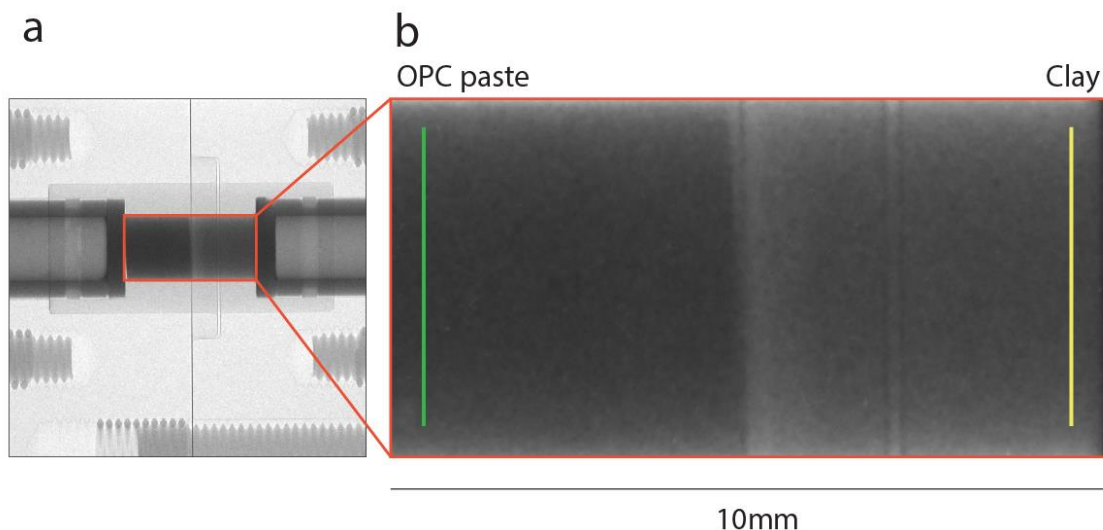


Fig. S2.1 a) Neutron radiography of the experimental cell containing OPC paste and clay (montmorillonite). b) blow-up of the interface sample. The reference unaltered regions used to perform the calibration (Shafizadeh, 2019; Shafizadeh et al., 2020) are shown for OPC paste (green) and for the clay side (yellow).

The two selected reference (calibration) regions are shown as example in Fig. S2.1 as green (cement) and yellow (clay) lines. The showed lines actually represent multiple regions / points of 10 x 10 pixels. For

every one of these regions the transmissivities $A = \ln \left[\frac{T_{dry}}{T} \right]$ are a projection of the cross sections, acquired for different d_w (water thicknesses). The effective water attenuation coefficient $\mu_{w,eff}$ can then be calculated:

$$\mu_{w,eff} = \frac{1}{\theta d_T} \ln \left[\frac{T_{dry}}{T} \right] \quad \text{eq. (S2.2)}$$

The effective attenuation coefficient can then be derived for every calibration region as a function of the total water thickness (Fig. S2.2). The μ_0 and β are estimated by a linear fitting of the obtained data. The most external part of the sample were excluded due to the very high scattering.

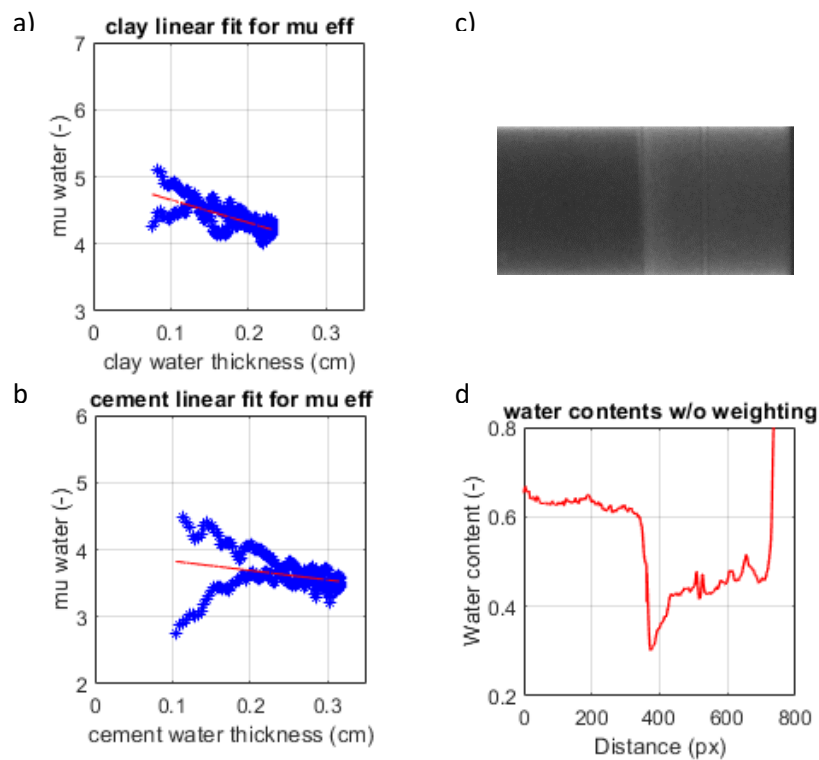


Fig. S2.2 Effective water attenuation coefficient $\mu_{w,eff}$ as a function of the water thickness in clay (a) and in Cement (b). c) Radiograph of a cement-clay interface sample. d) Corresponding 1D derived water content.

Supplementary Material (S3) – Neutron radiography

Sample C3

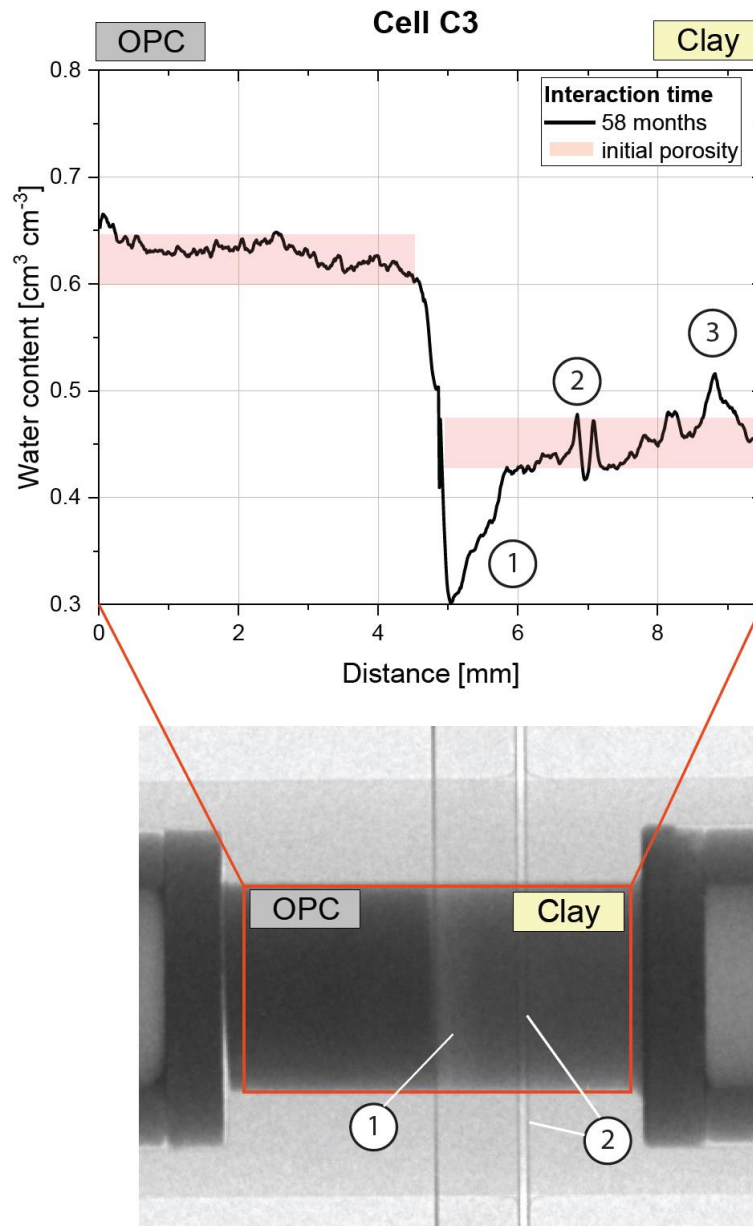


Fig. S3.1 Neutron radiography of the sample C3 (lower image) and corresponding 1D profile (upper image). The numbers on the figure indicate: the low-porosity region detected on the clay side (1). A disturbance in the porosity quantification due to the PEEK cell structural composition (2). A Disturbance in the porosity quantification due to the calibration procedure: heterogeneities in the dry clay sample (3).

Sample C11

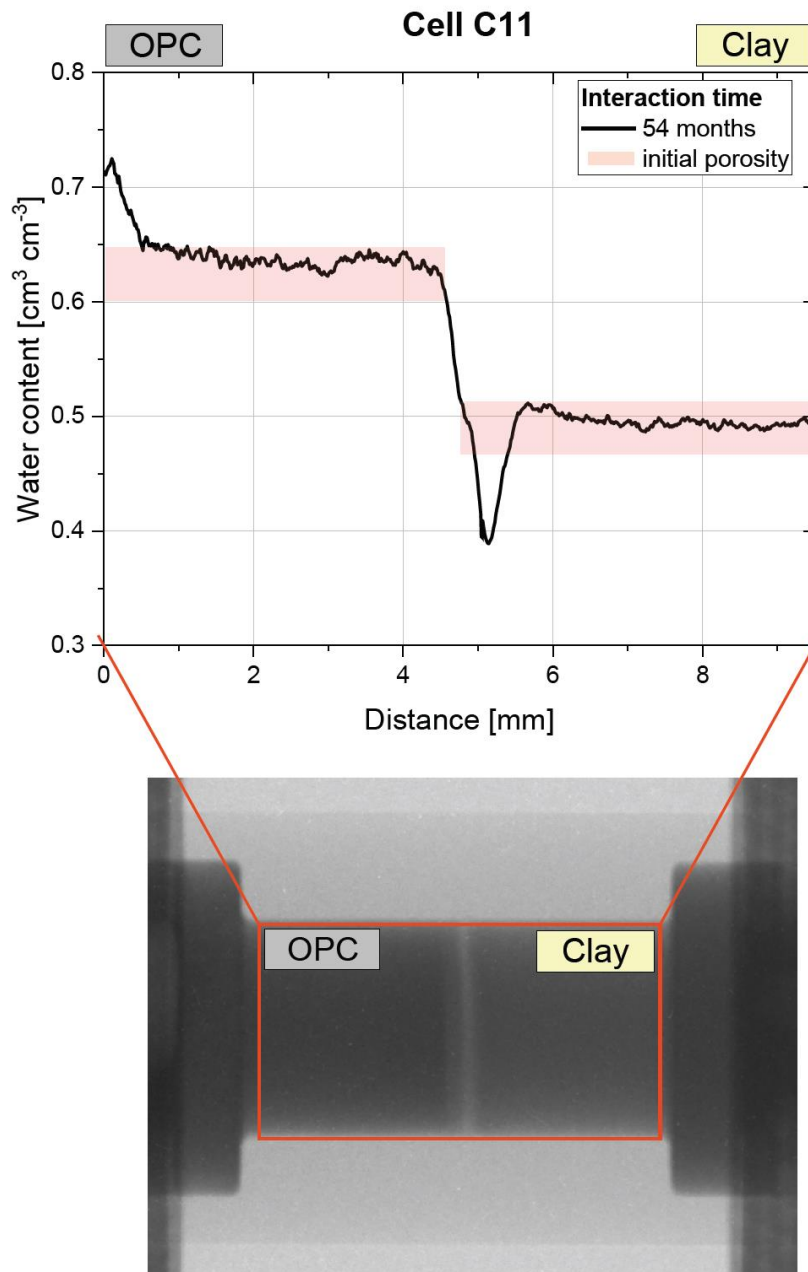


Fig. S3.2 Neutron radiography of the sample C11 (lower image) and corresponding 1D profile.

Supplementary Material (S4) – Cement paste and clay porewater

Composition of the porewater (total concentrations) for OPC (Wieland et al., 1998) and for Na montmorillonite (Shafizadeh, 2019).

	OPC [M]	Na-montmorillonite [M]
Na	0.114	0.3
K	0.18	-
Ca	1.6×10^{-3}	-
Cl	-	0.3
S^{VI}	3×10^{-3}	-
Al	5×10^{-5}	-
pH	13.3	8.7

Chemical composition (g/100g) of the used cement and clay (Shafizadeh et al., 2015).

	SiO ₂	Al ₂ O ₃	Fe ₂ O ₃	MnO	MgO	CaO	Na ₂ O	K ₂ O	TiO ₂	P ₂ O ₅	LOI	SrO	BaO	Li ₂ O	Rb ₂ O	CaO (free)	CO ₂	SO ₃
CEM I 52.5 N HTS ^a	22.3	2.7	1.9	-	0.85	65.7	0.13 (0.04 ^b)	0.22 (0.08 ^b)	-	-	-	0.16	0.002	0.03	<0.001	0.45	1.6	2.2
Montmorillonite (Milos)	62.5	20.4	1.94	0.01	3.72	0.02	2.96	0.22	0.16	<0.015	8.81	-	-	-	-	-	-	-

Supplementary Material (S5) – EDX maps of the sample C 29

EDX maps of chloride and carbon allow to detect the regions where the resin entered the high porous cement paste.

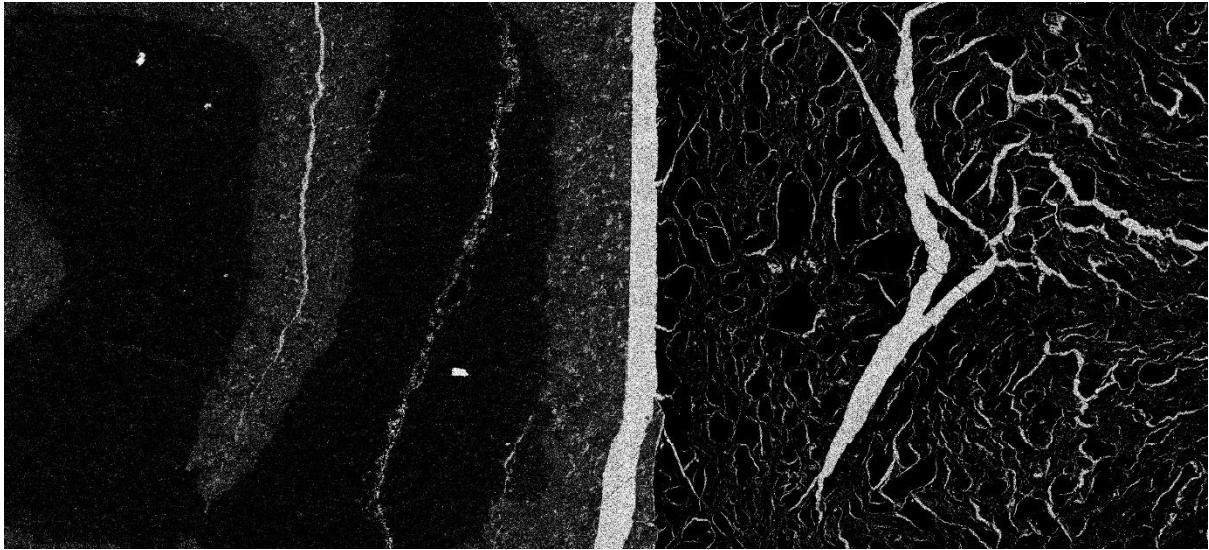


Fig. S5.2 EDX map of the carbon distribution

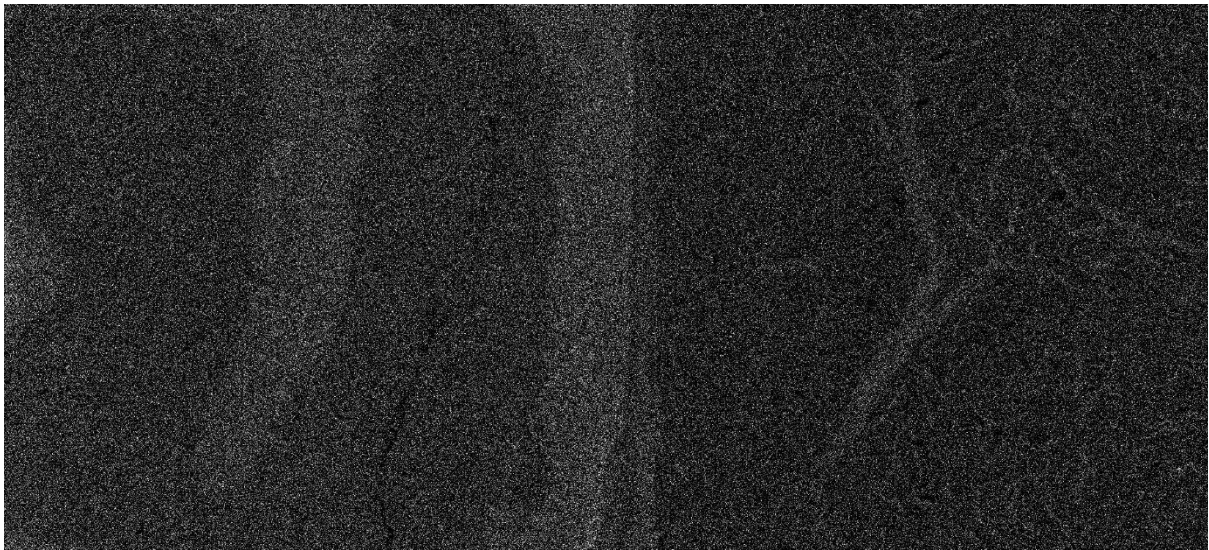


Fig. S5.2 EDX map of the chloride distribution

Supplementary Material (S6) – EDX profile Na/K

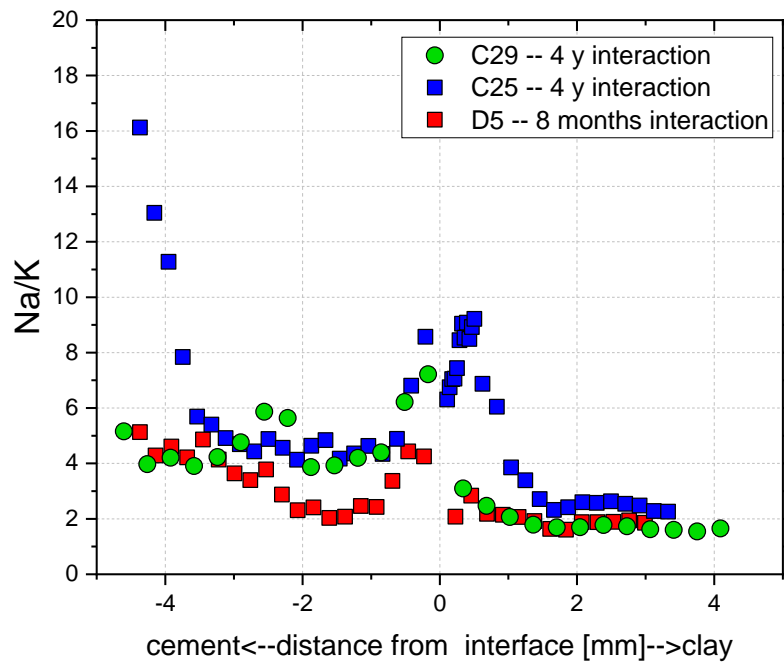


Fig. S6.1 1D profile of the Na/K distribution obtained by EDX.

Chapter 5

**Evolution of diffusive and mineralogical properties of cement-clay interfaces:
effects of cement and clay type**

-- Manuscript in preparation for publication --

Evolution of diffusive and mineralogical properties of cement-clay interfaces: effects of cement and clay type

Pietro Luraschi^{a,b,*}, Thomas Gimmi^{a,b}, Luc Van Loona, Michele Griffa^c, Frank Winnefeld^c, Sergey V. Churakov^{a,b}

^aLaboratory for Waste Management, Nuclear Energy and Safety, Paul Scherrer Institute, 5232 Villigen, Switzerland

^bInstitute of Geological Sciences, University of Bern, 3012 Bern, Switzerland

^cLaboratory for Building Science and Technology, Swiss Federal Laboratory for Materials Science and Technology, EMPA, 8600 Dübendorf, Switzerland

* Corresponding author

E-mail addresses: pietro.luraschi@psi.ch (P.Luraschi), thomas.gimmi@psi.ch (T. Gimmi)

Keywords: reactive transport, nuclear waste disposal, mineralogy, alteration

Abstract

Interactions between cement and clay materials are of great relevance in the context of radioactive waste disposal. The mineralogical alterations expected to occur at these interfaces will affect gas transport and solute diffusion and are thus of great interest with regard to the long-term safety assessment of the repository. Various cement and clay materials are currently under investigation; their chemical compositions affect the type and extent of mineralogical alterations which may take place in a repository. To investigate such variations, small (length of 1 cm) samples with cement-clay interfaces prepared from different materials were investigated by means of a suite of techniques. The following four materials were selected as components of the interface samples: bentonite (MX-80), Opalinus Clay, hardened OPC paste and low-alkali (low-pH) ESDRED mortar. The samples reacted under nitrogen atmosphere at room temperature for 2 years, during which the diffusive properties were monitored by means of through-diffusion experiments using tritiated water (HTO) as tracer. All interface samples displayed a decrease of the measured diffusivity after 2 years of interaction, with a decrease of the diffusion coefficient by 34% to 64% with respect to the initial values. The extensions of the alterations and the mineralogical modifications that lead to the decrease of the diffusivity were investigated by scanning electron microscopy (SEM/EDX), X-ray micro-tomography, neutron imaging, thermo-gravimetry (TGA) and X-ray diffraction (XRD). In general, for all samples types after two years of interaction the extent of the strongly altered region, with porosity variations and/or newly formed minerals, is restricted to 1-2 mm, similar as observed in previous experiments with samples prepared from Na-montmorillonite and OPC paste. The mineralogical modifications are, however, strongly dependent on the initial chemical composition of the interface samples.

Introduction

Many countries are developing concepts for the safe disposal of radioactive waste in deep geological formations. In such a repository, a combination of natural and engineered barriers is foreseen to isolate the waste from interacting with the biosphere for the necessary time (IAEA, 2009). Depending on the local geologic settings, every country-specific repository concept is confronted with different challenges and adapted specific solutions. Switzerland considers a repository emplaced in a clay-rich sedimentary formation: the Opalinus Clay (OPA). According to the current concept (Nagra, 2002; 2014), cement will be used as liner and as tunnel/cavern backfill. Cement and concrete will therefore be in contact with clay-rich materials. Due to the very different porewater compositions, cement-clay interfaces represent a highly reactive system with strong chemical gradients, which results in mineralogical alterations and consequent changes of the transport properties (Gaucher and Blanc, 2006; Savage et al., 2011). The evolution of cement-clay interfaces has been studied by the scientific community since more than 30 years. Attempts have been made to characterize the evolution of the mineralogical alteration and of the transport properties based on laboratory experiments, analogues and geochemical modelling, (Hodgkinson and Hughes, 1999; Savage et al., 2007; Dauzères et al., 2010; Kosakowski and Berner, 2013; Fernández et al., 2016; Mäder et al., 2017; Nagra, 2018; Wilson et al., 2021). The complexity of such systems is related to several factors: i) The small extension and the mechanical fragility of the altered interface regions, which makes their experimental study difficult, ii) the mineralogical variety and heterogeneity of cement and clay, iii) the variety of possible interfaces type, which depend on the selected cement and clay, and iv) the boundary conditions (temperature, degree of saturation, experimental setup), which influence the dynamics of the reactions. The main modifications occurring when cement and clay are put in contact are known and well characterized, such as alteration of the cation exchange capacity (CEC); porosity variations; reduction of diffusive properties and dissolution/precipitation reactions (Gaucher and Blanc, 2006; Wilson et al., 2021).

In the current Swiss concept of the geological repository for High-Level Waste (HLW), the waste is encapsulated in steel canisters which are surrounded by a bentonite granulate backfill (Nagra, 2014). The cementitious liner used to stabilize the tunnel walls will be in contact with the backfilling bentonite on the inner side and with the host rock (the Opalinus Clay) on the outer side. This liner might be made of low-pH cement.

Currently, one of the most challenging problems is the lack of information regarding the evolution of the transport properties, which are a deciding factor for middle- and long-term safety assessment. Some experimental studies on alteration of the clay's transport properties after interaction with alkaline solutions report a noticeable and clear decrease in diffusivity after months to years of interaction (Melkior et al., 2004; Yamaguchi et al., 2016). Luraschi et al. (2020) studied the diffusive properties of generic, idealized interface samples composed of high porosity hardened OPC paste and Na-montmorillonite (using HTO and $^{36}\text{Cl}^-$ as tracers) by means of specifically developed small reaction cells. They observed a decrease of the diffusivity of the entire interface samples for both HTO and $^{36}\text{Cl}^-$, with a much stronger effect for the anion tracer. The decrease was related to a low-porosity zone forming in the Na-montmorillonite, as evidenced by neutron imaging (Shafizadeh, 2019; Shafizadeh et al., 2020). By dividing the interface region

into several sections, Luraschi et al. (2020) estimated a decrease of the $D_{e, \text{HTO}}$ and $D_{e, \text{Cl}}$ for the 5-mm clay part by >60% and >95%, respectively after 6 years interaction. In a successive study, the same authors reported the formation of C-S-H phases within the Na-montmorillonite as the main cause for the porosity and diffusivity decrease in their samples (Luraschi et al., in prep.).

Here, using the methodology developed and discussed in Shafizadeh (2019), Shafizadeh et al., (2020) and Luraschi et al. (2020), interface samples with materials foreseen for the use in a repository were created at laboratory scale, namely one high porosity OPC paste, one low-pH ESDRED mortar and two clays (MX-80 bentonite, Opalinus Clay). The samples were reacting for 2 years under saturated conditions in a glovebox under a nitrogen atmosphere. During this period several through-diffusion experiments were performed, followed by various analytical characterizations (neutron imaging, X-ray tomography, XRD, TGA, SEM/EDX) to investigate the chemical and mineralogical alterations at the interface. The overall goal of the present study was to characterize similarities and differences of mineralogical alterations and the evolution of the diffusive properties for the various cement-clay combinations.

Methods

Experimental cell

The experimental cell was designed and developed by Shafizadeh (2019) to allow a combined non-destructive characterization of the same samples by through-diffusion experiments, X-ray tomography and neutron radiography. The experimental cell is composed of a PTFE cylindrical holder into which the cement and clay plugs are inserted. Cement and clay plugs are confined by a PEEK filter on each side, and an external aluminum ring ensures mechanical stability. Two PEEK screw caps cover the ends and allow to keep the interface in contact. In- and outlet channels and small reservoirs present in the caps allow the circulation of porewater on the outside of the filters on each side. A detailed description of the cell is given in Luraschi et al. (2020).

Clay materials

Bentonite samples were compacted to cylindrical plugs (5mm length, 5 mm diameter) with a specially designed press to a bulk dry density of $1500 \pm 100 \text{ kg m}^{-3}$ (Tab. 1). After compaction the plugs were inserted in the cells and pre-saturated for two weeks with the corresponding porewater solution (Tab. 2). The Opalinus Clay samples originate from a drill core obtained from the CI experiment at the Mont Terri Rock Laboratory (Jenni et al., 2014). Directly after extraction, the cores were embedded in resin, vacuum-packed and then stored at 4°C. Plugs of 5 mm diameter were drilled out of the bigger cores parallel to the bedding, while trying to avoid preexisting cracks and obvious mineral heterogeneity. Sample specifications are given in Table 1.

Cement materials

The OPC paste was cast in 2001 in cylindrical plexiglass molds (5 cm diameter, 10 cm length) and subsequently stored under nitrogen atmosphere in the corresponding porewater solution (Tits et al., 2003). The 5-cm cylinders were then cut into 1 cm thick slices, from which the cylinders with 5 mm diameter were produced using a diamond drill head. The samples were polished to the desired length and introduced into the cell in contact with the pre-saturated clays. This specific cement paste was chosen

because of its high porosity ($63 \pm 5 \%$; Jakob et al., 1999), which promotes the development of reactions near the interface. Further details regarding these samples (preparation, chemical composition and transport properties) are given in Shafizadeh et al. (2015; 2020) and Luraschi et al. (2020).

The low-pH mortar (ESDRED) originates from the CI experiment at the Mont Terri underground rock laboratory. The mortar was poured into holes drilled in the Opalinus Clay rock in 2012 creating ESDRED-OPA interfaces (Jenni et al., 2014). The overcores from this experiment were obtained in 2017. After extraction, the cores were emplaced into pre-vacuumed epoxy resin and then vacuum-packed. From one of these cores (BCI-20, 400-412; Jenni and Mäder, 2020), ESDRED mortar plugs of 5 mm diameter were drilled out, in a distance of > 8 cm from any interface. The mortar cylinders were polished to 5 mm length, pre-saturated with the corresponding solution and then inserted in the reaction cells. The chemical compositions of the used porewaters are listed in Table 2.

Table 1
Characteristics of the cements and clays for the different samples.

Sample	Interface	Contact	Clay			Cement		
			Length (mm)	Dry density (kg m^{-3})	Porosity (-)	Length (mm)	Dry density (kg m^{-3})	Porosity ² (-)
E4	OPA-OPC	10.04.2018	5	2300 ¹	0.13-0.16 ²	5	770 ⁴	0.63 ⁵
E20	OPA-OPC	29.06.2018	5	2300 ¹	0.13-0.16 ²	5	770 ⁴	0.63 ⁵
E21	OPA-OPC	29.06.2018	5	2300 ¹	0.13-0.16 ²	5	770 ⁴	0.63 ⁵
E14	OPA-ESDRED	28.06.2018	5	2300 ¹	0.13-0.16 ²	5	-	-
E16	OPA-ESDRED	28.06.2018	5	2300 ¹	0.13-0.16 ²	5	-	-
E17	OPA-ESDRED	28.06.2018	5	2300 ¹	0.13-0.16 ²	5	-	-
E22	Bentonite-OPC	02.07.2018	5	1500	0.44 ³	5	770 ⁴	0.63 ⁵
E23	Bentonite-OPC	02.07.2018	5	1500	0.44 ³	5	770 ⁴	0.63 ⁵
E24	Bentonite-ESDRED	02.07.2018	5	1500	0.44 ³	5	-	-
E25	Bentonite-ESDRED	02.07.2018	5	1500	0.44 ³	5	-	-
E26	Bentonite-OPC	20.01.2019	5	1500	0.44 ³	5	770 ⁴	0.63 ⁵

¹ Gimmi et al. (2014)

² Bossard et al. (2017)

³ Calculated from the dry density using a grain density of 2700 kg m^{-3}

⁴ Shafizadeh (2019)

⁵ Determined by MIP (Jakob et al., 1999)

Table 2
Composition of the used synthetic porewater (total concentrations) for OPC (Wieland et al., 1998), ESDRED mortar (Dolder, 2015), MX-80 Bentonite (Bradbury and Baeyens 2003, adapted for 1500 kg m^{-3} dry density) and Opalinus Clay (Pearson et al., 2003).

	OPC [mM]	ESDRED ¹ [mM]	Bentonite, Mx-80 [mM]	Opalinus Clay [mM]
Na	114	24	243	241
K	118	12	1.2	1.6
Ca	1.6	26	9.5	2.5
Mg	-	-	7.1	17
Cl	-	-	67.5	300
S ^{VI}	3	2	104	14
Al	0.05	-	-	-
Sr	-	-	0.08	0.51
C _{org.}	-	-	0.88	0.476
Formate	-	66	-	-
pH	13.3	11.3	8	7.6

¹ For ESDRED porewater Na, Ca and K are present as formate, according to Dolder (2015).

Neutron imaging

Neutron imaging represents a powerful tool to non-destructively investigate the compositional and structural properties of materials. Neutrons interact with the nucleus of atoms, and are differently attenuated (scattered or absorbed) depending on the material they are passing through. The scattering cross section μ [-] can be described as the interaction probability of different atoms with the neutron beam. Hydrogen possesses a high scattering cross section. In a water-saturated porous sample the water content can be considered as a proxy for the porosity, meaning that the latter can be quantified from neutron measurements. Shafizadeh (2019) developed a dedicated technique to derive the porosity of cement and clay samples using the same cells applied in this article.

The neutron radiographs were obtained at the cold neutron imaging facility of the Paul Scherrer Institut (ICON, Switzerland, Kaestner et al., 2011). When a sample is illuminated with the neutrons, the transmitted part of the beam is detected by a scintillator (field of view: 27 x 27 mm²). The neutrons are then converted into light and a CCD (charge-coupled device) sensor produces a gray-scale image.

The water quantification procedure relies on the on the Lambert-Beer law,

$$I_T(t) = I_0(t) \exp(-\sum_i \mu_i d_i) \quad (1)$$

I_T and I_0 represent the transmitted and the initial beam intensity respectively, whereas t is the time of the measurement. The interaction probability is a material specific property described by the attenuation coefficient μ_i . The material thickness is given by d_i . For 2D radiographs as obtained here, Eq. (1) applies for every pixel.

The porosity quantification technique is built on eq. (1), but is composed of several steps comprising different image corrections and a calibration with materials of known water content at each measurement time. These corrections and the calibration was necessary because of variations of the beam intensity histogram with time and multiple scattering effects that are not accounted for in Eq. (1). The evaluation procedure is described in detail in Shafizadeh (2019), Shafizadeh et al., (2020) and Luraschi et al. (in prep.).

X-ray Tomography

We performed laboratory-scale attenuation-contrast X-ray tomography, which allows obtaining a non-destructive view of the structural state of the interfaces. In an acquired tomogram, the gray scale voxel value (\sim intensity) is a proxy of the X-ray attenuation coefficient μ_{xray} [cm⁻¹]. The μ_{xray} is, considering a single photon energy, proportional to the product between ρ (the bulk mass density) and a nonlinear function of the effective atomic number Z_{eff} whose value increases with increasing Z_{eff} (Jackson and Hawkes, 1981). Within any single component material, a region characterized by a smaller average voxel value may be more porous than a region with larger average value. It need to be considered, that the difference in the measured (average) voxel values between the two materials may originate not only from a different bulk mass density but also from a different chemical composition. Details about the measurement settings are available in the Supplementary Data document. The voxel size of the tomograms was 6.2 or 6.4 μ m and the effective spatial resolution was about twice this value. To avoid clay swelling and

to reduce as much as possible carbonation of the cement paste, we performed the tomographic acquisition within ~1 hour for bentonite samples and ~2 hours for OPA specimens, but we optimized the measurement settings in order to limit the reduction in tomographic spatial resolution caused by higher image noise levels for shorter acquisition time.

Through-diffusion experiments

The diffusion experiments were performed in a glovebox under nitrogen atmosphere to avoid carbonation by atmospheric CO₂ dissolving in the porewater. HTO (GE healthcare, UK) tracer was added in 50-mL reservoirs connected to the cement side. For the experiments, the chosen activity was either 1000 Bq mL⁻¹ (high porosity OPC paste) or 2000 Bq mL⁻¹ (lower porosity ESDRED mortar). The HTO tracer then started to diffuse through the cement and the clay towards the external reservoir without tracer with a volume of 20 mL connected to the clay side. The solution in this reservoir was frequently replaced to keep the boundary concentration of tracer near zero. The accumulated activity on this 'low concentration' reservoir was measured by liquid scintillation counting (Tri-carb 2250 CA, Canberra-Packard); 5 mL solution were mixed with 15 mL of scintillation cocktail (Ultima Gold XR, Canberra-Packard). For some cells, the filters were exchanged when approximately a constant tracer flux was achieved to check whether any clogging of the filters occurred.

The effective diffusion coefficient D_e of a porous material can be defined as

$$D_e = \varepsilon \frac{D_0}{G}$$

with ε representing the porosity of the material, D_0 the tracer diffusion coefficient in bulk water, and G the so-called geometry factor, which increases with increasing tortuosity and decreasing connectivity of the pore space. From the cumulative activity on the low concentration side, the 'raw' effective diffusion coefficient of the entire system (consisting of filters, cement and clay) was determined as described in Luraschi et al. (2020). Knowing the properties of the filters (size, effective diffusion coefficient, see Luraschi et al., 2020), the effective diffusion coefficient of the cement-clay sample was then calculated by considering a system of diffusive resistances in series. No further discrimination between diffusion properties of cement and clay, or an altered zone, was attempted here, in contrast to Luraschi et al. (2020). A detailed description of the diffusivity derivation and of the data processing is given in Crank (1979) and Van Loon and Soler (2003).

SEM/EDX: sample preparation and measurement conditions

Energy dispersive X-ray (EDX) analysis provides semi-quantitative chemical information about the composition of a sample surface. The samples were first dried using a combination of liquid N₂ flash freezing and subsequent freeze drying. Then, the samples were introduced into a vacuum chamber, where pre-vacuumed resin was inserted, allowing the resin to enter into cracks and voids and increase the sample stability. The resin was pre-vacuumed to avoid the formation of air bubbles during filling. Subsequently, the samples were cut and polished. No coating was applied. A series of element maps was sequentially acquired by means of SEM/EDX and the average chemical composition was derived for different regions of

the samples. Since no coating was applied, the interfaces were measured in a low vacuum mode (18 Pa), working at a distance of ~9 mm. The beam acceleration voltage was 20kV and the current ~500 pA. Depending on the filament conditions, the current was increased up to ~1.2 nA to enhance the interaction and increase the count number.

Thermogravimetric analysis (TGA)

TGA was performed using a TGA/SDTA 851 instrument (Mettler Toledo). The measurements were performed between 25°C and 1000°C, with a heating rate of 20°C/min. The cement and the clay compartment were each split into two parts for the analysis: an external one (~3-5 mm from the interface) and an internal part (~0-1 mm from the interface). To obtain enough material considering some loss during the preparation of the subsamples (cutting, milling), in some cases a larger section was prepared (e.g., 0-2 mm from the interface). The samples were either freeze dried or stored in a desiccator for several days before analysis.

X-ray diffraction (XRD)

Due to the small size of the samples available for the analysis, glass capillaries were used for the measurements. After drying (freeze drying or desiccator storage), the cement and the clay slices were ground in an agate mortar and inserted in the glass capillary (outer diameter 0.5mm; wall thickness 0.01mm). The measuring device used was a PANalytical X'Pert³ powder diffractometer in capillary geometry with a Cu source ($\lambda = 1.5406 \text{ \AA}$ Cu K α) and a PIXcel^{3D} detector. Technical details and measurement conditions are described in detail in Luraschi et al. (in prep.).

Results

Neutron imaging

Investigation of OPC-bentonite samples (Fig. 1a) did not reveal large alterations of the porosity on the OPC side. Close to the interface the porosity appears to be slightly increased in the first ~1mm (compared to the extrapolation of the slightly decreasing background trend towards the interface). This variation could be related to mineral dissolution as described by Shafizadeh et al. (2020), but considering the uncertainty of the porosity determination this interpretation remains tentative. On the bentonite side there is a clear decrease of the porosity within the first mm of the compartment. The low-porosity region displays a minimal porosity of 0.35 very close to the interface. Outside the low-porosity region (> 1 mm from the interface), the porosity is close to the initial value (0.45), but it appears to be slightly increasing. Whether this increasing trend effectively represents a variation in porosity (and mineralogy) is, however, unclear. The ESDRED-bentonite sample (Fig. 1b) does not show any significant changes neither on the mortar nor on the clay side. It has to be considered that some porosity variations along the profile could be due to the presence of quartz grains in the mortar. The latter makes it also more difficult to resolve any small porosity alterations in this system.

Figure 1c shows the porosity profile of an OPC-OPA interface. Similar as for the OPC-bentonite sample, there seems to be a slight porosity increase in the first mm (compared to the extrapolation of the decreasing

background trend towards the interface), but with an even narrower extent. Again, considering the uncertainty of the porosity determination, it is unclear whether this increase is significant. Accordingly, the porosity of the OPC can be considered as about constant throughout the entire compartment apart from the $\sim 200\mu\text{m}$ zone close to the interface, where it appears to be slightly decreasing. On the OPA side close to the interface, no porosity variations are visible.

The ESDRED-OPA interface (Fig. 1d) appears to be unaltered with respect to the porosity. Similarly, as observed for the ESDRED-bentonite sample, the ESDRED mortar compartment shows more pronounced variations in the porosity profile, very likely due to the compositional heterogeneities.

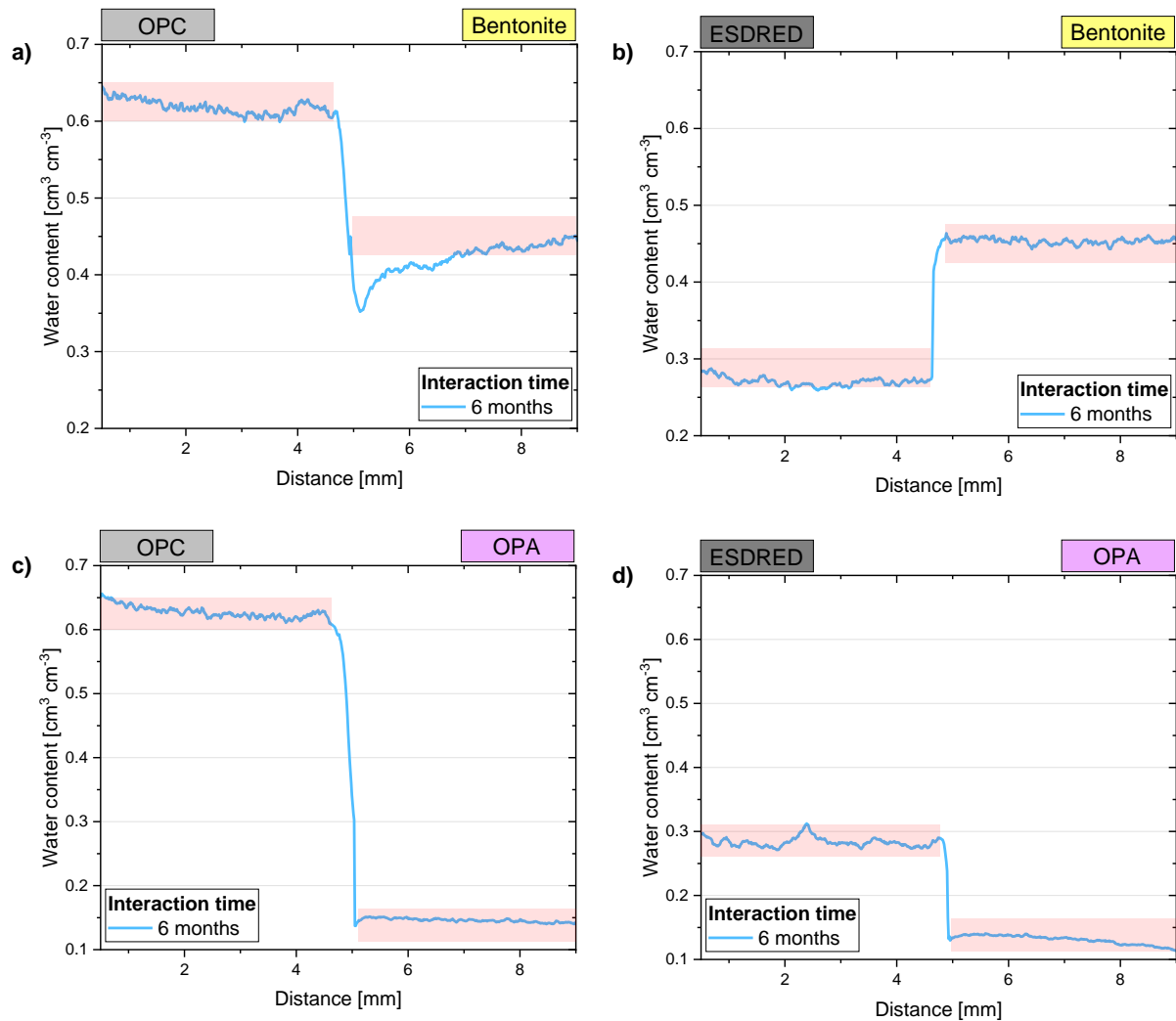


Figure 1 Porosity profiles measured for different cement-clay interfaces after six months of interaction: a) OPC-bentonite; b) ESDRED-bentonite; c) OPC-OPA; d) ESDRED-OPA. The zones marked in red represent the range of the initial porosity.

The unaltered ESDRED porosity (0.28) used for the calibration of the data shown in Figs. 1b and 1d was taken from data of the CI experiment at Mont Terri (Lerouge et al., 2017). Porosity estimation performed here, based on the saturation of a small cement sample (5 mm cylinder) and then oven drying ($>60^\circ\text{C}$), indicated a smaller porosity (<0.2). Thus, it is clear that the absolute porosity of the ESDRED sample is not exactly known. However, the data do not hint to any tendencies of porosity alteration towards the interface

in relative terms, meaning that, independent of the absolute value, porosity in the ESDRED mortar in contact with bentonite or OPA remained unaltered over these six months.

Through-diffusion experiments

For all the samples where diffusion experiments were performed, a clear decrease of the effective diffusion coefficient of HTO was observed after 2 years interaction. In general, the samples with a bentonite component displayed a higher reactivity (faster decrease of the D_e) than those with Opalinus Clay. For bentonite-OPC interfaces an average diffusivity decrease by 40% was observed after 8 months of interaction. The subsequent measurement after a total of 2 years indicated a decrease of the $D_{e, \text{HTO}}$ by 58% with respect to the initial unaltered interface sample (Fig. 1a). For OPA-OPC interfaces, the diffusivity was measured only after 2 years of interaction, showing a decrease by 45% with respect to the initial calculated value. The initial diffusion coefficient of ESDRED is not exactly known; it is only deduced from first experiments with samples with two components. Accordingly, the numbers given here for the decrease of $D_{e, \text{HTO}}$ in samples including ESDRED mortar are more uncertain than those including OPC. The ESDRED mortar has a lower porosity and consequently a lower diffusion coefficient compared to the used OPC. Therefore, the unaltered ESDRED-clay samples had a significantly lower initial (unaltered) $D_{e, \text{HTO}}$ (Fig. 2b) compared to the OPC-clay samples. ESDRED mortar-bentonite samples display a diffusivity decrease by 57% after 8 months interaction (with respect to the initial calculated value).

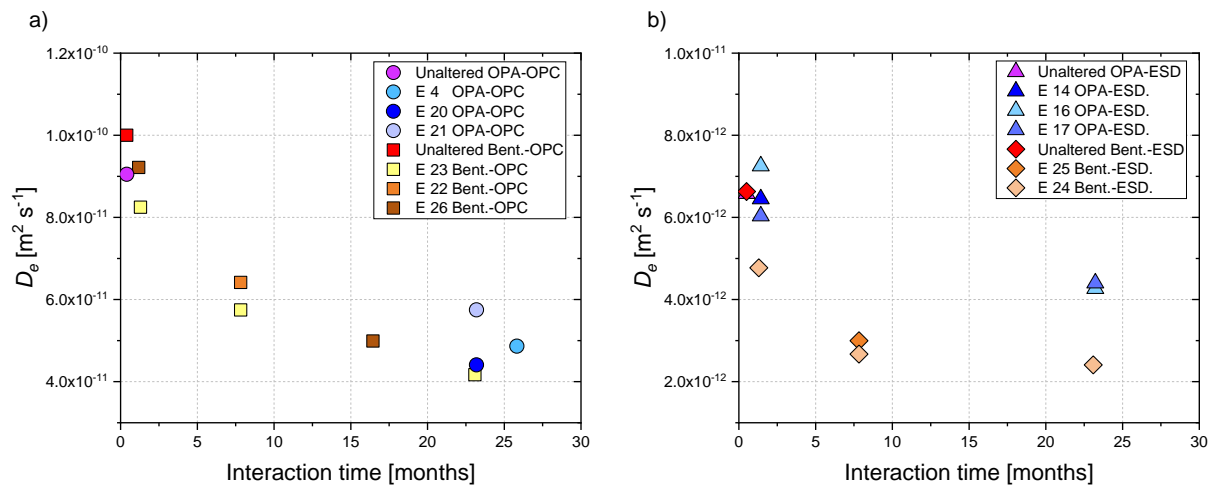


Figure 2 Evolution of the effective diffusion coefficient of HTO ($D_{e, \text{HTO}}$) for a) OPC paste in contact with bentonite and OPA; b) ESDRED mortar in contact with bentonite and OPA. Purple and red symbols represent calculated values for fresh interfaces (unaltered). For these calculations, the values of the individual materials given in Table 1 were used, and a length of 5 mm of each material.

Only a slight decrease in the following year is observed; the $D_{e, \text{HTO}}$ decreases after 2 years by 64%. This value is calculated with respect to the initial calculated diffusion coefficient. If we consider as initial value the $D_{e, \text{HTO}}$ of ESDRED-bentonite after 1.3 months interaction (Tab. 3), the diffusivity decrease is 50%. The ESDRED-OPA interfaces were also investigated after 2 years interaction. The results indicated a $D_{e, \text{HTO}}$ decrease by 34% with respect to the unaltered interface, that is, a smaller decrease (smaller reactivity) compared to ESDRED-bentonite samples. An overview of the derived diffusion coefficients is given in Table 3.

Table 3 Overview of the derived diffusion coefficients for the various types of interface samples.

Sample	Interface type	Interaction time [months]	D_e of the entire sample [m ² s ⁻¹]
E4	OPA-OPC	26.2	$4.9 \cdot 10^{-11}$
E20	OPA-OPC	23.5	$4.4 \cdot 10^{-11}$
E21	OPA-OPC	23.5	$5.7 \cdot 10^{-11}$
E14	OPA-ESDRED	1.5	$6.4 \cdot 10^{-12}$
E16	OPA-ESDRED	1.5	$7.3 \cdot 10^{-12}$
E16	OPA-ESDRED	23.5	$4.3 \cdot 10^{-12}$
E17	OPA-ESDRED	1.5	$6.0 \cdot 10^{-12}$
E17	OPA-ESDRED	23.5	$4.4 \cdot 10^{-12}$
E22	Bent.-OPC	8.0	$6.4 \cdot 10^{-11}$
E23	Bent.-OPC	1.3	$8.2 \cdot 10^{-11}$
E23	Bent.-OPC	8.0	$5.7 \cdot 10^{-11}$
E23	Bent.-OPC	23.4	$4.2 \cdot 10^{-11}$
E24	Bent.-ESDRED	1.3	$4.8 \cdot 10^{-12}$
E24	Bent.-ESDRED	8.0	$2.7 \cdot 10^{-12}$
E24	Bent.-ESDRED	23.4	$2.4 \cdot 10^{-12}$
E25	Bent.-ESDRED	8.0	$3.0 \cdot 10^{-12}$
E26	Bent.-OPC	1.2	$9.2 \cdot 10^{-11}$
E26	Bent.-OPC	16.7	$5.0 \cdot 10^{-11}$
Unaltered OPA ¹	-	-	$5.4 \cdot 10^{-11}$
Unaltered bentonite ²	-	-	$6.1 \cdot 10^{-11}$
Unaltered OPC paste ³	-	-	$2.8 \cdot 10^{-10}$
Unaltered ESDRED ⁴	-	-	$3.5 \cdot 10^{-12}$
Calculated initial values	OPA-OPC	0	$9.1 \cdot 10^{-11}$
	OPA-ESDRED	0	$6.6 \cdot 10^{-12}$
	Bent-OPC	0	$1.0 \cdot 10^{-10}$
	Bent-ESDRED	0	$6.6 \cdot 10^{-12}$

¹Bossart et al. (2017); ²Luraschi et al. (2020); ³Tits et al. (2003); ⁴estimated from the earliest through-diffusion experiments.

X-ray tomography

The samples were investigated after ~16 months of interaction. Figure 3 shows four panels, one for each system. At the bottom, a 2D cross-section (also called tomographic slice) from a small 3D region of interest (ROI) extracted from a respective tomogram is presented, focusing on the interface. At the top, in each panel a 1D profile along a direction approximately orthogonal to the interface is shown. The 1D profile was obtained from 3D regions by averaging the observed intensity within the planes parallel to the interface.

Figure 3a and b show the results for two samples where OPC paste was in contact with bentonite ad OPA, respectively. Fig. 3a (OPC-bentonite) shows on the OPC side, that the cement paste appeared unaltered, with stable portlandite, for distances larger than about 1.5 mm from the interface (zone (1)). Within the first 1.5 mm, two distinct zones, both with lower voxel value than in (1), can be recognized. Zone (2), at the interface, had an extension of ~400 μm and was characterized by higher voxel value compared to the following zone (3). The higher intensities in (2) may be due to new mineral formation. On the contrary, the drop in zone (3) can be attributed to portlandite dissolution. The OPC-bentonite system showed, on the bentonite side, a clear high voxel value zone (in comparison with the bentonite further away from the interface) whose center was located at ~250 μm from the interface (zone (4)).

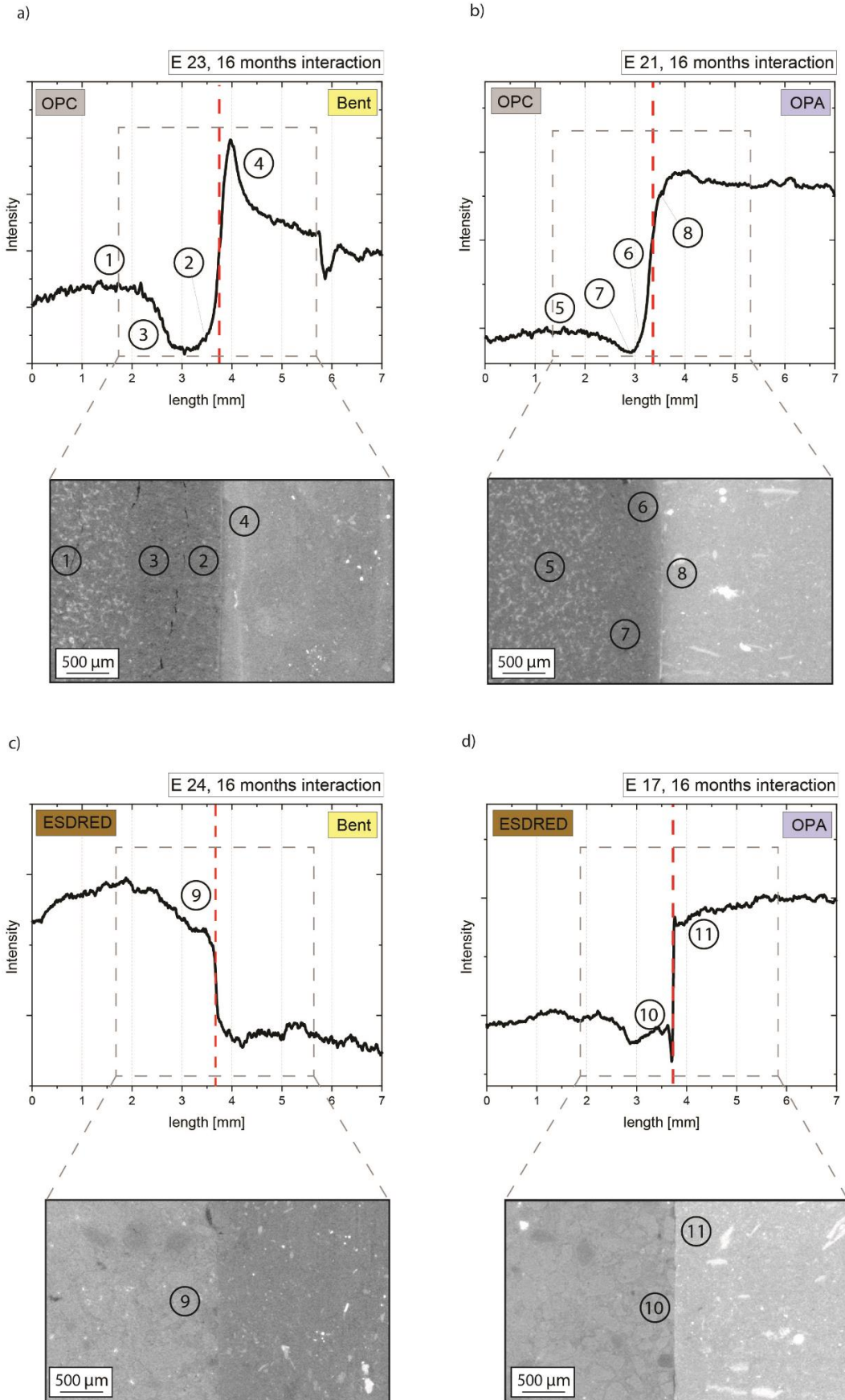


Figure 3 Intensity profiles with the corresponding 2D slice of the tomogram for different interface samples after about 16 months interaction. a) OPC-bentonite. b) OPC-OPA. c) ESDRED-bentonite. d) ESDRED-OPA

This bentonite higher density region had a relatively small extension (<200 μm). Beyond this zone, the average voxel value was characterized by a general decrease and significant fluctuations. Localized peaks may originate from the presence of heavy minerals (e.g. pyrite), which appear as very bright spots in the slice. A deep local minimum in the 1D profile is visible at about 2 mm from the interface. A large particle of the heavy minerals was located approximately at the same distance, whose volume was not crossed by the slice shown in Fig. 3a. The extremely high X-ray attenuation of such particle led to so-called metal artifacts in the tomographic reconstruction (Mouton et al, 2013).

For the OPC-OPA sample, on the OPC side, a spatial profile qualitatively similar to the one obtained from the OPC-bentonite system can be observed. The zone labelled as (5) and starting at about 1.5 mm from the interface, is characterized by a voxel value slightly fluctuating around a plateau. This zone could be considered as reference region, where portlandite seems to have remained stable. Towards the interface, the OPC paste appeared significantly altered with two distinct sub-zones. Zone (6) in Fig. 3b clearly exhibited higher voxel values compared with the average value in zone (5). It had a thickness of $\sim 400 \mu\text{m}$ and was followed by a zone labelled as (7) with significantly lower voxel values than in zone (5). On the OPA side, close to the interface, a zone with decreased voxel value (Fig. 3b feature (8)) compared with the rest of the volume on that side was visible.

The ESDRED-bentonite interface (Fig. 3c) did not show a clear zonation, contrary to what observable in Fig 3a and b. Heavy minerals, appearing as very bright particles in the slices, are recognizable in Fig. 3c, both on the bentonite side and within the ESDRED paste. The central part of the ESDRED side is characterized by a region with higher voxel value, which towards the interface tends to decrease to values comparable to the external part. Around the sand grains close to the interface, the cement paste exhibited slightly smaller voxel values (9) than what it did further away from the interface. The bentonite side showed relatively stable voxel values, with exception of a $\sim 300 \mu\text{m}$ thick region close to the interface with slightly higher voxel value.

For the ESDRED mortar-OPA interface sample, on ESDRED side, in the zone labelled as (10) and still close to the interface, the voxel value was also slightly lower than further away from the interface. The cement paste around the sand grains appeared also for this sample to be darker than further away from the interface. On the OPA side, Region (11) in Fig. 3d indicates a $\sim 500 \mu\text{m}$ zone, close to the interface characterized by a slight decrease in voxel value compared to the region further away from the interface. Beside these two features, the X-ray tomographic investigation of the ESDRED-OPA interface did not provide evidence of strong alterations of the interface itself.

X-Ray Diffraction (XRD)

Opalinus Clay in contact with OPC paste or ESDRED mortar did not show any significant variation in the mineralogy after 2 years interaction (Fig. 4a). The main minerals identified are: i) illite $8.9^\circ 2\theta \text{ CuK}\alpha$ ($d=10.0 \text{ \AA}$), and $19.7^\circ 2\theta \text{ CuK}\alpha$; ii) kaolinite, with a major reflection located at $12.3^\circ 2\theta \text{ CuK}\alpha$ ($d=3.6 \text{ \AA}$) and $24.8^\circ 2\theta \text{ CuK}\alpha$ ($d=7.2 \text{ \AA}$); iii) quartz ($26.6^\circ 2\theta \text{ CuK}\alpha$, $d=4.26 \text{ \AA}$); iv) calcite ($29.4^\circ 2\theta$, $d=3.03 \text{ \AA}$); v) pyrite ($33.0^\circ 2\theta \text{ CuK}\alpha$, $d= 2.71 \text{ \AA}$). The soft reflection located at $8.9^\circ 2\theta$ ($d=10 \text{ \AA}$), is indicated in Fig. 4a as corresponding to illite but could also partially be related to the presence of minor amount of chlorite (Mäder et al., 2017). At $19.7^\circ 2\theta$, a remarkable reflex is present. This peak is typical for clay minerals and

can indicate the presence of different clay types; for this case it is likely to be related to illite and possibly illite/smectite layers. The very strong intensity of the calcite reflection at 29.4° 2θ $\text{CuK}\alpha$ may hide the formation of C-S-H minerals, which normally have a main reflection located at $\sim 29^\circ$ 2θ $\text{CuK}\alpha$ (e.g., Fig. 4b, CSH).

Bentonite in contact with cementitious material reacted differently than Opalinus Clay. Fig. 4b shows the diffractogram of unaltered Na-montmorillonite (one of the main component of bentonites, Carlson, 2004) and of unaltered MX-80 bentonite. Na-montmorillonite has a prominent reflex at 19.7° 2θ $\text{CuK}\alpha$ corresponding in this case to sodium montmorillonite. Some traces of quartz (26.6° 2θ , $d=4.26$ Å) are also well recognizable. The weak reflection at 21.9° 2θ $\text{CuK}\alpha$ may be ascribed to cristobalite but possibly also to stacking faults within the montmorillonite structure (Jansen et al., 2024) Unaltered bentonite is characterized by the presence of a major reflection at $\sim 7.0^\circ$ 2θ $\text{CuK}\alpha$, $d=12.9$ Å), corresponding to Ca-Na montmorillonite. Quartz (26.6° 2θ $\text{CuK}\alpha$) and feldspars (23.6° and 27.6° 2θ $\text{CuK}\alpha$) reflections are also well visible. Furthermore, cristobalite (21.9° 2θ $\text{CuK}\alpha$) appear also to be present, as observed in Yokoyama et al. (2021).

The bentonite sample after two years contact with the ESDRED mortar shows a diffractogram relatively similar to unaltered bentonite: quartz, feldspar and montmorillonite are present. The cristobalite reflection, well visible in the unaltered sample, is reduced. Whether this represents cristobalite dissolution or sample heterogeneity is not clear at the moment.

Bentonite in contact with OPC paste shows as well a pattern similar to unaltered bentonite: montmorillonite, quartz and feldspars are present as well in this sample. The cristobalite reflection (21.9° 2θ $\text{CuK}\alpha$) is present but is relatively weak. The main difference compared to unaltered bentonite (and also to the one in contact with ESDRED) is the presence of a reflection at $\sim 29.3^\circ$ ($d=3.04$ Å) corresponding to C-S-H phases; minor C-S-H reflections at 32.05° ($d=2.7$ Å) and 50.07° 2θ ($d=1.8$ Å; not shown) were also observed. The bentonite skin formed at the interface in contact with OPC is therefore characterized by precipitation of C-S-H phases.

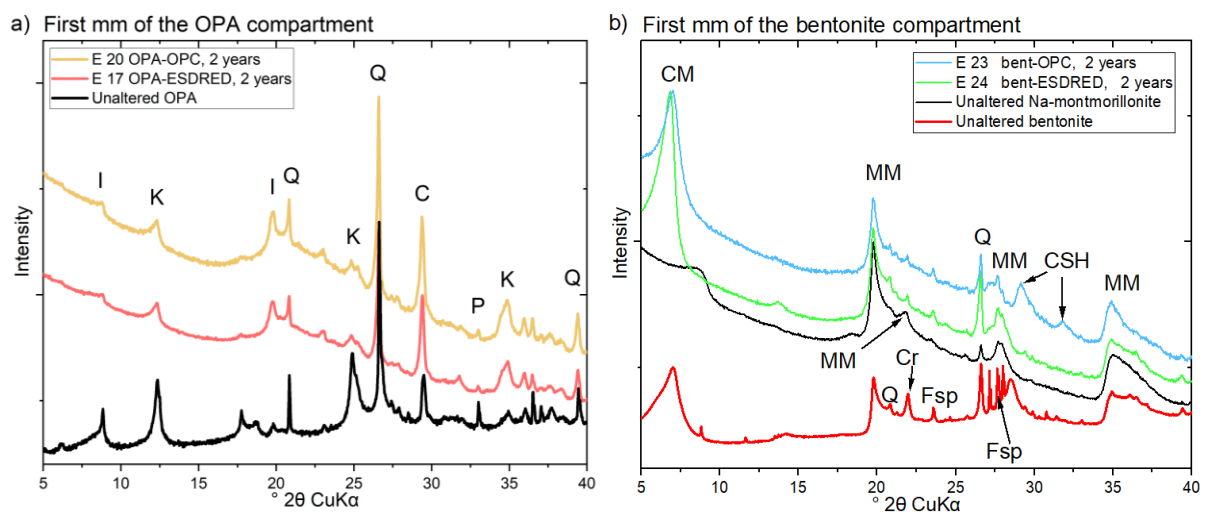


Figure 4 X-ray powder diffractogram of the first mm of a) Opalinus Clay and b) bentonite (MX-80) in contact with OPC and ESDRED for 2 years. Reflection identifications, I: illite, K: kaolinite, Q: quartz, C: calcite, P: pyrite, CM: Ca-Na montmorillonite, MM: Montmorillonite, Cr: cristobalite, Fsp: feldspar, CSH: C-S-H.

SEM/EDX

OPC - clay interfaces

Ordinary Portland cement paste samples in contact with clays were all characterized by a decrease of the Ca/Si ratio towards the interface (Fig. 5a). The ratio, which is about 2.4 far away from the interface, reaches a minimum value of ~ 1.7 at the contact with clay. EDX investigations (Fig. 5a; Annex 1, Ca map) indicate that this decrease is mainly attributed to portlandite dissolution related to the influence of the lower pH clay porewater. The longer the interaction time, the more the porewaters will tend to equilibrate (also depending on the diffusive properties of the interface). The decrease of the pH may also destabilize C-S-H phases, which most likely at least partially dissolve close to the interface. For OPC samples in contact with Opalinus Clay the region with reduced portlandite has an extension of 1-1.5 mm (Fig. 5a). Bentonite was compacted to a density of $1500 \pm 50 \text{ kg m}^{-3}$ and thus had a slight higher diffusivity and thus faster mass transport compared to Opalinus Clay. This fact may partially explain why, in OPC-bentonite samples a wider region formed where portlandite was unstable (2-3 mm, Annex 1). No significant alteration of the magnesium content is observed for OPC paste-clay interfaces (Fig. 5b). Regarding aluminum, on the cement side an increase of the Al/Si ratio is observed towards the interface (Fig. 5c) for the OPC-OPA sample. This suggests that clay minerals are dissolving and releasing Al^{3+} in solution, available for other reactions. The dissolution of clays and accessory minerals (e.g. quartz, cristobalite, feldspars) would also lead to the release of silica in solution. Sodium tends to decrease towards the interface on the OPC side, for both interface types (Fig. 5d).

On the clay side, Ca/Si is increased towards the interface in samples with OPC (Fig. 5a). The Ca/Si enrichment in the clay is more prominent in OPC-bentonite samples, consistent with the higher dissolution of portlandite in these samples. The diffused calcium very likely accumulates in the clay on the exchanger sites and/or precipitates as a new phase. The extension of the Ca enrichment measured on the clay side is $\sim 1 \text{ mm}$ for OPA and up to 2.5 mm for bentonites. For both, OPA and bentonite in contact with OPC paste, no relevant alteration of the magnesium concentration was observed on the clay side (Fig. 5b). Na instead appears to be slightly increasing towards the cement compartment (Fig. 5d).

ESDRED - clay interfaces:

A decrease of the Ca/Si ratio towards the interface is also seen in ESDRED mortar. In this case, due to the absence of portlandite, the measured ratio is mainly related to the C-S-H composition. The average value in the external part is 1.4. This value drops to 1.0 at 1 mm from the interface, and even to 0.8 in the first 200 μm of the cement paste, indicating that C-S-H are strongly decalcified and dissolving in this region (Fig. 5a, Annex 2). With respect to the unaltered Ca/Si ratio, no significant enrichment is visible on the clay side for bentonite and OPA, reflecting the lower amount of released Ca compared to samples composed of OPC.

For ESDRED-OPA samples a prominent magnesium enrichment within the first mm of the OPA was measured (Fig. 5b, Annex 1). On the ESDRED side, however, the Mg concentrations do not appear to be strongly modified with respect to the external, less altered part. For ESDRED-bentonite samples, a magnesium enriched region was also observed on the clay side, although less prominent; its extension is approximately 1 mm.

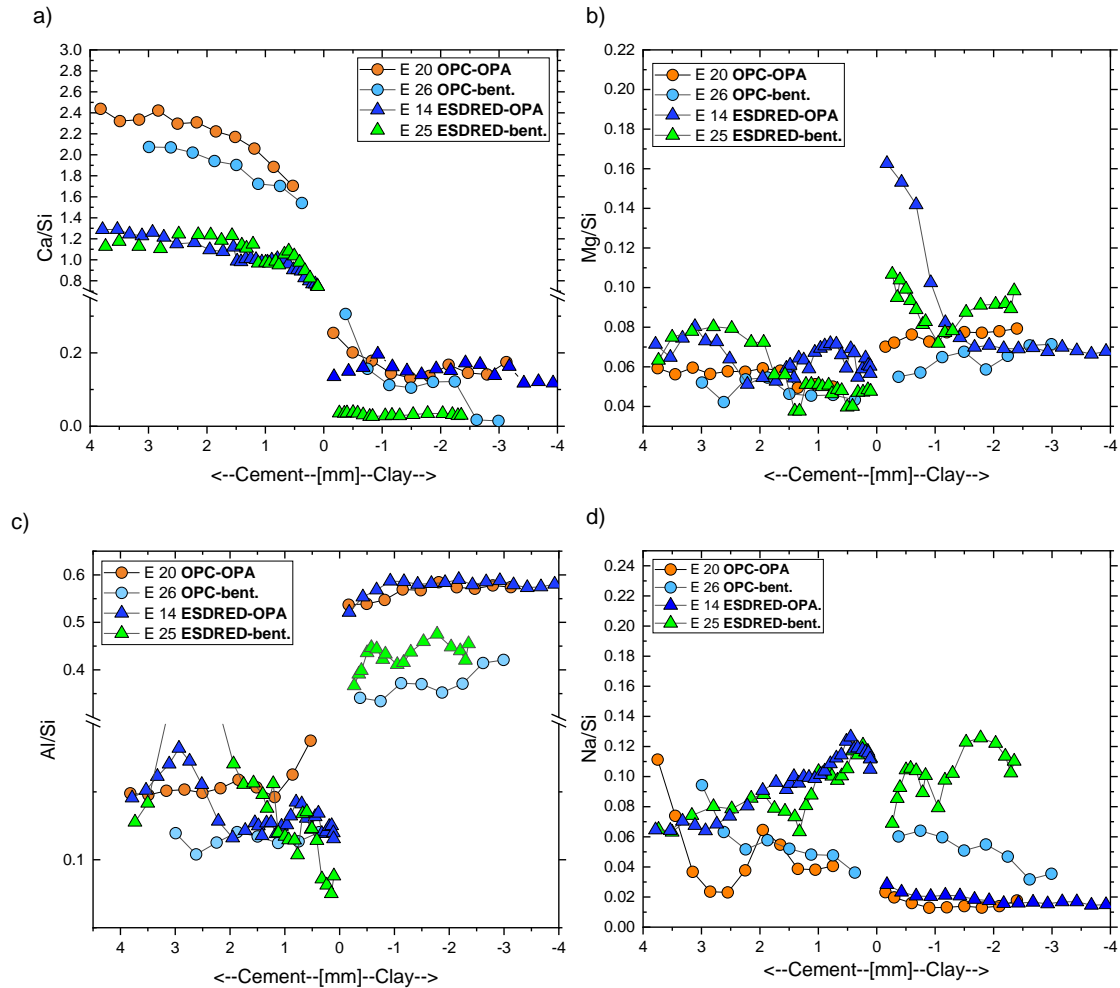


Figure 5 SEM/EDX chemical composition of different interfaces type after 2 years interaction. The data were obtained by averaging a series of maps, see Annex 1. ESDRED mortar data were obtained as punctual moving averages. Full data are given in Annex 2.

For this sample, on the ESDRED side, the Mg/Si ratio seems to be lowered towards the interface (Fig. 5b). For both interface type, aluminium appear to be decreasing towards the interface on the mortar (Fig. 5c) side. Sodium appears to be clearly enriched on the ESDRED side, while it was about constant in the bentonite or slightly enriched in the OPA near the interface.

Thermogravimetric analysis (TGA)

OPC paste

TGA investigation of unaltered OPC (black line, Fig. 6a) revealed a considerable dehydration between 50°C and 250°C, where the weakly bound water is released. This peak overlaps with the dehydration peaks of several cement phases; mainly: C-S-H, AFm and AFt phases. Portlandite dehydroxilation is visible at ~450°C. The slight portlandite peak shift between unaltered and reacted samples is related to different sample mass used for the measurement (Lothenbach et al., 2016). The presence of small amounts of calcite is indicated by the small negative peak in the region around 700°C. All the analyzed samples of OPC paste show a higher amount of carbonate with respect to the unaltered sample (650-750°C), possibly related to the atmospheric conditions during the measurements and the transport.

OPC having been in contact with Opalinus Clay shows an enhanced presence of minerals with weakly bound water (100-200°C) close to the interface (0-2 mm), possibly representing additionally formed C-S-H or C-(A)-S-H phases (Adler et al., 1999; L'Hôpital et al., 2015). To reach the minimum amount of mass necessary for TGA analysis, two millimeters of sample had to be cut and grinded. Therefore, the sample contained not only the cement skin seen in other investigations (e.g., Fig. 3) but also a part of an unaltered section of the OPC side. For this reason, a small peak related to dehydration of portlandite can still be observed at 450°C in the 0-2 mm slice. The negative peak at 700°C indicates the remarkable presence of newly formed calcite at the interface. The external part of the sample (3-5mm) is characterized by a composition generally similar to the unaltered OPC sample.

When OPC paste got in contact with bentonite, similarly as observed for OPA-OPC interfaces, a stronger negative peak can be observed between 100°C and 200°C for the region near the interface (0-2 mm), possibly related to C-S-H formation. The negative peak for enhanced carbonation (650°C-750°C) is weaker than for the sample having been in contact with OPA. Also, for OPC paste that was in contact with bentonite, portlandite is conserved in the external part of the sample.

ESDRED

The unaltered ESDRED sample is characterized by a small mass loss within the first 200°C, mainly related to C-S-H, AFm and AFt phases (Fig. 6b). A prominent negative peak is present between 200-300°C suggesting the presence of residual calcium aluminate hydrate $[Al(OH)_3]$. Most likely this negative peak is due to the presence of corundum grains originating from the abrasive paper used to produce the powder. A peak in this temperature range may theoretically also indicate dehydroxilation of calcium aluminate hydrate present in other phases such as Hydrogarnet, AFm or AFt (Lothenbach et al., 2016). However, the absence of other negative peaks does not support this hypothesis for the investigated samples. From 300°C on, no other significant peaks can be detected in the DTG analysis.

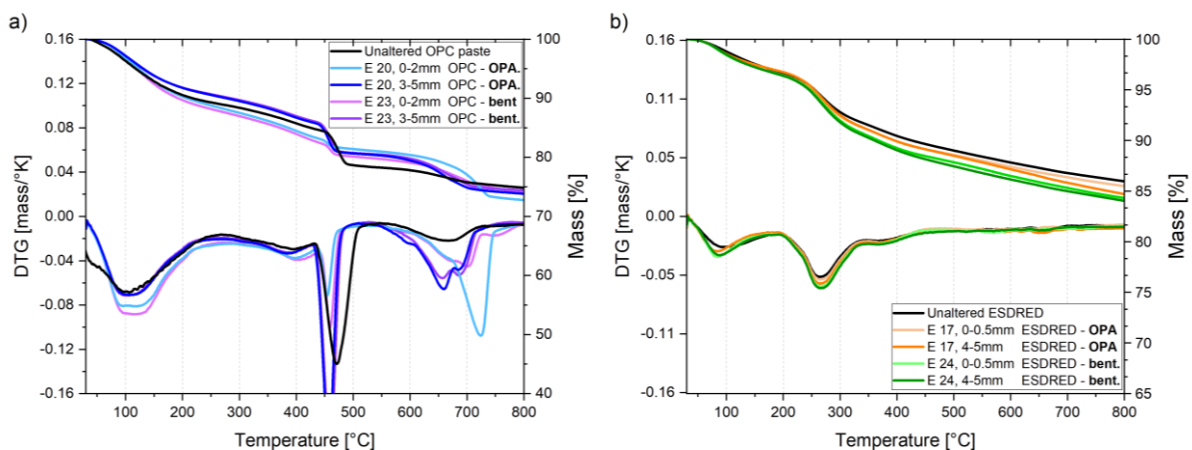


Figure 6 DTG analysis diagrams for cement from a) OPC paste – clay samples; b) ESDRED - clay samples. The top curves represent mass loss (right y-axis), the bottom curves DTG data (left y-axis).

Also, in the temperature window between 500°C and 700°C, typical for carbonates, no mineral phases were observed. All ESDRED samples, independent from the interface type, do not show any significant alterations. The DTG pattern is in general very similar to the unaltered sample, characterized by some

weakly bound water related mass loss around 100°C. With respect to the unaltered sample, a slightly higher mass loss is observed around 100°C.

Opalinus Clay

Unaltered Opalinus Clay (Fig. 7a) has a mineralogy dominated by clay minerals (illite, kaolinite, illite/smectite mixed layers, chlorite), quartz, calcite and some accessory pyrite and feldspars (Bossart and Thury, 2008). The DTG diagram of unaltered OPA allows recognizing a negative peak in the 30-150°C interval, representing the dehydration of interlayer water. The negative peak between 500-600°C represents the mineral kaolinite (Faqir et al., 2019). Siderite, present in minor amount in OPA, shows as well a peak at ~500°C; its presence may be in this case hidden by the larger amount of kaolinite contained in OPA. The peak at 700°C indicates the presence of calcite (as fossils and diagenetic-related fillings).

Opalinus Clay in contact with OPC paste is in the external part almost unaltered (3-5 mm from the interface), showing a similar pattern with respect to the unaltered OPA sample. The slice close to the interface (0-1 mm) shows instead a continuous mass loss between 100°C and ~350°C, suggesting the presence of some C-S-H phases (Fig. 7a, light blue line). The OPA sample in contact with the ESDRED mortar has a very similar DTG pattern with respect to unaltered Opalinus Clay. The main difference is represented by the presence of the peak between 500°C and 600°C. Especially close to the interface (0-1 mm) the mass loss related to this peak is remarkable. The peak may indicate the slight presence of magnesite ($MgCO_3$), but further investigation would be needed to confirm this hypothesis.

Both samples of OPA in contact with ESDRED mortar and OPC paste respectively, show a higher calcite content with respect to the unaltered sample. This observation is likely to be related to local mineralogical heterogeneities present inside the Opalinus Clay. In fact, for the unaltered sample a larger amount of material could be used, resulting in a more representative mineralogical composition.

MX-80 bentonite

The unaltered bentonite sample, mainly composed of montmorillonite, shows a strong peak at 80-90°C representing the interlayer water, and a wider peak at 700°C corresponding to the clay dehydroxylation. Bentonite in contact with OPC paste is characterized by a strong alteration of the mineralogy: between 50°C and 200°C, increased mass loss occurs leading to a wide DTG peak for the sample from 0-1 mm (purple line), which is not seen in the original bentonite. This feature indicates the presence of C-S-H minerals forming at the contact with the cement. At higher temperatures, the clay dehydroxylation peak is remarkably reduced. The 3-5 mm part of the bentonite that contacted OPC does not show new mineral formation, but displays a reduced interlayer water-related peak and also a reduced dehydroxylation peak, suggesting partial clay dissolution.

The bentonite samples in contact with ESDRED mortar do not show significant mineralogical alterations. Both samples (0-1 mm and 3-5 mm) have a very similar pattern with respect to the unaltered bentonite. Differently than observed for bentonite in contact with OPC, the interface sample (0-1 mm) has a very similar mineralogy with respect to the unaltered sample until 200 °C. Between 200°C and 700°C the sample displays a continuous mass loss. To be noted are the smaller sizes of the dihydroxylation peaks for bentonite in contact with OPC as compared with ESDRED, suggesting a larger dissolution of

montmorillonite in the first case. A slight peak shifting is also present and could partially be related to a difference in the composition and/or small mass changes present in the measuring crucible.

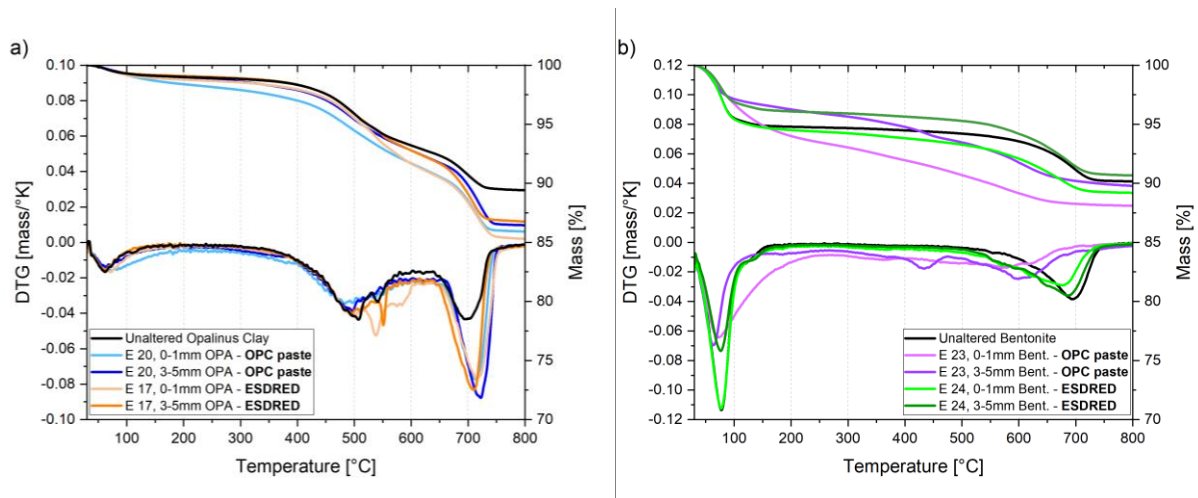


Figure 7 DTG analysis diagrams for clay from a) Opalinus Clay-cement samples; b) bentonite (MX-80) - cement samples. The top curves represent mass loss (right y-axis), the bottom curves DTG data (left y-axis).

Discussion

Mineralogical alterations

General observations on samples consisting of OPC paste and clays (bentonite or OPA)

On the OPC side, as result of the diffusive mixing of the cement and clay porewaters, dissolution of portlandite is observable. The decrease of the pH quickly destabilized portlandite leading to a calcium and pH plume which then diffused into the clay compartment. When portlandite was completely consumed, C-S-H destabilization started, providing additional calcium into solution. The alkaline plume diffusing into the clay lead to mineral dissolution (e.g., illite, montmorillonite) and a release of ions into solution (Bauer et al., 1998; Honty et al., 2010), which then could diffuse towards the cement compartment and form new minerals. SEM/EDX maps indicated an increase of aluminum close to the interface on the cement side, observation valid especially for OPC-OPA interfaces. The aluminum available in solution is possibly at least partially incorporated into C-S-H phases leading to the formation of C-(A)-S-H phases (L'Hôpital et al., 2015).

OPC paste – bentonite samples

For experiments using the same cement paste in contact with Na-montmorillonite, Luraschi et al. (in prep.) observed the formation of Cl-AFm on the cement side in contact with montmorillonite and the disappearing of ettringite close to the interface (for samples investigated after 4 years of interaction). Although no XRD data were acquired for the material from the cement paste side in the present study, both phenomena are expected to occur as well in the bentonite samples here (Fig. 8a). X-ray tomography allowed recognizing the formation of a high intensity region within the first 500 μm on the cement side (Fig. 3c). Furthermore, TGA analysis suggested an increased presence of hydrated phases in this region (Fig. 8a). Which phase is present could not be clearly determined, but potentially C-S-H or AFm may have formed. Similar observations were already made in other experiments (e.g., Fernández et al., 2016).

The bentonite side is characterized by an enrichment in calcium; the highest concentrations are measured within the first ~2 mm of the bentonite compartment (Fig. 5a). SEM/EDX investigations also evidenced a Na enrichment within the bentonite skin (0-2 mm from the interface). Approximately, in the same region neutron imaging evidenced a remarkable porosity decrease (Fig. 1a, 8a). TGA and XRD investigations showed the presence of C-S-H phases, which formed within the ~2 mm thick clay skin (0-2 mm, Figs, 4b, 7b). Outside the clay skin region (2-5mm) the clay appears mostly unaltered.

OPC paste – Opalinus Clay samples

The alteration of the cement paste is limited to ~1-1.5 mm from the interface. Inside this cement-skin region, portlandite is dissolved and calcite precipitation was observed within the first 500 µm of the cementitious compartment (Figs 6a, 3b), likely to locally decrease the porosity (Fig. 8c). Calcite precipitation is related to the high CO₂ partial pressure of OPA. According to Jenni et al. (2014) and Mäder et al. (2017), HCO₃⁻ diffuses into the cement compartment and precipitates – due to the presence of Ca²⁺ – as CaCO₃. The samples were stored for most of the time under a nitrogen atmosphere, therefore an influence of atmospheric CO₂ can be considered as of minor relevance. The similarity of the TGA patterns of OPC in contact with bentonite or OPA (Fig. 6a) suggests also the possible precipitation of C-S-H, and possibly AFm phases, although no clear evidence was observed. On the OPA side, TGA measurements suggest the possible formation of C-S-H within the first mm of the clay compartment (Fig. 7a). This observation is well understandable considering the alkaline conditions and the availability of calcium, aluminum and silica in solution. Nevertheless, the mineralogically dominating reaction at the interface of this sample type, at least in short term, is represented by the precipitation of calcite occurring on the cement side.

General observations on samples consisting of ESDRED and clays (bentonite or OPA)

Thermogravimetric analysis performed on samples did not reveal any strong mineralogical alteration within the ESDRED compartment (Fig. 6b). Likewise, neither XRD, neutron imaging nor X-Ray tomography did hint to significant alterations (Figs. 1, 3). This is probably related to the low diffusivity of the ESDRED mortar, which does not allow to observe significant modifications within 2 years. The decreasing Ca/Si ratios towards the interface observed by SEM/EDX (Fig. 5a, Annex 2) show that the mortar compartment did not react homogeneously; this trend indicates the progressive destabilization of C-S-H phases when approaching the interface. A magnesium enrichment within the first mm of both bentonite and OPA was observed (Fig. 5b). For OPA the Mg enrichment was particularly evident (Annex 1). On the mortar side, no Mg anomalies were detected for the sample with OPA, but a decrease towards the interface for the sample with bentonite. Sodium was increased towards the interface on the ESDRED side (Fig. 5d).

ESDRED-Opalinus Clay samples

A prominent Mg enrichment was observed on the OPA side, (Fig. 5b, 8d) but not on the mortar side. XRD measurements did not detect significant alteration of the OPA skin with respect to the unaltered Opalinus Clay (Fig. 4a). Mg enrichment within the first 1.5mm within OPA was also described by Bernard et al. (2020), who investigated OPA-ESDRED samples having reacted for up to 10 years by means of micro XRD. Furthermore, they describe a region at the interface with calcite precipitation, which in this study was not

observed. Calcite is considered to be forming from the available calcium (from ESDRED mortar) and carbonate (from clay) in solution. In contrast to XRD, TGA measurements indicated the possible neoformation of Mg-carbonate (MgCO_3) in OPA (Fig. 7a), which would partially explain the absence of calcite. Whether this is the only phase responsible for Mg-enrichment, or whether also M-S-H and LDH (Dauzères et al., 2016; Bernard et al., 2020) are present, is at the moment not clear. On the OPA side no relevant Ca enrichment was observed, which is possibly related to the low amount of Ca provided by the dissolution of C-S-H, which furthermore readily diffuses through the clay compartment and is thus not easily detectable. In addition, the high presence of carbonate fossils inside the Opalinus Clay (clearly visible with SEM, parallel to the bedding) need to be considered. Their presence can locally affect the obtained EDX results, especially for calcium.

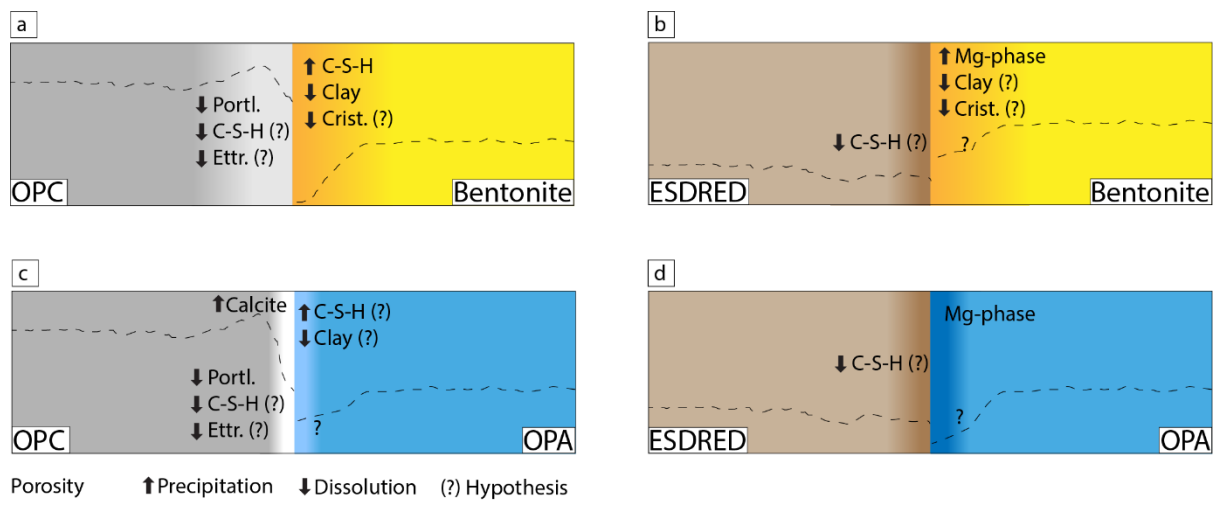


Figure 8 Schematic representation of the skin extension, the expected porosity evolution, and the main mineralogical alteration after 2-years interaction: a) OPC paste-bentonite (MX-80) interface; b) ESDRED-bentonite (MX-80); c) OPC paste-Opalinus Clay; d) ESDRED-Opalinus Clay. The dashed line represents the supposed porosity evolution. The intensities of the colors indicate qualitatively the skin extension. Drawings are not to scale.

ESDRED-bentonite samples

TGA did not show any detectable mineralogical modification of bentonite (Fig. 7b). The DTG pattern is in fact very similar to that one of unaltered bentonite. The XRD investigation evidenced as main modification (with respect to an unaltered bentonite) the possible reduction of the cristobalite reflection (Fig. 4b), although this feature may stem from the heterogeneities between the samples. SEM/EDX investigations indicated a slight enrichment of magnesium towards the interface (Fig. 5b) on the bentonite side. X-ray tomography showed i) a small decrease of intensity towards the interface (Fig. 3c) on the ESDRED side and ii) a slight increase of the intensity on the bentonite side towards the interface. These variations of the intensity are anyway difficult to relate to a specific reaction.

The magnesium distribution

Magnesium enrichment at cement-clay interfaces was described in field scale and laboratory experiments by several authors for different cement-clay systems. The location of the enrichment (cement or clay side) is dependent on the interface components (Jenni et al., 2014; Mäder et al., 2017; Lerouge et al., 2017; Fernández et al., 2017; González-Santamaría et al., 2020). The Mg enrichment is attributed to nano-

crystalline M-S-H phases (Dauzères et al., 2014; Bernard et al., 2020) or Mg-bearing layered double hydroxides (Bernard et al., 2020).

In our experiments, the Mg enrichment was observed only in the samples in contact with the low-pH ESDRED mortar (Fig. 5b, Annex 1); and only on the clay side of both OPA and bentonite. There are various possible reasons for the observed differences: i) The small size of our samples and the connection to the reservoir may have played a relevant role. As mentioned in the methods, the samples were not connected to the corresponding reservoir for the entire time. This possibly limited the Mg supply hindering the precipitation of Mg-phases. ii) The specific chemical composition of the high-porosity OPC paste may influence the precipitation, favoring the formation of other phases (the porewater of the used OPC paste does not contain Mg). iii) The different diffusive properties of the system, especially of the high porosity OPC paste, may lead to a different chemical equilibrium, favoring the formation of the observed phases. Unpublished data (to be submitted) for similar clay samples in contact with OPC paste, which were continuously attached to the reservoir, indicate the formation of a Mg enrichment on the bentonite side after eight months of contact (at 70°C), but not on the OPC side.

The performed investigations did not allow to precisely define which phase is related to the Mg enrichment within the clay compartment. For Opalinus Clay-ESDRED mortar interface samples, magnesite (MgCO_3) appeared to be present approaching the interface. Whether this is the only Mg phase present is, however, unclear.

Correlation between mineralogical alteration and diffusive properties

For OPC paste-bentonite interfaces, the diffusivity decrease observed in the samples (Fig. 2a) appears to be related to the formation of a C-S-H rich skin in the first mm near the interface on the clay side, leading to a porosity decrease (Fig. 1a) and therefore to a lower D_e . The magnitude of the decrease of the diffusion coefficient, the temporal evolution of the alteration and the mineralogical modifications correlate well with the observation made by Luraschi et al. (2020) for OPC paste Na-montmorillonite interface samples. They observed a decrease of the interface diffusivity by 46% after 17 months interaction, and then a subsequent lower (but ongoing) reduction of the diffusivity.

For bentonite samples in contact with ESDRED, a diffusivity decrease by 64% was observed after 2 years of interaction (Fig. 2b). The mineralogical investigation performed on these samples did not allow to clearly identify the phase responsible for the porosity alteration, but it may well be related to the formation of Mg-phases on the clay side. González-Santamaría et al. (2018) describe for a 70 days laboratory experiment with low-pH cement and bentonite similar phenomena as observed in the present study: decalcification of the cement paste close to the interface and Mg enrichment on the bentonite side. They also observed carbonation, which was not observed in the current study, likely because of the low $p\text{CO}_2$ of bentonite and the storing of the samples under nitrogen atmosphere.

The 45% decrease of the interface diffusion coefficient for OPA-OPC paste samples (Fig. 2a) is likely to be primarily related to the precipitation of calcite inside the cement paste pores at the interface (Figs. 3b, 6a). The mineral precipitation observed by means of TGA on the OPA side (possibly C-S-H), Fig. 7a) may also influence the diffusivity. As observed for the other interface samples with OPC paste, portlandite dissolution and C-S-H decalcification are present (Figs. 5a, c).

For OPA-ESDRED mortar samples, a clear decrease of the diffusion coefficient (by 34% after 2 years, Fig. 2b) was also observed. In this case, the main phase responsible for this is probably the magnesium enriched region observed on the clay side (Fig. 5a), as no calcite formation was observed on the cement side (Fig. 6b), in contrast to observations by Lerouge et al. (2017) and Bernard et al. (2020). TGA suggest the presence of magnesite in OPA close to the interface (Fig. 7a); this mineral, not described in the literature for similar samples, could thus represent one of the responsible phases for the diffusivity decrease in our experiments, even though no clear porosity reduction could be seen (Fig. 1d).

Conclusions

Cement-clay samples prepared from different materials (OPC paste, ESDRED mortar, MX-80 bentonite and Opalinus Clay) and reacted for up to 2 years allowed to characterize the changes in mineral phases at the interface between the two materials. Simultaneously, through-diffusion experiments allowed to monitor the evolution of the diffusivity of the different systems. All the investigated types of cement-clay sample showed a significant alteration of the diffusive properties after 2 years of interaction. For OPC-Na montmorillonite samples, Luraschi et al. (2020) demonstrated a rapid decrease of the diffusivity across a cement-clay sample within the first 12 months, followed by a slower but continuous decrease of the measured diffusion coefficient. This pattern is related to a negative feedback: a porosity decrease due to the precipitation of new mineral phases slows down diffusive exchange, which in turn reduces further alterations, that is, the overall reactivity of the interface region. The different interface samples displayed a 34-64% decrease of the diffusivity within two years. This is a relatively narrow range when considering the differences between samples and the multiple factors that can influence the derived diffusion coefficient. It thus appears that the $D_{e, \text{HTO}}$ across the various investigated cement-clay interface samples behave relatively similarly.

Mineralogically, the ESDRED mortar appears to be less aggressive towards the clay material as expected, which is certainly related to its lower pH. Nevertheless, also the ESDRED-clay samples displayed a remarkable diffusivity decrease at the interface. The collected data suggest that the details regarding the types of phases dissolving or precipitating, as well as regarding the locations and the timing of the reactions, vary clearly depending on the composition and properties of the used material. However, the disequilibrium present at the cement-clay interfaces leads in all cases to a similar evolution of the diffusive properties on the short term, independently from the initial chemical composition. This may be due to the mentioned negative feedback, which levels out the extent of reactions for the different materials. To verify this hypothesis, more data will have to be collected, and for longer periods. A possible solution to speed up experiments would be the increase of the temperature, to enhance diffusion and the interface reactivity, and thus to obtain a view on the long-time behavior.

References

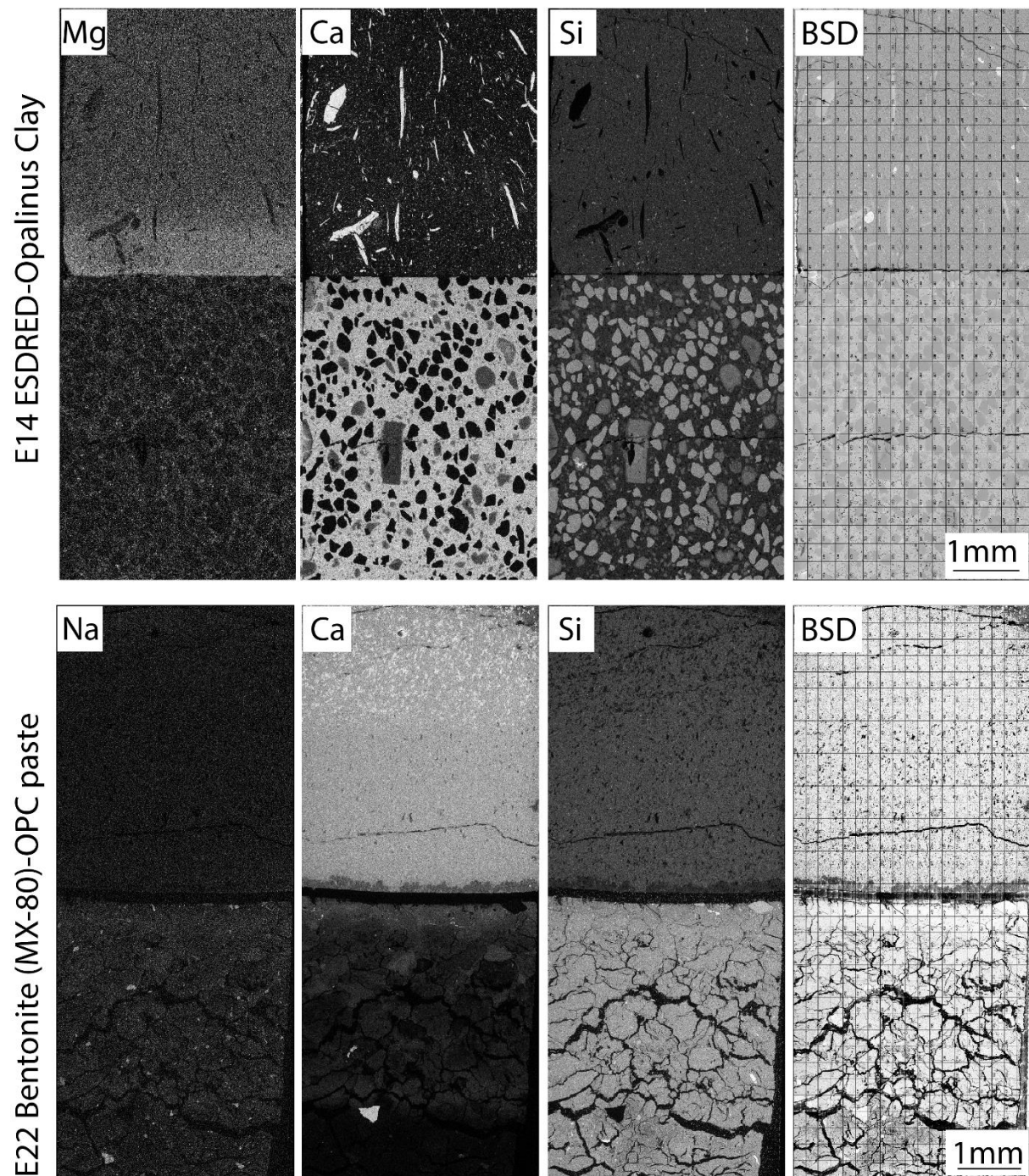
- Adler, M., Mäder, U., Waber, H.N., 1999. High-pH alteration of argillaceous rocks: an experimental study. *Schweiz. Mineral. Petrogr. Mitt.* 79, 445–454.
- Bauer, A., Berger, G., 1998. Kaolinite and smectite dissolution rate in high molar KOH solutions at 35 and 80 C. *Appl. Geochem.* 13, 905–916.
- Bernard, E., Jenni, A., Fisch, M., Grolimund, D., Mäder, U., 2020. Micro-X-ray diffraction and chemical mapping of aged interfaces between cement pastes and Opalinus Clay. *Appl. Geochem.* 115, 104538.
- Bossart, P., Thury, M., 2008. Mont Terri Rock Laboratory - Project, Programme 1996 to 2007 and results. Wabern: Reports of the Swiss Geological Survey no. 3.
- Bossart, P., Bernier, F., Birkholter, J., Bruggeman, C., Connolly, P., Devonck, S., Fukaya, M., Herfort, M., Jensen, M., Matray, J., Mayor, J., Möri, A., Oyama, T., Schuster, K., Shigeta, S., Vietor, T., Wieczorek, K., 2017. Mont Terri rock laboratory, 20 years of research: introduction, site characteristics and overview of experiments. *Swiss J. Geosci.* 110, 1–20.
- Bradbury, M.H., Baeyens, B., 2003. Porewater chemistry in compacted re-saturated MX-80 bentonite. *J. Contam. Hydrol.* 61, 329–338.
- Carlson, L., 2004. Bentonite mineralogy. Posiva working report, 2004-02, Posiva OY, Olkiluoto, Finland.
- Crank, J., 1979. *The Mathematics of Diffusion*. Oxford university press.
- Dauzères, A., Le Bescop, P., Sardini, P., Cau Dit Coumes, C., 2010. Physico-chemical investigation of clayey/cement-based materials interaction in the context of geological waste disposal: Experimental approach and results. *Cem. Concr. Res.* 40, 1327–1340.
- Dauzères, A., Achiedo, G., Nied, D., L'Hôpital, E., Alahrache, S., Lothenbach, B., 2014. M-S-H precipitation in low-pH concrete in clayey environment. *NUWCEM*.
- Dauzères, A., Achiedo, G., Nied, D., Bernard, E., Alahrache, S., Lothenbach, B., 2016. Magnesium perturbation in low-pH concretes placed in clayey environment - solid characterizations and modeling. *Cem. Concr. Res.* 79, 137–150.
- Dolder, F., 2015. *Experimental Characterization and Quantification of Cement-Bentonite Interaction using Core Infiltration Techniques Coupled with X-ray Tomography*. PhD Thesis. University of Bern, Bern, Switzerland.
- Faqir, N., Shawabkeh, R. A., Al-Harhi, M., Wahhab, H.A., 2018. Fabrication of Geopolymers from untreated Kaolin Clay for Construction Purposes. *Geotech. Geol. Eng.* 37, 129–137.
- Fernández, R., Ruiz, A.I., Cuevas, J., 2016. Formation of CASH phases from the interaction between concrete or cement and bentonite. *Clay Miner.* 51, 223–235.
- Fernández, R., Torres, E., Ruiz, A.I., Cuevas, J., Alonso, M.C., García Calvo, J.L., Rodríguez, E., Turrero, M.J., 2017. Interaction processes at the concrete-bentonite interface after 13 years of FEBEX-Plug operation. Part II: Bentonite contact. *Phys. Chem. Earth* 99, 49–63.
- Gaucher, E.C., Blanc, P., 2006. Cement/clay interactions – a review: experiments, natural analogues, and modeling. *Waste Manag.* 26, 776–788.
- Gimmi, T., Leupin, O.X., Eikenberg, J., Glaus, M., Van Loon, L.R., Waber, H.N., Wersin, P., Wang, H.A.O., Grolimund, D., Borca, C.N., Dewonck, S., Wittebroodt, C., 2014. Anisotropic diffusion at the field scale in a four-year multi-tracer diffusion and retention experiment - I: Insights from the experimental data. *Geochim. Cosmochim. Acta* 125, 373–393.

- González-Santamaría, Angulo, M., D.E., Ruiz, Fernández, R., A.I., Ortega, A., Cuevas, J., 2018. Low-pH cement mortar-bentonite perturbations in a small-scale pilot laboratory experiment. *Clay Min.* 53, 237–254.
- González-Santamaría, D.E., Fernández, R., Ruiz, A.I., Oretga, A., Cuevas, J., 2020. Bentonite/CEM-II cement mortar interface experiments: A proxy to *in situ* deep geological repository engineered barrier system surface reactivity. *Appl. Geochem.* 117, 104599.
- Hodgkinson, E.S., Hughes, C.R., 1999. The mineralogy and geochemistry of cement/rock reactions: high-resolution studies of experimental and analogue materials. *Chem. Cont.Waste in the Geosph.* 157, 195–211.
- Honty, M., De Craen M., Wang, L., Madejová, J. A., Pentrák, M., Stríček, I., Van Geet, M., 2010. The effect of high pH alkaline solutions on the mineral stability of the Boom Clay – Batch experiments at 60 °C. *Appl. Geochem.* 25, 825–840.
- IAEA, 2009. Geological Disposal of Radioactive Waste: Technological Implications for Retrievability. NW-T-1.19.
- Jackson, D.F., Hawkes, D.J., 1981. X-Ray attenuation coefficients of elements and mixtures. *Phys. Rep.* 70, 169–233.
- Jakob, A., Sarott, F.A., Spieler, P., 1999. Diffusion and sorption on hardened cement pastes - experiments and modelling results. Paul Scherrer Institut, PSI-Bericht, 99–05.
- Jansen, D., German, A., Ectors, D., Winnefeld, F., 2024. Stacking faults of the hydrous carbonate-containing brucite (HCB) phase in hydrated magnesium carbonate cements. *Cem. Concr. Res.* 175, 107371.
- Jenni, A., Mäder, U., Lerouge, C., Gaboreau, S., Schwyn, B., 2014. In situ interaction between different concretes and Opalinus Clay. *Phys. Chem. Earth, Parts A/B/C* 70, 71–83.
- Jenni, A., Mäder, U., 2020. CI Experiment: specification and comparison of the cements included in the different cement formulations. Mont Terri Project, Technical Note, TN 2020–53.
- Kaestner, A.P., Hartmann, S., Kuhne, G., Frei, G., Grunzweig, C., Josic, L. Schmid, F., Lehmann, E., 2011. The ICON beamline - a facility for cold neutron imaging at SINQ, *Nucl. Instrum. Methods Phys. Res. Section A*, 659, 387–393.
- Kosakowski, G., Berner, U., 2013. The evolution of clay rock/cement interfaces in a cementitious repository for low- and intermediate level radioactive waste. *Phys. Chem. Earth*, 64, 65–86.
- Lerouge, C., Gaboreau, S., Grangeon, S., Claret, F., Warmont, F., Jenni, A., Cloet, V., Mäder, U., 2017. In situ interactions between Opalinus clay and low alkali concrete. *Phys. Chem. Earth* 99, 3–21.
- Lerouge, C., Gaboreau, S., Duee, C., Fauchet, C., Maubec, N., Touzelet, S., Wille, G., 2017. CI Experiment phase 21: in-situ interaction for 2 years between different cement pastes and Opalinus Clay. Mont Terri Project, Technical Note, TN 2016-36.
- L'Hôpital, E., Lothenbach, B., Le Saout, G., Kulik, D., Scrivener, K., 2015. Incorporation of aluminium in calcium-silicate-hydrates. *Cem. Concr. Res.* 75, 91–103.
- Lothenbach, B., Durdziński, P. and De Weerd, K., 2016. Thermogravimetric analysis. In: K. L. Scrivener, R. Snellings and B. Lothenbach, Eds. *A Practical Guide to Microstructural Analysis of Cementitious Materials*. Boca Raton, London and New York: CRC Press, 177-211.
- Luraschi, P., Gimmi, T., Van Loon, L.R., Shafizadeh, A., Churakov, S.V., 2020. Evolution of HTO and ³⁶Cl diffusion through a reacting cement-clay interface (OPC paste-Na montmorillonite) over a time of six years. *Appl. Geochem.*, 119, 104581.

- Mäder, U., Jenni, A., Lerouge, C., Gaboreau, S., Miyoshi, S., Kimura, Y., Cloet, V., Fukaya, M., Claret, F., Otake, T., Shibata, M., Lothenbach, B., 2017. 5-year chemico-physical evolution of concrete-claystone interfaces. *Swiss J. Geosci.*, 110, 307–327.
- Melkior, T., Mourzagh, D., Yahiaoui, Y., Thoby, D., Alberto, J.C., Brouard, C., N. Michau, N., 2004. Diffusion of an alkaline fluid through clayey barriers and its effect on the diffusion properties of some chemical species. *Appl. Clay Sci.*, 26, 99–107.
- Mouton, A., Megherbi, N., Slambrouck, K.V., Nuyts, J., Breckon, T.P., 2013. An experimental survey of metal artefact reduction in computed tomography. *J. X-Ray Sci. Technol.*, 21, 193–226.
- Nagra, 2002. Project Opalinus Clay – Safety Report, Demonstration of Disposal Feasibility for Spent Fuel, Vitrified High-level Waste and Long-lived Intermediate-level Waste ("Entsorgungsnachweis"). Nagra Tech. Rep. NTB 02–05, Nagra, Wettingen, Switzerland.
- Nagra, 2014. SGT-Etape-2: Vorschlag weiter zu untersuchender geologischer Standortgebiete mit zugehörigen Standortarealen für die Oberflächenanlage: Charakteristische Dosis intervalle und Unterlagen zur Bewertung der Barrierensysteme. Nagra Tech. Rep. NTB 14–03, Nagra, Wettingen, Switzerland.
- Nagra, 2018. A review of Cement-Clay Modelling. Nagra Arbeitsber. NAB 28–24.
- Pearson, F. J., Arcos, D., Bath, A., Boisson, J.-Y., Fernandez, A., Gaebler, H.-E., Gaucher, E., Gautschi, A., Griffault, L., Hernan, P., Waber, H. N., 2003. Geochemistry of Water in the Opalinus Clay Formation at the Mont Terri Rock Laboratory (Synthesis Report). Geological Report, No. 5, p. 321. Federal Office of Topography (swisstopo), Wabern.
- Savage, D., 2011. A review of analogues of alkaline alteration with regard to long-term barrier performance. *Min. Mag.*, 75, 2401–2418.
- Savage, D., Walker, C., Arthur, R., Rochelle, C., Oda, C., Takase, H., 2007. Alteration of bentonite by hyperalkaline fluids: a review of the role of secondary minerals. *Phys. Chem. Earth, Parts A/B/C* 32, 287–297.
- Shafizadeh, A., Gimmi, T., Van Loon, L.R., Kaestner, A., Lehmann, E., Mäder, U., Churakov, S.V., 2015. Quantification of water content across a cement-clay interface using high resolution neutron radiography. *Phys. Proc.* 69, 516–523.
- Shafizadeh, A., 2019. Neutron Imaging Study of Evolution of Structural and Transport Properties of Cement-Clay Interfaces. PhD Thesis. University of Bern, Bern, Switzerland.
- Shafizadeh, A., Gimmi, T., Van Loon, L.R., Kaestner, A.P., Mäder, U.K., Churakov, S.V., 2020. Time-resolved porosity changes at cement-clay interfaces. *Cement Concr. Res.* 127, 105924.
- Ramirez, S., Cuevas, J., Vigil, R., Leguey, S., 2002. Hydrothermal alteration of "La Serrata" bentonite (Almeria, Spain) by alkaline solutions. *Appl. Clay Sci.* 21, 257–269.
- Taylor, H.F.W., 1997. *Cement Chemistry*, 2nd Edition. Thomas Telford, London.
- Tits, J., Jakob, A., Wieland, E., Spieler, P., 2003. Diffusion of tritiated water and $^{22}\text{Na}\beta$ through non-degraded hardened cement pastes. *J. Contam. Hydrol.* 61, 45–62.
- Van Loon, L.R., Soler, J.M., 2003. Diffusion of HTO, $^{36}\text{Cl}^-$, $^{125}\text{I}^-$ and $^{22}\text{Na}^+$ in Opalinus Clay: Effect of Confining Pressure, Sample Orientation, Sample Depth and Temperature. Nagra Technical Report, NTB 03-07.
- Wieland, E., Tits, J., Dobler, J.P., Spieler, P., 1998. Interaction of Eu(III) and Th(IV) with Sulphate-resisting Portland cement. *Mater. Res. Soc. Symp. Proc.* 506, 573–578.

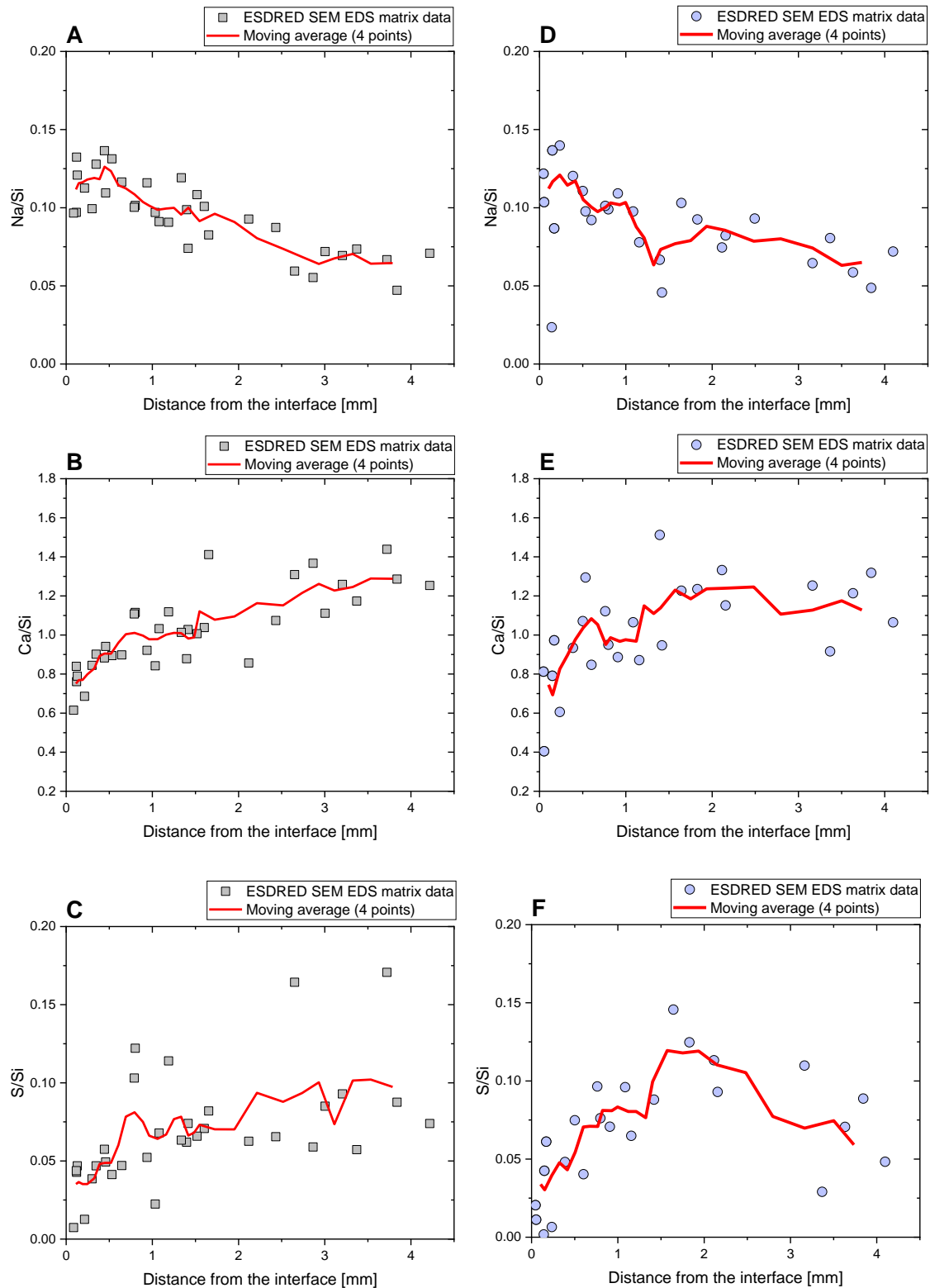
- Wilson, J., Bateman, K., Tachi, Y., 2021. The impact of cement on argillaceous rocks in radioactive waste disposal systems: A review focusing on key processes and remaining issues. *Appl. Geochem.* 130, 104979.
- Yamaguchi, T., Sawaguchi, T., Tsukada, M., Hoshino, S., Tanaka, T., 2016. Mineralogical changes and associated decrease in tritiated water diffusivity after alteration of cement–bentonite interfaces, *Clay Miner.* 51, 279–287.
- Yokoyama, S., Shimbashi, M., Minato, D., Watanabe, Y., Jenni, A., Mäder, U., 2021. Alteration of Bentonite Reacted with Cementitious Materials for 5 and 10 years in the Mont Terri Rock Laboratory (CI Experiment). *Min.* 11, 251.

Annex 1



Annex 1 Elemental and back scatter maps (BSD) obtained by SEM/EDX mapping of an ESDRED-OPA sample (upper image) and OPC-bentonite (lower image).

Annex 2



Annex 2 Measured EDX data points from the ESDRED matrix and corresponding moving averages for different elemental ratios. Sample E14 representing ESDRED-OPA (A,B,C) and sample E25, representing ESDRED-bentonite (D,E,F).

Supplementary material

X-ray tomography was performed on the four clay-cementitious interface systems with the EasyTom XL tomograph manufactured by RX Solutions (<https://www.rxsolutions.fr/>) and located at Empa's Center for X-ray Analytics (<https://www.empa.ch/web/s499/nano-ct>).

The X-ray source of such tomograph consists of an open X-ray tube, manufactured by Hamamatsu Photonics K.K. (model L10711-23), which was equipped with a LaB₆ filament (when we performed the measurements) and a 1 μm -thick W target deposited on a 500 nm-thick diamond substrate. When operated at less than 100 kV of acceleration voltage, such X-ray tube can focus the accelerated electron beam on the W target within a focal spot with size slightly smaller than 1 μm , thus allowing reducing the source-related blur in the X-ray images to the sub- μm scale.

The tomograph is equipped with an X-ray detector being a 2D flat panel of 1920 \times 1536 amorphous-Si pixels, each coated with a CsI X-ray scintillator screen. The X-ray photons transmitted through the specimen are converted into visible light photons by the CsI thin film. The latter get converted at each pixel into electrical charge. The physical pixel size of such detector is $p = 127 \mu\text{m}$.

For each tomography measurement, we used approximately the same settings, except for small differences leading to distinct total acquisition time. The X-ray source acceleration voltage and current were set to 90 kV and 55 μA , corresponding to a power delivered on the target of 4.4 W. 2400 and 1792 projection images of the specimens (called radiographs) were acquired for the tomograms of the specimens with the Opalinus clay and those with the bentonite, respectively. Each radiograph was acquired at a distinct orientation angle, θ , of specimen around an axis passing approximately through its center of mass and parallel to the vertical direction of the detector's plane. θ spanned the range 0° - 360°, typical for cone beam tomography measurements. Each radiograph consisted of the pixel-wise average of 12 or 8 distinct and successive radiographs acquired with θ fixed (frame averaging), for the Opalinus- and bentonite-containing specimens, respectively. The acquisition time *per* frame was 250 ms. In addition to the 2400 or 1792 radiographs with the specimen into the X-ray beam, 128 in the absence of the specimen and 128 with the X-ray source switched off were acquired at the start of the measurement for performing the flat-field and dark current corrections of the specimen radiographs, respectively.

The X-ray source-to-detector distance was $d_{s-d} = 257.96 \text{ mm}$ and the source-to-specimen distance was $d_{s-s} = 12.59 \text{ mm}$, leading to a geometrical magnification factor $M = \frac{d_{s-d}}{d_{s-s}} \cong 20.49$ for the specimen's projection onto the detector plane, as a consequence of the conical geometry of the X-ray beam. The voxel/pixel size of the tomogram/radiographs was thus $\tilde{p} = \frac{p}{M} \cong 6.2 \mu\text{m}$. We remind the reader that the effective spatial resolution of the tomogram/radiographs is always a multiple of the actual voxel size. A heuristic estimate of the upper bound of the spatial resolution is $2 \times \tilde{p} \cong 12.4 \mu\text{m}$.

Each tomogram was obtained from the respective set of 2400 or 1792 radiographs by using an implementation of the Feldkamp-David-Kreiss cone beam filtered back-projection tomographic reconstruction algorithm into RX Solutions' XAct Ver. 1.0 software, optimized for GPU-processing. The reconstructed tomograms, with real-valued voxel, were then saved in the format of a stack of 2D 16-bit unsigned integer TIFF images (tomographic slices), spaced along the vertical axis or rotation at a distance \tilde{p} . The voxel values in the range 0.45 - 2 were mapped from real to integer numbers between 0 and $2^{16}-1$ with a linear transform. Such mapping was performed for all tomograms in order to make the range of voxel values comparable across the tomograms.

Feldkamp, L.A., Davis, L.C., Kress, J.W., 1984. Practical cone-beam algorithm, J. Opt. Soc. Am A. 1, 612-619.

Chapter 6

OPC paste-clay interaction at 70°C: Eight months monitoring of properties at materials interfaces

-- Manuscript in preparation for publication --

OPC paste-clay interaction at 70°C: Eight months monitoring of properties at materials interfaces

Pietro Luraschi^{a,b,*}, Thomas Gimmi^{a,b}, Luc Van Loon^a, Michele Griffa^c, Frank Winnefeld^c, Sergey V. Churakov^{a,b}

^aLaboratory for Waste Management, Nuclear Energy and Safety, Paul Scherrer Institut, 5232 Villigen, Switzerland

^bInstitute of Geological Sciences, University of Bern, 3012 Bern, Switzerland

^cSwiss Federal Laboratories for Materials Science and Technology, Empa, 8600 Dübendorf, Switzerland

* Corresponding author

E-mail addresses: pietro.luraschi@psi.ch (P. Luraschi), thomas.gimmi@psi.ch (T. Gimmi)

Keywords: reactive transport, precipitation, dissolution, high temperature, clogging, nuclear waste disposal

Abstract

The interaction between cementitious materials and clay is of relevance in environmental systems and engineering applications, for instance in the context of geological disposal of hazardous waste. Cement and concrete are used as construction material, and clays (e.g., bentonite) are used for sealing. When brought in contact, geochemical reactions are triggered due to the geochemical differences of the two materials. Here we report on reactions observed in cement-clay samples that were kept for eight months at an elevated temperature of 70°C under a nitrogen atmosphere. The samples were prepared from three different material combinations: a high porosity hardened Portland cement paste was in contact with Opalinus Clay, Na-montmorillonite or bentonite (MX-80). The experiments were performed at 70°C to accelerate diffusion, and to increase the reactivity of the system and possibly the crystallinity of newly formed minerals, which, at room temperature, would tend to be more amorphous. During the experiments, the porewater chemistry and the pH evolution at both ends of the samples were monitored. The diffusive properties of the altered interface samples were studied by through-diffusion experiments after eight months of interaction using HTO as a tracer. Subsequently, the samples were investigated by means of several techniques (TGA, XRD, X-ray tomography, SEM/EDX) to observe the mineralogical alterations. A decrease of the diffusion coefficient with respect to the initial unaltered conditions occurred for samples including bentonite or montmorillonite. On the cement-side, portlandite dissolution and, towards the interface, an enrichment of aluminium and sodium was evidenced. On the clay side, for bentonite and montmorillonite the formation of C-S-H minerals within the first mm of the interface was detected. A thin region with magnesium enrichment was also present at 1.5 mm from the contact with the hardened cement paste. The samples with Opalinus Clay were characterized by minor alteration (possibly related to incomplete contact to the paste): mainly calcite precipitation near the interface on the cement side and a slight portlandite dissolution near the interface, also on the cement side.

Introduction

Cementitious materials, thanks to their mechanical and chemical properties, are foreseen for construction of underground repositories for radioactive waste, and they are also used for conditioning waste. Different rock formations are considered to host the underground repository in different countries, including clay-rich as well as crystalline rocks. Independently of the chosen rock, the contact of the highly alkaline cement porewater with other materials (host rock, sealing materials) is a topic of research for all the countries facing the challenge of radioactive waste disposal (IAEA, 2009). The Swiss repository will be located in a clay-rich sedimentary rock, the Opalinus Clay (OPA). The Swiss concept foresees the use of concrete and cementitious materials as stabilizers for the tunnel walls, and as a cavern back fill material (Nagra, 2002; 2008). The mineralogical differences between cement paste and clay are reflected in their respective porewaters. The contact of these two different porewaters leads to solute fluxes across the material interface and consequently mineralogical alterations including a variation of the porosity at the interface (Gaucher and Blanc, 2006; Savage, 2011; Wilson et al., 2021). After a short period of interaction, a region of limited spatial extension (mm) with altered physico-chemical properties, often denoted as a skin region, is formed. Interactions between alkaline solutions and clays have been studied since decades and a large amount of data has been acquired. Studies with samples where concrete or cement paste came into contact with clay also exist. Extensive reviews are provided by Gaucher and Blanc (2006), Savage (2011), Wilson et al., (2021) and Nagra (2018; 2022). Nevertheless, several questions remain open. Of special interest is the evolution of the diffusive properties and the characterisation of the effective rates of the mineral alterations. The evolution of the transport properties is a key factor in the field of radioactive waste disposal. It is expected that the steel canisters containing high-level waste, spent fuel or (depending on design) also low- and intermediate-level waste will fail after a given time, leading to the release of radionuclides to the surroundings. At that time the host rock and the engineered barriers must be operational, i.e., retard the migration of radionuclides towards the biosphere (Nagra, 2002). A clogging of the pore space at the interface between cement and clay, on one hand, would be a positive effect with respect to retention of radionuclides. On the other hand, one of the major concerns is the gas production (Nagra, 2016), related to the anoxic corrosion of steel (formation of H_2) and degradation of organic materials in the waste matrix (formation of CH_4). Luraschi et al. (2020), using the same setup as in this study, observed a very low diffusivity of anions (for some interface samples no flux at all) for OPC-Na montmorillonites interfaces which reacted at room temperature for up to 6 years. Whether the diffusivity of gas molecules such as H_2 and CH_4 will also be reduced, possibly leading to a pressure build-up, is unclear. Porosity evolution and ultimately diffusivity evolution near the cement-clay interfaces are therefore relevant topics when assessing the safety of a repository.

The diffusive and mineralogical alterations of systems composed of a high-porosity OPC paste and Na-montmorillonite, bentonite (MX-80) or Opalinus Clay at room temperature have already been investigated (Shafizadeh, 2019; Shafizadeh et al., 2020; Luraschi et al., 2020; Luraschi et al., in prep), but no data exist for elevated temperatures. Knowing the reactivity at elevated temperatures is relevant for several reasons. Elevated temperatures prevail in-situ at the considered repository depths (several hundred metres), and heat is typically also released by emplaced high-level waste. Furthermore, higher

temperatures are expected to accelerate solute diffusion and reactions, and thus to possibly shorten the times needed to detect significant alterations in experiments. The present study focused on three different types of interface samples (high-porosity OPC paste in contact with Na-montmorillonite, bentonite (MX-80) or Opalinus Clay), which reacted for eight months at 70°C under a nitrogen atmosphere. During this period the porewater and the pH evolution were monitored. After eight months, the cells were removed from the oven and a series of through-diffusion experiments using tritiated water (HTO) as a tracer were conducted at room temperature. Subsequently the interface samples were investigated using different analytical techniques, to correlate the observed diffusivity variations with the mineralogical alterations. The results of the new samples reacted at 70°C were then compared with previous data for identical samples (Luraschi et al., 2020; in prep.) to derive the effect of temperature on the overall reactivity of the system.

Materials

Sample components: the cement and the clays

Na-montmorillonite (Milos, Greece) and bentonite (MX-80) were compacted using a specifically designed press to a bulk dry density of $1500 \pm 50 \text{ kg m}^{-3}$. After compaction, the clay plugs of 5 mm length and 5 mm diameter were introduced into PTFE (Polytetrafluoroethylene) sleeves in aluminium cells and saturated for 14 days with the corresponding porewater solution (Tab.1).

Table 1

Composition of the synthetic porewater (total concentrations) derived for OPC (Wieland et al., 1998), MX-80 Bentonite (Bradbury and Baeyens, 2002, adapted for 1500 kg m^{-3} dry density) and Opalinus Clay (Pearson et al., 2003). The reported porewater compositions correspond to equilibrium at ambient conditions.

	OPC [mM]	Na-montmorillonite [mM]	Bentonite, Mx-80 [mM]	Opalinus Clay [mM]
Na	114	300	243	241
K	118	-	1.2	1.6
Ca	1.6	-	9.5	2.5
Mg	-	-	7.1	17
Cl	-	300	67.5	300
S^{VI}	3	-	104	14
Al	0.05	-	-	-
Sr	-	-	0.08	0.51
C_{org}	-	-	0.88	0.476
pH	13.3	7	8	7.6

To maintain the desired degree of compaction during equilibration, a steel dummy was inserted into the cell to fill the space foreseen for the cement paste plug. The details of the setup (Fig. 1) are given in (Luraschi et al., 2020). OPA was obtained from a drill core produced in the Mont Terri Underground Laboratory. Plugs of 5 mm diameter were drilled parallel to the bedding plane, trying to avoid micro cracks and regions enriched in fossils or accessory minerals. After careful polishing the plugs to the desired length of 5 mm, they were pushed into the PTFE sleeve of the cell and saturated with a synthetic porewater solution (Tab.1). Again, a steel dummy was placed instead of a cement paste plug during the saturation process. A high porosity ($63 \pm 5\%$) hardened Ordinary Portland cement paste (Type CEM I 52.5 N HTS) cast in 2001 (Tits et al., 2003) was used to prepare the cement part of the samples. After casting, the cement was cut into slices and put under the corresponding porewater solution (Tab. 1) calculated by Wieland et al. (1998). Plugs of 5 mm diameter were drilled out,

shortened to 5 mm length and introduced into the PTFE sleeve of the cell to obtain an interface with the presaturated clay. The cement bulk chemical composition is given in Shafizadeh et al. (2015).

Experimental setup

Figure 1 displays a schematic view of the experiment (see Luraschi et al., 2020, for more details). Six cells containing three different interface samples were connected to the corresponding porewater reservoirs (50 mL for this phase at both sides) through a filter (thickness 1.5 mm) and a small reservoir of 30 μL inside the cell on each side. The interface samples were saturated under N_2 atmosphere at room temperature ($25 \pm 2^\circ\text{C}$) for an additional week. Then, the cells were emplaced in an oven at $70 \pm 2^\circ\text{C}$ for eight months. The pump and the porewater reservoirs were placed outside the oven.

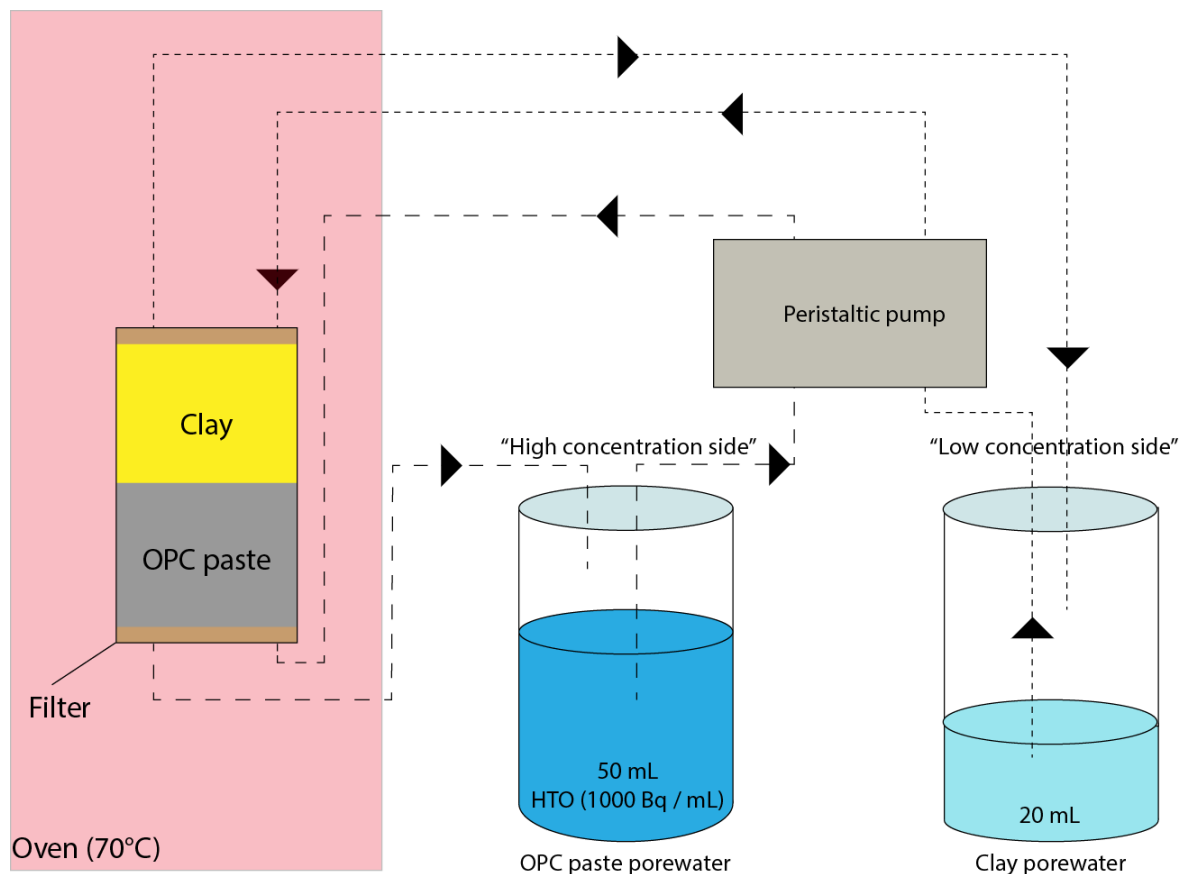


Fig.1 Schematic view of the experimental setup. The reservoir volumes shown (50 and 20 mL) relate to the through-diffusion experiments; previously, 50 mL was used on both sides. The samples reacted at 70°C for eight months. Through-diffusion experiments were performed at room temperature (25°C).

The flow rate was set to 0.1 mL s^{-1} to avoid excess pressure and to ensure a diffusive transport regime across the experimental cell. Even though the solution volumes to be circulated within the cell were small (small dead volume of tubing inside the oven, the small reservoir of $30 \mu\text{L}$ inside the cell and in the filters) and thermal equilibration is comparably fast, it is possible that at the very external part of the samples the temperature was lower than 70°C . The concentrations of Ca^{2+} , Mg^{2+} , Na^+ , K^+ and the pH in the reservoirs with the cement and clay porewater were repeatedly monitored during the experiment. After eight months of interaction, the samples were taken out of the oven and cooled down for 24 hours to room temperature. Subsequently, after a week, a series of through-diffusion experiments was started using HTO as a tracer added at the OPC paste side. The samples were kept for the entire duration of the

experiment under a nitrogen atmosphere (<0.1 ppm O₂). The porewater solutions were also prepared under N₂ atmosphere and exposed only for short times (some minutes) to air conditions.

Methods

Through-diffusion experiments

After cooling down, both reservoirs with cement and clay porewater were replaced with 50 mL fresh solution. The tubings were completely exchanged because some precipitates were observed, especially on the cement side, indicating that the solutions were not perfectly stable at 70°C. For the same reason also the filters were replaced by new ones. After one week, a solution containing 1000 Bq mL⁻¹ HTO (GE Healthcare, UK) was connected to the cement side (high concentration side). On the clay side (low concentration side), a 20 mL reservoir containing the corresponding porewater solution was attached (Fig. 1). This reservoir was exchanged every 2-3 days to keep the HTO concentration in this reservoir as low as possible. The accumulated diffused activity was measured by sampling 5 mL solution from the low concentration side, subsequently mixed with 15 mL Ultima Gold XR Scintillation Cocktail (Canberra-Packard). The 20 mL solution-cocktail mixtures were then measured by liquid scintillation counting (Tri-carb 2250 CA, Canberra-Packard).

The investigated cement paste-clay interface system can be approximated as a 1D domain of a given length, where the solute diffuses with a certain flux J . Once steady state conditions were reached, Fick's first law was applied,

$$J = -D_e \frac{\partial C}{\partial x} \quad (1)$$

where J is the solute flux per total cross section [mol m⁻² s⁻¹], D_e represents the effective diffusion coefficient that includes the porosity [m² s⁻¹], C is the tracer concentration in the solution [mol m³] and x is the spatial coordinate [m]. An extensive description of the derivation and of the error estimation procedure is given in Van Loon and Soler (2003) and Luraschi et al. (2020).

The obtained diffusion coefficient (D_e) represents an average for the entire system, composed of filters, cement and clay. The system can be considered as a series of resistances R_x (Glaus et al., 2015), such that:

$$R_{tot} = R_{clay} + R_{cem} + 2R_{filters} \quad (2)$$

where R is

$$R = \frac{\Delta x}{D_e} \quad (3)$$

Since the length and the properties of the different domains are known (Tab. 2), the properties of the newly formed skins, when observed, can be calculated (Luraschi et al., 2020).

Table 2 Characteristics of the used materials. The diffusion coefficients apply to room temperature.

	Length [mm]	Diffusion coefficient (D_e) [$\text{m}^2 \text{s}^{-1}$]
OPC paste	5.0 ± 0.1	2.8×10^{-10} (Tits et al., 2003)
OPA	5.0 ± 0.1	5.4×10^{-11} (Bossart et al., 2017)
Bentonite (MX-80)	5.0 ± 0.1	6.1×10^{-11} (Luraschi et al., 2020) ¹
Na-montmorillonite	5.0 ± 0.1	6.1×10^{-11} (Luraschi et al., 2020)
Peek filters	1.5	1.1×10^{-10} (Glaus et al., 2008)

¹Luraschi et al., (2020) derived $D_{e, \text{HTO}}$ values for Na-montmorillonite, here uses as a proxy for unaltered bentonite

X-ray tomography

The three different types of interface samples were investigated using attenuation-contrast X-ray tomography (Swiss Institute for Material Sciences, EMPA, Dübendorf, Switzerland). The measurements were performed after approximately one year of interaction: 8 months at 70°C and 4 months at room temperature when performing the diffusion experiments. The aluminium parts of the cells were removed and the samples were measured within the PTFE holder only. Extracting the sample from the aluminium holder allowed to significantly increase the spatial resolution. During the measurements, the samples were exposed to normal air conditions. To reduce the carbonation potential and the excessive swelling of the clay, a relatively short measuring time was selected. The analyses were performed using a nano computer tomography cone beam set-up (RX Solutions Easy Tom XL). The device is composed of a rotational table, a flat panel detector and a micro-focus X-ray tube. The small sample dimension (10 mm diameter including PTFE sleeve) allowed reaching a voxel size of $\sim 14 \mu\text{m}$. A total of 1179 projections were acquired during ~ 60 minutes. Dark- and flat field images were acquired and used to correct for camera and beam inhomogeneity. After a series of corrections related to reconstruction features and measuring conditions the data set was reconstructed to a three-dimensional object. The segmentation analysis was performed using the 3D visualization and analysis software Avizo (ThermoFisher).

Thermogravimetric analysis (TGA) and X-ray diffraction (XRD)

The cement paste-clay interface samples were flash-frozen with N_2 , subsequently freeze dried for several hours, cut into small slices parallel to the interface and measured in parallel with TGA and XRD at EMPA (Dübendorf, Switzerland). In general, four regions of the samples were investigated: i) one each from the external part of the cement paste and of the clay away from the material interface, supposed to be least altered, ii) one each from the regions close to the interface (from 0 to 1 mm or to 2 mm from the interface). The slices of 1-2 mm (depending on the material) were finely crushed in an agate mortar. For TGA, ~ 10 -15 mg of material was introduced into a crucible and stepwise heated ($20^\circ\text{C}/\text{min}$) until 1000°C . The measurements were performed using a TGA/SDTA 851 instrument (Mettler Toledo). XRD investigations were performed using an XRD diffractometer (PANalytical X'Pert Powder) in a capillary geometry with a Cu source ($\lambda = 1.5406 \text{ \AA}$ Cu $K\alpha$) and a PIXcel^{3D} detector. The limited amount of available sample material required a capillary glass (outer diameter: 0.5 mm, wall thickness: 0.01mm) for the investigations. The samples were scanned between 5° and 70° 2θ (continuous scan, step size of 0.026°

2 θ) during approximately one hour; subsequent phase identification was done using a specific software (X'Pert Highscore software V. 4.9.).

Chemical composition of the porewater

During the 8 months of interaction, the cement and the clay porewater in the reservoirs connected to the cells were monitored. Small samples of 200 μ L were regularly taken from both reservoirs and measured using an Ion Chromatography (IC) device (Dionex DX 600 IC/HLPC System coupled with Chromeleon software). Four major cations were measured: Na⁺, K⁺, Mg²⁺ and Ca²⁺. At the same time, the pH evolution of the reservoirs was monitored with a pH-Meter. To perform the IC measurements, the solutions were diluted into Methanesulfonic acid (MSH) to buffer the high pH of the cement porewater, which would otherwise lead to calcite precipitation when the solution is exposed to normal atmospheric condition.

SEM/EDX imaging

Due to the mechanical fragility of the dried cement paste-clay interface samples, they were prepared using a special procedure composed of liquid N₂ flash freezing, freeze drying and resin embedding under vacuum (the procedure is described in detail in Luraschi et al., in prep.). Once embedded in the resin, the samples were cut in half and polished using non-polar liquids. Since no coating was applied to the samples, SEM investigations were performed in low-vacuum mode (18 Pa) using a SEM (Zeiss EVO-50 XVP). The working distance was \sim 9 mm, the current 500 pA and the beam acceleration 20 kV. During the mapping, depending on the filament condition, the current was increased up to 1.2 nA to increase the count to noise ratio. Using Energy Dispersive Spectroscopy (EDX) the samples were investigated by means of the GENESIS software. The samples were divided into small (\sim 300 x 250 μ m) rectangles, which were mapped individually and subsequently joined to obtain a chemical map of the entire interface and a semi quantitative distribution of the main elements.

Results

Scanning Electron Microscopy (SEM) / Energy Dispersive Spectroscopy (EDX)

Mapping the different interface samples by means of SEM/EDX clearly indicated decalcification of the cement paste for the interfaces in contact with Na-montmorillonite and bentonite. The decrease in the Ca/Si ratio in the cement towards the interface (Fig. 2a) is mainly related to the dissolution of portlandite, which is recognizable in EDX maps (e.g., Supplementary Materials S1- S2). For the two investigated interface samples, with the clay side composed Na-montm. and bentonite, the extension of the region without portlandite (\sim 1.5 mm) on the cement paste side is similar in both interface samples. On the OPC paste side, no significant variations of the magnesium content were detected (Fig. 2c). A slight progressive enrichment of aluminium in the paste towards the clay contact appear to be present for these two sample type. Aluminium displays the same distribution through the cement paste side as silica (Fig. 2e). Fig. 2d indicates an increase of the Al/Mg ratio towards the interface. It is not clear whether Mg is slightly decreasing towards the interface, or aluminum and silica are enriched towards the interface.

On the bentonite and the Na-montmorillonite sides, a clear enrichment in calcium is visible within the first mm (Fig. 2a) from the interface. Sodium as well is enriched in the first mm of the clay compartment. Fig. 2f indicates that for montmorillonite, Na reaches a relatively constant concentration only at 3 mm from the interface, whereas for bentonite already at 1.5 mm. Magnesium is enriched in both

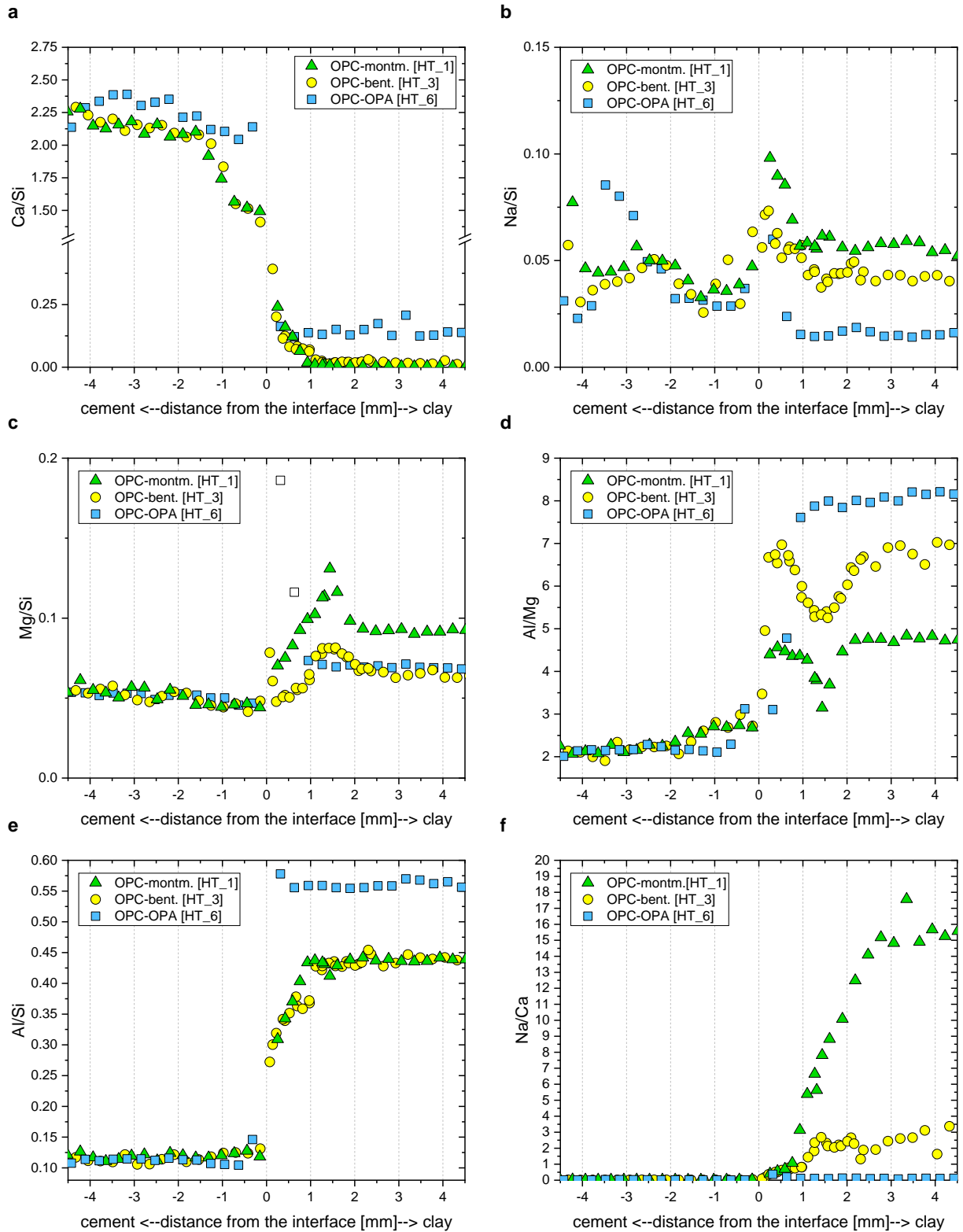


Fig. 2 SEM/EDX maps of the three different interfaces for different elements. A) Ca/Si; B) Na/Si; C) Mg/Si; D) Al/Mg; E) Al/Si; F) Na/Ca. The white squares in Figure 2c indicate high Mg values which originate from local enriched regions in the OPC-OPA sample (Supplementary Material S3) and necessitate a careful interpretation.

montmorillonite and bentonite in a zone at ~ 1.5 mm from the interface (Fig. 2c). This is further away from the interface than the zone of sodium and calcium enrichment, located at $\sim 0-1$ mm (Fig. 2a, b).

The OPC-OPA interface sample displayed only limited alterations. This is mostly related to an incomplete contact between the cement paste and the clay solids (Supplementary materials, S4). Nevertheless, within the first 200 μm of the OPC side portlandite is dissolved (Ca Map, S3). Crystals of a Ca-Si-Al-Si-K phase formed within the gap (attached to the OPC paste), indicating that the gap was filled by solution, but possibly not homogeneously (S4). The higher Ca/Si value observed within OPA is related to the high amounts of calcified fossils (e.g., Fig. 3c). Two data points with the magnesium concentration obtained at the interface (Fig. 2c) are displayed as white squares since their interpretation is not straightforward. It appears that where water was present in the gap between OPC paste and OPA, locally a magnesium enrichment formed (Supplementary materials, S3-S4). It is not clear at the moment whether these regions with increased Mg content are an artefact mostly related to imperfect contact would also be observed in situations with full contact.

X-ray tomography

On the external part of the cement paste in contact with montmorillonite or bentonite, a mineral with high voxel values is observed with a spotty distribution. Towards the interface, this mineral disappears (regions demarked by the dashed blue line, Fig. 3a, b). The extension of these regions is 1.5 mm for samples with Na-montmorillonite and about 3 mm for those with bentonite. Based on the EDX data and on previous investigations performed on similar samples (Luraschi et al., in prep), it can be stated that this mineral represents portlandite. For the montmorillonite samples a relatively sharp transition is visible (Fig. 3a), whereas for bentonite a region with partially dissolved portlandite is present (Fig. 3b). The precipitation of some new (high voxel value) phases seems to have happened in the voids left by portlandite dissolution. Where no precipitation occurred, dark empty pores are visible. On the cement side but right at the interface, a very thin region with high voxel values is visible for the OPC in contact with Na-montmorillonite.

On the montmorillonite and especially on the bentonite side, several accessory minerals are present (mainly quartz and feldspars according to EDX maps). Bentonite has a high content of pyrite resulting in spots with high voxel values (due to the high atomic weight). For Na-montmorillonite a region with high voxel values with ~ 0.8 mm extension formed at the contact with the cement paste (yellow line, Fig. 3a). The remaining part of the clay side appears to be undisturbed. Bentonite also displays a similar alteration region with high voxel values, which is less homogeneous and more extended (~ 2 mm) compared to the corresponding region within Na-montmorillonite.

Fig. 3c shows that there was probably no direct contact between OPA and OPC as mentioned in the previous section. Although the gap was probably at least partly filled by solution (Supplementary Material S4), it may have lowered the degree of transformation. This idea is supported by the fact that portlandite is stable nearly up to the interface, whereas in a study at room temperature with full contact of Opalinus Clay and OPC, it dissolved up to a distance of ~ 1 mm within 16 months (Luraschi et al., in prep.). Nevertheless, a thin layer of a mineral with a high voxel value formed right at the contact with the gap, suggesting that the gap was at least partially filled with solution. This high voxel value region

may have a low porosity, such that further diffusive exchange and portlandite dissolution was reduced. It is unclear whether the presence of the gap or the higher reaction temperature favoured the formation of this thin layer.

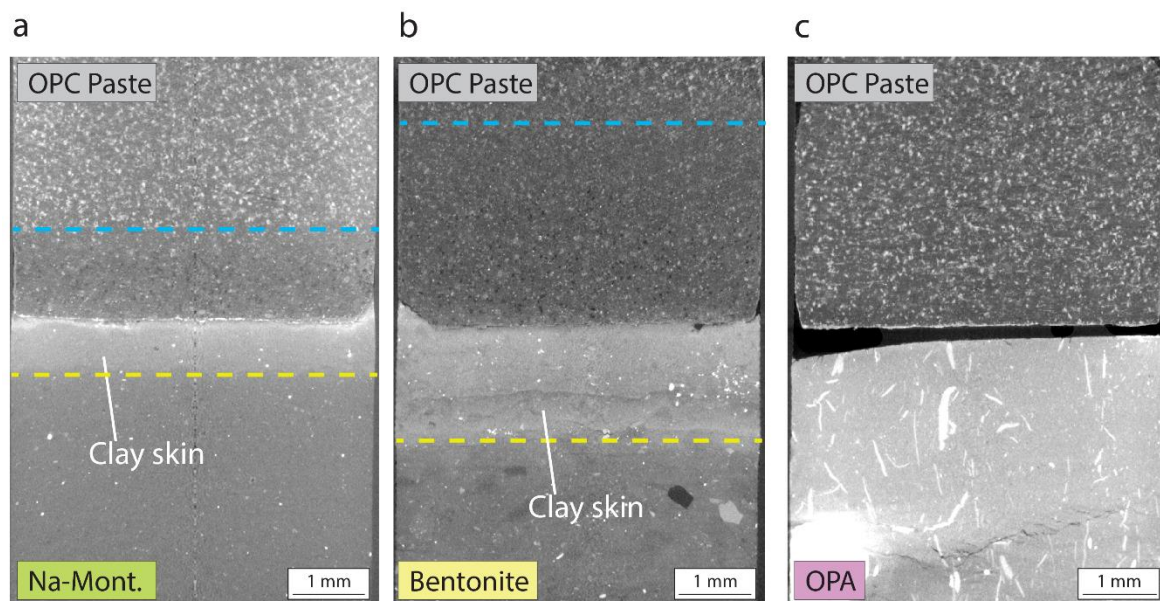


Fig. 3 Cross-sections extracted from the tomography for a) OPC-Na montmorillonite, b) OPC-bentonite (MX-80), c) OPC-OPA. The dashed lines represents the estimated extensions of the altered region in the cement paste (blue) and in the clay (clay skins, yellow).

TGA

Fig. 4a shows the TGA results for four different sections of OPC paste which have been in contact with Na-montmorillonite or bentonite. It can be seen how portlandite (characteristic peak at $\sim 450^\circ\text{C}$) is unstable towards the interface (0-2 mm), resulting in a less prominent peak. This part represents 2 mm of cement paste, which is the minimum amount to reach enough mass to perform the analysis. For this reason, some portlandite is still observable especially for the OPC in contact with Na-montmorillonite (light blue line Fig. 4a). The residual portlandite originates mainly from the more external part of the prepared section (1.5-2 mm), as observable in the images obtained by means of X-ray tomography (Fig. 3a). All the measured sections displayed a greater mass loss between the interval $300\text{-}450^\circ\text{C}$ with respect to the unaltered sample. The exact mineral responsible for this mass loss was not identified. The two external compartments (3-5 mm) also display a slight increase of calcite (650°C), possibly related to CO_2 contamination during transport or other measurements, which exposed the samples for short times to normal atmospheric conditions. Between $\sim 100^\circ\text{C}$ and $\sim 200^\circ\text{C}$ the sections from 0-2 mm show a more prominent and wider temperature range of dehydration compared to unaltered OPC, likely related to the formation of new hydrated minerals (e.g., AFm, C-S-H). In a study of similar samples but investigated at ambient temperature, Luraschi et al. (in prep.) reported the presence of Friedel's salt in OPC near interfaces; this mineral is may be present in this system as well.

On the clay side (Fig. 4b), for unaltered bentonite and montmorillonite, a significant mass loss is visible between 50°C and 150°C , representing the dehydration of the clay interlayers (M1, Fig. 4b). At 700°C another loss of water related to the transformation of montmorillonite (dehydroxylation) is visible (M2, Fig. 4b). Both the bentonite and the montmorillonite skin regions (0-1 mm) are characterized by

remarkably stronger mass loss in the interval 50-200°C (with a smaller, but much broader peak compared to unaltered material), possibly also related to C-S-H dehydration (Fig. 4, CS). The mass loss continues then constantly until ~600°C. The absence of the dehydroxilation peak at 700°C for the 0-1 mm region suggests a decrease of the clay content close to the material interface.

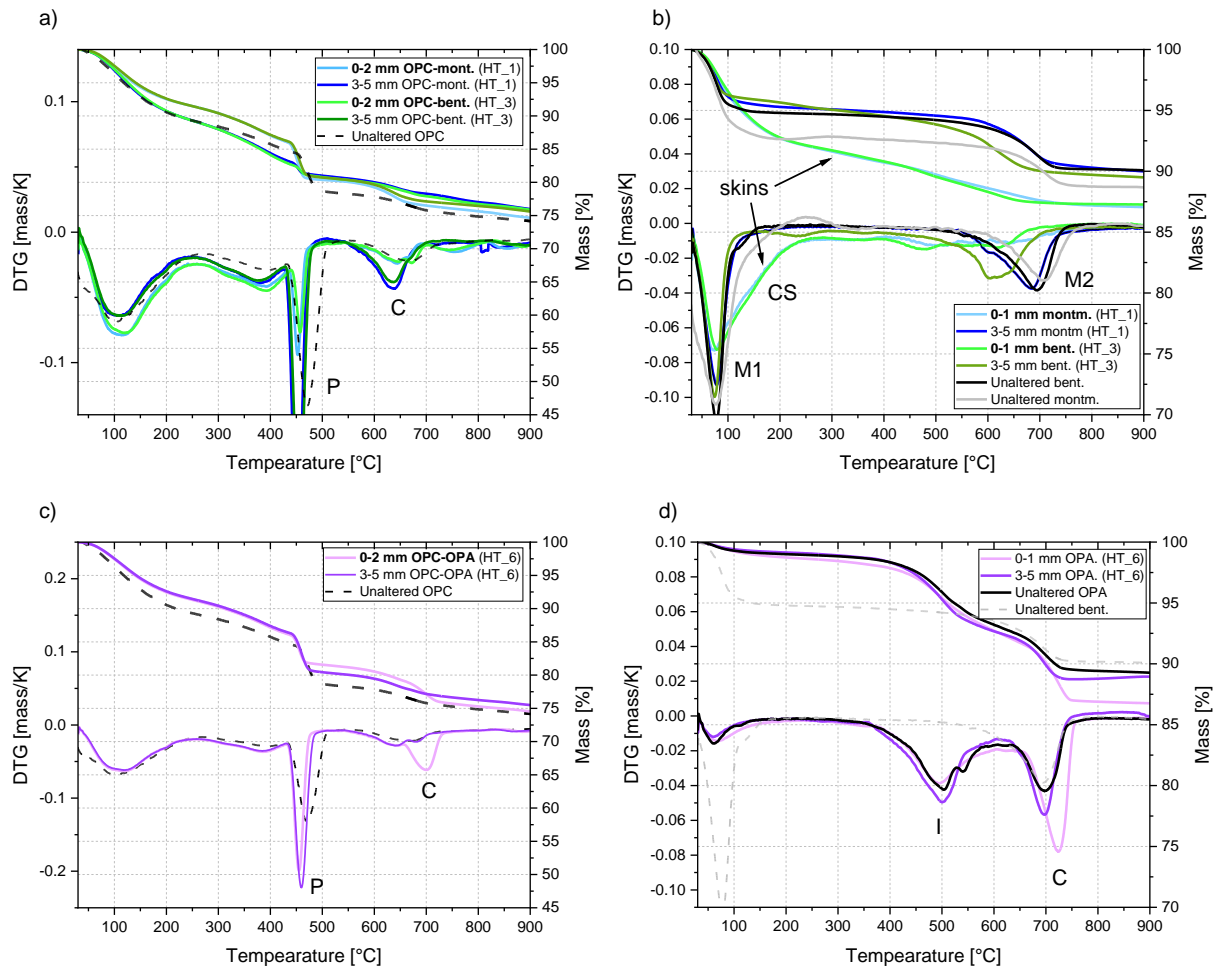


Fig. 4 TGA results for a) OPC paste after contact with Na-montmorillonite (green) and bentonite (blue). b) Na-montmorillonite (green) and bentonite (blue) after contact with OPC paste. c) OPC paste after contact with OPA. d) OPA after contact with OPC paste. Peak identification: P: portlandite, C: calcite, CS: C-S-H, M1: montmorillonite (interlayer water), M2: montmorillonite (dehydroxilation), I: illite. All the samples were flash frozen with liquid N₂ and subsequently freeze-dried.

For OPC in contact with OPA, the 0-2 mm sample shows no significant reduction in the portlandite content, suggesting that not much solute exchange took place. The most prominent feature on the OPC side is the presence of calcite, evident from the clear mass loss at 700°C. This signal could possibly originate from the thin bright layer at the beginning of the OPC see in the X-ray image (Fig. 3c). Carbonation of cement paste in contact with OPA was often described in the literature (Jenni et al., 2014; Mäder et al., 2017). The 3-5 mm OPC sample shows no significant alteration.

Opalinus Clay is characterized by three regions of mass loss: the first between 30°C and 150°C, where clay minerals lose their interlayer water. The grey dashed curve (bentonite) serves as comparison to indicate the typical dehydration of montmorillonite-rich samples. The second peak represents the dehydroxilation of illite (~500°C) and the third one calcite decarbonation, at around 700°C. Although the OPA-OPC contact was not optimal, some reactions appear to have taken place through solution in

the gap (Fig. 4c, d). The 0-1 mm OPA sample displays a slightly wider negative peak between 30-100°C compared to the unaltered sample, possibly indicating the formation of new hydrated minerals. The calcite peak is increased within the 0-1 mm. As the other investigations did not hint to a clear alteration in this respect, it is not clear whether this feature represents a real calcite enrichment or is mainly related to the OPA heterogeneity. The outer part of the OPA sample 3-5 mm appears to be unaltered.

Evolution of the porewater: pH

For all the samples, the pH on the in the reservoir on the cement side remained stable (~13.3) for the entire duration of the experiment (Fig. 5h). This fact was expected due to the very high initial pH and the comparably large reservoir volume (50 mL reservoir). The clay side started with a lower pH (7 to 8 for the different samples, Fig. 5). Due to technical reasons, no measurements could be performed during the first 50 days of the experiment. After 50 days of interaction, a clear pH increase was visible for all samples, but the values and the further development varied depending on the type of sample.

For Na-montmorillonite, after a significant and rapid increase to 10.5-11.0, the pH kept increasing relatively constantly and reached after eight months of interaction a value of almost 12.0. For bentonite and OPA, after the initial rapid increase to 8.9 - 9.5 the pH increased only slightly further or appeared to stabilize. It appears that the capacity of the Na montmorillonite to buffer a high pH is lower than that of bentonite or Opalinus Clay, possibly due to the lower amount of accessory minerals. During a precedent work on similar interface samples (Luraschi et al., in prep), it was already noticed that the high pH-plume moves fast from the cement paste side towards the clay reservoir (~2 weeks). While the observed direction of the pH change is plausible, the specific characteristics of the experimental setup have to be considered in the interpretation: i) the size of the cells was very small (total length of 10 mm). ii) The OPC paste sample had a high porosity and a higher diffusion coefficient compared to the clay sample, propagating the properties of the cement reservoir comparably quickly towards the interface. In the real case, the cement likely has a lower porosity, leading to a slower pH increase on the clay side. Also, the reservoir represented by the host rock has a larger size and thus (on the long range) a larger buffer potential.

Evolution of the porewater: Cationic composition

Bentonite and OPA porewaters are characterized by higher initial Mg, Ca and Na concentrations compared to Na-montmorillonite porewater (Fig. 5). Cation concentrations in the OPA and in the bentonite reservoirs behaved in a similar way: Na, Mg and Ca were quite stable during the entire experiment, with only small fluctuations visible. The potassium concentration instead increased clearly in the bentonite reservoirs (especially for sample HT_4, less so for sample HT_3), and only slightly in the

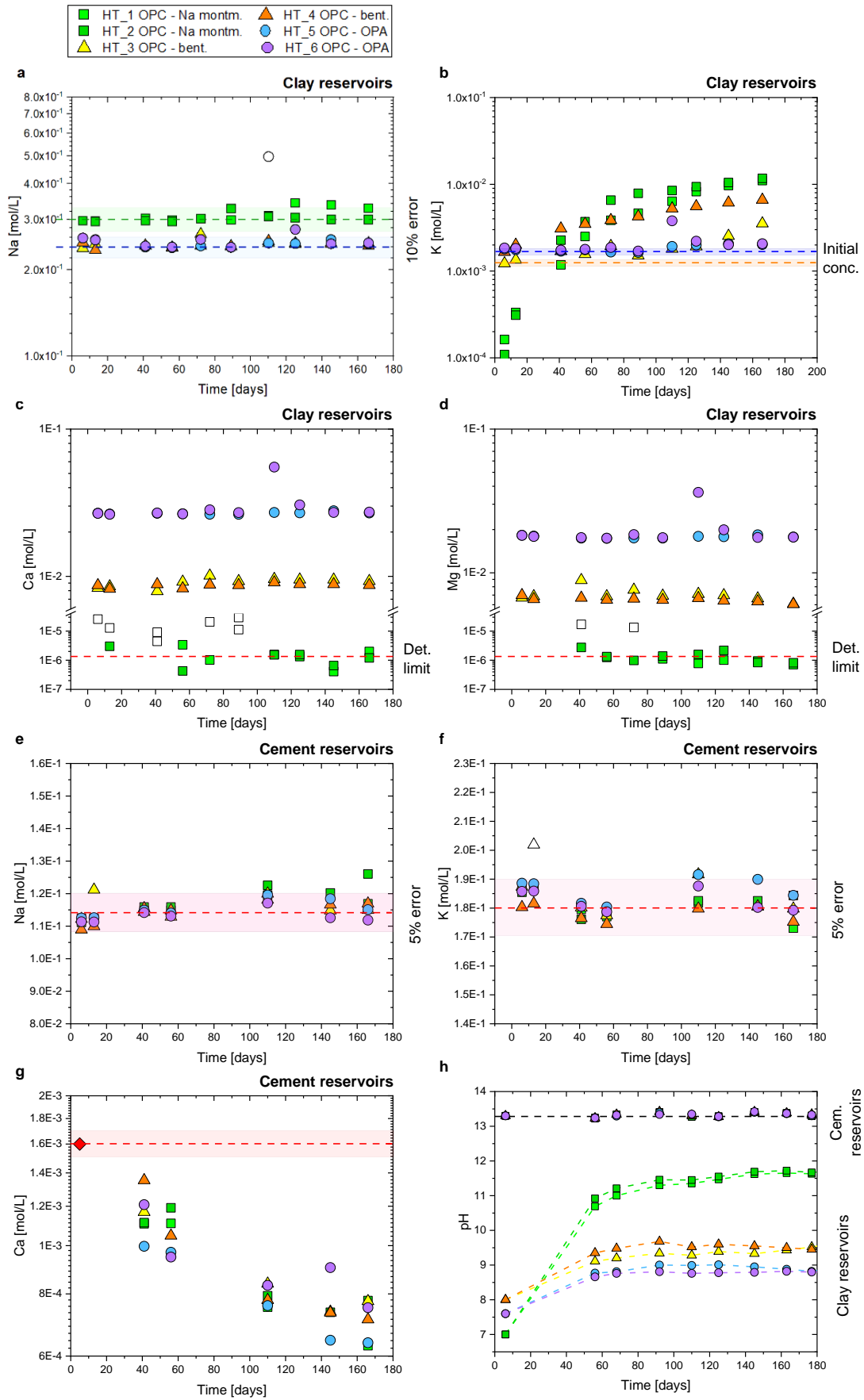


Fig. 5 Evolution of the concentration of different cations and the pH for the cement and clay reservoirs. a) Na, clay reservoirs. b) K, clay reservoirs. c) Ca, clay reservoirs. d) Mg, clay reservoirs. e) Na, cement reservoirs. f) K, cement reservoirs. g) Ca, cement reservoirs. h) pH, cement and clay reservoirs. For cations, where present, dashed lines represent the initial concentrations or the detection limit (Ca, Mg clay reservoirs). Empty symbols are considered as outliers.

OPA reservoirs. In the Na-montmorillonite reservoirs, containing initially only sodium chloride, a clear potassium enrichment was observed. Especially of interest is the variation of calcium and magnesium in the Na-montmorillonite reservoirs, which may originate from the dissolution of hydrated cement phases and clay minerals respectively. After 8 months interaction, on the montmorillonite side no Ca and Mg inside the reservoirs was measured (detection limit: 1 $\mu\text{mol/L}$, red dashed line, Fig 5c). This indicates that, while Ca and Mg may have been present in the clay pore solution near the material interface, no Mg or Ca diffused up to the montmorillonite reservoirs.

On the cement side, for all the sample types, no significant variations were observed in the concentrations of Na, K and Mg (not shown) cations in the reservoirs during the duration of the experiment. In contrast, a clear decrease of Ca over time was observed in the OPC paste reservoirs for all types of interface samples. The Ca decrease observed within the reservoirs is likely to be related to the white precipitate observed in the tubing and reservoirs. The precipitate was tested with HCl (1M) and did not react, indicating that no calcite was present.

X-ray diffraction

The first mm of clay from the three different types of samples was investigated by means of XRD. The unaltered Na-montmorillonite diffractogram is characterized by a main reflection at $\sim 19.6^\circ$ 2θ $\text{CuK}\alpha$ (gray in Fig. 6a), related to clay minerals, here Na-montmorillonite. A small reflection related to quartz is also visible (26.6° 2θ $\text{CuK}\alpha$). Unaltered bentonite (black line, Fig. 6a) is characterized by Ca-Na montmorillonite (7.0° 2θ $\text{CuK}\alpha$), quartz (26.6° 2θ $\text{CuK}\alpha$), cristobalite (21.9° 2θ $\text{CuK}\alpha$) and feldspars (23.6° and 27.6° 2θ $\text{CuK}\alpha$).

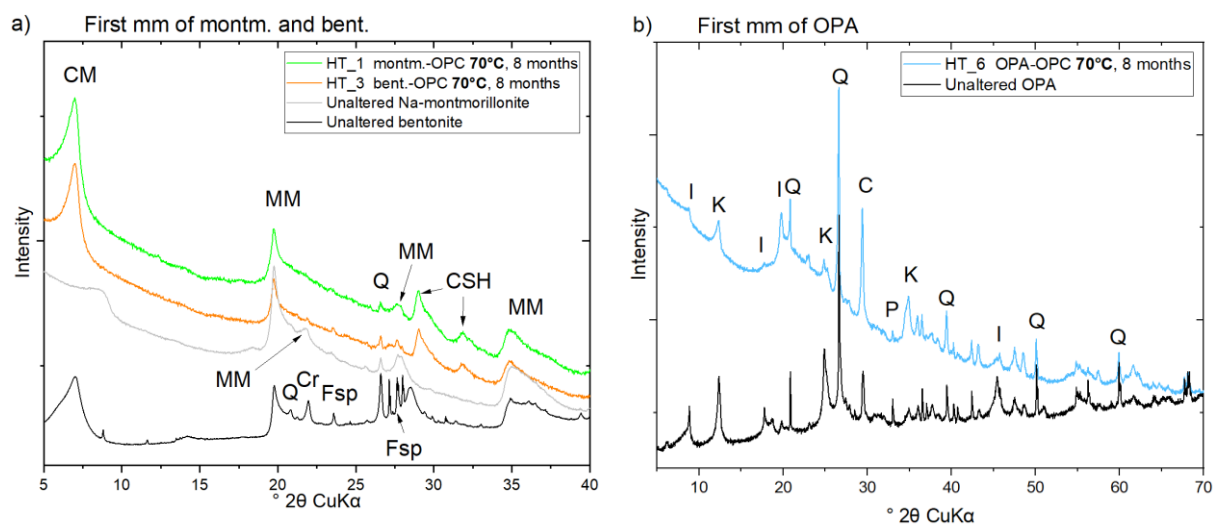


Fig. 6 X-Ray powder diffraction of a) the first mm of Na-montmorillonite (green) and bentonite (orange) and b) Opalinus Clay (blue) having been in contact with OPC paste for 8 months at 70°C . Reflection identification. CM: Ca- Na montmorillonite, MM: montmorillonite, Q: quartz, Cr: cristobalite, Fsp: feldspars, CSH: C-S-H, I: illite, K: kaolinite, C: calcite, P: pyrite.

The montmorillonite sample showed after contact with OPC a new reflection at $\sim 7.0^\circ$ 2θ $\text{CuK}\alpha$, indicating that part of the montmorillonite was transformed into Ca-Na montmorillonite (initially Na-montmorillonite). Furthermore, the decrease of the reflection at 19.7° 2θ $\text{CuK}\alpha$ (characteristic for clay minerals), compared to unaltered montmorillonite, points towards possible clay minerals dissolution

(although a quantification by means of XRD only is not straightforward). A major reflection appeared at $\sim 29.3^\circ$ 2θ $\text{CuK}\alpha$ ($d=3.04 \text{ \AA}$), indicating the presence of C-S-H phases.

The diffractogram of the 0-1 mm slice from bentonite show the presence quartz, feldspar and Ca-Na montmorillonite, similarly as observed in the unaltered sample. For the bentonite sample as well, C-S-H formed as visible in Fig. 6a (reflection at $\sim 29.3^\circ$ 2θ $\text{CuK}\alpha$). The cristobalite reflection (21.9° 2θ $\text{CuK}\alpha$), quite prominent in unaltered bentonite, is still observable but strongly reduced after two years of contact with OPC. It has to be mentioned that this may be partially related to sample heterogeneity.

In contrast, the first mm of the Opalinus Clay sample (Fig. 6b) does not show any alteration with respect to the unaltered sample. Illite (8.9° 2θ $d=10 \text{ \AA}$, 19.7° 2θ $\text{CuK}\alpha$), kaolinite (29.4° 2θ $\text{CuK}\alpha$ $d=7.2 \text{ \AA}$), calcite (29.4° 2θ $\text{CuK}\alpha$, $d=3.03 \text{ \AA}$), quartz (26.6° 2θ $\text{CuK}\alpha$) and pyrite (33.0° 2θ $\text{CuK}\alpha$, $d= 2.71 \text{ \AA}$) are still present in similar amounts. In a precedent study for the same sample type (OPC paste-OPA at room temperature), no significant alteration of the OPA was observed after two years of interaction (Luraschi et al., in prep). There, it was also suggested that due to the high amount of calcite (having similar reflexes as C-S-H), the presence of a small amount of C-S-H cannot be completely excluded.

Through-diffusion experiments

The initial effective diffusion coefficients expected for the unaltered samples composed of two materials were calculated using literature data (Tab. 2). After eight months interaction, samples with Na-montmorillonite displayed an average D_e of $4.7 \times 10^{-11} \text{ m}^2 \text{ s}^{-1}$, which represents 47% of the initial calculated value ($1.0 \times 10^{-10} \text{ m}^2 \text{ s}^{-1}$). Bentonite also shows a clear decrease of the diffusive flux, resulting in an average diffusion coefficient of $4.4 \times 10^{-11} \text{ m}^2 \text{ s}^{-1}$, 44% of the initial value. The two replicate samples with bentonite and montmorillonite show a similar evolution of the diffusion coefficient (Fig. 7).

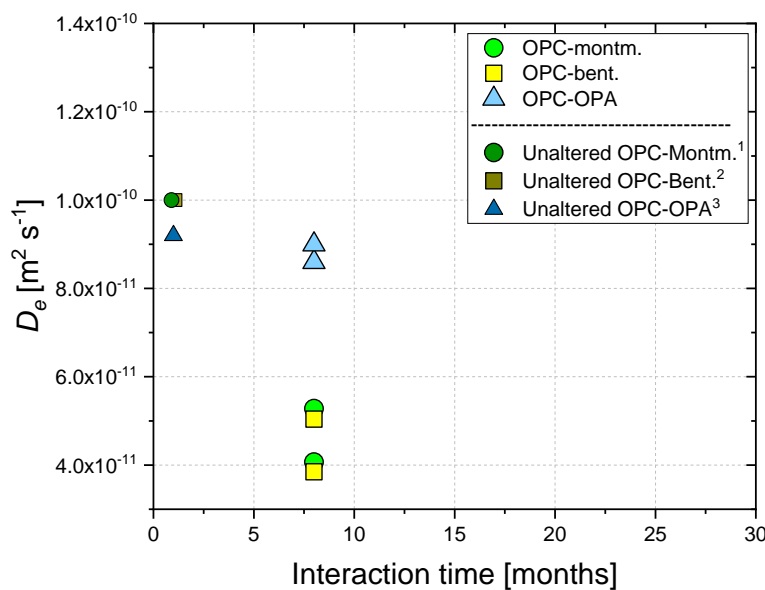


Fig.7 Measured diffusion coefficients of the entire system (OPC-clay) at 70°C for the three different types of interface samples after eight months interaction time.

^{1,2,3} Calculated from data in Table 2.

The OPA-OPC paste samples did not show a significant reduction of the diffusion coefficient. This is consistent with the comparably little alterations seen in this case, and it may also be related to the imperfect contact between the two components of the sample. Diffusion coefficients of different sample parts can be derived by applying a relation equivalent to eq. (2). The following four subunits were considered here: i) unaltered cement, ii) cement skin, iii) clay skin and iv) unaltered clay. As long as the main resistance to diffusion is in the low-porosity clay skin, a variation of the properties of the cement paste side would only marginally affect the derived properties of the clay skin, as already discussed by Luraschi et al. (2020). This applies very likely for the present samples with Na-montmorillonite and bentonite, but may be less for the Opalinus Clay, where no skin was detected. The minor effect of a potentially larger diffusion coefficient for the zone without portlandite was ignored. The tomographic images allowed to determine the skin thickness for Na-montmorillonite (~0.8 mm) and bentonite (~2 mm). Using eq. (2), an average diffusion coefficient of $6.4 \times 10^{-12} \text{ m}^2\text{s}^{-1}$ for the first and $1.3 \times 10^{-11} \text{ m}^2\text{s}^{-1}$ for the latter was derived. It has to be noted here that the used skin thickness has a deciding effect on the derived skin D_e value.

Table 3 Summary of the derived diffusion coefficients for the different components of the samples. The values for the entire clay compartment or the clay skin were calculated using D_e values of the entire cement given in Table 2. The experiments were performed at $25 \pm 1^\circ\text{C}$ using HTO as tracer.

Sample	Interface type	D_e entire sample [$\text{m}^2 \text{s}^{-1}$]	D_e entire clay compartment [$\text{m}^2 \text{s}^{-1}$]	D_e clay skin [$\text{m}^2 \text{s}^{-1}$]	¹ Skin extension [mm] on the clay side
HT_1	Na-montm.-OPC	5.3×10^{-11}	2.9×10^{-11}	7.8×10^{-12}	0.8 ± 0.2
HT_2	Na-montm.-OPC	4.1×10^{-11}	2.2×10^{-11}	5.0×10^{-12}	0.8 ± 0.2
HT_3	Bentonite-OPC	3.8×10^{-11}	2.1×10^{-11}	1.1×10^{-11}	2 ± 0.5
HT_4	Bentonite-OPC	5.0×10^{-11}	2.8×10^{-11}	1.5×10^{-11}	2 ± 0.5
HT_5	OPA-OPC	8.6×10^{-11}	5.1×10^{-11}	-	(?)
HT_6	OPA-OPC	9.0×10^{-11}	5.4×10^{-11}	-	(?)
Unaltered values	Na-montm.-OPC	1.0×10^{-10}	-	-	-
	Bentonite-OPC	1.0×10^{-10}	-	-	-
	OPA-OPC	9.1×10^{-11}	-	-	-

¹Estimated from the X-ray tomography and SEM/EDX data.

Discussion

Porewater and pH evolution

During the entire experiment the pH on the cement side did not vary significantly, and stayed at a value of ~13.3. On the clay side instead, a significant pH increase was observed in all samples, and most prominently in the montmorillonite porewater. The comparably low alteration of the pH on OPA side (from 7.6 to ~9) was related to i) the lower diffusivity of the OPA, ii) the high amount of accessory minerals, which can dissolve and buffer the pH, and iii) possibly also the discontinuous material contact at the interface which may have influenced the diffusive processes. Bentonite is mainly composed of montmorillonite but, unlike Na-montmorillonite, contains various accessory minerals, which play a key role in the pH buffering and thus reduce the pH increase compared to Na-montmorillonite. For all the interface samples, after a rapid pH increase during the first 2 months, the further pH rise was small or even absent. It cannot be excluded that the rapid initial pH increase took place mostly during the first days or weeks of the experiment. The formation of a low-porosity region in montmorillonite and

bentonite samples is likely to be responsible for the slowing down of the pH increase. At the same time, slow kinetics of dissolution processes that buffer the pH increase may also be partially responsible for the change in slopes.

Before starting the experiment, the cement paste was stored in the porewater used in the reservoir, meaning that equilibrium conditions are expected to prevail. All the OPC paste reservoirs were characterized by a near-linear decrease of the (initially comparably low) calcium concentration during the eight months interaction. This may in part be caused by the white precipitate well observable inside the tubing connecting the cell and the reservoir on the cement side. The nature of this phase is unknown. Due to the absence of CO₂, it is likely to represent an amorphous cementitious phase (e.g. C-S-H). Interestingly, Ca decreased also in OPA-OPC systems, where no low-porosity region formed, and where the Ca gradient is actually pointing towards the cement side. Potassium and sodium, which are present in high concentrations in the cement porewater, remained stable. No magnesium could be detected during the entire experiment in the cement reservoirs; even though bentonite and OPA porewater contain considerable concentrations of it. This fact suggests that Mg was consumed (exchanged/sorbed or precipitated) locally.

On the clay side, the most striking feature (observed in every sample type) is the increase of potassium, which from the beginning on rapidly diffuses from the cement porewater reservoir through the sample towards the clay porewater reservoir. Sodium remains stable throughout the experiment in the reservoirs on both sides, although there is a gradient from the clay reservoir to the cement reservoirs. Another interesting factor is the absence of calcium and magnesium in the Na-montmorillonite reservoir (initially 0.3 M NaCl). This observation indicates that calcium ions precipitated as new phases within the sample and/or completely exchanged on montmorillonite sites. The dissolution of clay minerals released magnesium. This does not diffuse towards the reservoirs, but remains in the samples, either adsorbed/exchanged or as part of new solid phases.

Mineralogical alteration of the interfaces

In the OPC paste adjacent to the clay, portlandite dissolution occurs, which takes place as soon as the pH drops below 12.5 (Atkins and Glasser, 1992) or the Ca concentration in the pore solution decreases. Depending on the system, either one factor or the other can be the driving force of the process. Na-montmorillonite porewater has a low pH and a low Ca content, whereas OPA and bentonite porewater have initially a higher calcium content than the cement paste porewater, making the pH the dominant factor. Once all portlandite is dissolved, C-S-H dissolution is the next process buffering the pH. Although it was not clearly evidenced by the performed analysis, it is likely that at the interface C-S-H starts to destabilize (decalcify and dissolve) at least locally. Luraschi et al. (in prep.) describe the precipitation of Friedel's salt and hypothesize a possible aluminium incorporation in C-S-H in identical samples investigated at 25°C. The OPC paste interfacing OPA, although not properly connected, showed calcite precipitation at the interface (Figs. 3c, 4c), as already described by Jenni et al. (2014), Mäder et al. (2017) and Luraschi et al. (in prep.). Calcite precipitation, related to the high partial pressure of CO₂ inside OPA, is the major process responsible for porosity and diffusivity decrease at the interface of OPC with OPA. On the OPA side a Mg-enrichment was locally observed (Supplementary Material, S3), although it was

not clear, whether it represents an artefact due to the bad interface contact, or a real enrichment. Montmorillonite and bentonite are instead characterised by low carbonate content, and therefore no carbonates precipitated at the OPC interface with these minerals. Partial dissolution of clay and possibly other silicates (quartz and feldspars) release aluminium and silica in solution. These may be partially incorporated into C-S-H phases, but no clear evidence was found.

On the clay side, newly formed C-S-H were detected in bentonite and montmorillonite close to the interface with OPC, forming a skin with different properties. Also here, if present, aluminium would likely be incorporated into C-S-H phases (Fernández et al., 2016). The montmorillonite or bentonite region outside the skins remained largely unaltered (except for the Ca-Na exchange in montmorillonite). The extension of the skin varies, depending on the system, between ~0.8 mm (montmorillonite) and ~2 mm (bentonite). An increase of sodium (Fig. 2b, peak of Na/Si) was observed towards the interface in both clays; it was especially strong in the Na-montmorillonite. This observation was already made by Luraschi et al. (in prep.). Na may partially be incorporated into C-A-S-H as discussed by Bernard et al. (2020). The XRD investigation (Fig. 6a) evidenced a prominent reflection at $6.9\ 2\theta^\circ$ ($d=12.9\text{\AA}$) in the first mm of these clays. This reflection is likely to represent Ca-(Na) montmorillonite, but could theoretically also be ascribed to zeolites or Na-beidellite, an aluminum rich clay which can form in cement paste-clay systems (Bouchet et al., 2004; Karnland et al., 2004; Ramirez et al., 2005). Ca-(Na) montmorillonite, originating from the partial substitution of Na by Ca inside the interlayer, is likely present and extends more than just over the first mm of the clay (Fig. 2f, Na/Ca ratio much lower compared to the external part of the sample. Together with the occurrence of, for instance, beidellite in the clay skin, this could explain the peak of Na/Si in the first mm (Fig. 2b). While the precipitation of a Na-rich phase in the clay skin probably would reduce the diffusive transport, the exchange of Na by Ca would tend to increase diffusive transport and decrease the swelling capacity.

In montmorillonite and bentonite, a clear magnesium enrichment (compared to Si or Al) was observed at ~1.4 mm from the interface. The enriched region is very thin ($<500\mu\text{m}$) (Fig. 2c, d). Mg alteration was not observed in similar samples at room temperature (Luraschi et al., in prep.). These authors hypothesized the absence of a Mg enrichment as being partly related to the prolonged detachment of the samples from the reservoir solutions. The formation of magnesium-enriched regions was already described by several authors. The nature of this Mg enriched region is still not clear. It may represent M-S-H phases (Bernard et al., 2020; Dauzères et al., 2016) or Mg bearing layered double hydroxides.

With respect to the experiments described in Luraschi et al. (2020; in prep.), where the samples reacted at room temperature for up to six years, the skins here have a slightly smaller extension and the element gradients detected by EDX are generally located closer towards the interface. The Na enrichment in montmorillonite reported by Luraschi et al. (in prep.) has a similar magnitude but is slightly shifted away from the OPC paste-montmorillonite contact (peak at ~500 μm from the interface, whereas here peak is right at interface).

Evolution of the interface diffusivity

Interface samples composed of montmorillonite and bentonite show a similar evolution of the diffusive properties. In both cases, the $D_{e, \text{HTO}}$ strongly decreased already after 8 months interaction at 70°C ,

indicating a porosity decrease. The HTO diffusion coefficient (for the entire interface) decreased on average to 47% of the initial value for montmorillonite and 44% for bentonite. Figure 8 shows the diffusive properties of different skins in montmorillonite and bentonite measured over the years in this and two previous studies. It can be noted how the $D_{e, \text{HTO}}$ values for skin regions from interface samples reacted for 8 months at 70°C are similar to values derived after 24 months of interaction at ~25°C. The increase of the storage temperature led to increased solute diffusion coefficient, solute flux and therefore to a general increased interface reactivity.

The Arrhenius law can be used to study the effect of different storage temperatures on the diffusive properties of the interface samples. Considering an activation energy for HTO diffusion in clays of 22 kJ mol⁻¹ (Van Loon et al., 2002), increasing the temperature from 25°C to 70°C results in a ~3 fold increase of the $D_{e, \text{HTO}}$. Although some differences are present between the different samples (e.g. porosity, density, chemical composition), an increase by a factor of about 3 in temperature lead to an overall increase of the rate of the alteration close to the interface by a similar rate. This observation suggest that the overall rate of the modifications and alterations during the present experiments are dominated by transport, and not by the kinetics of the reactions. This could in turn also mean that mainly comparably fast geochemical reactions were involved during the investigations lasting 8 or 24 months.

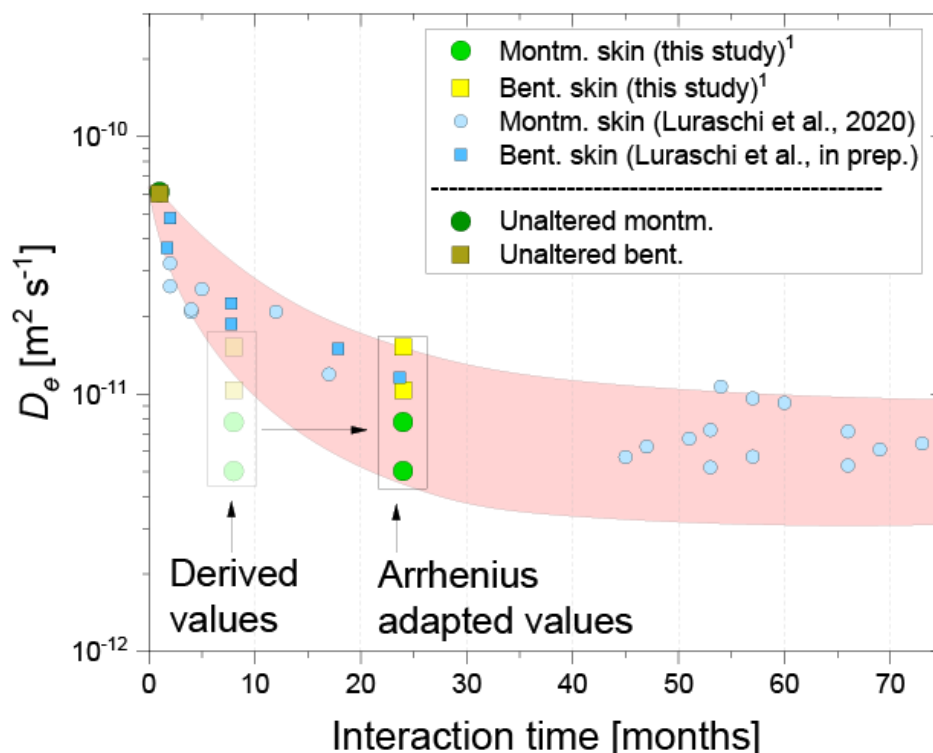


Fig. 8 Diffusion coefficients D_e of pristine bentonite and Na-montmorillonite and values of the skin regions in such clays derived from samples having been in contact with OPC paste (all D_e values obtained at room temperature). The samples were let react at room temperature for the indicated interaction times in the previous experiments (blue symbols), while the samples in this study were kept at 70°C for eight months (yellow and green semi-transparent symbols). For comparison, the D_e values obtained in the present study are also shown at a three times longer interaction time of 24 months (Arrhenius adapted values; time adapted to account for ca. three times larger D_e at 70°C compared to room temperature).

Using equation (2) and making some further assumptions, it is possible to subdivide the interfaces in different regions. Figure 8 shows the derived clay skin properties compared with precedent results

obtained on similar samples (Luraschi et al., 2020; in prep.). Considering the effect of the three times higher temperature as a three times faster rate of chemical alteration, the skin properties are shown at 8 and 24 months (3 times faster) interaction time (Fig. 8).

No relevant changes of the diffusion coefficient in the interface samples of Opalinus Clay with the OPC was observed after 8 months of interaction. This observation may have several reasons: i) the contact between the materials composing the interface was not perfect. The presence of air at the interface reduced the interface reactivity. ii) The presence of fractures within the cement paste or the OPA may have affected the diffusivity, preventing the formation of a homogenous skin. iii) The formation of altered skins is slowed down by the lower diffusivity of OPA. iv) Reaction kinetics may be more relevant for OPA compared to montmorillonite, reducing the overall reactivity. The diffusive data alone do not allow judging which hypotheses are most likely to have occurred.

Effect of temperature

For interface samples composed of montmorillonite and bentonite, the increase of the storage temperature from 25°C to 70°C led to a ~3-fold increase of the interface reactivity in terms of observed diffusion coefficients. The decrease of the HTO diffusivity after 8 months of storage at 70°C is similar to that experienced after 24 months of storage at 25°C. It seems that the evolution happened about three times as fast at the higher temperature (fig. 8).

The degrees of alterations observed here in terms of changes of element or mineral composition are similar as those reported for OPC-Na montmorillonite samples at room temperature (Luraschi et al., in prep.). This is especially true for the clay side, where the formation of C-S-H phases within the montmorillonite and the bentonite skin was evidenced as main modification. In the clay, a Mg enrichment was observed in Na-montmorillonite or bentonite that was not reported in the earlier study with the same materials at 25°C (no clear Mg enrichment was seen here in OPA). On the cement side, the zone of portlandite dissolution in the OPC paste sample contacting bentonite (8 months, 70°C) reached ~1.5 mm for one sample (Fig.2a) and ~3 mm for another sample (Fig. 3b). Luraschi et al. (in prep.) reported for similar samples reacted at room temperatures portlandite dissolution up to 2.5 mm from the interface.

Portlandite dissolution in OPC paste in contact with Na-montmorillonite appeared to be less extended at 70°C. It did reach only the first ~1.5 mm in the 8 months at 70°C, while it already reached ~2 mm in 8 months at 25°C, and >2.5-3 mm in 4 years (Luraschi et al., in prep). These differences may be related i) to differences between the samples (heterogeneity); ii) to the complex interplay of several temperature dependent variables (e.g., kinetic rates, ion activities, pH) or iii) to the fact that the cells were in Luraschi et al., (in prep) not constantly connected to the reservoirs. Regarding OPC paste-OPA samples, the formation of calcite on the cement side close to the interface was observed by Luraschi et al. (in prep.). The results indicate that the increased temperature did not affect the type of mineralogical alteration occurring at the interface. Precipitation of zeolites, which is described for cement-clay interface samples reacted at elevated temperature (Gaucher and Blanc, 2006), was not observed in this study. The reservoirs and the tubing on all the OPC paste sides were characterized by the precipitation of a white phase, likely composed of calcium and silica. The white precipitate was not observed at room

temperature; it suggests that the OPC paste porewater solution was not completely stable at 70°C. This should be considered for further experiments.

Conclusions

Combining porewater analysis, diffusion experiments and post-mortem chemical investigations of samples reacted at 70°C allowed to obtain complementary information regarding the evolution of cement paste-clay interface samples. For interface samples composed of OPC and montmorillonite or bentonite, it was demonstrated that an increase of the temperature by a factor of ~3 with respect to room temperature leads to a similar increase in the interface reactivity. After 8 months interaction at 70°C, the observed diffusion coefficients for the entire sample were analogous to those observed for the same interface types after ~24 months at 25°C. Similarly as observed by Luraschi et al. (in prep.), C-S-H precipitated in the interface proximity forming a so called -skin- and led to a porosity decrease, responsible for the reduction of the diffusivity. This region with an extension of about 1-2 mm (depending on the sample type) showed a clear enrichment in Na and Ca. Right behind the skin-region a thin enrichment in magnesium was observed. The nature of this Mg enrichment is not clear at the moment. The monitoring of the pH evidenced an initially rapid, but later slower increase of pH values across the clay samples. The change in rate may be partially due to the porosity decrease at the interface, but also due to the kinetics of dissolution reactions buffering the pH. Porewater measurements indicated that calcium (originating from portlandite and possibly C-S-H dissolution) does not reach the reservoir on the clay side, but remains probably mostly within the first mm of the interface, where it was mainly used for C-S-H precipitation or exchanged on clays. The OPC-OPA sample, which displayed no full contact between the two materials, was characterized by local precipitation of calcite at the interface and inside the first mm of the cement paste. The OPA compartment remained nearly unaltered; although a Mg enrichment was locally observed close to the interface. The monitoring of the porewater allowed to observe the extension of the zone with a chemically altered porewater, which is effectively rather limited during the times of investigation except for pH or K, even at higher temperatures.

The experiments at higher temperature correlate well with experiments at room temperature, provided the scaling of the diffusive transport is accounted for. Therefore, such experiments can be considered as a valuable tool to accelerate the processes and efficiently study the evolution of these system.

References

- Atkins, M., Glasser, F.P., 1992. Application of Portland cement-based materials to radioactive waste immobilization. *Waste Manag.* 12, 105–131.
- Bernard, E., Jenni, A., Fisch, M., Grolimund, D., Mäder, U., 2020. Micro-X-ray diffraction and chemical mapping of aged interfaces between cement pastes and Opalinus Clay, *Appl. Geochem.* 115, 104538.
- Bossart, P., Bernier, F., Birkholzer, J., Bruggeman, C., Connolly, P., Dewonck, S., Fukaya, M., Herfort, M., Jensen, M., Matray, J.-M., Mayor, J.C., Möri, A., Oyama, T., Schuster, K., Shigeta, N., Vietor, T., Wieczorek, K., 2017. Mont Terri rock laboratory, 20 years of research: introduction, site characteristics and overview of experiments. *Swiss J. Geosci.* 110, 1–20.
- Bouchet, A., Cassagnabère, A., Parneix, J.C., 2004. Batch experiments: results on MX80. In: Michau, N. (Ed.), *Ecoclay II: Effect of Cement on Clay Barrier Performance Phase II*. Final report. (ANDRA) European contract FIKW-CT-2000-0028.
- Bradbury, M.H., Baeyens, B., 2003. Porewater chemistry in compacted re-saturated MX-80 bentonite. *J. Contam. Hydrol.* 61, 329–338.
- Dauzères, A., Achiedo, G., Nied, D., Bernard, E., Alahrache, S., Lothenbach, B., 2016. Magnesium perturbation in low-pH concretes placed in clayey environment—solid characterization and modeling. *Cem. Concr. Res.* 79, 137–150.
- Fernández, R., Ruiz, A.I., Cuevas, J., 2016. Formation of C-A-S-H phases from the interaction between concrete or cement and bentonite. *Clay Min.* 51, 223–235.
- Gaucher, E.C., Blanc, P., 2006. Cement/clay interactions—a review: experiments, natural analogues, and modeling. *Waste Manag.* 26, 776–788.
- Glaus, M.A., Rossé, R., Van Loon, L.R., Yaroshchuk, A.E., 2008. Tracer diffusion in sintered stainless steel filters: measurement of effective diffusion coefficients and implications for diffusion studies with compacted clays. *Clay Clay Min.* 56, 677–685.
- Glaus, M.A., Aertsens, M., Maes, N., Van Laer, L., Van Loon, L.R., 2015. Treatment of boundary condition in through-diffusion: a case study of $^{85}\text{Sr}^{2+}$ diffusion in compacted illite. *J. Contam. Hydrol.* 177–178, 239–248.
- González-Santamaría, D.E., Fernández, R., Ruiz, A.I., Ortega, A., Cuevas, J., 2020. Bentonite/CEM-II cement mortar interface experiments: A proxy to *in situ* deep geological repository engineered barrier system surface reactivity. *Appl. Geochem.* 117, 104599.
- IAEA, 2009. *Geological Disposal of Radioactive Waste: Technological Implications for Retrievability*. NW-T-1.19
- Karnland, O., 2004. Laboratory experiments concerning compacted bentonite contacted to high pH solutions. In: Michau, N. (Ed.), *Ecoclay II: Effect of Cement on Clay Barrier Performance Phase II*. Final Report. (ANDRA) European contract FIKW-CT-2000-0028.
- Jenni, A., Mäder, U., Lerouge, C., Gaboreau, S., Schwyn, B., 2014. In situ interaction between different concretes and Opalinus Clay. *Phys. Chem. Earth, Parts A/B/C* 70–71, 71–83.
- Luraschi, P., Gimmi, T., Van Loon, L.R., Churakov, S.V., Shafizadeh, A., 2020. Evolution of HTO and $^{36}\text{Cl}^-$ diffusion through a reacting cement-clay interface (OPC paste-Na montmorillonite) over a time of six years. *Appl. Geochem.* 119, 104581.

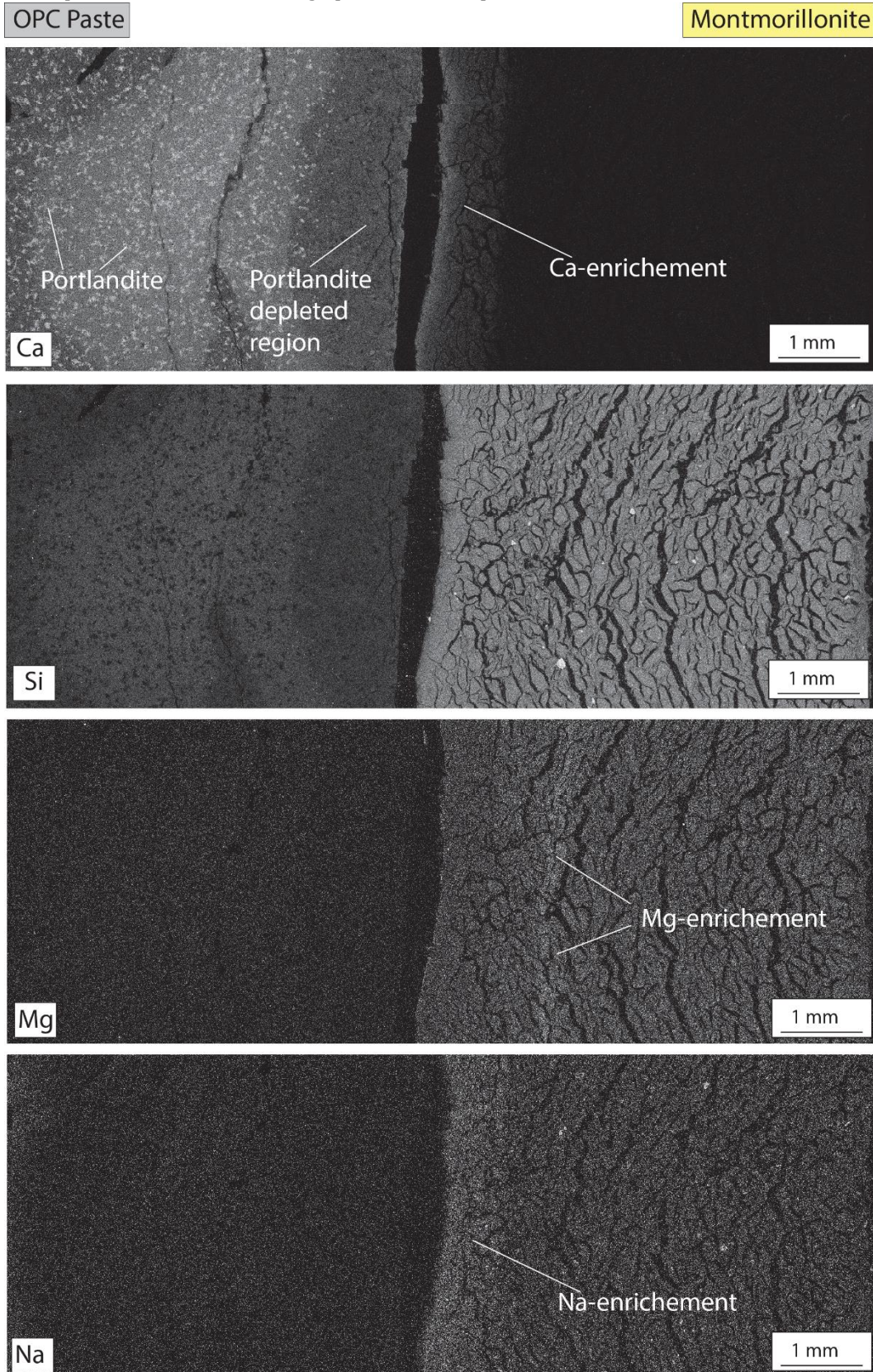
- Mäder, U., Jenni, A., Lerouge, C., Gaboreau, S., Miyoshi, S., Kimura, Y., Cloet, V., Fukaya, M., Claret, F., Otake, T., Shibata, M., Lotenbach, B., 2017. 5-year chemico-physical evolution of concrete–claystone interfaces, Mont Terri Rock Laboratory (Switzerland). *Swiss J. Geosci.* 110, 307–327.
- Nagra, 2002. Project Opalinus Clay – Safety Report, Demonstration of Disposal Feasibility for Spent Fuel, Vitrified High-level Waste and Long-lived Intermediate-level Waste ("Entsorgungsnachweis"). Nagra Tech. Rep. NTB 02-05.
- Nagra, 2008. Vorschlag geologischer Standortgebiete für das SMA- und das HAA Lager. Darlegung der Anforderungen, des Vorgehens und der Ereignisse. Nagra Tech. Rep., NTB 08-03.
- Nagra, 2016. Production, consumption and transport of gases in deep geological repositories according to the swiss disposal concept. Nagra Tech. Rep. NTB 16-03.
- Nagra, 2018. A review of cement-clay modelling. Nagra Arbeitsber. NAB 18-24.
- Pearson, F. J., Arcos, D., Bath, A., Boisson, J.-Y., Fernandez, A., Gaebler, H.-E., Gaucher, E., Gautschi, A., Griffault, L., Hernan, P., & Waber, H. N., 2003. Geochemistry of Water in the Opalinus Clay Formation at the Mont Terri Rock Laboratory (Synthesis Report). Geological Report, No. 5, p. 321. Federal Office of Topography (swisstopo), Wabern.
- Ramirez, S., Vieillard, P., Bouchet, A., Cassagnabère, A., Meunier, A., Jacquot, E., 2005. Alteration of the Callovo-Oxfordian Clay from Meuse-Haute Marne underground laboratory (France) by alkaline solution. I.A XRD and CEC study. *Appl. Geochem.* 20, 89–99.
- Savage, D., 2011. A review of analogues of alkaline alteration with regard to long-term barrier performance. *Min. Mag.* 75, 2401–2418
- Shafizadeh, A., Gimmi, T., Van Loon, L.R., Kaestner, A., Lehmann, E., Mäder, U., Churakov, S.V., 2015. Quantification of water content across a cement-clay interface using high resolution neutron radiography. *Phys. Proc.* 69, 516–523.
- Shafizadeh, A., Gimmi, T., Van Loon, L.R., Mäder, U., Churakov, S.V., 2019. Neutron Imaging Study of Evolution of Structural and Transport Properties of Cement-Clay Interfaces. PhD Thesis. University of Bern, Bern, Switzerland.
- Shafizadeh, A., Gimmi, T., Van Loon, L.R., Kaestner, A.P., Mäder, U.K., Churakov, S.V., 2020. Time-resolved porosity changes at cement-clay interfaces. *Cement Concr. Res.* 127, 105924.
- Tits, J., Jakob, A., Wieland, E., Spieler, P., 2003. Diffusion of tritiated water and $^{22}\text{Na}^+$ through non-degraded hardened cement pastes. *J. Contam. Hydrol.* 61, 45–62.
- Van Loon, L.R., Gimmi, T., Iijima, K., 2002. Activation energy of the self-diffusion of water in compacted clay systems: a case study with opalinus clay. *Clay In Natural And Engineered Barriers For Radioactive Waste Confinement. International Meetin, Reims, France.* 327–328.
- Van Loon, L.R., Soler, J.M., 2003. Diffusion of HTO, $^{36}\text{Cl}^-$, $^{125}\text{I}^-$ and $^{22}\text{Na}^+$ in Opalinus Clay: Effect of Confining Pressure, Sample Orientation, Sample Depth and Temperature. Nagra, Wettingen, Switzerland. Nagra Technical Report, NTB 03-07.
- Wieland, E., Tits, J., Dobler, J.P., Spieler, P., 1998. Interaction of Eu(III) and Th(IV) with Sulphate-resisting Portland cement. *Mater. Res. Soc. Symp. Proc.* 506, 573–578.
- Wilson, J., Bateman, K., Tachi, Y., 2021. The impact of cement on argillaceous rocks in radioactive waste disposal systems: A review focusing on key processes and remaining issues. *Appl. Geochem.* 130.

Supplementary Material

Supplementary Material S1

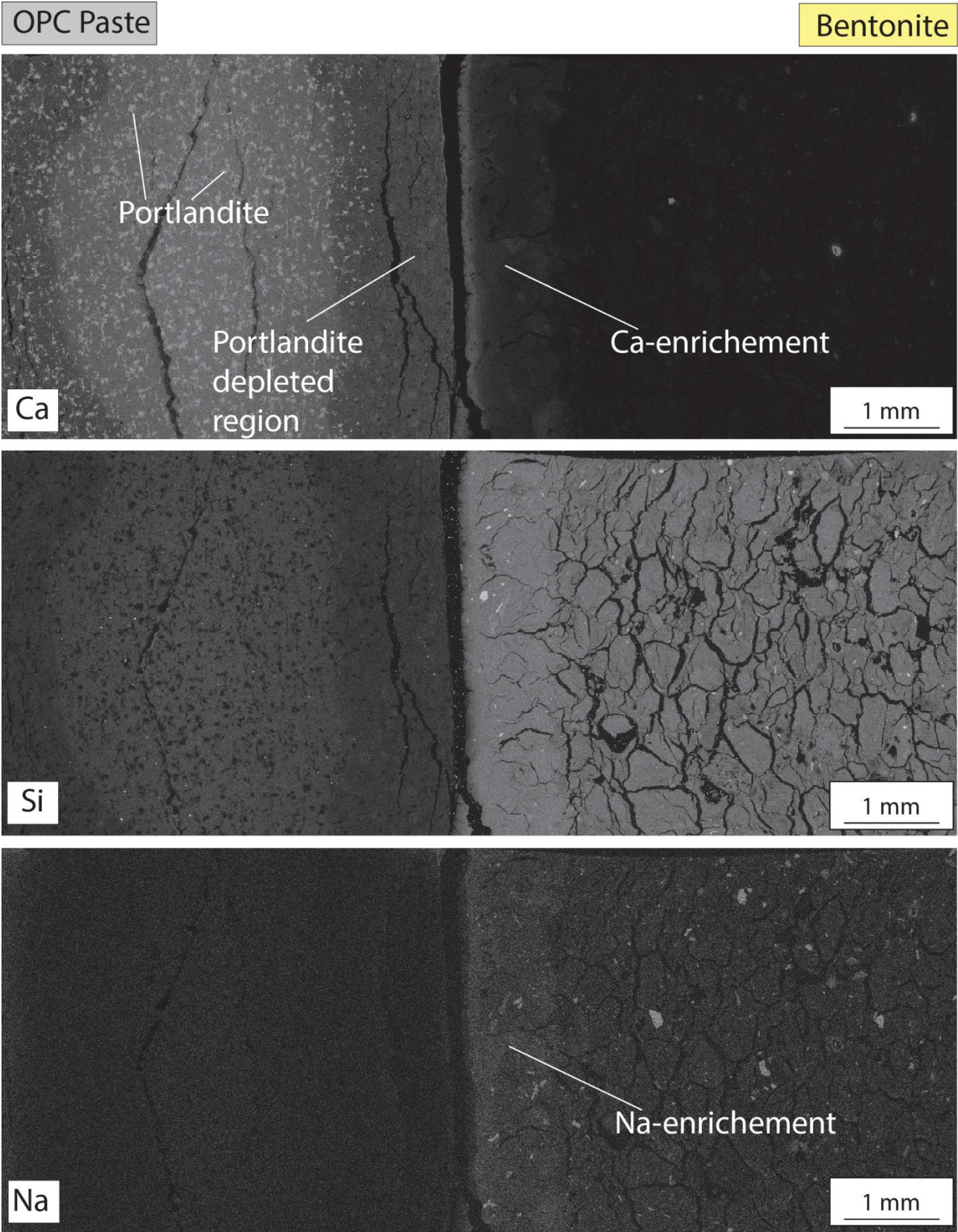
SEM/EDX maps (Ca, Si, Mg, Na) of sample HT_1 OPC-Na montmorillonite.

The zonation visible close to the interface on the cement side (e.g., in the portlandite depleted region) are related to the presence of resin in the high porous cement paste.



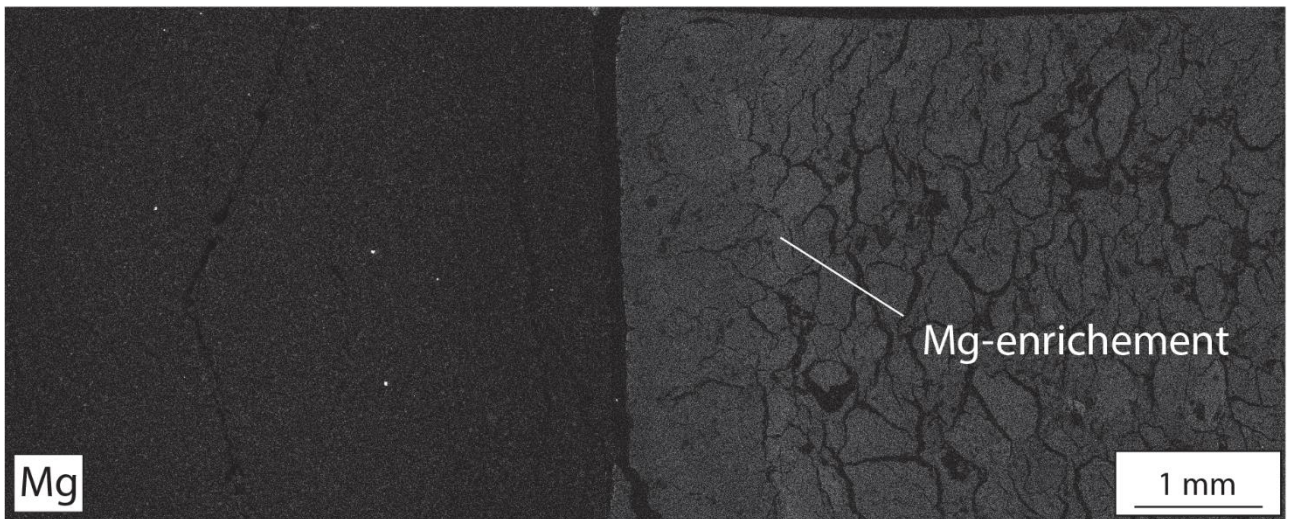
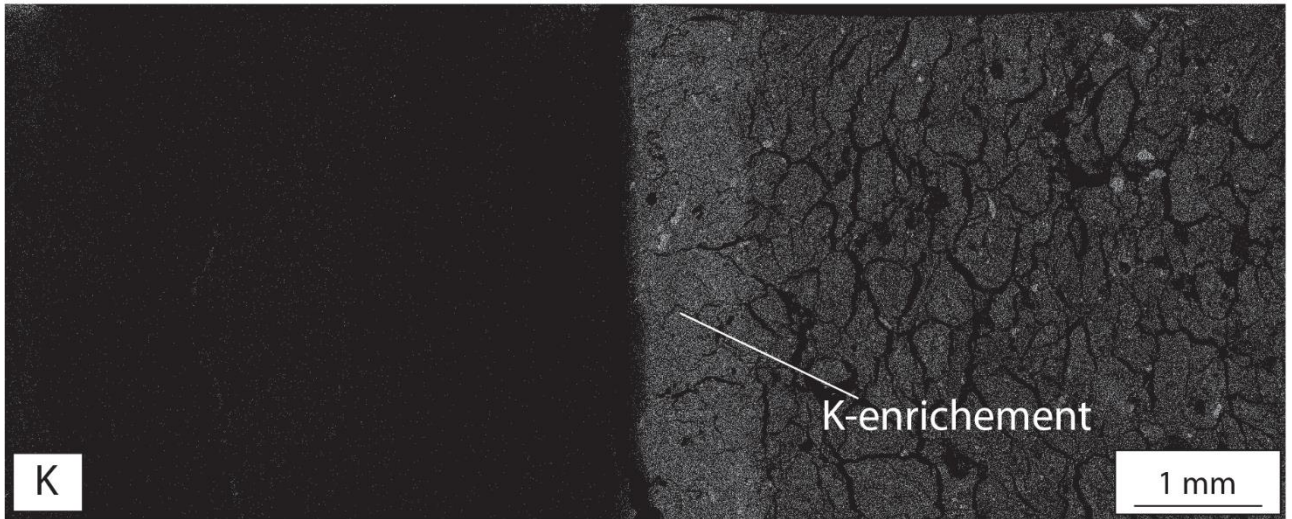
Supplementary Material S2

SEM/EDX maps (Ca, Si, Mg, Na) of sample HT_3 OPC-bentonite.



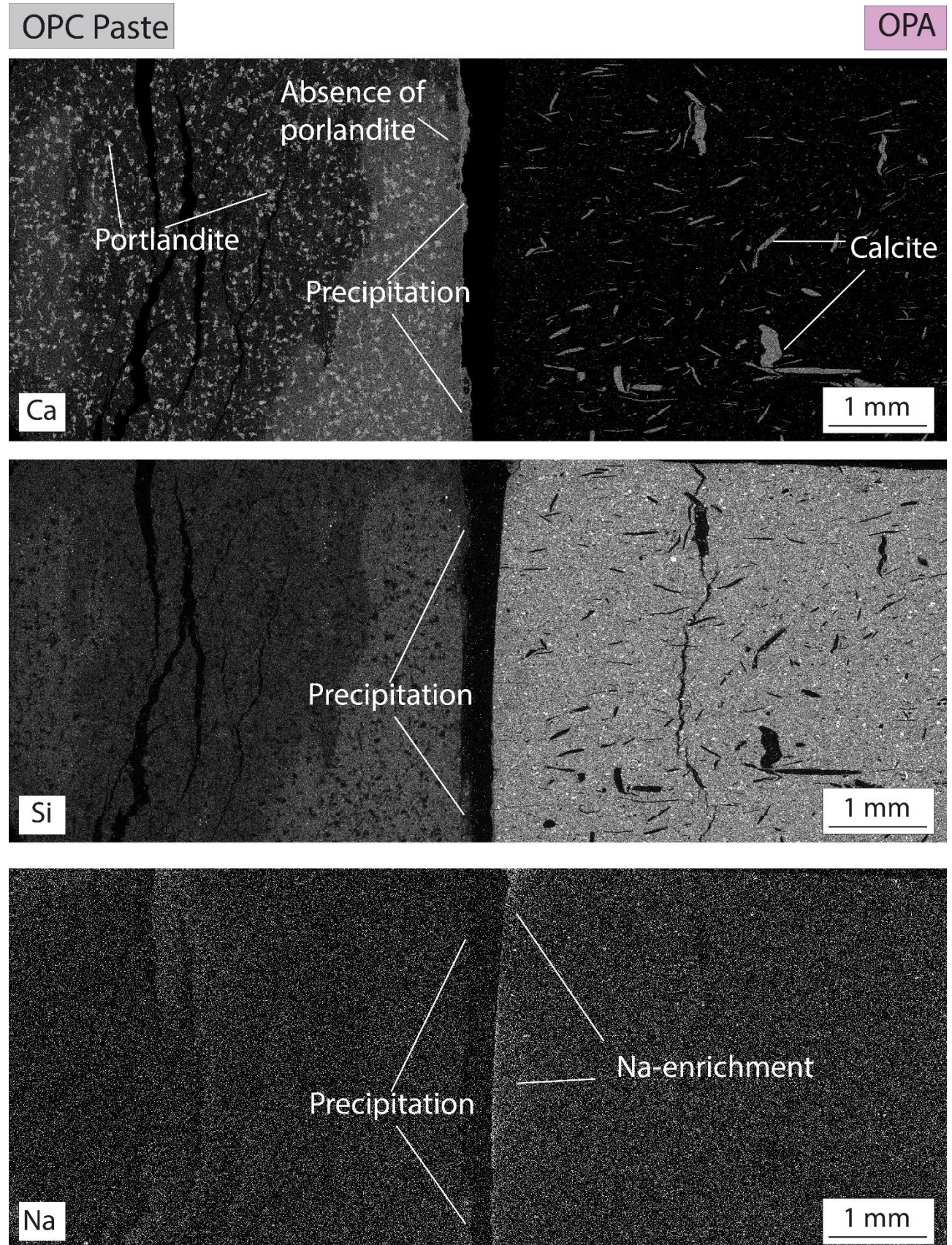
OPC Paste

Bentonite



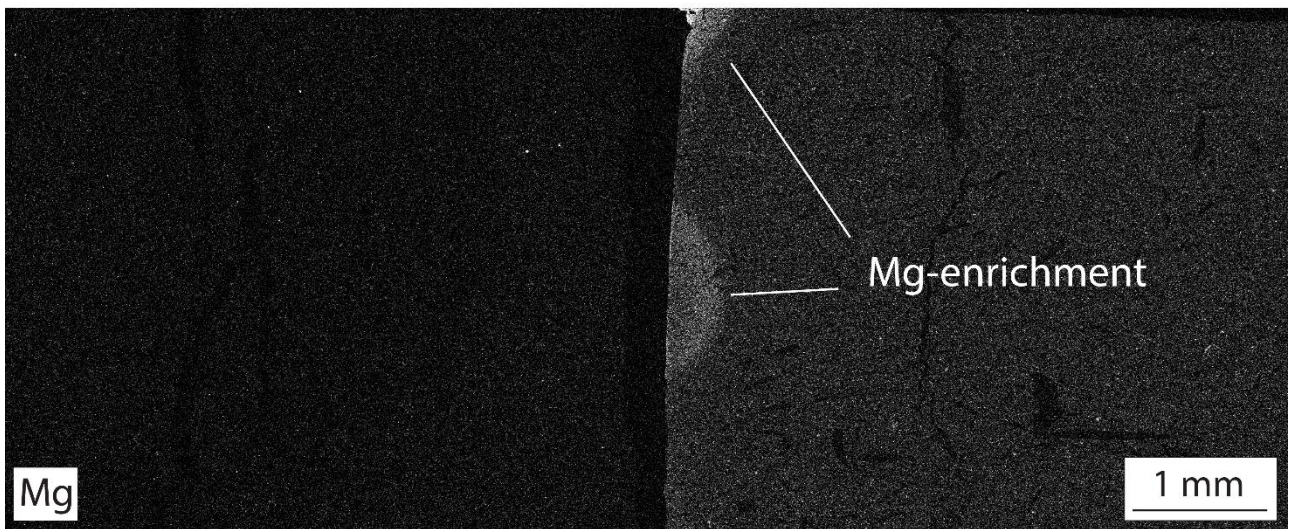
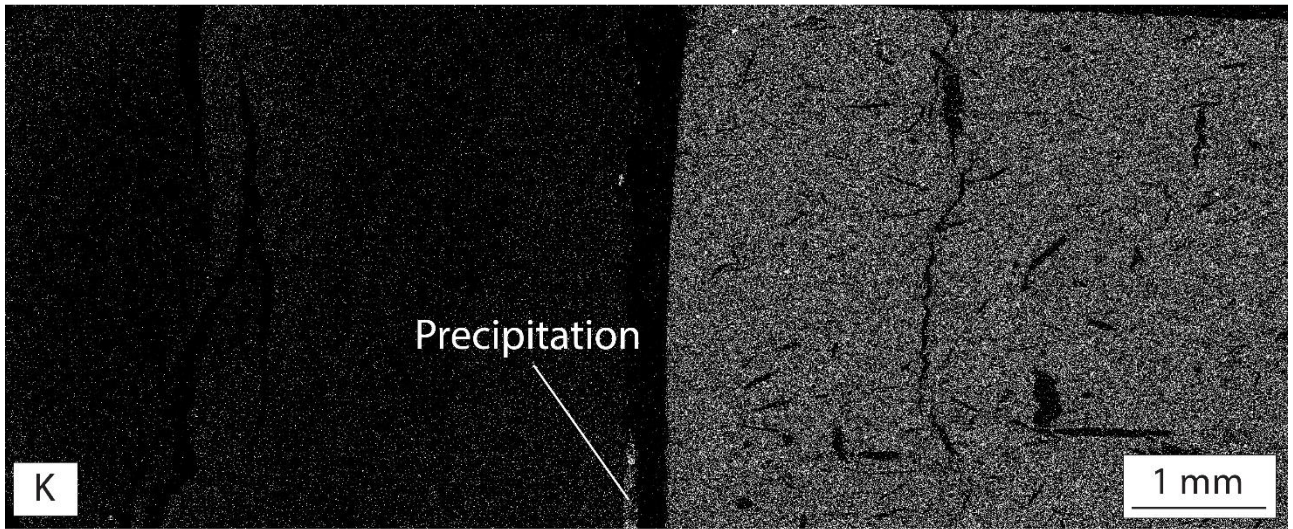
Supplementary Material S3

SEM/EDX maps of sample HT_5 OPC-OPA



OPC Paste

OPA



Supplementary Material S4

Crosssection from X-ray tomography of the sample HT_6 OPC-OPA

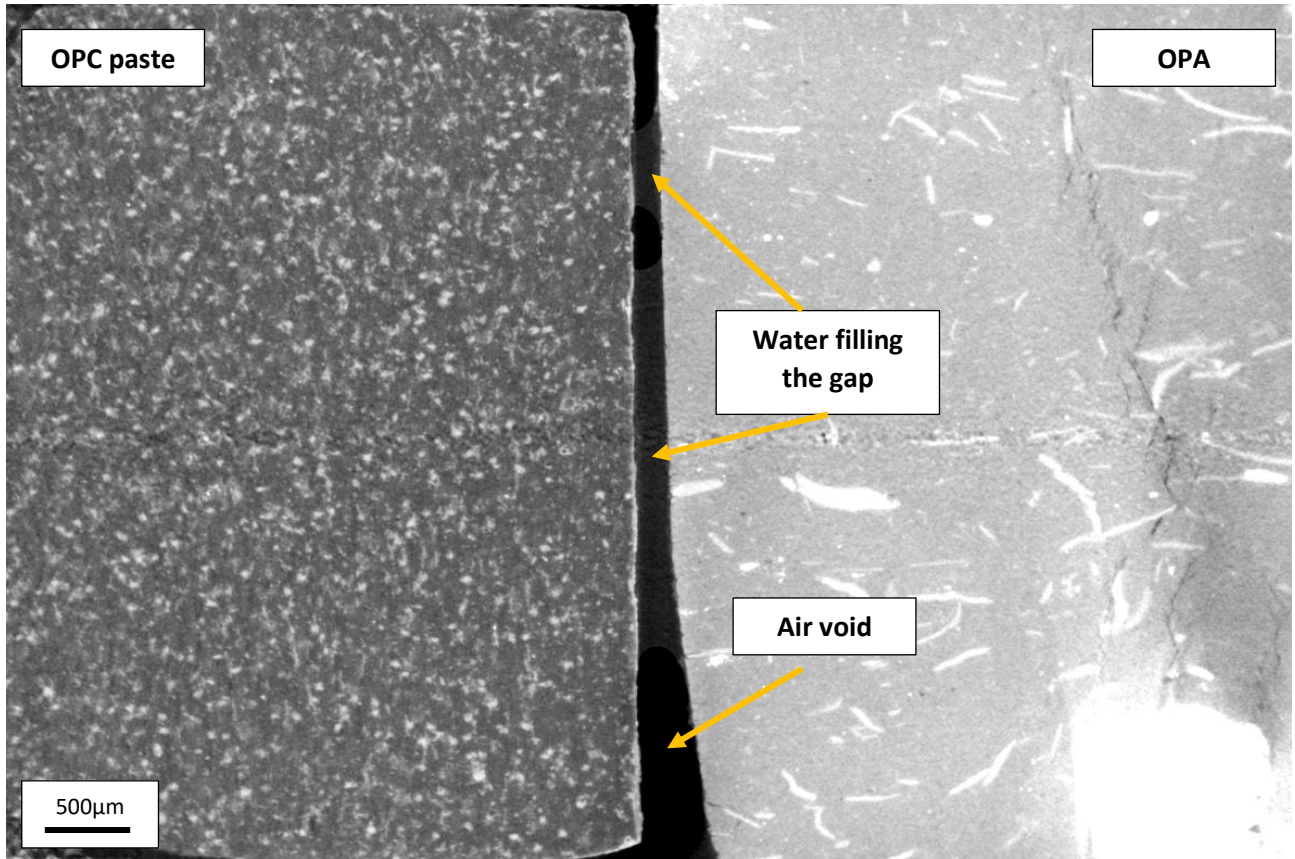


Fig. S4 crossection obtained from an X-ray tomography for a OPC-OPA sample.

Chapter 7

Discussion and conclusions

7. Discussion and conclusions

7.1 The evolution of the different types of cement-clay interfaces

In the L/ILW repository, cement-OPA interfaces will be present when a cement-based liner will be applied to the tunnel walls or caverns. In the case of HLW/SF there will be an additional interface related to the contact between the cement-based liner and bentonite. A summary of the insights gained during this thesis regarding the different interface types are presented and discussed in the following paragraphs.

7.1.1 Cement-Na montmorillonite and cement-bentonite interactions

A first series of experiments was conducted with OPC-Na montmorillonite interface samples at room temperature (Chapters 3, 4). In a second series of experiments, OPC-bentonite (MX-80) samples were investigated also at room temperature (Chapter 5). Finally, in a third series, the OPC interaction with montmorillonite and bentonite at 70°C was studied. The reactions observed in the first system with Na-montmorillonite turned out to be very similar to those in the second system, where the clay part was composed of MX-80 bentonite. Remarkably, the mineralogical alterations at 70°C for montmorillonite and bentonite are as well very similar to the alterations at room temperature. A considerable amount of data was collected over the years regarding the evolution of the cement and the montmorillonite or bentonite part of the samples. The experimental results described in detail in Chapters 3-6 are summarized in Table 1.

Through-diffusion experiments performed on OPC-Na montmorillonite samples with both HTO and chloride tracers allowed gaining relevant insight regarding the location of the precipitation of the new minerals and the porosity distribution within the clay (see Chapter 3). The diffusion coefficient of both tracers decreased significantly with increasing interaction time. The chloride D_e showed a clearly stronger decrease than that of HTO, indicating that the main mineral precipitation within montmorillonite occurs in the so-called free porosity (accessible for anions; dual porosity concept). Complementary mineralogical investigations evidenced the formation of altered regions (skins) of variable thickness, on both the cement and the clay side. The formation of C-S-H phases within the first millimetre of the montmorillonite compartment is mainly responsible for the diffusivity decrease. It led to a porosity decrease within the clay skin of $\sim 0.1 \text{ m}^3 \text{ m}^{-3}$ with respect to the outer unaltered clay side. The observed dissolution of clays suggests that aluminium is present in solution. It is therefore possible that part of it will be incorporated into C-S-H leading to C-A-S-H formation. Nevertheless, the presence of C-A-S-H could not be confirmed, it could be the focus of further studies.

Table 1 Summary of observations related to physical and mineralogical properties of the investigated cement-bentonite interface samples. ↑ indicates mineral precipitation. ↓ represents mineral dissolution.

Interface type	Temp.	Interact. time	HTO Diffusivity decrease (entire sample) ¹	Clay altered zone			Cement altered zone	
				Extension	Mineral. variations	Porosity (neutron img.)	Extension	Mineral. variations
OPC-montm.	25 °C	Up to 6 years	-64%	~1 mm	↑ C-S-H ↓ montm.	0.30-0.35 General decrease of ~0.1	~3-4 mm	↓ portlandite, ettringite, C-S-H (?) ↑ Cl-AFm
OPC-bentonite	25 °C	2 years	-58%	~2-3 mm	↑ C-S-H ↓ montm.	0.35 General decrease of ~0.1	~3 mm	↓ portlandite, C-S-H, ettringite (?) ↑ Cl-AFm (?)
OPC-bentonite	70 °C	8 months	-56%	~2 mm	↑ C-S-H, Mg-phase ↓ montm.	No measurements	~1.5 mm	↓ portlandite, C-S-H, ettringite (?) ↑ Cl-AFm (?)
OPC-montm.	70 °C	8 months	-53%	~0.8 mm	↑ C-S-H, Ca-montm., Mg-phase ↓ montm.	No measurements	~1-1.5mm	↓ portlandite, C-S-H, ettringite (?) ↑ Cl-AFm (?)
ESDRED-bentonite	25 °C	2 years	-64%	~0.5-1 mm	↑ Mg-phase (?) ↓ montm. (?)	No variations detected	~0.5-1mm (?)	↓ C-S-H (?)

¹The diffusivity decrease represents the average experimental value of the HTO diffusion coefficient across the cement-clay sample after interaction compared to the (experimental or calculated) initial diffusion coefficient of the unaltered interface sample. Question marks (?) represent hypotheses of mineral alterations that were assumed to occur, but were not confirmed (e.g., no suitable method used to detect this phase, or no measurement performed to verify the hypothesis).

To enhance the complexity of the system and approximate the real repository conditions, in the second series investigations were also performed on bentonite (MX-80) in contact with a low pH mortar (ESDRED) in addition to those with bentonite and the high-porosity OPC. The interface samples reacted for two years at ambient temperature in an oxygen-free atmosphere. The ESDRED-bentonite samples appeared to react remarkably less compared to samples with OPC (Chapter 5): no porosity modification could be detected in either part of the sample, and also mineralogically only small changes were noted. Nevertheless, the diffusivity across the ESDRED-MX-80 samples decreased significantly within the experimental time period, similarly as that across bentonite-OPC paste samples. The pattern is the same as that observed for OPC-montmorillonite interfaces (Chapter 3): a first phase of fast decrease (<1 year) followed by a second phase (>1 year) with a slower decrease, pointing to a reduced reactivity of the system. The decrease of the sample diffusion coefficient is likely related to different reactions for the two interface samples, depending on the initial mineralogy and porosity of the system. In the OPC-bentonite sample, it is very likely related to a porosity reduction following the precipitation of newly formed C-S-H phases that were identified on the bentonite side. In the ESDRED-bentonite samples, it might be related to the formation of a Mg phase, even though no porosity decrease could be observed.

The experimental design described in Chapter 6 (experiments at 70°C) allowed to better define the extension of the alteration zones for OPC reacting with bentonite and montmorillonite. On the bentonite side, the strongly altered region (clay-skin) displayed an extension of ~1 mm and showed a heterogeneous

chemical zonation. Ca and Na were enriched within the skin and C-S-H phases were detected. A Mg-enrichment was present at 1.5 mm from the interface. From 2 mm on, the bentonite was generally unaltered (if continuously connected to a porewater reservoir of sufficient size on the external side). For OPC-montmorillonite samples, the clay skin showed an extension of ~0.8 mm and a strong enrichment in calcium and sodium with respect to the external clay side. Newly formed C-S-H phases were detected inside the skin. As in bentonite, a Mg-enrichment located at 1.5 mm from the interface was observed on the montmorillonite side.

The extension of the altered region on the OPC paste side was about 1-1.5 mm for both sample types, independent of whether bentonite or montmorillonite was used. Portlandite dissolution was observed with different methods. It has to be considered that to enhance the reactivity of the system a high-porosity hardened cement paste ($\varepsilon = 0.63$) was used. In general, it was confirmed that the formation of the low porosity region on the bentonite or montmorillonite side slowed down the overall reactivity at the interface, and therefore also slowed down the further extension of the altered region within the cement paste. For samples not constantly connected to the corresponding porewater reservoir, the alteration on the cement side reached in some cases 4-4.5 mm within 6 years (Chapter 3). This is probably related to the lack of buffering on the external side during the times of disconnection. The high temperature experiments (Chapter 6) demonstrated that if a sufficiently large reservoir is present, the alteration is limited to 1-1.5 mm from the interface.

7.1.2 Cement-OPA interaction

The results of the experiments performed with cement-OPA interface samples allowed to shed light on the small-scale alterations occurring near the interface during a maximum of 2 years interaction time. An overview of the main observations for the interface samples involving Opalinus Clay is given in Table 2.

The investigation of the diffusive properties of OPC-OPA interface samples by means of HTO showed a significant decrease of the diffusion coefficient after 2 years interaction. Similarly, ESDRED-OPA interface samples denoted a remarkable decrease of the HTO diffusion coefficient. For both interface sample types, no complete blocking of the pore space occurred within the time of the experiments. Especially for ESDRED-OPA samples it was not possible to detect any relevant porosity variation. Several aspects may have led to this, e.g.: i) neutron imaging was performed only after six months of interaction, which may have been too early for noticeable changes. ii) Both materials (ESDRED and OPA) have a comparably low porosity, and the used neutron imaging setup has a too low resolution to detect small porosity variations. The absence of a noticeable porosity change is, however, not necessarily at odds with the measured decrease of the diffusivity. The ESDRED-OPA system with its low porosity has a certainly a high sensitivity with respect to any small changes of the pore structure. This means that a relatively small decrease in the porosity (e.g., 0.03), undetected by the used neutron imaging setup, may have a great influence on the diffusivity.

Table 2 Summary of the physical and mineralogical properties regarding the investigated cement-OPA interfaces. ↑ indicates mineral precipitation. ↓ represents mineral dissolution.

Interface type	Temp.	Int. time	HTO Diffusivity decrease (entire sample)	Clay altered zone			Cement altered zone	
				Extension	Mineral. variations	Porosity (neutron img.)	Extension	Mineral. variations
OPC-OPA	25 °C	2 years	-45%	~0.5-1 mm	↑ C-S-H?, Ca-clays (?) ↓ silicates, clays (?)	Slight decrease on cement side (right at the interface)	<1 mm	↑ Calcite ↓ portlandite, ettringite (?), C-S-H (?)
OPC-OPA ¹	70 °C	8 months	No data	<~0.5 mm	↑ C-S-H ?, Ca-clays (?) ↓ Silicates, clays (?)	No measurements	<~0.3 mm	↑ Calcite, Mg-phase (?) ↓ portlandite, ettringite (?), C-S-H (?)
ESDRED-OPA	25 °C	2 years	-34%	~1 mm (?)	↑ Mg Phase ↓ Silicates (?), clays (?)	No relevant variations detected	~0.5mm (?)	↓ C-S-H (?)

¹The OPC-OPA interface samples used in this experiment displayed an imperfect contact of the two materials at the interface, which probably affected the evolution of the samples (cf. Chapter 6). Question marks (?) represents hypotheses of mineral alterations, that were assumed to occur but were not confirmed (e.g., no suitable method used to detect this phase or no measurements performed to verify the hypothesis).

Mineralogical and structural investigations of the OPC-OPA samples reacted at 25°C revealed a narrower altered region at the interface compared to OPC-bentonite samples. Calcite precipitation was observed close to the interface within the first 500 µm of the cement side, whereas the main cement phases tended to dissolve (portlandite, and possibly C-S-H) within the first mm of the OPC compartment. On the OPA side, C-S-H phases may have formed very close to the interface, although they were not unambiguously identified.

ESDRED-OPA interface samples were characterized by a clear 1-mm thick magnesium-enriched region on the OPA side. The nature of the newly forming phase is not completely clear at the moment. The ESDRED compartment was likely characterized by partial dissolution of C-S-H phases within the first 0.5-1mm of from the interface. Beside this observation, the cement paste side appeared to be mineralogically relatively unaltered.

It is important to note that the diffusive properties of OPA and especially those of the ESDRED mortar differ significantly from those of bentonite and the used high porous hardened OPC paste. It is thus possible that much longer interaction times than two years would be required to observe significant (detectable) mineralogical alterations. Nevertheless, the observed clear reduction of diffusivity indicates that some mineralogical alterations leading to a change in the pore connectivity took place.

7.2 Cement-clay interfaces: relevance of the observed results for a repository

7.2.1 Porosity decrease at the interface and bentonite re-saturation

The performed experiments indicated that a porosity and diffusivity decrease will be present at the interface, the latter independently from the cement material used for a liner. These reactions are expected to start after bringing a wet cement in contact with Opalinus Clay or bentonite, even though especially the

latter is not fully and uniformly saturated at this stage. If the diffusivity in the Opalinus Clay will be reduced, the re-saturation of the bentonite surrounding the canisters will very likely be slowed down compared to an unaltered system. It is difficult to quantify the expected magnitude of the porosity reduction for a real repository, as the geometries and the material properties will probably differ from the ones used here. The investigations on OPC-Na montmorillonite samples (Shafizadeh, 2019; Luraschi et al., in prep.,) revealed a remarkable porosity reduction on the clay side. The porosity of the clay skin varied in fact from the initial 0.39-0.53 to ~0.30-0.35 (within the clay skin) after up to 6 years of interaction. Porosity measurements in OPC-bentonite samples indicated the same trends as observed for Na-montmorillonite interface samples (Chapter 5). We have to mention here that while, for instance, the decrease of the porosity in the clay is proven by various measurements, the absolute values of the porosities derived from neutron imaging have a non-negligible error estimated to be in the order of ± 0.05 . It is furthermore likely that in a real case, the interface region will show some heterogeneity, such that the porosity reduction will also not develop uniformly, for instance due to the occurrence of aggregates. More likely is the formation of a region with a general, but not uniform porosity decrease, with a relatively small extension perpendicular to the interface that depends on the interaction time.

The saturation of bentonite will be dominated by advective flow of water from the Opalinus Clay towards the caverns (even though a diffusive component of vapour transport may also play a role at early phases). Once enough porewater is available in the bentonite, geochemical reactions following the contact with the cement liner may also occur in the bentonite. There is no direct correlation between the derived diffusion coefficients and the hydraulic conductivity that governs advective water flow, but both parameters are related to the porosity and the connectivity of the pore space. The observed porosity reduction indicates that the hydraulic conductivity will also be reduced and therefore the saturation of the bentonite will be slowed down.

Bentonite saturation is expected to occur within the first hundreds to thousands of years (see Chapter 2). Figure 1 shows a summary of the diffusion coefficients of the montmorillonite and bentonite skins (with extents of ~1-2 mm) derived during this thesis. From the obtained values, an extrapolation to 10 years (Fig. 1a) and 100 years (Fig. 1b) was performed (red area). The extrapolation indicates that the diffusion coefficient of the skin can be described by a power function, and would reach according to the current data a value $>10^{-12}$ after 100 years interaction, i.e., a value about a factor of 10 or more lower than the initial value. This extrapolation assumes of course that the boundary conditions remain constant. The saturation of bentonite would in this case be slowed down, but no estimation of the prolongation of the re-saturation can be indicated due to the many feedback mechanisms between water saturation, water flow, solute transport and geochemical reactions in a real repository. An eventual strong decrease of the total porosity (close to a total pore clogging) would only occur over longer terms, likely beyond the saturation time of bentonite (several centuries, to thousands of years, according to the last indications). It needs furthermore to be mentioned that the skins, if subjected to high mechanical stress (e.g. due to increasing bentonite swelling pressure, or gas production) may fracture, which then leads to an increase of the diffusivity and conductivity of the interface.

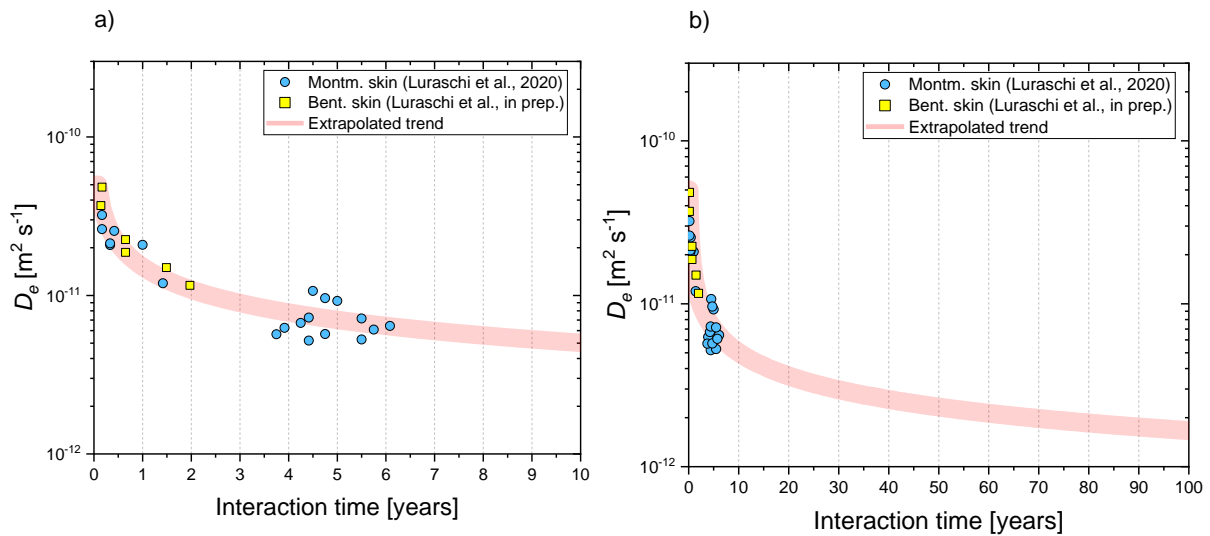


Figure 1 Derived montmorillonite and bentonite skin diffusion coefficients ($D_{e,HTO}$) and extrapolation of the D_e over a) 10 years and b) 100 years.

7.2.2 Radionuclide migration

A decrease of the diffusivity at the cement-clay interface is positive with respect to radionuclide retention. The low diffusivity of the interface region will further slow down any diffusive transport towards the biosphere. The experiments reported in Chapter 3 allowed to recognize the effect of mineral precipitations on the diffusivity of HTO and chloride. It was concluded that C-S-H minerals tended to precipitate in the free porosity, leaving only the interlayer porosity available for diffusive processes. The interlayer porosity in compacted montmorillonite represents, depending on the bulk dry density, a large part of the total porosity (Van Loon et al., 2007; Krejci, 2023), but is not accessible to anions, which leads to the strong observed decrease of anion diffusion. Anion diffusion is a topic of relevance because some of the dose relevant radionuclides are negatively charged (e.g. iodine and selenium) and will therefore not be sorbed on clay surfaces, and thus not be retarded. The porosity and diffusivity decrease near cement-clay interfaces have therefore a positive, retarding effect especially on transport of negatively charged radionuclides. This effect was observed even for a Opalinus Clay or bentonite in contact with a high-porosity cement paste. Accordingly, such highly porous cements could be a good compromise allowing a relatively “fast” bentonite re-saturation but at the same time strongly slowing down anion diffusion.

7.2.3 Cement clay interfaces and their role in gas transport processes

Gas transport is a key topic regarding the long-term safety assessment of a repository. Anoxic steel corrosion is in fact expected to produce relevant quantities of H_2 gas. Although in minor amount, alkanes (e.g., CH_4), originating from microbiological reactions, are also expected to be present. In situ experiments in the Mont Terri underground rock laboratory, and experiments on drill cores of OPA demonstrated that gas can migrate in different ways through a clay rock. At low gas pressures, diffusion in the water phase will be dominant. If the gas entry pressure (capillary threshold pressure) is reached (and if it is lower than the stress acting within the rock), gas transport will also occur by porewater displacement (Marshall et al.,

2005). This process will lead to a desaturation of the OPA. Marshall et al. (2005) reported also evidence for dilatancy-controlled gas transport at somewhat elevated pressures. The formation of gas related fractures would occur only if the gas pressure would exceed the sum of minimal principle stress and tensile strength of the rock.

A strong reduction of the macroporosity (defined as pores with radii > 25 nm) or even a total clogging of the pore space at cement-clay interfaces would reduce gas transport and could thus lead to an increased pressure build up. The diffusion experiments presented in Chapter 3 indicated a very strong decrease of the diffusivity of chloride after 6 years interaction for OPC paste-Na montmorillonite interfaces. Inside the repository, if part of the macroporosity will be affected by precipitation of new mineral phases as observed in the OPC-montmorillonite (and bentonite) experiments, diffusion of dissolved gases will have to occur through meso- and micropores. Gases are uncharged, but if gas molecules are large (e.g., CH₄), dissolved gases will tend to share (at least partially) the same porosity as anions. In the case of a very strong porosity decrease at the interface, which would clog great parts of the free porosity and possibly indirectly parts of the interlayer porosity, the diffusive transport of large dissolved gas molecules will similarly be restricted as that of anions. Hydrogen molecules are significantly smaller compared for example to methane. This means that H₂ is able to diffuse through smaller-sized pores and would therefore be less affected by a reduction of the free porosity than large gas molecules, similar as HTO in comparison to Cl. Precipitations mainly in the macropores will also lower the gas entry pressure, possibly leading to a larger pressure build-up. However, as already mentioned, a strong pressure build-up may also increase the chance of mechanically breaking the low porosity skins formed at the interface.

Several numerical models predict that a complete clogging of the porosity will occur at a certain time (Chapter 2). Due to the difficulty of producing reliable experiments studying the gas transport, only a small amount of data is present about gas migration through clays, and, to the knowledge of the author, none about gas transport across cement-clay interfaces.

With the data acquired in this thesis it is not possible to make a definitive statement about the transport of gases through cement-clay interfaces. However, any reduction of porosity and especially of the free porosity, as observed for OPC-bentonite interfaces, would also reduce the transport of dissolved gases.

7.2.4 Liner composition: OPC vs ESDRED

Our observations do not allow to clearly define which cement would be most suitable to be used as a liner. The OPC and the ESDRED used in this project differed significantly in their initial porosity. Due to the short experiment duration, the porosity and diffusivity differences have a major impact on the experimental outcomes. Reproducing the same experiments with OPC and ESDRED with comparable initial porosity would allow a better comparison. Nevertheless, some considerations based on our observations can be made:

- Low-pH cements induce less dissolution of clays and silicates in the clay compartments. This difference with respect to normal cements is interesting, since less clay and accessory mineral dissolution means also a smaller amount of ions available for precipitation of new minerals. Although the quantification of clay dissolution is not straightforward, the TGA results (Chapter 5) indicated little

changes in bentonite in contact with ESDRED compared to bentonite in contact with OPC. Experiments with longer durations would be needed on this topic.

- Although the used ESDRED and OPC had significantly different initial diffusive properties, samples with both cements displayed a remarkable decrease of the HTO diffusion coefficient after two years interaction. This experimental observation suggests that using a cement with low pH is not sufficient to reduce the interface reactivity (i.e., porosity decrease), at least over relatively short times.

References

- Krejci, P., 2023. Diffusion of sorbed cations in clays: Development, improvement and application of new and existing models. PhD Thesis. University of Bern, Bern, Switzerland.
- Marschall, P., Gorseman, S., Gimmi, T., 2005. Characterisation of Gas Transport Properties of the Opalinus Clay, a Potential Host Rock Formation for Radioactive Waste Disposal. *Oil & Gas Sci. Tech.* 60, 121-139
- Van Loon, L.R., Glaus, M.A., Müller, W., 2007. Anion exclusion effects in compacted bentonites: towards a better understanding of anion diffusion. *Appl. Geochem.* 22, 2536–2552.

Chapter 8

Outlook

8. Outlook

The experiments and analytical investigations performed during this work allowed increasing the understanding of several fields regarding interactions at cement-clay interfaces. This included the quantification of the time-dependent evolution of diffusive properties, of the porosity, and of mineralogical alterations, as well as the characterization of differences of the reactions occurring in samples prepared from different clay and cement materials. Although a relevant amount of new clarifying information was acquired, there are still several aspects that would deserve further investigations, building on the knowledge collected in this project. In the following, some ideas and hints are presented, and possible improvements regarding further experiments are proposed.

Neutron imaging

This technique demonstrated to have a great potential to investigate the porosity variations near cement-clay interfaces. Two aspects which could be deepened in the future are described in the following.

- i) Improvement and verification of the water quantification procedure by measuring a dry sample of a clay skin. The water quantification procedure relies on several steps. One of them is represented by the production of an image of the dry sample. This is done by measuring unaltered dry cement paste and clay samples (allowing to create a 'dry image'). The image of the saturated samples is then normalized by the dry image to quantify the water content. If the mineralogy of the clay skin is strongly altered compared to the unaltered state, the used dry image is no longer adequate, and this normalization procedure could produce an under- or overestimation of the true water content. As long as the total H content of the solid would not alter much, the effect would be minor, or at least small compared to an increase or decrease of the H content following the change in water content. So far, no neutron measurements of altered dry samples were possible. Measuring a dry clay skin would allow to verify the current procedure to evaluate the water content.
- ii) The ICON beam line at PSI offers the possibility to perform measurements using a neutron microscope. This setup allows obtaining a considerably better spatial resolution than the standard one. The drawback of this setup is that smaller samples are required (diameter in the order of two millimetres). Attempts were started in this direction, but they were unsuccessful. Due to the limited beam time and the smaller size of the sample, which implies practical difficulties, it is strongly advised to produce several samples and possibly perform previous investigations with other imaging techniques to verify the quality of the samples, notably of the interface contact. Identical samples inserted in cells of different compositions (e.g. peek) could be investigated in advance with X-Ray tomography, allowing inferring precious structural information such as zonations, heterogeneities to be investigated, or simply bad samples. Due to the small size of the samples required, a considerable time should be invested in developing a procedure to produce good quality samples.

High temperature experiments

The greatest limit of experimental techniques related to cement-clay interfaces is the reactivity of the system. In the field of radioactive waste disposal, the time of interest is thousands to millions of years, which is obviously not replicable in laboratory. Accelerating the experiments by increasing the interface reactivity could therefore represent a key to be considered for the future. The experiments performed at 70°C and discussed in Chapter 6 showed how such experimental design can significantly accelerate the reactivity of the system. For the future, it could be interesting to produce interface samples with material identical as the one which will be used in the repository and further investigate the interaction at increased temperature.

Size of the samples and cells

Ideally, a cement-clay interface sample should be as realistic as possible (e.g., regarding the composition), and it should be investigated with all the possible techniques. The size of the experimentally reproduced interfaces is often very small due to the measurement conditions and handling setup (e.g., size of glove box, of the oven or size of the cell).

Certain investigations, e.g. the imaging techniques, necessitate a small sample size. Unfortunately, small samples produce little amount of material available for the investigations and therefore only selected methods can be applied. As an example, the altered region formed inside the bentonite investigated in this thesis was made of some tens of milligrams.

A bigger reaction cell would allow performing different analyses on the same sample, but would reduce the resolution of the imaging techniques. As a solution, the experiments could be performed in parallel, using small and bigger cells. This would allow to use the small cells for imaging techniques and the bigger cells, which should basically have reacted in the same way, for the rest of the investigations.

Improvement of the experimental setup

The outer ring stabilizing the cells used in these experiments was composed of aluminium, which has a low interacting probability with neutrons. Due to the strong X-Ray attenuation of aluminium, to perform X-ray tomography the ring was generally removed to improve the resolution (the samples were still contained in a PTFE sleeve, but had open ends). The production of some rings less interacting with X-Rays (e.g. peek) could be interesting. Having peek rings would allow to quickly exchange the aluminium ring when necessary (inside the glove box), and perform X-Ray tomography without opening the cell. This would slightly decrease the resolution due to increased distance sample to detector, but air contamination could be avoided and therefore longer acquisition times could be used, resulting in higher resolution.

High-porosity low-pH cement

It could potentially be interesting to produce a cement paste that represents a middle ground between the two used so far: low-pH and high porosity. To allow a faster re-saturation of the bentonite, the porosity of the cement paste plays a relevant role. It could be conceivable to use a high porosity low-pH cement or mortar. This combination would theoretically guarantee i) a reduced clay dissolution, and ii) higher

diffusive properties of the interface region (cement-bentonite), facilitating the bentonite re-saturation. Such samples could be produced in laboratory to investigate their evolution.

Through-diffusion experiments using different tracers

Most of the diffusion experiments were performed using HTO. Only for OPC-Na montmorillonite interface samples the diffusivity of chloride was additionally investigated. It could be interesting to produce new realistic interfaces (e.g. ESDRED-OPA, OPC-OPA) and investigate the diffusivity evolution using HTO, chloride and sodium. This would allow acquiring information on the diffusivity of differently charged species and on the effect of the mineralogical and porosity alteration on the various diffusion coefficients. Especially performing through diffusion experiments through cement-clay interfaces with cations would give new information that could shed light on, for instance, the location(s) of the new mineral precipitates.

Gas migration experiments through cement-clay interface

It would certainly be interesting to develop a cell in which experiments could be performed with gases, maybe initially only in fully saturated samples. Constructing a cell that is gas tight and measuring the concentration variations of gases is certainly not a simple undertaking, but it would provide valuable information. The effect of newly formed skins with altered porosity on the transport of different gases could be investigated. Performing the experiments at different water saturations would add significant and very valuable information, but would also imply additional challenges.

To simplify the experiments, a clay (e.g., montmorillonite) could be put in contact in cells solely with an artificial porewater of cement. This would lead to the formation of a clay skin but avoid the presence of the cementitious compartment.

Production of a 3D porous sample

The 3D printing techniques allow nowadays producing materials of small size with very high precision. It would be interesting to produce a porous material and simulate a cementitious-clay interface. For example, the porewater of cement and clay could be put in contact similarly as performed in this thesis, but without the physical presence of cement and clay. The result could be the formation of a skin within the synthetically produced material, provided these reactions would occur independently of any mineral dissolution. The advantage would be that all the precipitated material would represent newly formed skin material. Furthermore, diffusion experiments could be performed and the diffusivity could be investigated. It would of course be interesting to perform diffusion experiments using differently charged tracers and subsequently investigate the mineralogy by means of different analytical techniques. If possible, the production of materials with different porosity or pore sizes would then allow acquiring further interesting information.

Annex

Annex A

A brief history of the nuclear sciences and nuclear energy use

The issue of radioactive waste disposal is obviously related to the evolution of the nuclear sciences and the nuclear energy production. The beginning of the nuclear era is difficult to be set precisely in history: towards the end of the 19th century a series of scientific discoveries have radically changed the physics-based description of nature. The major events are briefly summarized as follows.

In 1865, J.C. Maxwell published a set of equations theoretically describing the electromagnetic radiations (Maxwell, 1865). During those years several scientists were using variations of vacuum tubes to study electron beams. In 1895 W. Röntgen, a German physicist, was able to produce the first X-Ray radiography image. Röntgen's results indirectly inspired Henri Becquerel, who started experimental investigations with a fluorescent material in 1896 (Becquerel, 1896). The material turned out to be a uranium salt. He discovered that the material was producing an unknown radiation which was able to traverse a paper. During his experiments, Becquerel noted that the salt was able to emit so called "uranic radiations" also in absence of an energy source (Becquerel, 1896). Two years later Polonium and Radium were first isolated from pitchblende minerals (later called uranite) by Marie and Pierre Curie (Curie and Curie, 1898; Radvanyi and Villain, 2017). In the following years, many other radioactive elements were discovered, the different ionizing radiations were identified and the fundamentals of the nuclear science started to be theorized and investigated.

In 1933, the Hungarian physician Leo Szilard recognized as first the feasibility of the nuclear fission. One year later Enrico Fermi started experimenting with the bombarding of uranium by neutrons. In 1938 a group of scientists led by Otto Hahn and Lise Meitner observed a chain reaction triggered by interaction of uranium with neutrons and detecting several decay products (e.g. barium). A few years later, the Manhattan project started; and in less than five years, the members of the project were able to use the fission reaction for military purpose, developing the first weapon made of an uncontrolled chain reaction.

In 1948, the American Energy Commission (AEC) started the first plan directed towards the development of nuclear reactors for energetic purposes (Mazzuzan and Walker, 1984), officially starting the race towards nuclear energy production. Some years later, in summer 1955, the first international conference focused on the atomic energy took place in Geneva (Switzerland). The USA attended the conference with a small "swimming-pool" demonstrative reactor, which not only impressed all the visitors with the bewitching Cherenkov radiation, but was also subsequently bought by the Swiss government. The reactor was renamed SAPHIR and placed in the newly founded "Reaktor AG", which 30 years later became the Paul Scherrer Institute (Nägelin, 2007). In 1957, the Euratom and the International Atomic Energy Agency (IAEA) were founded, marking the beginning of a new period in the nuclear era. The potential of nuclear power was just discovered, and the danger of radioactivity was not well known yet, or considered irrelevant. Therefore, several "futuristic" studies started. One of them was the Plowshare project, which aimed to use nuclear explosions to modify the landscape (Kirsch, 2005). Nuclear explosions were also investigated as a potential means to gain resources from the underground (gas, oil and minerals). One of these experiments with an underground nuclear detonation resulted in high amounts of gas production,

which could not be used due to its radioactivity (Freeman, 1982). In 1964, the first nuclear reactor able to produce energy (in a more cost efficient way than burning fossil fuels) was installed (Weinberg, 1994). All around the world, hundreds of reactors were planned to be built in the following decades. Also in Switzerland, up to ten reactors were planned (Kupper, 2003).

Although many scientists had already pointed out the potential danger of nuclear reactors, accelerators and radioactive waste (e.g. Scherrer, 1945), the threat of ionizing radiation and the sustainable management of radioactive waste was at that time underestimated, especially in the beginning of the nuclear energy era (Weinberg, 1994). The “anti-atom” activism and the resistance of the population against nuclear power plants (NPP) steadily grew; it was accentuated by some severe accidents that occurred worldwide (Freeman, 1982; Cooke, 2011; Kuruc and Mátel, 2011). From the 70ties, a large part of the population in the USA and in western Europe were following the activist movements of that historic period and started to oppose to the use of atomic energy.

The development of nuclear reactors and the consequent production of High-Level Waste (HLW) led to the need of a solution for the waste disposal, which were previously either accumulated in disposal sites on the surface or diluted into rivers and seas (Lipschutz, 1981; Milnes, 1985). A variety of concepts were investigated by the scientific community as possible ways to eliminate the radioactive waste. The possibility of dumping active material into space was one among them, as described in Burns et al. (1978). Another idea proposed to dispose the waste on the surface of the Greenland or Antarctica ice sheet such that the residual heat would melt the ice and the waste would be transferred deeply below the surface. (Philberth, 1958; Zeller et al., 1973).

From the 70ties, the disposal into deep geological formations started to be considered as the most suitable option. Several programs started in different countries with the goal to explore the underground in search for a geological formation most suitable to host the waste safely for a long period of time.

Nuclear energy in Switzerland

Already before the development of the nuclear energy sector, radioactive materials were produced by industry (e.g., watches), medicine and research. In the 30ties, the dominant energy sources in Switzerland were hydropower and fossil fuels (Axpo, 2019). After the Second World War, the Swiss government, together with the industry, launched significant investments in the development of nuclear power, not only for energetic purposes (Wildi, 2003). The main actors pushing the development in Switzerland were Walter Boveri, active in the energy industry, and Professor Paul Scherrer, a particle physicist (Buser, 2019). In 1965 the construction of the first Swiss nuclear power plant (Beznau I) started. It operates a 350 MW turnkey reactor delivered by Westinghouse Electric. In parallel, with the goal to develop an own reactor, the underground facility of Lucens (VD) was opened in 1967, where a Swiss made experimental reactor was constructed in an underground cavern. In 1969, a severe accident occurred in Lucens, involving a partial melting of the core. This definitely signed the end of the plan to developing an own Swiss made nuclear reactor (Wildi, 2003; Nägelin 2007). Shortly after, the first two imported nuclear reactors were

started: Beznau 1 (1969) and Beznau II (1971). Other three reactors were then constructed in the next 15 years: Mühleberg, (1971), Gösgen (1979) and Leibstadt (1984). Several additional nuclear power plants were planned to be built in the next years; e.g. Kaiseraugst, AG; Graben, BE; Verbois, GE (Axp0, 2019).

The first major nuclear accident of Tschernobyl (26.4.1986), related to a chain of human errors, strongly changed the perception of the peoples towards nuclear energy. The second major accident occurred in Fukushima (11.03.2011), caused by a Tsunami following a magnitude 9 earthquake. This second severe accident led the Swiss federal council in the year 2011 to set an end to the use of nuclear energy. The law states that the Swiss nuclear power plants will be operated as long as safety can be demonstrated and then will be dismantled; no new nuclear NPP will be built. The population approved a new energy legislation in 2017, apparently signing the end of the nuclear energy in Switzerland. The five Swiss reactors will be operated until their end life, without being substituted. In December 2019, the NPP Mühleberg was shut down and the dismantling was started. The remaining three power plants will probably continue to operate for several years. The dismantling of a single plant will last more than a decade and costs several billion Swiss francs (Swissnuclear, 2020).

Today (August 2023), the unstable geopolitical situation and the energetic crisis make it difficult to predict the future strategies. Although renewable energy seems to be the next energy source (at least in the so-called western world) already for more than a decade, the era of nuclear power in Switzerland may not be over after all.

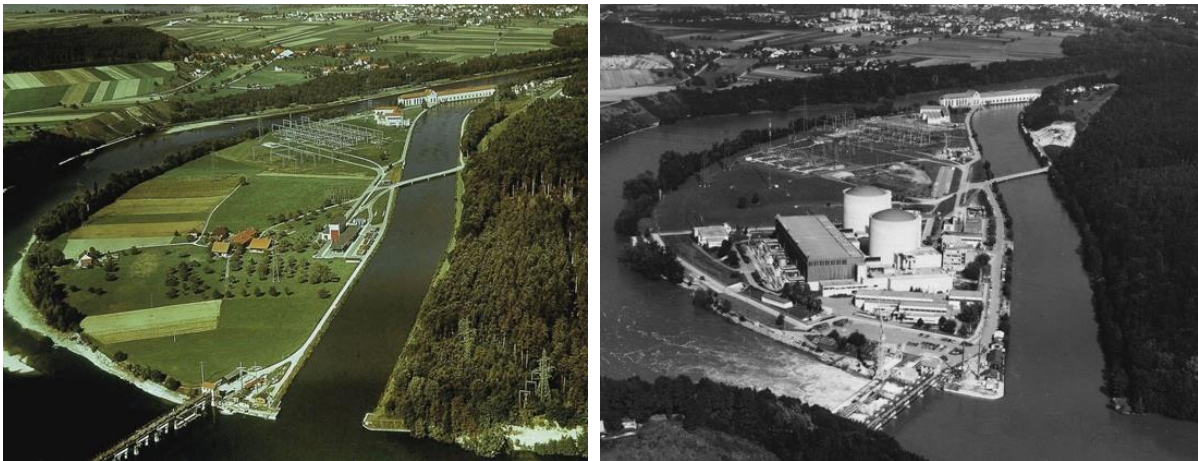


Figure 1 Location of the Beznau NPP, located between the Aare river and a channel excavated for the hydropower plant. Left: before the construction of the first Swiss nuclear powerplant. On the upper part, the building containing the gas turbines are visible. Right: after the construction of the two reactors (Axp0, 2019).

The disposal of radioactive waste in Switzerland

The beginning: Waste production and temporary storage

In 1955, the first guidelines regarding the handling and disposal of radioactive waste were indicated by the Swiss federal government. At that time only low-level waste (LLW) was produced, mainly by the watchmaking industry (Emmenegger and Studer, 2018) and medicine. Due to the poor knowledge of radiological impact on the biosphere at the beginning of the 20th century, the Swiss federal government suggested in the beginning to store the waste in a near surface disposal sites or to dilute them into

canalizations (Hadermann et al., 2014). In 1959, the first nuclear law was put in place, giving guidelines regarding the transport and handling of the radioactive “rests”. Four years later (1963) the first radio-protection ordinance followed, declaring that the low- and intermediate-level radioactive waste (LMA) will be yearly collected by the government. In 1967, considering the future building of NPPs, the government declared the producer of highly-active waste (HLW) responsible for the disposal of this waste.

The amount of low- and intermediate-level radioactive waste produced by research and medicine steadily increased during the years; the surface deposits could not keep pace with the waste production. For this reason, between 1969 and 1983 Switzerland participated, in cooperation with the Nuclear Energy Agency (NEA), in several actions of waste disposal into the North Sea (Hadermann et al., 2014).



Figure 2 Waste disposal into the see (Hadermann et al., 2014).

The construction of the Beznau NPP in 1969-71 forced the industry to increase the effort to develop a concept for the long-term management of the produced high-level waste. The nuclear fuel was at the beginning reprocessed in foreign countries; the highly active material left by the reprocessing did not need to be transported back to Switzerland. Towards the end of the 70ties new contracts signed with the companies responsible for the reprocessing changed the situation, forcing Switzerland to take back the residues of the reprocessing. This fact, together with the building of the five Swiss reactors, increasingly emphasized the problematic of the waste.

Underground waste disposal: The search of a suitable site

The storage of waste disposal containers into geological formations started to be considered towards the end of the 70ties. First investigations in Switzerland were made in the northeastern part (Table Jura), where gypsum formations were investigated. This site was then disregarded due to a tectonic structure

(thrust fold) discovered in the underground, which would compromise the necessary long-term stability (Wildi, 1975).

In 1972, the owners of the nuclear power plants founded Nagra (Nationale Genossenschaft für die Lagerung radioaktiver Abfälle), a cooperative including the powerplant owners and the Swiss confederation. Nagra is financed by the cooperative owners, whereas the disposal costs are included in the produced electricity (~1 cent per kWh on the energy of nuclear origin). The cooperative has a mandate to look for the most suitable place in Switzerland and develop a concept for geological disposal of the radioactive waste. The first studied geologic formations were evaporitic rocks (anhydrite) located in different regions within the Swiss Alps, among these, Bex (JU), and Airolo (TI), where several sites were investigated by means of drilling campaigns (Gassmann et al., 1979; Nagra, 1981).

In 1978 the Swiss government decided that a license to build new powerplants, and also to continue operating the already active ones, would have been granted only if the safe and long-term storage of the produced waste could be assured. So the project “guarantee 1985” (Projekt Gewähr 1985) was started, which had the goal to demonstrate, before 31.12.1985, that the safe disposal of radioactive waste was possible. The project was focusing on crystalline basement rocks located in Northern Switzerland. This project was supposed to find a suitable host rock for a high-level waste repository within the following seven years. From 1982, several deep boreholes were drilled and seismic investigations were performed to study the crystalline basement of Northern and Central Switzerland (Nagra, 1994). The results did not fulfill the expectations (sufficient size of a stable undisturbed crystalline basement could not be guaranteed), and therefore this option had to be withdrawn.

Between 1978 and 1981 several lithologies were investigated as possible host rock. In the end, only three sites were considered as potential repository locations: Glaive (VD, anhydrite), Oberbauenstock (UR, marl) and Piz Pian Grand (GR, crystalline rocks). All three sites were only suitable to host low- and intermediate-level waste (L/ILW). In 1986, Wellenberg (NW, Marls) was added to the previous three sites, especially because for high-level waste (HLW), the repository should be located clearly below the valley floor.

In parallel to the investigation on crystalline rocks, as an alternative solution, several Swiss sedimentary formations have been studied (Nagra, 1988). From 1989, a clay-rich sedimentary rock formation started to be considered as a possible host rock for a future repository: the Opalinus Clay (Schaeren and Norbert, 1989; Tripet et al., 1990). This sedimentary formation appeared promising thanks to a series of properties that allow to efficiently isolate the waste from the biosphere for long periods. From 1996 on, with the inauguration of the Mont Terri Underground Rock Laboratory (canton of Jura), the Opalinus Clay (OPA) became the central focus of the program for the storage of radioactive waste. The initial Mont Terri Project was driven by Marc Thury; his pioneering efforts played a decisive role for the starting of the project, which encountered considerable resistance at the beginning (personal communication). For the last 30 years, this rock formation and its properties were extensively studied under a multitude of aspects to confirm its suitability to host a repository.

In September 2022, Nagra announced the intent to submit the general license application for a combined repository (HLW, L/ILW) in Opalinus Clay.

References

- Axpo, 2019. 23.04.2019. 50 Jahre KKW Beznau. Ein halbes Jahrhundert klimafreundliche Stromproduktion. www.axpo.ch
- Becquerel, H., 1896. Sur les radiations émises par phosphorescence. C. R. hebd. Séanc. Acad. Sci. Paris, 122, 420–421.
- Becquerel, H., 1896. Sur diverses propriétés des rayons uraniques. C. R. hebd. Séanc. Acad. Sci. Paris, 123, 855-858.
- Buser, M., 2019. Wohin mit dem Atommüll? Das Nukleare Abenteuer und seine Folgen – Ein Tatsachenbericht. Rotpunktverlag.
- Burns, R.E., Causey W.E., Galloway W.E., Nelson, R.W., 1978. Nuclear Waste Disposal in Space. NASA Technical Paper 1225.
- Cooke, S., 2011. Atom. Die Geschichte des nuklearen Irrtums, Kiepenheuer & Witsch.
- Curie, P., and Marie S. Curie, M.,S., 1898. On a New Radioactive Substance Contained in Pitchblende. *Comptes Rendus*, no. 127.
- Emmenegger, L., and Studer, B., 2018. Die Verwendung von Radiumleuchtfarben in der Schweizer Uhrenindustrie (1907–1963). Historischer Bericht. Abteilung für Schweizer und Neueste Allgemeine Geschichte.
- Freeman, J.L., 1982. Nuclear Witnesses, Insiders speak out, Norton & Company.
- Gassmann, J., Gysel, M., Schneider, J.F., 1979. Anhydrit als Wirtgestein für die Endlagerung Radioaktiver Abfälle in der Schweiz. Nagra Technischer Bericht, 12.
- Hadermann, J., Issler, H., Zurkinden, A., 2014. Die Nukleare Entsorgung in der Schweiz 1945-2006. NZZ.
- Kirsch, S., 2005. Proving Grounds. Project Plowshare and the Unrealized Dream of Nuclear Earthmoving. Rutgers University Press.
- Kupper, P., 2003. Atomenergie: und die gespaltene Gesellschaft. Die Geschichte des gescheiterten Projektes Kernkraftwerk Kaiseraugst. Chronos.
- Kuruc, J., Mátel, L., 2007. 30th Anniversary of reactor Accident in A1-Nuclear Power Plant Jaslovske Bohunice. Technical report INIS-SK-2007-02.
- Lipschutz, R., 1980. Radioactive Waste. Politics, Technology and Risks, Union of Concerned Scientists.
- Maxwell, J.C., 1865. A Dynamical Theory of the Electromagnetic Field.
- Mazzuzan, G. and Walker, J. S. Controlling the atom. The Beginnings Of Nuclear regulation 1946-1962, University of California press.
- Milnes, A.G., 1985. Geology and Radwaste. Academic Press Geologic Series.
- Nägelin, R., 2007. Geschichte der Sicherheitsaufsicht über die schweizerischen Kernanlagen, 1960 – 2003. Villigen: Hauptabteilung für die Sicherheit der Kernanlagen (HSK).
- Nagra, 1981. Die Endlagerung schwach-und mittel radioaktiver Abfälle in der Schweiz. Potentielle Standortgebiete für ein Endlager Typ B. Nagra Tech. Rep. NTB 81-04.
- Nagra, 1988. Sedimentstudie Zwischenbericht Möglichkeiten zur Endlagerung langlebiger radioaktiver Abfälle in den Sedimenten der Schweiz. Nagra Tech. Rep. NTB 88-25.

- Nagra, 1994. Kristallin-I. Gesamtsynthese der regionalen Untersuchungen zur Endlagerung hochaktiver Abfälle im kristallinen Grundgebirge der Nordschweiz. Nagra Tech. Rep. NTB 93-09.
- Philberth, B. 1958. Disposal of atomic fission products in Greenland or Antarctica. Union Géodésique et Géophysique Internationale. Association Internationale d'Hydrologie Scientifique. Symposium de Chamonix.
- Radvanyi, P., Villain, J., 2017. The discovery of radioactivity. *Comptes Rendus Physique*, 18 (9-10), 544–550.
- Schaeren, G., and Norbert, J. 1989. Tunnels du Mont Terri et du Mont Russelin — La traversée des “roches à risques”: Marnes et marnes à anhydrite. Juradurchquerungen aktuelle Tunnelprojekte im Jura Mitteilungen der Schweizerischen Gesellschaft für Boden- und Felsmechanik 119, 19–24.
- Scherrer, P., Atomenergie, Neue Zürcher Zeitung, 28 November 1945, Mittagsausgabe, Beiblatt “Technik”.
- Swissnuclear, 2020. Stilllegungs- und Entsorgungskosten der Kernenergie: Vergleich Schweiz – Finnland. www.swissnuclear.ch
- Tripet, J. P., Brechbühler, Y. A., Haarpaintner, R. T., Schindler, B., 1990. Hydrogéologie des milieux à faible perméabilité: Étude des Marnes aaléniennes dans la galerie de reconnaissance du Mont Terri (Canton du Jura). Bulletin de la Société Neuchâteloise des Sciences Naturelles 113, 179–189.
- Weinberg, A. 1994. The First Nuclear Era. The life and Times of a technological Fixer. AIP Pres.
- Wildi, W., 1975. Die Mettauer Überschiebung im Aargauischen Tafeljura (Nordschweiz). *Eclogae Geologicae Helvetiae*.
- Wildi, T., 2003. Der Traum vom eigenen Reaktor. Die schweizerische Atomtechnologieentwicklung 1945-1969. Chronos.
- Zeller, E.J., Sanders, D.F., Angino, E.E. 1973. Putting radioactive wastes on ice. A proposal for an international radionuclide repository in Antarctica. *Bulletin of the Atomic Scientists* 29, 4–9, 50–52.

Annex B

FT-IR ATR

FT-IR ATR investigation was performed on a single of OPC paste-Na montmorillonite sample (C25). The results were therefore added as additional information in the annex B.

Method

Fourier transform infrared spectroscopy (FTIR)

Polished cement clay interfaces were investigated by means of FTIR using an INVENIO FTIR Spectrometer coupled with a HYPERION 3000 Microscope (Bruker). Transmission measurements were performed using an Attenuated Total Reflectance (ATR) objective coupled with a single spot Mercury Cadmium Telluride (MCT). Environmental contamination by CO₂ or H₂O was limited thanks to a plexiglass chamber with controlled airflow. Spectral analysis was performed over the range 4000-650 cm⁻¹ with a spectral resolution of 4 cm⁻¹. Spot analysis and profiles were performed across the cement-clay interface to study the mineralogical variation along the samples. The data were further elaborated using the OPUS® software (Bruker).

Results

Portlandite is easily identified with FTIR using the characteristic peak at 3640 cm⁻¹, related to O-H stretching vibrations (Horgnies et al., 2013). FTIR studies of the sample reacted for 4 years (Fig. 1) indicate that portlandite in the cement paste is dissolved at the interface and is present only at distances more than 3 mm away from the interface to the clay. Small amounts of portlandite could still be detected at 2.4 mm from the interface (blue line, 2420 μm from the interface, Fig. 1a) in agreement with observations made with other methods (see Chapter 3). C-S-H can be detected based on the characteristic Si-O vibration bands at ~970 cm⁻¹. However, the de- and polymerization of the silica chains inside the C-S-H structure can result in some shifting of the IR bands (Yu et al., 1999; Horgneis et al., 2013). In the analyzed samples, the C-S-H related peak is consistently located at 960 cm⁻¹ throughout the entire cement sample. Besides the disappearance of the portlandite peak towards the interface (compared to the external part of the sample), the cement sample shows about a constant composition (no measurements could be achieved from 0 to 660 μm, at the contact with the clay).

The interpretation of the FTIR spectra collected for the clay compartment is more challenging. This is related to the variable composition of clays, which contain several types of substitution and exchangeable ions within their structure (Mitchell and Soga, 1992). The pristine clay material was composed of Na-montmorillonite, an Al-rich 2:1 dioctahedral smectite. The negative charge mainly originates from substitution within the octahedral sheet with Fe²⁺ or Mg²⁺ substituting for Al³⁺. According to Madejová et al. (2017) Al³⁺ substitution is visible in two peaks representing the bending vibration of (Al₂OH) at 916 cm⁻¹ and (AlMgOH) at 847 cm⁻¹ (observed here in a slightly shifted position: 918 and 829 cm⁻¹ respectively). A broad peak between 1000 cm⁻¹ and 1040 cm⁻¹ be recognized in spectra collected in the unaltered region and in the clay skin (except at 110 and 190 μm from the interface). Farmer (1974b) assigned absorption

bands in the 1030-1040 cm^{-1} region to Si-O stretching in dioctahedral smectites. The peak width depends on the degree of the cationic disorder inside the TOT layer. For the external part of the clay sample (>1 mm from interface) the absorption band is located between 1000 and 1030 cm^{-1} .

The FTIR spectra collected for the clay skin clearly shows differences with respect to the unaltered part of the sample. The main change is represented by the presence of a prominent absorption band located at $\sim 960 \text{ cm}^{-1}$. Furthermore, the two absorption bands described previously (918 and 828 cm^{-1}) are remarkably less pronounced and are well recognizable only starting at the external part of the clay-skin (>1mm from the cement). The broad peak between 1000 and 1040 cm^{-1} is still present, except for the region closest to the interface (110 μm and 190 μm). For the region between 500 and 700 μm from the cement interface the 956 cm^{-1} peak is more prominent than the $\sim 1000 \text{ cm}^{-1}$ peak. The identification of single minerals in such a complex environment is not completely certain but, in agreement with precedent observations the 956 cm^{-1} peak is likely to represent Si-O stretching vibration of C-S-H (see Fig. 1a for comparison).

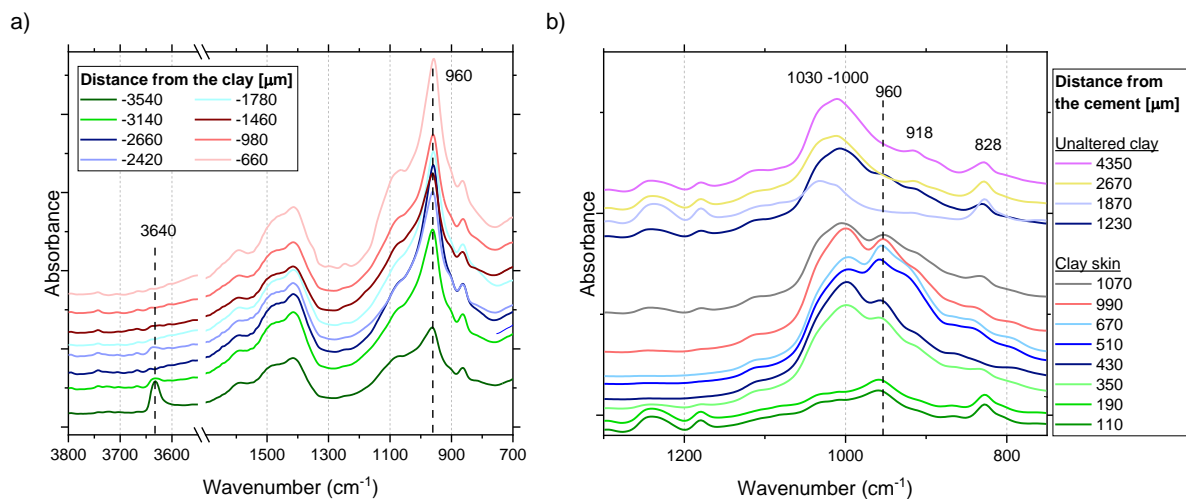


Fig. 1 FTIR spectra for a) the cement part and b) the clay part of the interface sample, subdivided in “unaltered region” and “clay skin”.

References

- Farmer, V.C., 1974b. Site group to factor group correlation tables. In *The Infrared Spectra of Minerals*, Mineralogical Society, London, 515–525.
- Horgnies, M., Chen, J.J., Bouillon, C., 2013. Overview about the use of Fourier Transform Infrared spectroscopy to study cementitious materials. *Mat. Charact.* VI, 251–262.
- Madejová, J., Gates, W.P., Petit, S., 2017. Infrared and Raman Spectroscopies of Clay Minerals, 107–149. In: *Infrared and Raman Spectroscopies of Clay Minerals*. 1st Edition, Volume 8, Elsevier.
- Mitchell, J.K., Soga, K., 1992. *Fundamentals of Soil Behaviour*, 3rd Edition. John Wiley and Sons.
- Yu, P., Kirkpatrick, R.J., Poe, B., McMillan, P.F., Cong, X., 1999. Structure of Calcium Silicate Hydrate (C-S-H): Near-, Mid-, and Far-Infrared Spectroscopy. *J. Am. Ceram. Soc.* 82, 742–748.

Annex C

Porewater composition for the samples discussed in chapter 6: **clay reservoirs.**

Interaction time [days]		HT_1	HT_2	HT_3	HT_4	HT_5	HT_6		HT_1	HT_2	HT_3	HT_4	HT_5	HT_6
6	Ca	1.3×10^{-4}	2.6×10^{-5}	8.3×10^{-3}	8.7×10^{-3}	2.7×10^{-2}	2.7×10^{-2}	Na	3.0×10^{-1}	3.0×10^{-1}	2.4×10^{-1}	2.5×10^{-1}	2.6×10^{-1}	2.6×10^{-1}
13		1.3×10^{-5}	3.0×10^{-6}	8.5×10^{-3}	8.2×10^{-3}	2.6×10^{-2}	2.6×10^{-2}		3.0×10^{-1}	2.9×10^{-1}	2.5×10^{-1}	2.3×10^{-1}	2.6×10^{-1}	2.5×10^{-1}
41		4.4×10^{-6}	9.2×10^{-6}	7.9×10^{-3}	8.8×10^{-3}	2.7×10^{-2}	2.7×10^{-2}		3.0×10^{-1}	3.0×10^{-1}	2.4×10^{-1}	2.4×10^{-1}	2.4×10^{-1}	2.4×10^{-1}
56		3.4×10^{-6}	4.3×10^{-7}	9.2×10^{-3}	8.3×10^{-3}	2.7×10^{-2}	2.7×10^{-2}		3.0×10^{-1}	3.0×10^{-1}	2.4×10^{-1}	2.4×10^{-1}	2.4×10^{-1}	2.4×10^{-1}
72		1.0×10^{-6}	2.1×10^{-5}	1.0×10^{-2}	8.8×10^{-3}	2.6×10^{-2}	2.8×10^{-2}		3.0×10^{-1}	3.0×10^{-1}	2.7×10^{-1}	2.4×10^{-1}	2.4×10^{-1}	2.6×10^{-1}
89		2.9×10^{-5}	1.1×10^{-5}	9.3×10^{-3}	8.7×10^{-3}	2.6×10^{-2}	2.7×10^{-2}		3.0×10^{-1}	3.3×10^{-1}	2.4×10^{-1}	2.4×10^{-1}	2.4×10^{-1}	2.4×10^{-1}
110		1.6×10^{-6}	1.5×10^{-6}	9.6×10^{-3}	9.1×10^{-3}	2.7×10^{-2}	5.5×10^{-2}		3.1×10^{-1}	3.1×10^{-1}	2.5×10^{-1}	2.5×10^{-1}	2.5×10^{-1}	5.0×10^{-1}
125		1.3×10^{-6}	1.6×10^{-6}	9.5×10^{-3}	8.8×10^{-3}	2.7×10^{-2}	3.1×10^{-2}		3.4×10^{-1}	3.0×10^{-1}	2.5×10^{-1}	2.5×10^{-1}	2.5×10^{-1}	2.8×10^{-1}
145		4.1×10^{-7}	6.6×10^{-7}	9.5×10^{-3}	8.8×10^{-3}	2.8×10^{-2}	2.7×10^{-2}		3.4×10^{-1}	3.0×10^{-1}	2.5×10^{-1}	2.5×10^{-1}	2.5×10^{-1}	2.5×10^{-1}
166		2.0×10^{-6}	1.2×10^{-6}	9.3×10^{-3}	8.7×10^{-3}	2.7×10^{-2}	2.7×10^{-2}		3.3×10^{-1}	3.0×10^{-1}	2.5×10^{-1}	2.4×10^{-1}	2.5×10^{-1}	2.5×10^{-1}
Interaction time [days]		HT_1	HT_2	HT_3	HT_4	HT_5	HT_6		HT_1	HT_2	HT_3	HT_4	HT_5	HT_6
6	K	1.6×10^{-4}	1.1×10^{-4}	1.2×10^{-3}	1.7×10^{-3}	1.8×10^{-3}	1.8×10^{-3}	Mg	5.0×10^{-3}	5.0×10^{-3}	6.7×10^{-3}	7.0×10^{-3}	1.8×10^{-2}	1.8×10^{-2}
13		3.3×10^{-4}	3.1×10^{-4}	1.4×10^{-3}	2.0×10^{-3}	1.8×10^{-3}	1.8×10^{-3}		5.1×10^{-3}	5.0×10^{-3}	6.9×10^{-3}	6.6×10^{-3}	1.8×10^{-2}	1.8×10^{-2}
41		1.2×10^{-3}	2.3×10^{-3}	1.7×10^{-3}	3.1×10^{-3}	1.7×10^{-3}	1.7×10^{-3}		1.7×10^{-5}	2.7×10^{-6}	8.9×10^{-3}	6.7×10^{-3}	1.7×10^{-2}	1.8×10^{-2}
56		2.5×10^{-3}	3.7×10^{-3}	1.6×10^{-3}	3.5×10^{-3}	1.8×10^{-3}	1.8×10^{-3}		1.3×10^{-6}	1.3×10^{-6}	6.9×10^{-3}	6.5×10^{-3}	1.7×10^{-2}	1.7×10^{-2}
72		3.9×10^{-3}	6.6×10^{-3}	1.9×10^{-3}	3.9×10^{-3}	1.7×10^{-3}	1.9×10^{-3}		1.3×10^{-5}	9.9×10^{-7}	7.6×10^{-3}	6.6×10^{-3}	1.7×10^{-2}	1.8×10^{-2}
89		4.6×10^{-3}	7.9×10^{-3}	1.5×10^{-3}	4.3×10^{-3}	1.6×10^{-3}	1.7×10^{-3}		1.1×10^{-6}	1.4×10^{-6}	6.9×10^{-3}	6.5×10^{-3}	1.7×10^{-2}	1.8×10^{-2}
110		6.4×10^{-3}	8.5×10^{-3}	1.8×10^{-3}	5.3×10^{-3}	1.9×10^{-3}	3.8×10^{-3}		7.8×10^{-7}	1.6×10^{-6}	7.1×10^{-3}	6.7×10^{-3}	1.8×10^{-2}	3.6×10^{-2}
125		8.2×10^{-3}	9.4×10^{-3}	1.9×10^{-3}	5.6×10^{-3}	2.0×10^{-3}	2.2×10^{-3}		1.0×10^{-6}	2.2×10^{-6}	7.0×10^{-3}	6.4×10^{-3}	1.8×10^{-2}	2.0×10^{-2}
145		9.7×10^{-3}	1.0×10^{-2}	2.5×10^{-3}	6.2×10^{-3}	2.1×10^{-3}	2.0×10^{-3}		9.4×10^{-7}	8.3×10^{-7}	6.6×10^{-3}	6.3×10^{-3}	1.8×10^{-2}	1.8×10^{-2}
166		1.1×10^{-2}	1.2×10^{-2}	3.5×10^{-3}	6.6×10^{-3}	2.0×10^{-3}	2.1×10^{-3}		7.1×10^{-7}	8.2×10^{-7}	6.1×10^{-3}	6.1×10^{-3}	1.8×10^{-2}	1.8×10^{-2}

Porewater composition for the samples discussed in chapter 6: **cement reservoirs**.

Interaction time [days]		HT_1	HT_2	HT_3	HT_4	HT_5	HT_6		Interaction time [days]		HT_1	HT_2	HT_3	HT_4	HT_5	HT_6
41	Ca	1.1×10^{-3}	1.1×10^{-3}	1.2×10^{-3}	1.35×10^{-3}	9.97×10^{-4}	1.21×10^{-3}		6	Na	1.1×10^{-1}					
56		1.1×10^{-3}	1.2×10^{-3}	2.7×10^{-3}	1.05×10^{-3}	9.70×10^{-4}	9.49×10^{-4}		13		1.1×10^{-1}	1.1×10^{-1}	1.2×10^{-1}	1.1×10^{-1}	1.1×10^{-1}	1.1×10^{-1}
110		7.5×10^{-4}	8.0×10^{-4}	8.4×10^{-4}	7.77×10^{-4}	7.58×10^{-4}	8.32×10^{-4}		41		1.2×10^{-1}	1.2×10^{-1}	1.1×10^{-1}	1.2×10^{-1}	1.2×10^{-1}	1.2×10^{-1}
145			7.4×10^{-4}	7.4×10^{-4}	7.33×10^{-4}	6.46×10^{-4}	9.04×10^{-4}		56		1.2×10^{-1}	1.2×10^{-1}	1.1×10^{-1}	1.2×10^{-1}	1.1×10^{-1}	1.1×10^{-1}
166		6.3×10^{-4}	7.8×10^{-4}	7.8×10^{-4}	7.11×10^{-4}	6.38×10^{-4}	7.51×10^{-4}		110		1.2×10^{-1}					
									145			1.2×10^{-1}	1.2×10^{-1}	1.2×10^{-1}	1.2×10^{-1}	1.1×10^{-1}
									166		1.2×10^{-1}	1.3×10^{-1}	1.2×10^{-1}	1.2×10^{-1}	1.2×10^{-1}	1.1×10^{-1}
Interaction time [days]		HT_1	HT_2	HT_3	HT_4	HT_5	HT_6									
6	K	1.9×10^{-1}	1.9×10^{-1}	1.9×10^{-1}	1.80×10^{-1}	1.9×10^{-1}	1.9×10^{-1}									
13		1.9×10^{-1}	1.9×10^{-1}	2.0×10^{-1}	1.8×10^{-1}	1.9×10^{-1}	1.9×10^{-1}									
41		1.8×10^{-1}	1.8×10^{-1}	1.8×10^{-1}	1.8×10^{-1}	1.8×10^{-1}	1.8×10^{-1}									
56		1.8×10^{-1}	1.8×10^{-1}	1.8×10^{-1}	1.7×10^{-1}	1.8×10^{-1}	1.8×10^{-1}									
110		1.8×10^{-1}	1.8×10^{-1}	1.9×10^{-1}	1.8×10^{-1}	1.9×10^{-1}	1.9×10^{-1}									
145		-	1.8×10^{-1}	1.8×10^{-1}	1.8×10^{-1}	1.9×10^{-1}	1.8×10^{-1}									
166		1.7×10^{-1}	1.8×10^{-1}	1.8×10^{-1}	1.8×10^{-1}	1.8×10^{-1}	1.8×10^{-1}									

Measured pH for the samples discussed in chapter 6: **cement and clay reservoirs.**

	Cement side						Clay side					
Interaction time [days]	HT_1	HT_2	HT_3	HT_4	HT_5	HT_6	HT_1	HT_2	HT_3	HT_4	HT_5	HT_6
6	13.30	13.30	13.30	13.30	13.30	13.30	7.00	7.00	8.00	8.00	7.60	7.60
56	13.25	13.22	13.24	13.22	13.25	13.24	10.69	10.92	9.11	9.35	8.77	8.66
68	13.33	13.34	13.34	13.34	13.29	13.32	11.00	11.21	9.20	9.48	8.81	8.76
92	13.41	13.39	13.42	13.41	13.39	13.34	11.30	11.46	9.34	9.68	9.00	8.81
110	13.28	13.27	13.29	13.32	13.34	13.35	11.35	11.45	9.28	9.52	8.99	8.76
125	13.29	13.28	13.27	13.27	13.27	13.28	11.47	11.55	9.39	9.60	9.01	8.78
145	13.41	13.41	13.39	13.42	13.40	13.42	11.62	11.69	9.33	9.55	8.95	8.79
163	13.38	13.38	13.38	13.38	13.36	13.37	11.65	11.72	9.43	9.50	8.88	8.82
177	13.29	13.31	13.35	13.31	13.30	13.33	11.63	11.67	9.52	9.45	8.82	8.80
230	13.33	13.35	13.34	13.29	13.30	13.33	11.88	11.88	9.97	9.20	9.30	8.81

Annex D

Design and structure of the experimental cell

Image taken from the PhD thesis of Shafizadeh (2019)

Isometrie
1:1

Oberflaechenbehandlung:
-Oberflaechche fettfrei!!!

Allgemeintoleranzen ISO 2768-mK

Pos.	Menge	Ein- heit	Sachnummer	Benennung / Merkmale
6	2 Stk	ET-70.0762	0-RING 6.00X1.00	FKM NT 80.7/70
5	2 Stk	43.3.6081	COVER	
4	1 Stk	43.3.6079	TUBE	
3	1 Stk	43.3.5394	PROBENROHR	
2	2 Stk	43.3.5390	3D, EINFahrPROBE	
1	2 Stk	43.3.5389	3D, PEEKFILTER D7.7 X 1.5	

Fremdnummer:

a	18-03-2013	SH94	e	Gezeichnet	28-01-2013	STEBOLD	Massst.
b	01-05-2013	SH94	f	Geprueft	28-01-2013	VAN LOON	2:1
c			g				
d			h	Archiviert		9424	

Anlage DIFFUSIONSPROZESSE
Baugruppe
ZUSAM. SING REAKTOR

Ersetzt durch	
Ersetzt fuer	
Stueckl. Nr.	
Zusammenst. Nr.	

3-43.3.6080B

b: 0-Ringe hinzu
a: Tube und Cover geändert

ZUSAM. CONTAINER
Paul Scherrer-Institut
CATIA

Internes Dokument des Paul Scherrer Instituts, CH 5202 Villigen PSI.
Unauthorized use and reproduction is prohibited.
Internal Document of Paul Scherrer Institut, CH 5202 Villigen PSI.

Erklärung

gemäss Art. 18 PromR Phil.-nat. 2019

Name/Vorname:

Matrikelnummer:

Studiengang:

Bachelor

Master

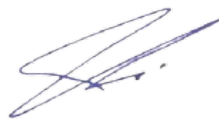
Dissertation

Titel der Arbeit:

LeiterIn der Arbeit:

Ich erkläre hiermit, dass ich diese Arbeit selbständig verfasst und keine anderen als die angegebenen Quellen benutzt habe. Alle Stellen, die wörtlich oder sinngemäss aus Quellen entnommen wurden, habe ich als solche gekennzeichnet. Mir ist bekannt, dass andernfalls der Senat gemäss Artikel 36 Absatz 1 Buchstabe r des Gesetzes über die Universität vom 5. September 1996 und Artikel 69 des Universitätsstatuts vom 7. Juni 2011 zum Entzug des Dokortitels berechtigt ist. Für die Zwecke der Begutachtung und der Überprüfung der Einhaltung der Selbständigkeitserklärung bzw. der Reglemente betreffend Plagiate erteile ich der Universität Bern das Recht, die dazu erforderlichen Personendaten zu bearbeiten und Nutzungshandlungen vorzunehmen, insbesondere die Doktorarbeit zu vervielfältigen und dauerhaft in einer Datenbank zu speichern sowie diese zur Überprüfung von Arbeiten Dritter zu verwenden oder hierzu zur Verfügung zu stellen.

Ort/Datum



Unterschrift